

This PDF was created from the British Library's microfilm copy of the original thesis. As such the images are greyscale and no colour was captured.

Due to the scanning process, an area greater than the page area is recorded and extraneous details can be captured.

This is the best available copy

DX

184647

THE BRITISH LIBRARY

BRITISH THESIS SERVICE

TITLE LANTHANIDE AND TRANSITION METAL
COMPLEXES OF NITROGEN AND OXYGEN
DONOR MACROCYCLIC LIGANDS.

AUTHOR Evagoras George
EVAGOROU

DEGREE Ph.D

**AWARDING
BODY** University of North London

DATE 1994

**THESIS
NUMBER** DX184647

THIS THESIS HAS BEEN MICROFILMED EXACTLY AS RECEIVED

The quality of this reproduction is dependent upon the quality of the original thesis submitted for microfilming. Every effort has been made to ensure the highest quality of reproduction. Some pages may have indistinct print, especially if the original papers were poorly produced or if awarding body sent an inferior copy. If pages are missing, please contact the awarding body which granted the degree.

Previously copyrighted materials (journals articles, published texts etc.) are not filmed.

This copy of the thesis has been supplied on condition that anyone who consults it is understood to recognise that its copyright rests with its author and that no information derived from it may be published without the author's prior written consent.

Reproduction of this thesis, other than as permitted under the United Kingdom Copyright Designs and Patents Act 1988, or under specific agreement with the copyright holder, is prohibited.

C12

**LANTHANIDE AND TRANSITION METAL
COMPLEXES OF
NITROGEN AND OXYGEN DONOR
MACROCYCLIC LIGANDS**

By

EVAGORAS GEORGE EVAGOROU

A thesis submitted in partial fulfilment of the requirements of the
University of North London
for the degree of **Doctor of Philosophy**

This research program was carried out in collaboration with
Amersham International plc

JULY 1994

To my Parents

ABSTRACT

This thesis is concerned with the synthesis and characterisation of altogether twenty 18- and 24-membered macrocyclic ligands, incorporating the pyridyl and phenolic substituents in the cavity, coupled with their lanthanide and transition metal complexes. Initially a survey of the synthesis and characteristics of related macrocycles is presented. The application of lanthanide metal complexes as contrast agents for magnetic resonance imaging (MRI) is discussed.

Schiff condensation of a dicarbonyl (2,6-pyridinedialdehyde and 2,6-diacetylpyridine) and a diamine (1,2-diaminoethane, 1,2-diaminobenzene and (\pm)-*trans*-1,2-diaminocyclohexane) in the presence of a metal (Ba^{2+} , Y^{3+} and Ln^{3+}) led to the *in-situ* synthesis of the [2+2] tetraimine Schiff bases L^1 , L^2 and the novel ligand L^5 . The use of hydrated $\text{Ba}(\text{ClO}_4)_2$, $\text{La}(\text{NO}_3)_3$, YCl_3 , GdCl_3 and $\text{Dy}(\text{NO}_3)_3$ afforded monomeric [2+2] species of which $[\text{GdL}^5(\text{H}_2\text{O})_3]\text{Cl}_3(3\text{H}_2\text{O})$ was characterised crystallographically. The application of hydrated $\text{Y}(\text{NO}_3)_3$ and $\text{Nd}(\text{NO}_3)_3$ yielded the dimeric compounds, $[\{\text{LnL}^5(\text{NO}_3)_2\}_2\text{NO}_3(\text{OH})]$ ($\text{Ln} = \text{Y}, \text{Nd}$), where two [2+2] monomers are linked *via* a nitrate anion. The isolation of the two novel macrocycles, L^5 and L^6 , was successfully achieved for the first time *via* the direct synthesis. For the synthesis of L^6 , the presence of Ba^{2+} yielded the metal-free 18-membered L^6 and the [7+12+7] tricyclic product, S1.

Borohydride reduction of $[\text{BaL}^1]^{2+}$, $[\text{BaL}^2]^{2+}$, L^5 and L^6 resulted in the corresponding demetallated new tetraamine derivatives L^7 , L^8 , L^9 and L^{10} . One of the *meso* forms was isolated from the diastereomeric mixture of L^8 and the structure was elucidated by ^1H NMR and CD spectroscopy and the absolute configuration by X-ray crystallography. The latter technique revealed that first and second row transition metal (Zn^{2+} and Cd^{2+}) co-ordination of L^9 causes the ligand to octahedrally twist and wrap helically around the metal ion adopting a *meridional* arrangement. The ligand in $[\text{LaL}^9(\text{NO}_3)_3]$ adopts a boat conformation analogous to the corresponding lanthanide imine structures.

The reaction of L^7 or L^8 with 2,4-dimethylphenol and aqueous methanal caused the addition of pendant arms and the formation of two new N_6O_4 decadentate ligands, L^{11}H_4 and L^{12}H_4 . On complexation with lanthanide metals all the pendant arms are co-ordinating to the metal although the hydroxy groups are not necessarily deprotonated. $[\text{Gd}(\text{L}^{11}\text{H}_3)\text{NO}_3]\text{NO}_3(3\text{H}_2\text{O})$ was analysed crystallographically. A similar reaction with L^9 yielded L^{15} where two tertiary nitrogen atoms are bridged by a methylene group forming two 5-membered rings and reducing the macrocyclic cavity from 18- to 16-membered.

The reaction of 2,6-diformylphenol and (\pm)-*trans*-1,2-diaminocyclohexane led to the [2+2] macrocycle, L^{17}H_2 . In solution, L^{17}H_2 undergoes solvolytic attack and exists in equilibrium with its carbinolamine. Complexes of L^{18}H_2 , incorporating 1,3-diaminopropane, were isolated when lanthanide metals were used as templates. When Dy^{3+} was employed, a [4+4] dinuclear macrocycle, $[\text{Dy}_2\text{L}^{19}(\text{NO}_3)_4]^+$, was obtained. A mechanism to the formation of the [4+4] dinuclear compounds and the [2+2] dimeric products, where the pyridyl unit is concerned, is proposed.

The relaxation rates of $[\text{GdL}^5(\text{H}_2\text{O})_3]\text{Cl}_3(3\text{H}_2\text{O})$ and $[\text{Gd}(\text{L}^{11}\text{H}_3)\text{NO}_3]\text{NO}_3(3\text{H}_2\text{O})$ proved to be high enough to be considered as potential contrast agents for MRI.

ACKNOWLEDGEMENTS

I wish to express my great appreciation for the guidance, encouragement and continual interest shown by my supervisor, Dr S. W. A. Bligh, throughout the duration of this work.

My thanks also go to Dr W. J. Cummins for his many useful comments and suggestions and also for his and Mr C. Ruddock's supervision during the radioactive experiments at the Amersham International Laboratories.

Prof. M. McPartlin and Mr N. Y. C. Choi are thanked for carrying out the X-ray crystallographic studies and Prof. J. Charalambous for elucidation concerning mass spectrometry. My appreciation is also extended to the technical staff at the School of Applied Chemistry of the University of North London, in particular Mr B. McBride, Miss P. Haria, Mr S. Boyer, Mr J. Crowder, Mr W. Dissanayake, Mr G. Alexandrou, Mrs Z. Khan, Mr H. Dato, Mr L. Williams and Mr A. Bashal.

Thanks are also due to collaborators at Birkbeck College, University of London; Dr H. Parkes and Mr D. Shipp for kindly running NMR spectra at 270 and 500 MHz, Prof. P. J. Sadler for the use of the Bruker minispec spectrometer and Dr A. Drake for running the CD spectra.

A research studentship from the Science and Engineering Research Council (SERC) and a CASE award from Amersham International plc are greatly acknowledged.

I am also extremely grateful for the funding provided by the SERC, Amersham International plc and the Faculty of Science, Computing and Engineering of the University of North London, to attend conferences or short courses at the Universities of Aberdeen, Surrey, Durham, Oxford, London, Reading, Basel (Switzerland) and San Diego (California).

ABBREVIATIONS

aq.	aqueous
Å	Angstrom
B.M.	Bohr Magnetons
B_0	magnetic field (longitudinal component)
BMA	bis methyl amide
CD	circular dichroism spectroscopy
CN	co-ordination number
COSY	correlated spectroscopy
CT	computerised tomography
DAP	diacetylpyridine
DCTA	<i>trans</i> -1,2-diaminocyclohexane tetraacetic acid
DEPT	distortionless enhanced polarisation transfer
DMP	dimethylphenol
dien	diethylenetriamine
dipy	dipyridyl
DMSO	dimethyl sulphoxide
DOTA	1, 4, 7, 10-tetraazacyclododecane-N, N', N'', N''' - tetraacetic acid
DTPA	diethylenetriamine-N, N, N', N'', N'''-pentaacetic acid
ϵ	extinction coefficient
EDTA	ethylenediamine-N,N-tetraacetic acid
EI	electron impact mass spectrometry
en	ethylenediamine
ESD	estimated standard deviation
FAB	fast atom bombardment mass spectrometry
fig(s)	figure(s)
FT	Fourier transform
h	hour(s)

HDB	2-hydroxy-3,5-dimethylbenzyl
HSAB	hard soft acid base theory
I	spin quantum number
IR	infra-red
ITLC	instant thin layer chromatography
IUPAC	International Union of Pure and Applied Chemistry
LD ₅₀	lethal dose of a compound which causes the mortality rate of 50% in an animal population
LFSE	ligand field stabilisation energy
lit.	literature
Ln	any lanthanide metal
LSIMS	liquid secondary ionisation mass spectrometry
M	magnetisation
M	any metal
m.p.	melting point
MHz	megahertz
min	minute(s)
μ	magnetic moment
MRI	magnetic resonance imaging
M _x , M _y , M _z	magnetisation vectors
NMG	N-methylglucamine
NMR	nuclear magnetic resonance
NOTA	1,4,7-triazacyclononane-N, N', N'', triacetic acid
p.p.m.	parts per million
PDA	pyridinedialdehyde
py	pyridine
q	number of metal-co-ordinated water molecules
R	relaxivity or relaxation rate
ref(s)	reference(s)
s	second(s)
S	electron spin number
T ₁	longitudinal or spin-lattice relaxation time

T_2	transverse or spin-spin relaxation time
TE	echo delay time
TETA	1, 4, 8, 11-tetraazacyclotetradecane-N, N', N'', N'''- tetraacetic acid
TGA	thermogravimetric analysis
TI	inversion delay time
TLC	thin layer chromatography
TM	any transition metal
TR	(pulse) repetition time
TTHA	triethylenetetraamine-N, N, N', N'', N''', N''''- hexaacetic acid
τ_c	correlation time
τ_s	electron spin relaxation time
UV-VIS	ultra violet-visible

Ligand Nomenclature

- L¹ 2, 7, 13, 18-tetramethyl-3, 6, 14, 17, 23, 24-hexaazatricyclo-[17, 3.1.1^{8,12}]-tetracos-1(23), 2, 6, 8, 10, 12,(24), 13(14), 17, 19, 21-decaene
- L² 3, 6, 14, 17, 23, 24-hexaazatricyclo-[17, 3. 1. 1^{8,12}]-tetracos-1(23), 2, 6, 8, 10, 12,(24), 13(14), 17, 19, 21-decaene
- L³ 3, 10, 18, 25, 31, 32-hexaazapentacyclo-[25, 3. 1.1^{12,16}, O^{4,9}, O^{19,24}]-dotriaconta-1(31), 2, 4, 6, 8, 10, 12, 14, 16(32), 17, 19, 21, 23, 25, 27, 29-hexadecaene
- L⁴ 2, 11, 17, 26-tetramethyl-3, 10, 18, 25, 31, 32-hexaazapentacyclo-[25, 3. 1.1^{12,16}. O^{4,9}, O^{19,24}]-dotriaconta-1(31), 2, 4, 6, 8, 10, 12, 14, 16(32), 17, 19, 21, 23, 25, 27, 29-hexadecaene
- L⁵ 4(*R*), 9(*R*), 19(*S*), 24(*S*)-3, 10, 18, 25, 31, 32, hexaazapentacyclo-[25, 3.1.1^{12,16}.O^{4,9},O^{19,24}]-dotriaconta-1(31), 2, 10, 12, 14, 16(32), 17, 25, 27, 29-decaene
- L⁶ 4(*R*), 9(*R*), 19(*S*), 24(*S*)-2, 11, 17, 26-tetramethyl-3, 10, 18, 25, 31, 32, hexaazapentacyclo-[25, 3.1.1^{12,16}.O^{4,9},O^{19,24}]-dotriaconta-1(31), 2, 10, 12, 14, 16(32), 17, 25, 27, 29-decaene
- L⁷ 3, 6, 14, 17 23, 24-hexaazatricyclo-[17, 3.1.1^{8,12}]-tetracos-1(23), 8, 10, 12(24), 19, 21-hexaene
- L⁸ 2, 7, 13, 18-tetramethyl-3, 6, 14, 17, 23, 24-hexaazatricyclo-[17, 3.1.1^{8,12}]-tetracos-1(23), 8, 10, 12(24), 19, 21-hexaene
- L⁹ 4(*R*), 9(*R*), 19(*S*), 24(*S*)-3, 10, 18, 25, 31, 32-hexaazapentacyclo-[25, 3.1.1^{12,16}.O^{4,9},O^{19,24}]-dotriaconta-1(31), 12, 14, 16(32), 27,29-hexaene

- L¹⁰ 4(*R*), 9(*R*), 19(*S*), 24(*S*)-2, 11, 17, 26-tetramethyl-3, 10, 18, 25, 31, 32-hexaazapentacyclo-[25, 3.1.1^{12,16}.O^{4,9},O^{19,24}]-dotriaconta-1(31), 12, 14, 16(32), 27,29-hexaene
- L¹¹H₄ 3, 6, 14, 17-tetrakis-(3,5-dimethyl-2-hydroxybenzyl)-3, 6, 14, 17, 23, 24-hexaazatricyclo-[17, 3.1.1^{8,12}]-tetracos-1(23), 8, 10, 12(24), 19, 21-hexaene
- L¹²H₄ 2, 7, 13, 18-tetramethyl-3, 6, 14, 17-tetrakis-(3,5-dimethyl-2-hydroxybenzyl)-3, 6, 14, 17, 23, 24-hexaazatricyclo-[17, 3.1.1^{8,12}]-tetracos-1(23), 8, 10, 12(24), 19, 21-hexaene
- L¹³H₆ 3, 6, 9, 17, 20, 23-hexakis-(3,5-dimethyl-2-hydroxybenzyl)-3, 6, 9, 17, 20, 23, 29, 30-octaazatricyclo-[23, 3.1.1^{11,15}]-triaconta-1(29), 11, 13, 15(30), 25, 27-hexaene
- L¹⁴H₆ 2, 10, 16, 24-tetramethyl-3, 6, 9, 17, 20, 23-hexakis-(3,5-dimethyl-2-hydroxybenzyl)-3, 6, 9, 17, 20, 23, 29, 30-octaazatricyclo-[23, 3.1.1^{11,15}]-triaconta-1(29), 11, 13, 15(30), 25, 27-hexaene
- L¹⁷H₂ 31, 32-bis-hydroxy-3, 10, 18, 25-tetraazapentacyclo-[25, 3.1.1^{12,16}.O^{4,19},O^{19,24}]-dotriaconta-1(31), 2, 10, 12, 14, 16(32), 17, 25, 27, 29-decaene
- L¹⁸H₂ 25, 26-bis-hydroxy-3, 7, 15, 19-tetraazatricyclo-[19, 3.1.1^{9,13}]-hexacos-1(25), 2, 7, 9, 11, 13(26), 19, 21, 23-decaene
- L²⁰H₄ 2, 31, 32-tris-hydroxy-3, 10, 18, 25-tetraazapentacyclo-[25, 3.1.1^{12,16}.O^{4,9},O^{19,24}]-dotriaconta-1(31), 10, 12, 14, 16(32), 17, 25, 27, 29-nonaene

TABLE OF CONTENTS

Title	i
Dedication	ii
Abstract	iii
Acknowledgements	iv
Abbreviations	v
Ligand nomenclature	viii
Table of contents	x

CHAPTER 1

SURVEY OF THE SYNTHESIS AND USES OF MACROCYCLES . . .	1
1.1 Definition of a Macrocyclic Ligand	1
1.2 Synthesis of Macrocycles	1
1.2.1 Metal Cation Size and the Macrocyclic Ligand Cavity	5
1.2.2 Ring Contraction and Expansion Under Cation Control	5
1.2.3 Co-ordination Template Effects	11
1.2.3.1 The Macrocyclic Effect	13
1.3 A General Overview of the 18-membered macrocyclic Ligands and their Metal Complexes	15
1.4 The Lanthanide Metals	19
1.4.1 The Lanthanide Contraction	19
1.4.2 Co-ordination Chemistry	20
1.4.3 Chelates of Lanthanide Metals	20
1.5 Magnetic Resonance Imaging (MRI)	21
1.5.1 The Technique of NMR Imaging as a Diagnostic Tool	22
1.5.2 Relaxation Processes in NMR Spectroscopy	24
1.5.2.1 Spin-lattice Relaxation	24
1.5.2.2 Spin-spin Relaxation	24
1.5.3 Applying the Mechanism of Relaxation to MRI	25
1.5.4 The Development of Contrast Agents	27

1.5.4.1	Mode of Action of Contrast Agents	28
1.5.4.2	Essential Properties of Contrast Agents	30
1.5.4.3	Recent Advances on Contrast Agents For MRI	31
1.6	References	37

CHAPTER 2

SYNTHESIS AND CHARACTERISATION OF 18-MEMBERED HEXAAZA MACROCYCLES AND THEIR LANTHANIDE METAL

COMPLEXES		43
2.1	Introduction	43
2.2	Synthesis and Characterisation of $BaL^1(NO_3)_2$	43
2.3	The Template Synthesis of L^3 with Gadolinium(III)	45
2.4	Synthesis, Characterisation and Metal Complexation of L^5 and L^6	
	Incorporating the Cyclohexyl Unit	48
2.4.1	The Template Synthesis of L^5	48
2.4.1.1	Infrared Studies	50
2.4.1.2	Liquid Secondary Ionisation Mass Spectrometry of L^5 and its Metal Complexes	53
2.4.1.2	Nuclear Magnetic Resonance Spectroscopy	57
2.4.1.3	The Solid State Characterisation of $[GdL^5(H_2O)_3]Cl_3 \cdot 3H_2O$	64
2.4.2	The Non-Template Synthesis of L^6	71
2.4.2.1	Spectroscopic Characterisation of L^6 and S1	75
2.4.2.2	The X-Ray Crystal Structure of L^6	82
2.4.3	Metal Complexation of L^6	85
2.4.3.1	Complexation of L^6 with Lanthanide Metals	85
2.4.3.2	Complexation of L^6 with Copper(II)	86
2.4.4	Relaxation Rate Studies of $[GdL^5(H_2O)_3]Cl_3 \cdot 3H_2O$	88
2.4.5	Electronic Spectroscopy of $[NdL^5(NO_3)_2]_2NO_3(OH)$	93
2.4.6	Instant Thin Layer Chromatography of $[YL^5Cl_2(H_2O)]^+$	98
2.5	Conclusion	102
2.6	References	103

CHAPTER 3

REDUCTION, DEMETALLATION AND METAL COMPLEXES OF

18-MEMBERED HEXAAZA MACROCYCLIC LIGANDS	108
3.1 Introduction	108
3.2 The Macrocyclic Ligands L ⁷ and L ⁸	110
3.2.1 Infrared Spectrophotometry	110
3.2.2 Mass Spectral Analyses	111
3.2.3 NMR and Circular Dichroism Spectroscopy of [L ⁷ H ₄]Br ₄ and [L ⁸ H ₄]Br ₄	112
3.2.4 The Absolute Configuration of L ⁸ - <i>meso</i>	120
3.3 The Macrocyclic Ligands L ⁹ and L ¹⁰ Incorporating the Cyclohexyl Group	122
3.3.1 Infrared and Mass Spectrometry	122
3.3.2 Nuclear Magnetic Resonance Spectroscopy	124
3.3.3 Isolation and Characterisation of [L ⁹ H ₄](ClO ₄) ₄	132
3.4 Metal Complexation of L ⁹ and L ¹⁰	135
3.4.1 Transition Metal Complexes of L ⁹ and L ¹⁰	135
3.4.1.1 Infrared Spectrophotometry and Magnetic Data	136
3.4.1.2 Liquid Secondary Ion Mass Spectrometry	137
3.4.1.3 NMR Spectroscopy of [ZnL ⁹](ClO ₄) ₂ and [CdL ⁹](ClO ₄) ₂	139
3.4.1.4 X-ray Crystallographic Studies of [ZnL ⁹](ClO ₄) ₂ .MeOH and [CdL ⁹](ClO ₄) ₂	145
3.4.2 Yttrium and Lanthanide Metal Complexes of L ⁹	153
3.4.2.1 Infrared Spectrophotometry and Magnetic Moments	153
3.4.2.2 Liquid Secondary Ion Mass Spectrometry	154
3.4.2.3 Nuclear Magnetic Resonance Spectroscopy of [LaL ⁹ (NO ₃) ₃]	155
3.4.2.4 Solid State Characterisation of [LaL ⁹ (NO ₃) ₃].MeCN	157
3.5 Conclusion	160
3.5 References	161

CHAPTER 4

HEXAAZA AND OCTAAZA MACROCYCLES WITH ADDITIONAL PHENOLIC PENDANT ARM FUNCTIONALITIES 164

4.1	Introduction	164
4.2	Synthesis of L ¹¹ - L ¹⁴ Incorporating the 2-hydroxy-3,5-dimethylbenzyl Pendant Arms	165
4.3	Characterisation of the Ligands	168
4.3.1	Infrared Spectrophotometry	168
4.3.2	Liquid Secondary Ion Mass Spectrometry	170
4.3.3	Nuclear Magnetic Resonance Spectroscopy	172
4.3.3.1	The NMR Spectra of L ¹¹ H ₄ and L ¹² H ₄	172
4.3.3.2	The NMR Spectra of L ¹³ H ₆ and L ¹⁴ H ₆	177
4.3.4	X-Ray Structural Studies of L ¹² H ₄	181
4.4	Yttrium, Lanthanide and Transition Metal Complexes of L ¹¹ H ₄	183
4.4.1	Infrared Spectrophotometry and Magnetic Moments	184
4.4.2	Mass Spectrometry	187
4.4.3	NMR Spectroscopy	190
4.4.4	The X-Ray Crystal Structure of [Gd(L ¹¹ H ₃)NO ₃]NO ₃ .3H ₂ O	196
4.4.5	Electronic Spectroscopy	201
4.4.6	Relaxation Rate Measurements of [Gd(L ¹¹ H ₃)NO ₃]NO ₃ .3H ₂ O	206
4.4.7	Fluorescence Experiments of [Eu(L ¹¹ H ₃)NO ₃]NO ₃ .3MeOH	206
4.5	Metal Complexes of L ¹³ H ₆ and L ¹⁴ H ₆	209
4.6	The Reaction of L ⁹ with 2,5-dimethylphenol and aqueous methanal; Synthesis of L ¹⁵ and L ¹⁶ H ₂	210
4.6.1	NMR Spectroscopy of L ¹⁵	212
4.6.2	NMR Spectroscopy of L ¹⁶ H ₂	213
4.7	Conclusion	218
4.7	References.	220

CHAPTER 5

TETRAAZA MACROCYCLES WITH BRIDGE PHENOLIC GROUPS 223

5.1 Introduction 223

5.2 Synthesis of L¹⁷H₂ and Lanthanide Metal Complexes of L¹⁷H₂
and L¹⁸H₂ 224

 5.2.1 Infrared Spectrophotometry 225

 5.2.2 Electronic Spectroscopy and Magnetic Moments 227

 5.2.3 NMR Spectroscopy 228

 5.2.4 Structure Adaptation of L¹⁷H₂ 230

 5.2.5 Thermogravimetric Analysis 237

2.6 Conclusion 239

5.5 References 240

CHAPTER 6

EXPERIMENTAL 242

6.1 Reagents and General Analytical Techniques 242

6.2 Syntheses and Reactions 243

6.3 References 263

APPENDIX

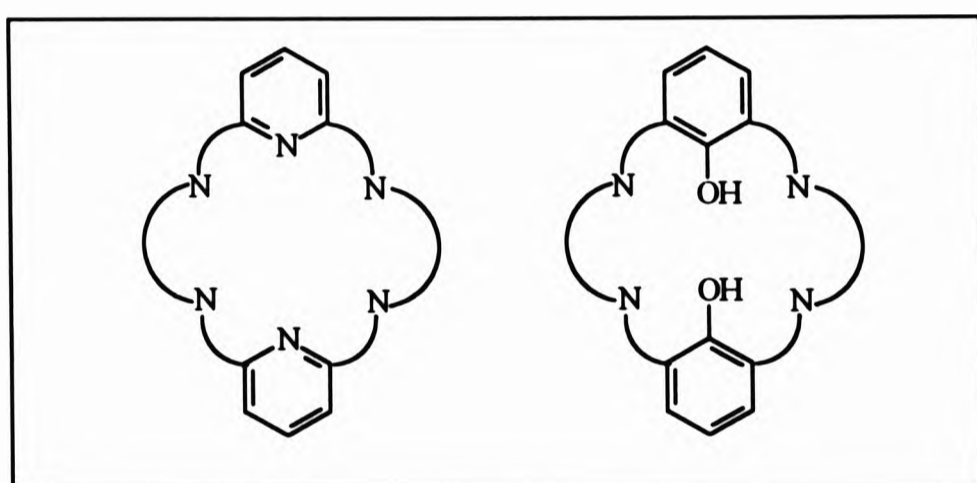
PUBLICATIONS

CHAPTER 1

CHAPTER 1: SURVEY OF THE SYNTHESIS AND USES OF MACROCYCLES

(References to this Chapter are listed on pages 37 - 42)

The work covered in this thesis will attempt to overview and contribute to an important area of macrocyclic chemistry, mainly the area of tetraaza, hexaaza and octaaza symmetrical macrocycles incorporating the pyridyl and phenolic groups coupled with their rare earth and transition metal chemistry. The use and relevance of these complexes in clinical applications and analysis will also be discussed.



Prior to an in-depth discussion of this field the basis, synthesis and basic background to macrocyclic chemistry will be given.

1.1 Definition of a Macrocyclic Ligand

A cyclised structure containing a minimum of three hetero-atoms in the cavity, which itself must be at least nine-membered is defined as a macrocycle.^[1] This definition distinguishes macrocyclic ligands from cyclised *organic* structures which are not capable of chelating to a metal.

1.2 Synthesis of Macrocycles

The synthesis of macrocyclic ligands will be restricted relative to the structures which will be discussed for this work. The general synthesis used here was as shown

in Fig. 1.1.

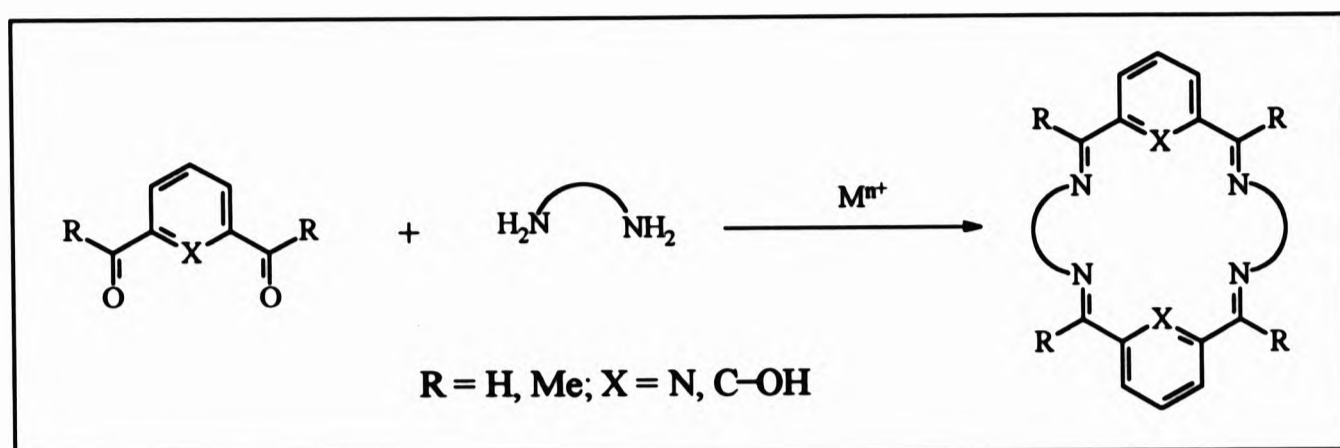


Fig. 1.1. *The general synthesis to the macrocyclic backbone used in this study*

The *direct synthesis* of a macrocycle in the absence of a metal ion is often a low-yield reaction as a result of competing linear polymerisation reactions which may dominate the cyclisation process.^[2] The yield of the cyclised product may be improved by affecting the ring-closing step at high dilution. More effective, however, is the addition of a metal ion during or before this step which leads to an overwhelming improvement in the yield of the required macrocycle as its metal complex. The improvement in yield of the latter *in-situ* method, is a consequence of one or more metal-ion effects that are categorised under the heading *co-ordination template effects* (§ 1.2.3).

The isolation of the metal-free macrocycle before its use to prepare metal derivatives has often certain advantages compared with the *in-situ* method; purification may be accomplished more readily than purification of its complexes.

A major disadvantage of the template,^[3] *in-situ* method, is that the excess presence of one of the organic reactants, which are often chelating agents themselves, may lead to contamination of the required cyclic product with acyclic impurities.

Among the many synthetic ways of preparing macrocyclic structures is the Schiff's condensation of a dicarbonyl and a diamine resulting in symmetrical Schiff bases. The orientation of [1+1] and [2+2] condensation between diamines and dicarbonyls was studied by Nelson *et al.*,^[4] the outcome being summarised in Fig. 1.3.

The formation of the cyclised structures (4) and (5) depends on the proportions and nature of the dicarbonyl (1) and diamine (2) and the size of the metal cation. The initial step is always product (3) resulting from the reaction between one molecule of the diamine and one molecule of the dicarbonyl in the presence of a metal cation. The next step is dependent on the factors mentioned above. If the diamine (2) has sufficient chain length to span the two carbonyl groups of (1) then intramolecular condensation leading to the [1+1] ring, (4), can be formed. If the diamine chain length is insufficient or too rigid to fit by folding, then the [2+2] macrocycle (5) is obtained. Also, if the metal cation is too large for the resulting [1+1] cavity, [2+2] condensation proceeds. The latter two reasons led to the metal template macrocycles reported here for this work.

Nelson and co-workers also suggested that the co-ordination type can also play a rôle in the orientation. A strongly co-ordinated NH_2 group in (3) favours [2+2] condensation in particular when heteroatoms are present in the diamine chain (Fig. 1.2a).

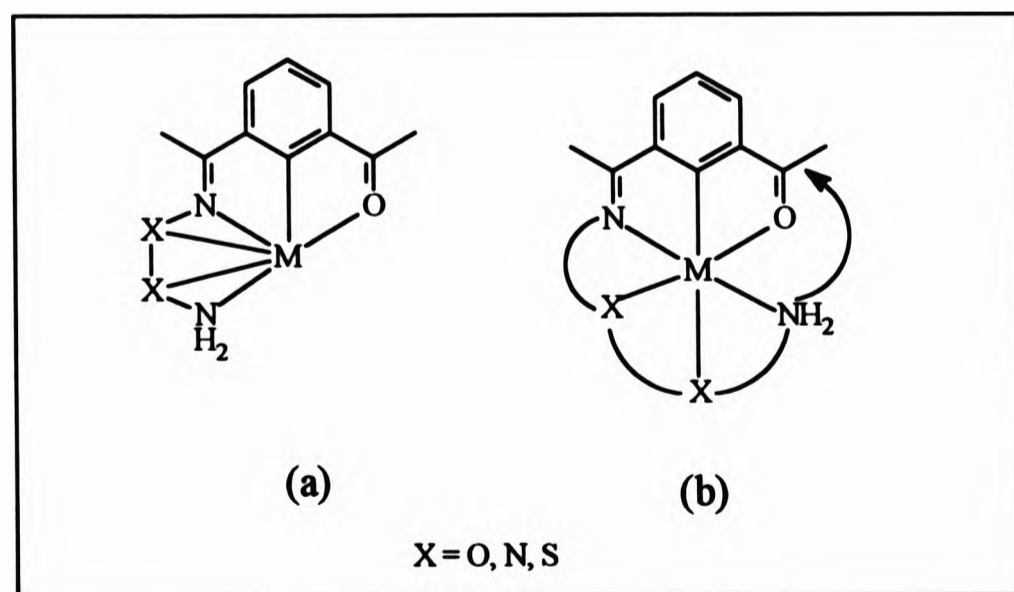


Fig. 1.2 Co-ordination type leading to (a) [2+2] and (b) [1+1] condensation

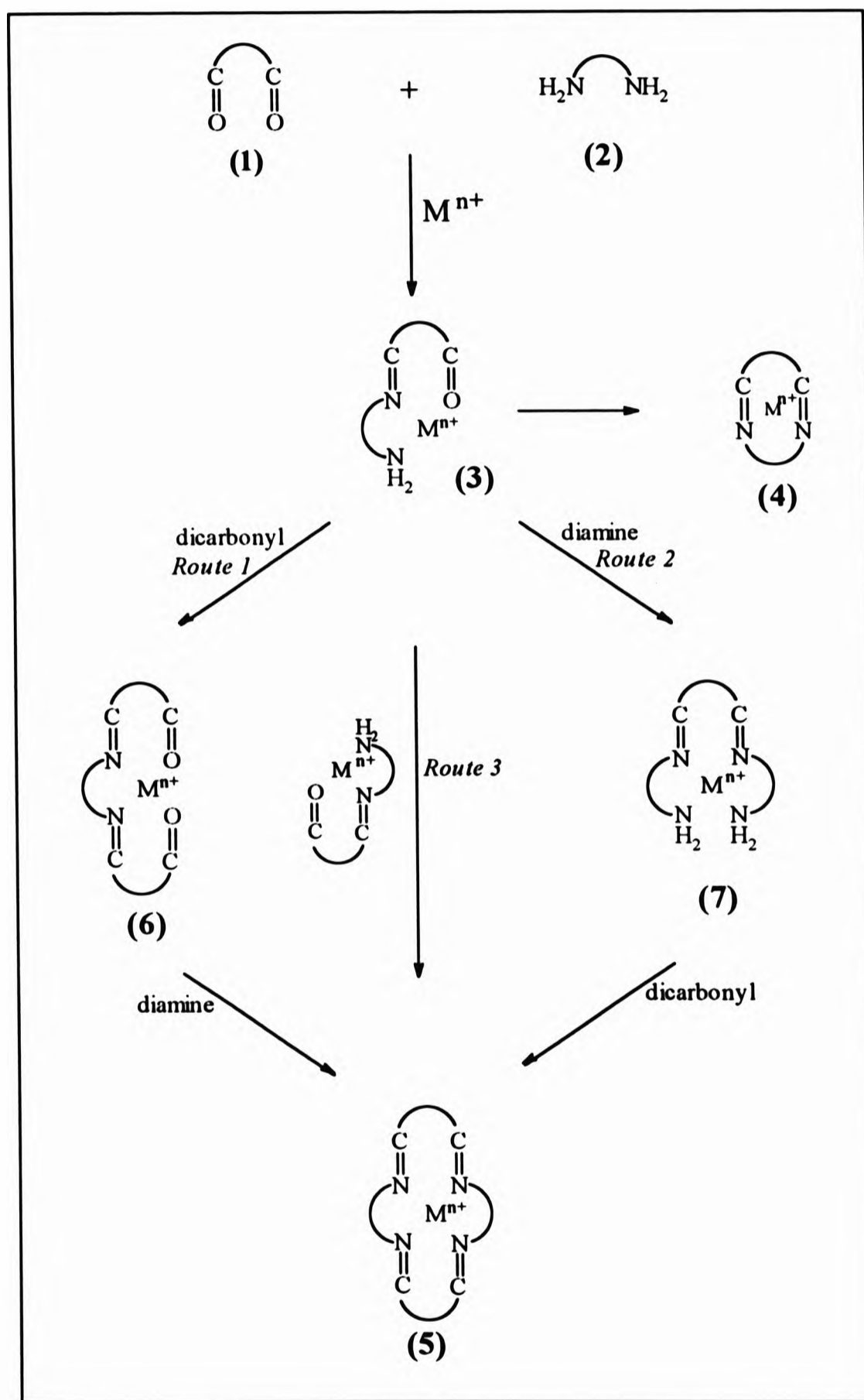


Fig. 1.3 The proposed mechanism of condensation of a diamine and a dicarbonyl (reproduced from ref. 4)

Axial co-ordination of the cation in (3) (Fig. 1.3) favours the [1 + 1] cyclisation (Fig. 1.2b) if the chain is long enough. Once the synthesis of [2+2] cyclisation has been established three routes can be followed from structure (3) leading to the product (5); (3) may react with a dicarbonyl molecule (1) to form the new dicarbonyl (6). Condensation of (6) with one molecule of the diimino-diamino species (7) is formed which on condensation with a molecule of the dicarbonyl (1) yields (5). The third route involves the condensation of two molecules of (3).

1.2.1 Metal Cation Size and the Macrocyclic Ligand Cavity

It is by now well established that the metal cation size plays an important part in the formation of the cavity size of the macrocyclic ligand. This will be illustrated by the reaction of 2,6-diacetylpyridine with 3,6-dioxaoctane-1,8-diamine.

In the absence of a metal cation, the reaction of 2,6-diacetylpyridine and 3,6-dioxaoctane-1,8-diamine gave exclusively oligomers.^[5] The same reaction in the presence of Mg^{2+} , Mn^{2+} , Fe^{2+} , Fe^{3+} , Zn^{2+} or Cd^{2+} led to [1 + 1] condensation and a 15-membered macrocyclic cavity, the cavity being large enough to accommodate these small cations^[6,7] (Fig. 1.4{I}). In the presence of Pb^{2+} or Ag^+ dinuclear complexes of the [2 + 2], 30-membered macrocycles were isolated (Fig. 1.4{III}). In the case where barium(II) or strontium(II) were used as templates an open chain [1 + 2] (Fig. 1.4{II}) complex was isolated, initially complying with structure (7) in Fig. 1.3. On reaction of (7) with one mole equivalent of 2,6-diacetylpyridine, the structure cyclised forming the [2 + 2] product (Fig. 1.4{III}). These observations were repeated when 2,6-diacetylpyridine was replaced by 2,6-pyridinedialdehyde or 2,5-furandialdehyde.

1.2.2 Ring Contraction and Expansion Under Cation Control

Similar to the example above, the reaction of 2,6-diacetylpyridine (1 mol equivalent) and dien (2 mol equivalent) with Ba^{2+} as a template led to the [1 + 2] open chain product {IV}.^[8]

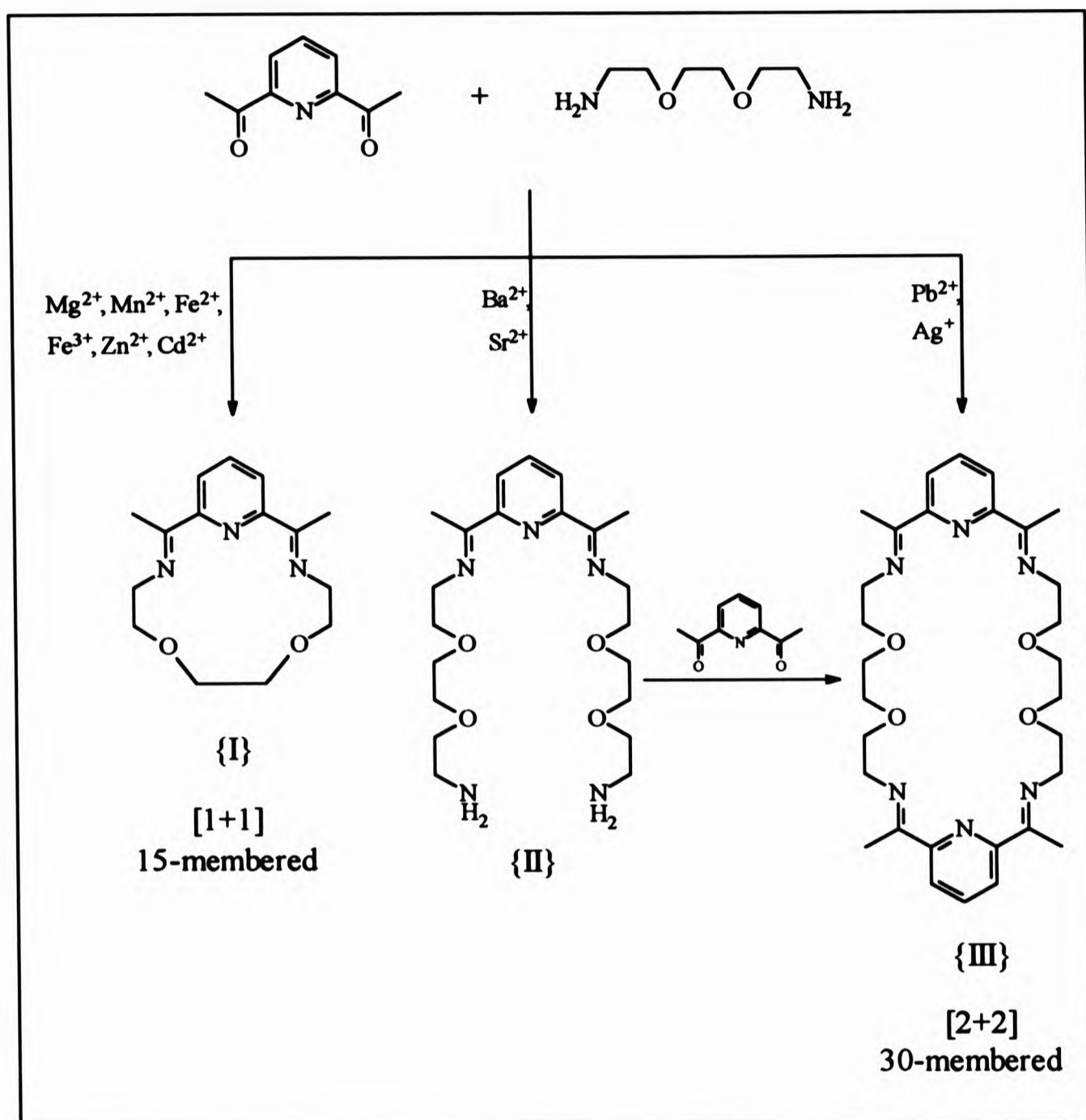
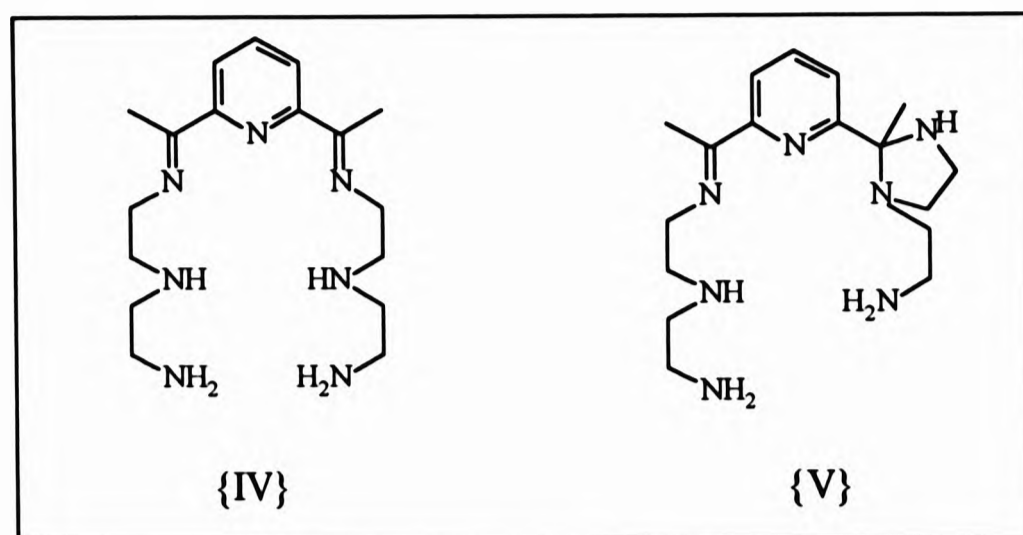


Fig. 1.4. The synthesis of 15- or 30-membered macrocyclic ligands resulting from small and large metal cations respectively

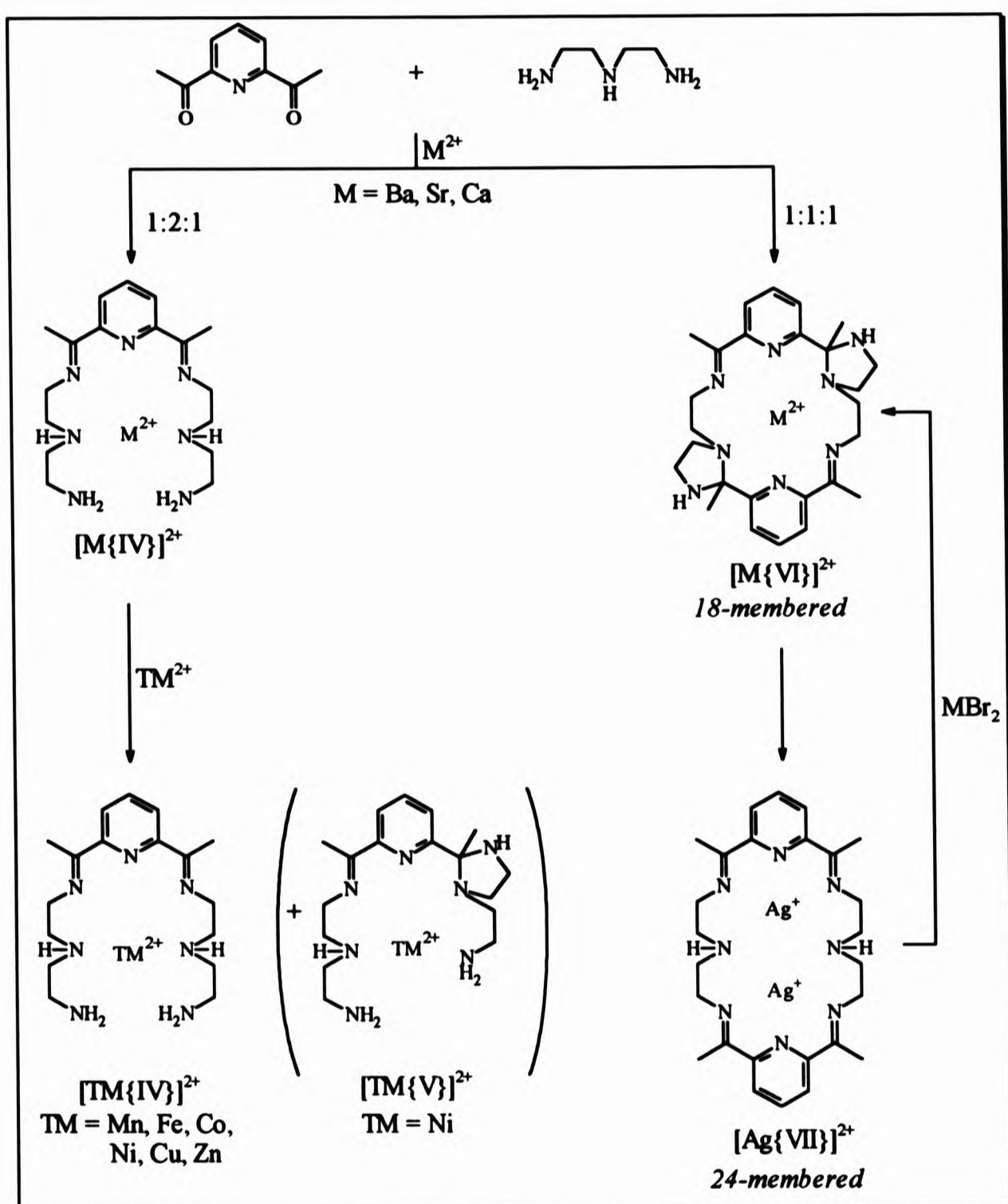
Transmetalation with first row transition metals resulted in the otherwise unobtainable seven co-ordinate complexes^[9] of Mn²⁺, Fe²⁺, Co²⁺, Cu²⁺ or Zn²⁺. Where nickel(II) was concerned, complexes of the heptadentate {IV} and hexadentate {V} were both isolated.^[10]



When the initial reaction was repeated in the molar ratios 1:1:1 (2,6-diacetylpyridine : Ba²⁺ : dien), complexes of the 18-membered macrocycle {VI} (Fig. 1.5) were isolated^[8] as opposed to the 24-membered ring {VII} expected. Treatment of [Sr{VI}(ClO₄)₂] with silver(I) resulted in the binuclear complex [Ag₂{VII}](ClO₄)₂ of the 24-membered macrocyclic ligand. When the latter complex was itself transmetallated with barium(II), [Ba{VI}(ClO₄)₂] was reformed. This process suggests that the macrocycle expands or contracts adopting an arrangement suitable for the metal cation size. The process is summarised in Fig. 1.5.

Similarly, the reaction of 2,6-diacetylpyridine and 1,3-diamino-2-hydroxypropane in the presence of a metal resulted in different ligand orientations depending on the metal template employed (Fig. 1.6). In the presence of barium(II), the mononuclear complex of the [2+2], 20-membered, macrocycle [H₂{VIII}] was formed.^[11] In contrast, in the presence of lead(II) the contracted 18-membered macrocyclic complex of {IX} was formed incorporating two oxazolidine rings. Transmetallation of [Ba{VIII}H₂(ClO₄)₂] with copper(II) yielded the dinuclear mono-deprotonated complex of H{VIII}.^[12] Manganese(II) complexes of {X} were isolated both by the *in-situ* method and by transmetallation of [Ba{VIII}H₂(ClO₄)₂]. With the former method a mixture of [2+2] dimeric and [4+4] condensation products formed.^[13] A trinuclear [3+3] condensation product, {XI}, was obtained when the lanthanide metals were employed as templates in the same reaction.^[14] Fig. 1.6 shows the crystallographic solid state structures of the ligand {VIII} with different metals.

Fig. 1.5 Macrocyclic ring contraction and expansion under metal cation control. (ratios are in the order *dap:dien:M²⁺*)



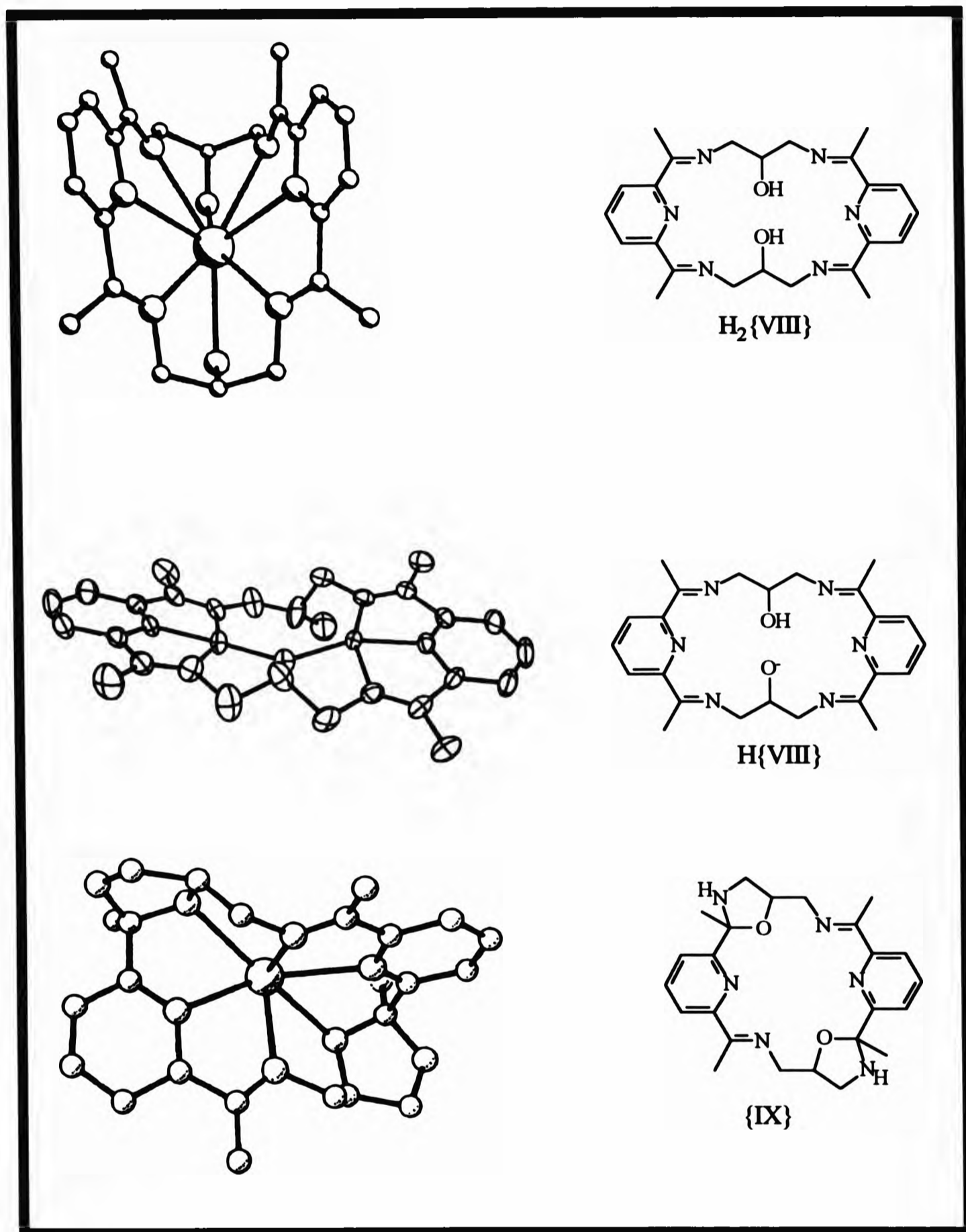
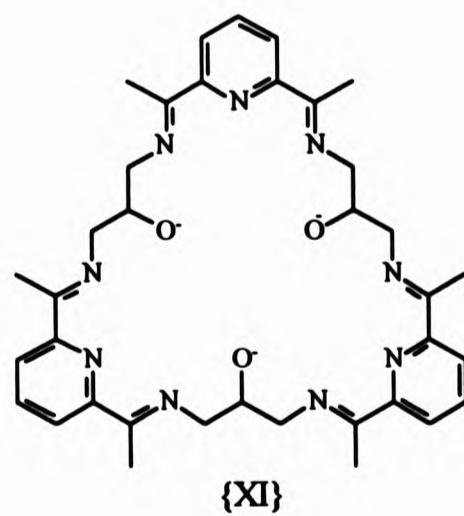
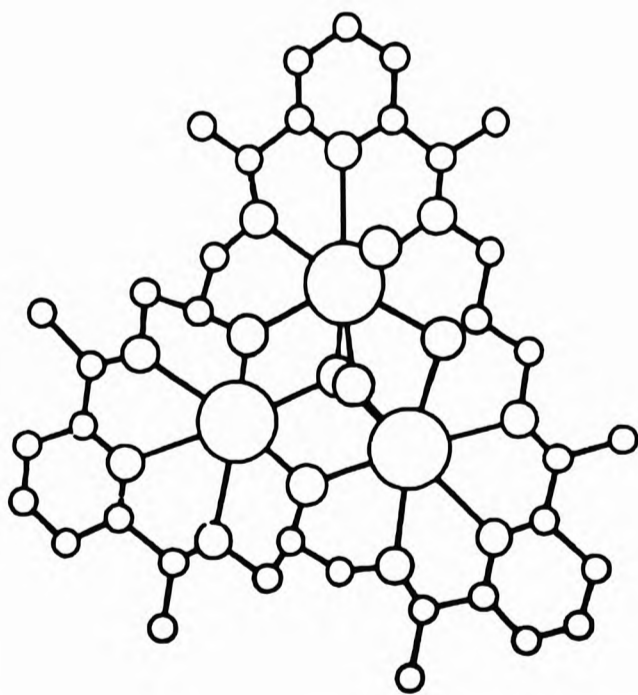
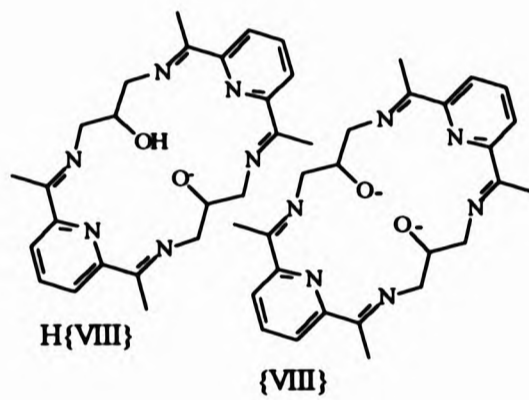
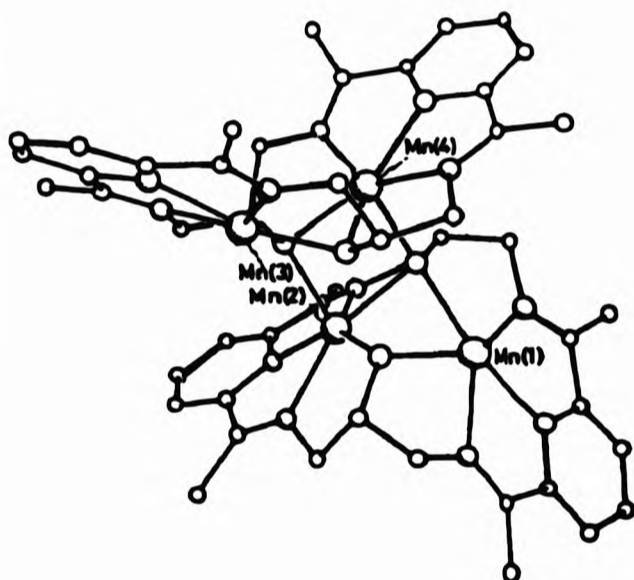
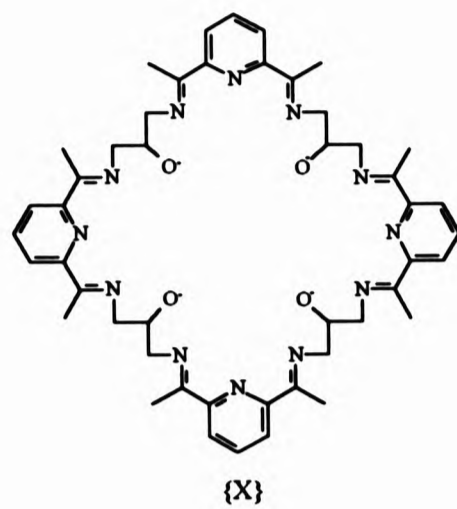
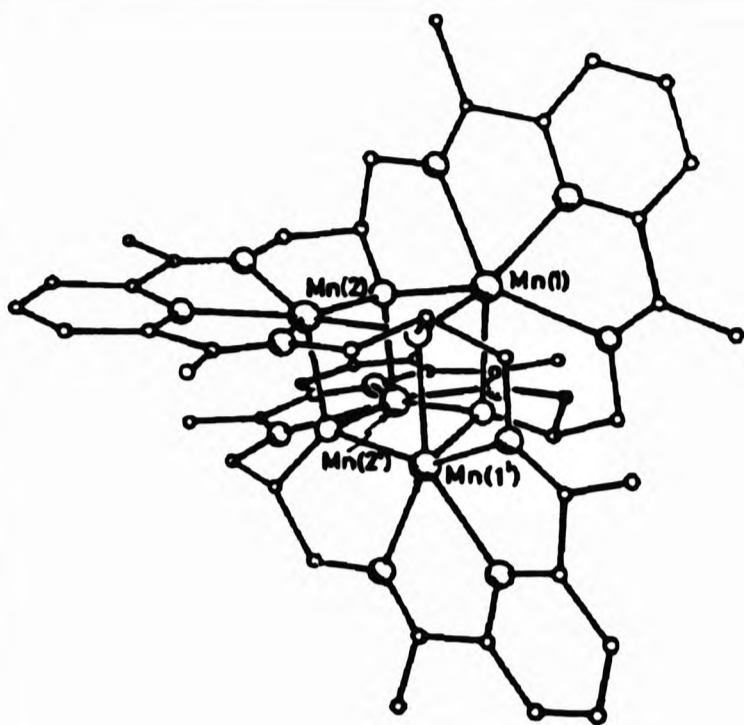


Fig. 1.6a The solid state structures adopted by the ligand $\{VIII\}$ with different metal cations. From top: $[Ba\{VIII\}]^{2+}$, $[Cu_2H\{VIII\}]^{2+}$, $[Pb\{IX\}]^{2+}$. Co-ordinated or unco-ordinated counterions or solvent molecules are omitted for clarity. (reproduced from refs 15, 12 and 15 respectively)

Fig. 1.6b (preceding page) From top: $[Mn_4\{X\}]^{4+}$, $[Mn_4\{VIII\}(H\{VIII\})]^{4+}$, $[La_3\{XI\}]^{3+}$. (reproduced from refs 13, 13, 14 respectively)

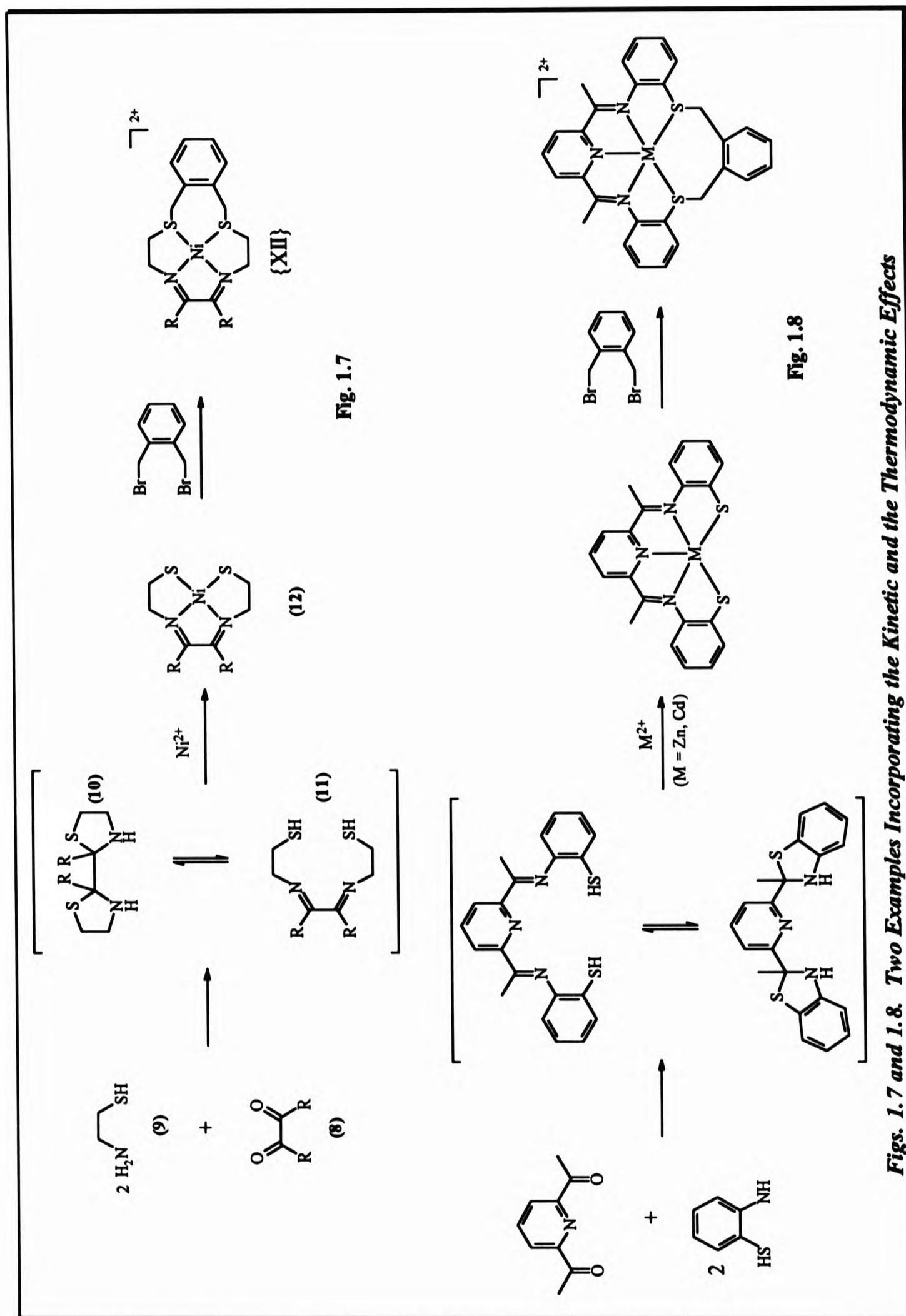


1.2.3 Co-ordination Template Effects

Co-ordination template effects is a term used to collectively describe the effect a metal ion has towards the formation of the final product in a reaction. If the metal ion directs the steric course of a sequence of stepwise reactions, then the process is described as the *kinetic template effect*. Where, in an organic system, the metal ion disturbs an equilibrium to form the required product as its metal complex, the process is known as the *thermodynamic template effect*. An example, whereby both of these co-ordination template effects are employed to obtain the desired product, is in the synthesis of the macrocyclic ligand {XII} (Fig. 1.7).

The reaction of a 1,2-diketone (8) with 2-aminoethanethiol (9) resulted in a thiazoline (10).^[16] In solution the thiazoline exists in equilibrium with the desired Schiff base compound (11). In the presence of nickel(II), since (11) is better suited for chelation, it is sequestered from the equilibrium and isolated in high yield as the nickel(II) complex, (12),^[17] this being an example of the thermodynamic template effect.

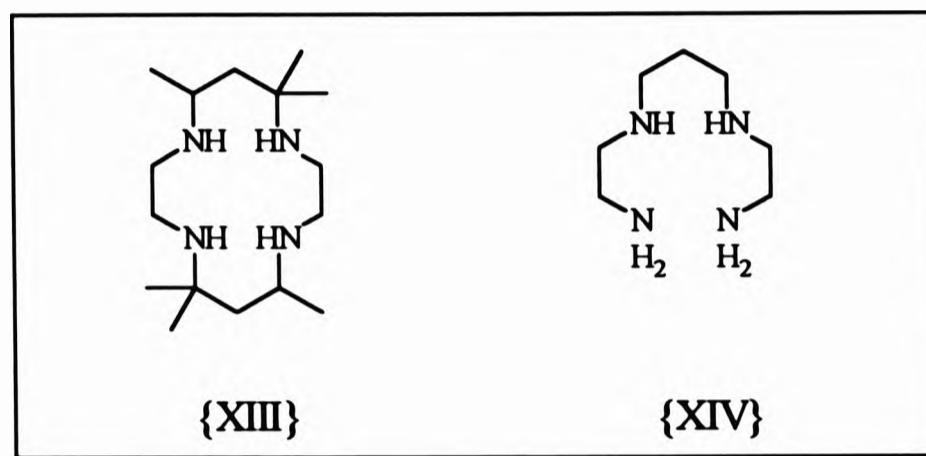
Reaction of (12) with benzyl bromide afforded the required macrocyclic ligand {XII} as its nickel(II) complex and this was achieved as a result of the kinetic template effect where the metal ion was used to sterically control the geometry of the thiol groups for the chemically selective cyclisation (Fig. 1.7). Fig. 1.8 shows another example of the co-ordination template effects.^[18]



Figs. 1.7 and 1.8. Two Examples Incorporating the Kinetic and the Thermodynamic Effects

1.2.3.1 The Macrocyclic Effect

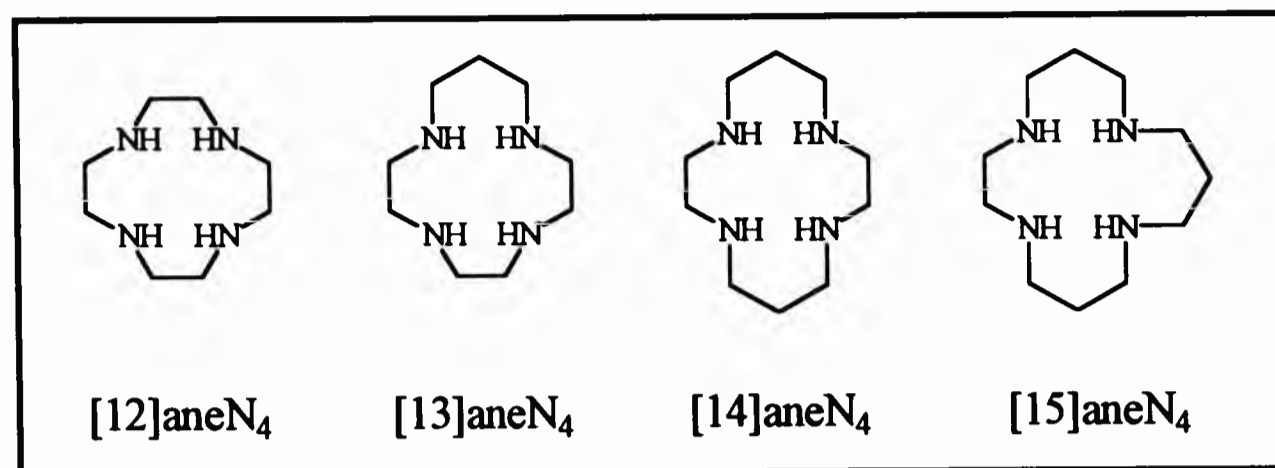
It is apparent from the chelate effect that complex stability increases as the number of chelate rings increases. The macrocyclic effect was pioneered when the stability constant of the copper(II) complex of the macrocyclic ligand {XIII} was discovered to be approximately 10^4 times higher than the copper(II) complex of the open-chain analogue {XIV}.^[19] This marked increase in stability was greater than expected from an additional chelate ring.



Initially, the extra stability was credited, by Kodama and Kimura, to entropy factors^[20,21] and, by Hinz and Margerum, to enthalpy factors.^[22,23] Prior to this, the macrocyclic effect was described as being the combination of both the restrained configuration, resulting from entropic effects, and the diminished solvation, an enthalpy effect, of the free macrocyclic ligand compared to the non-cyclic ligand.^[19] Overall, the effect is considered to represent Gibbs free energy (ΔG°) for the metathetical reaction:



where L represents the macrocycle and L' the non-cyclic analogue. It has, by now, been accepted that the dependence of the macrocyclic effect on enthalpy may vary from ligand to ligand and extensive studies on nitrogen donor ligands have shown that the entropy term is more favourable.



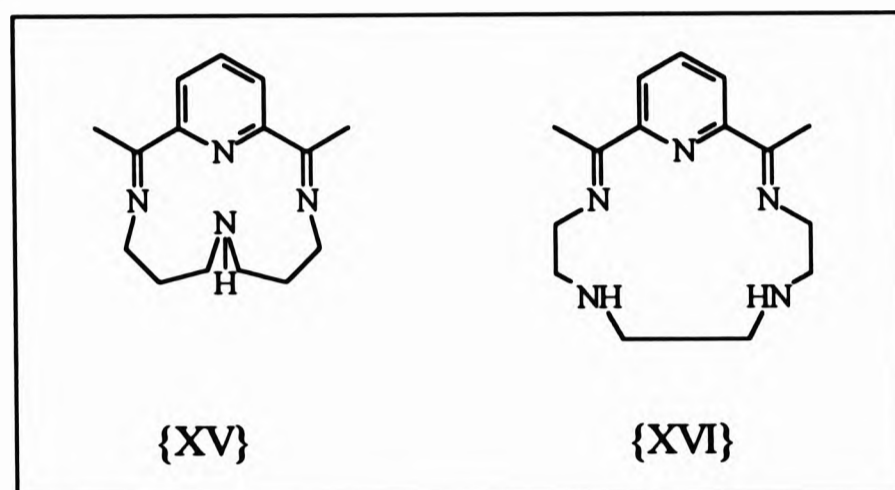
Another factor which contributes to the enhanced stability in macrocyclic complexes is the match of the metal ion size to the macrocyclic cavity size. Fabbrizzi, Paoletti and Clay^[24] showed, with a series of copper(II) complexes with macrocyclic ligands of different ring sizes, [12]aneN₄, [13]aneN₄, [14]aneN₄ and [15]aneN₄, that the enthalpy of the macrocyclic complex reaches a maximum at {Cu[14]aneN₄}²⁺. This was attributed to the planar arrangement of the metal ion and the four nitrogen atoms in the complex resulting in a close metal ion-cavity size match and hence minimum conformational strain. Busch discovered that there is an ideal ring size for any metal ion having a given metal-donor atom distance and that ring sizes slightly smaller than the best fit ring show abnormally strong metal-donor bonds while rings that are slightly oversized show substantially decreased metal-donor interactions.^[25]

The implication is that acyclic ligands require more energy in rearranging from the planar conformation, in the non-complexed form, to the non-planar arrangement on co-ordination where the donor atoms need to be positioned around the metal ion and the ligand will therefore experience steric resistance in the process. In contrast, the macrocyclic ligand, having its donor atoms synthetically pre-positioned for chelation, will undergo less geometrical change than the acyclic analogue and exert the strongest and most effective metal-to-donor interactions assuming a *perfect* metal-to-cavity size match. Hence there will be less disorder in the case of the macrocyclic ligand resulting in a more favourable configurational entropy contribution to the overall thermodynamic stability.^[26]

To conclude, the overall effect is of both enthalpic and entropic origin, the relative importance of these two contributions varying from case to case.^[27]

1.3 A General Overview of the 18-membered Macrocyclic Ligands and their Metal Complexes

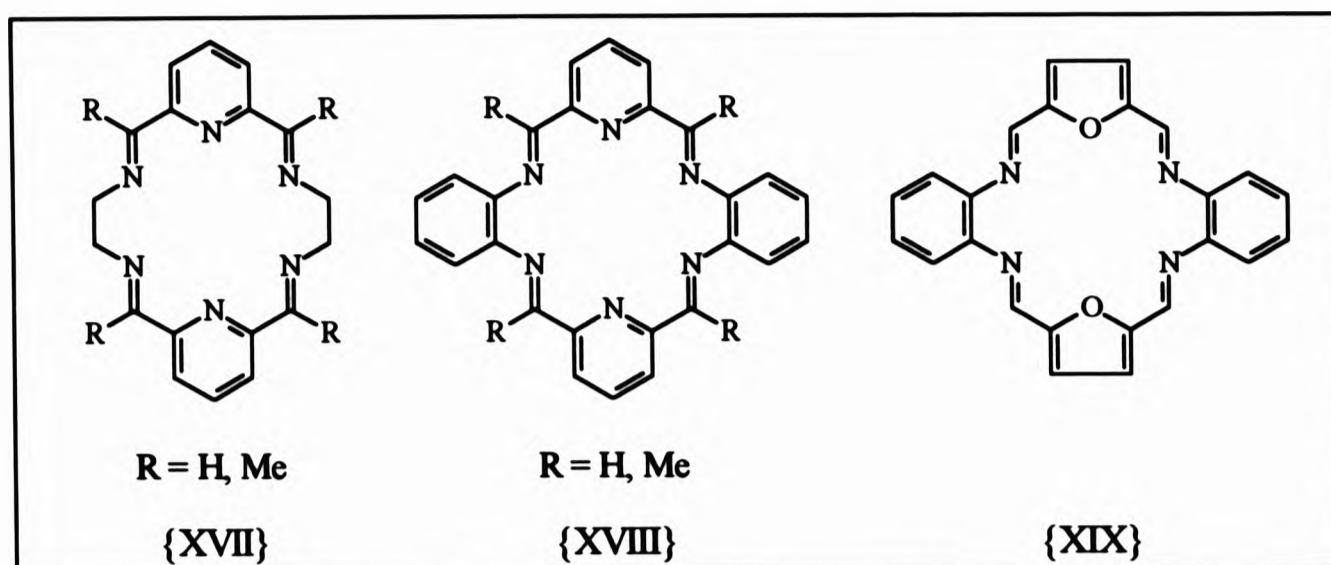
Busch and Curry^[28] were among the first to demonstrate the reaction of 2,6-diacetylpyridine with certain polyamines in the presence of metal ions (Mn^{2+} , Fe^{3+} , Co^{2+} , Ni^{2+} , Cu^{2+}) led to the [1+1] macrocycles of the type {XV}^[29,30] and {XVI}.^[31,32]



The presence of the pyridine group between the two carbonyl functions in 2,6-diacetylpyridine assures the initial tridentate chelation of the reactants and the activation of the co-ordinated carbonyl groups towards the reaction with a free amine group of an amino ligand that is chelated within the same co-ordination sphere. The presence of the metal does not alter the Schiff condensation mechanism although it may control the reactivity of the amine, the carbonyl or the resulting imine as well as the conformation of the product.^[33] Nelson *et al.* investigated the systems of 14 - 17-membered [1+1] macrocycles very thoroughly.^[34]

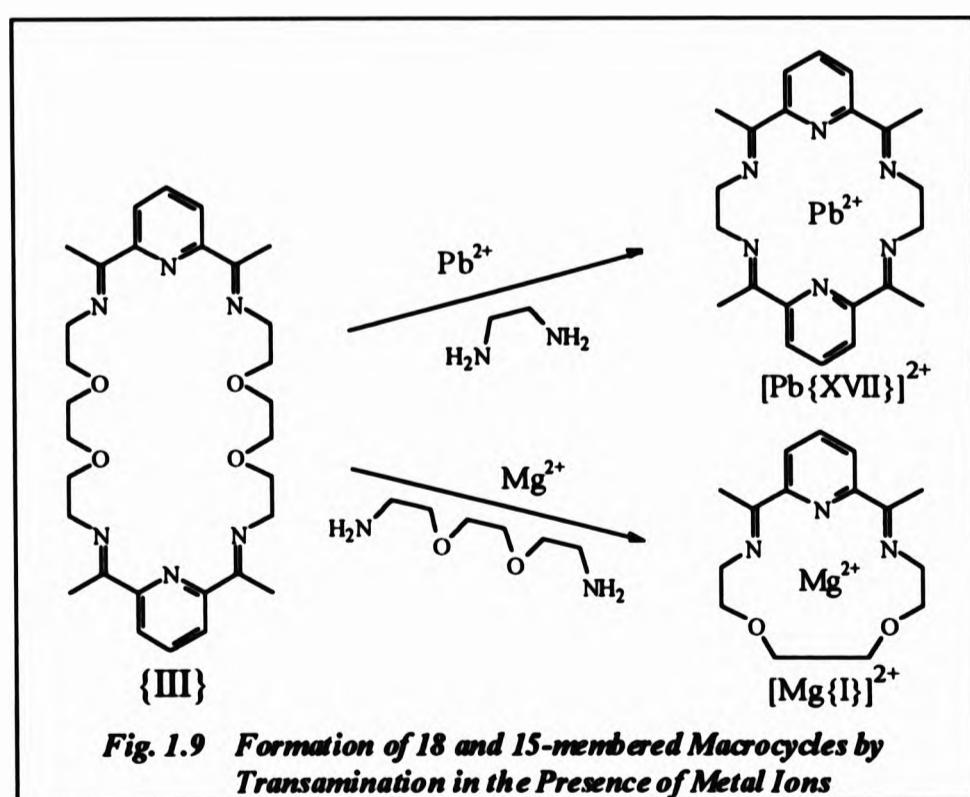
Reaction of 2,6-pyridinedicarbonyl with 1,2-diamines such as 1,2-diaminoethane or 1,2-diaminobenzene in the presence of first row transition metals does not yield any macrocyclic products as the amine is not lengthy enough to span the two carbonyl functionalities. The use of much larger metals ions, in particular the divalent alkali earths (except magnesium) and also lead(II) in the *in-situ* procedure yielded the [2+2], 18-membered macrocycles {XVII} - {XIX}.^[34-37]

Lanthanide metals, having similar ionic radii to the alkali earth metals, Ca^{2+} , Ba^{2+} ,

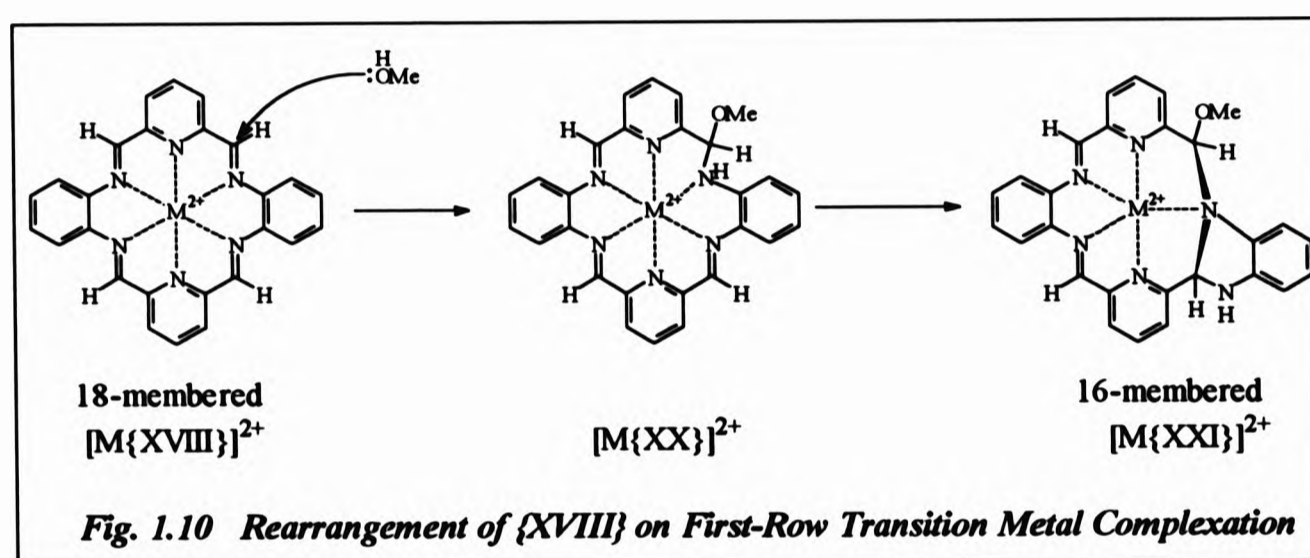


and Sr^{2+} , also facilitate such [2+2] condensation, of which the chemistry of these metal complexes with macrocyclic ligands has been extensively studied by many researchers (See Chapter 2). The discussion which follows is based on the reaction of 2,6-pyridinedialdehyde or 2,6-diacetylpyridine with 1,2-diaminoethane or 1,2-diaminobenzene and will be kept minimal as more insight into this field will be given as necessary in the subsequent Chapters.

An indirect route to the synthesis of {XVII} ($R = Me$) is *via* the transamination reaction of $[Pb\{III\}]^{2+}$ with 1,2-diaminoethane.^[38] Similar treatment with 3,6-dioxaoctane-1,8-diamine in the presence of Mg^{2+} yields $[Mg\{I\}]^{2+}$ (Fig.1.9).



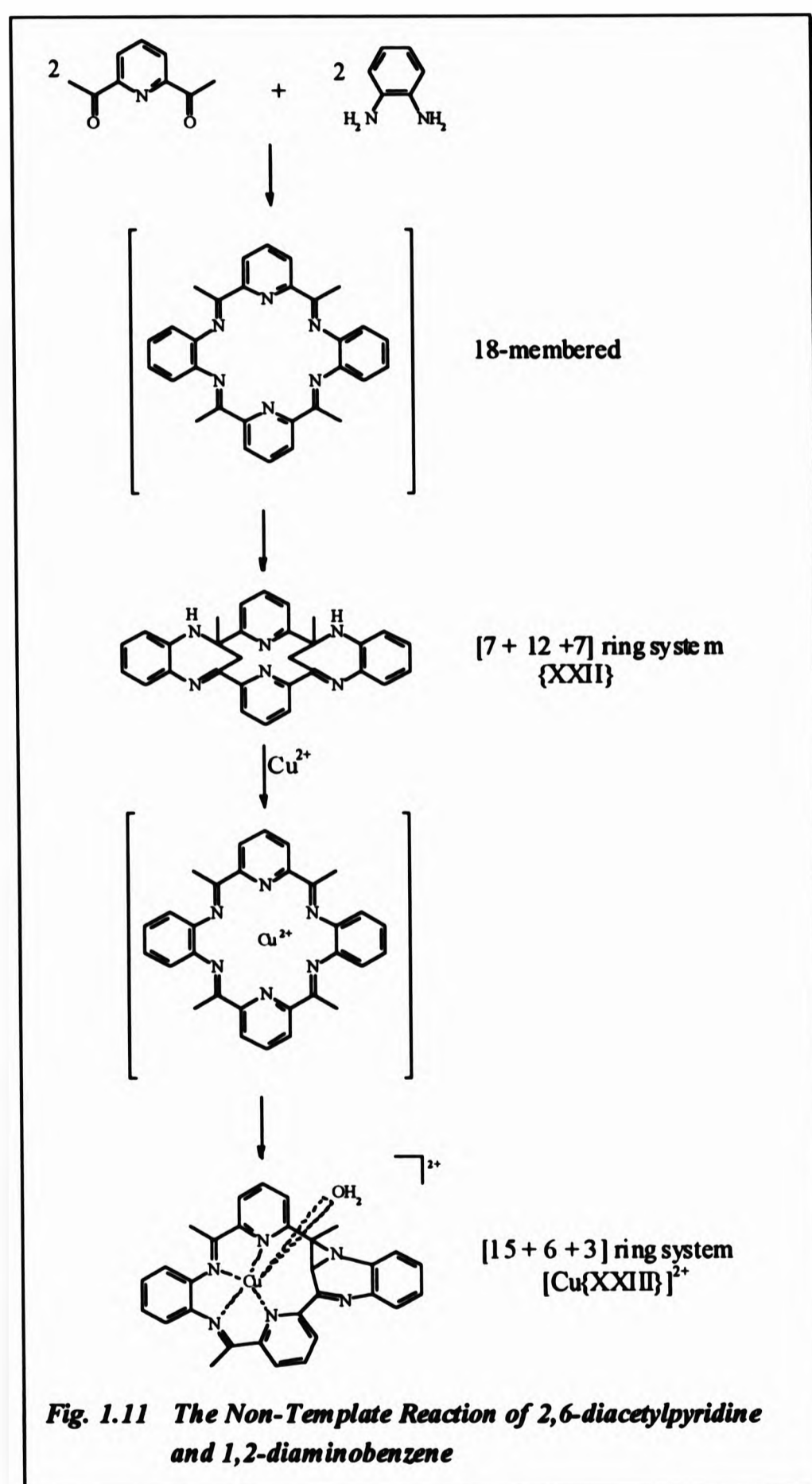
The macrocyclic cavity of {XVIII} is too large to accommodate first row transition metals. On complexation of the free ligand (R = H) or by transmetalation of its barium(II) complex, $[\text{Ba}\{\text{XVIII}\}_2]^{2+}$, the new metal would be lost unless the macrocycle was to undergo chemical transformation to form a close metal-ligand fitting. This is impossible due to the macrocycle being rigidly planar. Yet, stable, non-labile, complexes of the first row transition metals are formed as a result of metal-initiated nucleophilic addition at the imine groups,^[33] the complexation reaction in methanolic solution results in the attack of methanol on one of the imine bonds on the initially formed complex, $[\text{M}\{\text{XVIII}\}]^{2+}$ (M = Mn, Fe, Co, Zn) forming $[\text{M}\{\text{XX}\}]^{2+}$ (Fig. 1.10).



Although the reduction of the imine bond causes the macrocycle to pucker and reduce the hole-size, the cavity is still too large to accommodate these metals so the ligand intramolecularly rearranges further to reduce the hole-size even more, resulting in a 16-membered macrocycle with the formation of a benzimidazole ring outside the cavity. These rearrangements have been crystallographically proved.^[35,36]

Similar rearrangements occur when 2,6-diacetylpyridine is employed for the non-template synthesis of {XVIII} (R = Me) as shown in Fig. 1.11. Steric hinderance between the methyl groups and the hydrogen atoms on the phenylene rings prompt the synthesis of {XXII} incorporating the [7 + 12 + 7] ring system.^[39] On complexation with copper(II) the structure rearranges back to the 18-membered

macrocycle but as copper has a small ionic radius compared to the macrocyclic cavity the ligand again rearranges itself to a [15 + 6 + 3] ring system, {XXIII}, the larger ring snugly accommodating the metal .^[40]



1.4 The Lanthanide Metals

The lanthanide metals originally earned the historical name of *rare earths* to describe the elements lanthanum to lutetium which could not be separated from each other as they closely resemble themselves chemically and physically; they are by no means rare. IUPAC nomenclature outlines three classifications; *lanthanides* for the elements cerium to lutetium ($Z = 58 - 71$), *lanthanoids* for lanthanum to lutetium ($Z = 57 - 71$) and *rare earths* for scandium, yttrium and the series lanthanum to lutetium, the latter category representing group 3 of the Periodic Table. The discussion which follows will refer to yttrium and the series lanthanum to lutetium where the term *lanthanides* and the symbol Ln will be used loosely in this thesis to refer to these metals.

The chemical similarity of the lanthanide metals served them little consideration until very recently where their importance in the optical industry and as NMR shift reagents^[41-43] attracted vast attention and opened a gateway to extensive research and the discovery of many applications. Their use in industrial catalysts, electronic and optical components, high temperature superconductors, X-ray intensifying materials, relaxation agents for imaging techniques (§ 1.5), or radioisotopes for pharmaceutical applications are just a few examples of lanthanide metal uses and importance.

1.4.1 The Lanthanide Contraction

The electronic configuration of the lanthanide metals involves the progressive filling of the 4f electron shell from $[\text{Xe}]4f^0$ (La) to $[\text{Xe}]4f^4$ (Lu). Resulting from poor shielding of the 4f inner electrons, a reduction in size is experienced in atoms and ions, across the lanthanide series, with increasing atomic number. The lanthanide contraction is caused by the electrostatic effect increasing the nuclear charge experienced by each additional 4f inner electron resulting in shrinkage in the size of the entire 4f shell.^[44]

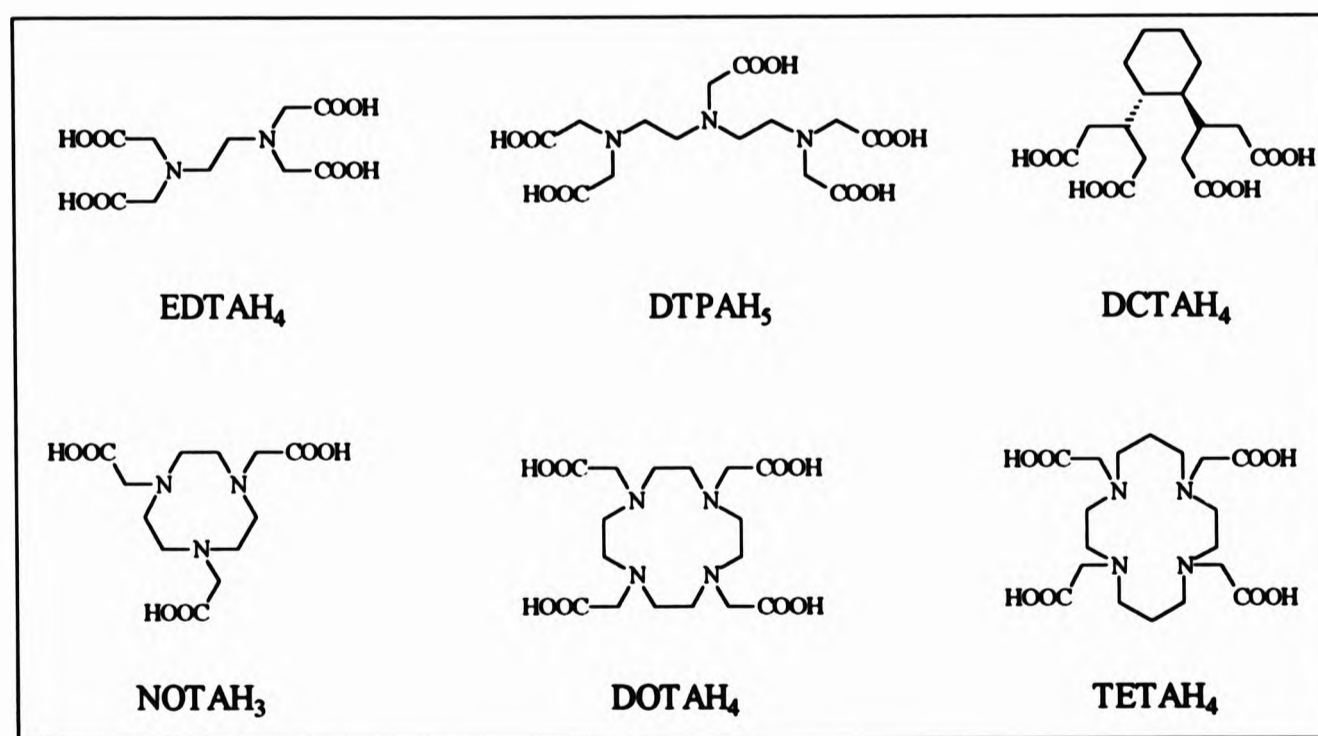
1.4.2 Co-ordination Chemistry

Since the 4f electrons are generally uninvolved in metal-ligand bonding, the lanthanide metals have a major oxidation state of +3. Behaving as hard acids, these elements form stable complexes with highly electronegative hard bases containing fluoride, oxygen and nitrogen donor atoms, in the order $F > O > N$.^[45] Oxygen donor ligands have been studied most extensively.^[46]

The absence of interactions between the ligand and the 4f orbitals is supported by observations that chelating agents have only a small effect upon the magnetic moments of the trivalent ions and upon the positions of their sharply defined, characteristic absorption bands in the UV-VIS region. The lack of ligand field stabilisation effects (LFSE) reduces the overall stability of lanthanide complexes but provides greater flexibility in geometry and co-ordination number which are restricted in transition metals by the requirement of metal-ligand orbital overlap.^[47]

1.4.3 Chelates of Lanthanide Metals

As discussed above the most stable and common lanthanide chelates are those incorporating oxygen donor atoms, in particular polyaminopolycarboxylic acid anions,^[47] EDTA⁴⁻, DTPA⁵⁻, DCTA⁴⁻.



Due to the weak basicity of the carboxylate groups in these compounds, the high stability of lanthanide chelates is owed to the chelation of the nitrogen donor atoms which, in their non-chelation, would lead to unsuitable and unstable chelate ring sizes.^[48]

Even more stable are the lanthanide complexes of the macrocyclic polyazapolycarboxylic acids, *e.g.* DOTAH₄, TETAH₄ and NOTAH₃. The high stability of these macrocyclic ligands with lanthanide metals depends on acid pKa values of the carboxylate groups, the basicity of the nitrogen donor atoms in the macrocyclic ring and the size and rigidity of the ring itself. The latter two factors also contribute to the slow dissociation kinetics as they cause shielding of the metal ion from water attack as it is well known that hydration generally causes decomplexation in macrocyclic complexes. The stabilities of the lanthanide complexes with NOTAH₃, DOTAH₄ and TETAH₄ were found to have a stability relative to EDTAH₄ of:^[49,50]



Because of high stability and kinetic inertness the lanthanide (in particular Gd³⁺ and Dy³⁺) complexes of such aminocarboxylate ligands have been considered as potential *in vivo* MRI contrast agents.

1.5 Magnetic Resonance Imaging (MRI)

Prior to prescribing the appropriate therapy for a tumour, the type of tumour and its precise location need to be identified and diagnosed.

The development of MRI, as a NMR technique, for imaging the human body and its introduction as a diagnostic imaging technique in the early 1980s has led to a breakthrough in medicine.^[51] MRI is generally more expensive than any other imaging technique and much slower than X-ray computerised tomography (CT) to perform. As a non-invasive method, which does not use ionising radiation, such as

X-rays, γ -rays or positrons, MRI (or more appropriately, NMRI), has no known hazards, which compensates for the above disadvantages.

As well as the physiological and medicinal use of MRI, there is a wide scope of applications in particular the determination of water-content in cooked food without causing its destruction and the monitoring of water content in old manuscripts and books. A biological application is the examination of oil content in seeds such as corn which has led to new and high-yielding varieties.^[52] Analytical applications range from structure determination and solvent diffusion of polymers and composites to solvent mobility in inorganic materials such as ceramics.^[53]

1.5.1 The Technique of NMR Imaging as a Diagnostic Tool

MRI is a tomographic technique yielding three-dimensional images in the form of slices of tissue. Imaging used in diagnostic medicine is similar to spectroscopy in chemistry. The important differences are the addition of gradient coils, a sample specific receiver coil and software for imaging purposes. Although other nuclei, ^7Li ,^[54] ^{13}C ,^[55] ^{19}F ,^[56] ^{23}Na ^[57] and ^{31}P ^[58] have been used for *in vivo* NMR experiments, to date imaging is restricted to protons, specifically water protons. There are two main reasons for the proton's universal popularity; hydrogen is the most abundant element in the body (98.98% of hydrogen exists as the ^1H isotope) and is present mostly in water or lipids. It is also the most sensitive NMR nucleus (except for tritium, ^3H).

The whole basis of the technique is to provide a contrast (difference in intensities) between normal and pathological tissues. The signal intensity from a particular tissue or the contrast between two tissues is dependent on the relative rôle played by various factors (Fig. 1.12). The factors responsible are proton density, spin-lattice (T_1) and spin-spin (T_2) relaxation times, motion or flow, gradient coils and the NMR pulse sequence.

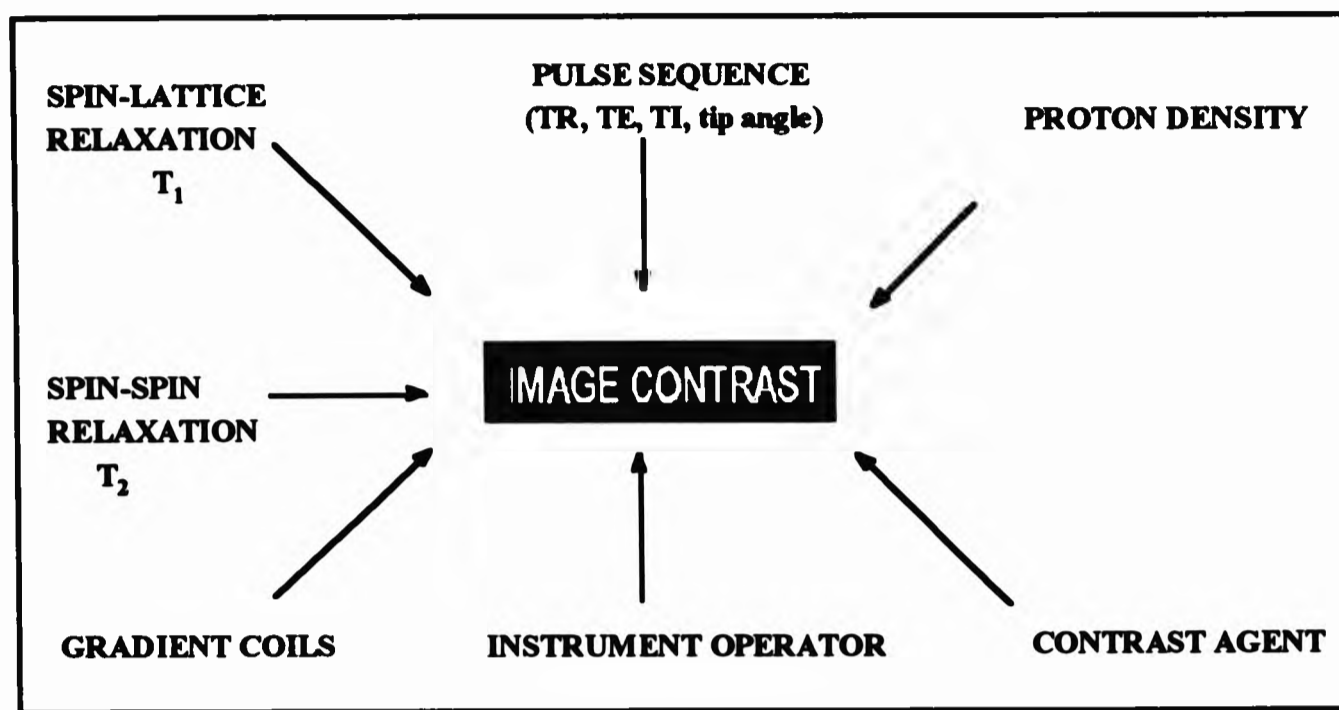


Fig. 1.12 The dependence of image contrast on various parameters

The T_1 and T_2 relaxation times, proton density and signal void caused by flowing blood are responsible, primarily, for providing the differentiation or contrast between normal and pathological tissue in spin-echo imaging. Through appropriate selection of several operator parameters an image may be obtained that will provide a weighting to represent either the T_1 or T_2 relaxation times or the proton density of the tissue under investigation. These pulse sequence parameters include the pulse repetition time (TR), the echo delay time (TE), the inversion delay time (TI) in inversion recovery imaging or the tip/ flip angle in fast scanning techniques.

Spatial information is obtained by making the resonance frequencies position dependent. Gradient coils create an opposing field to the applied field at each of thousand of points in a fixed volume of tissue.^[57] The water protons then resonate at slightly different frequencies at each point, spatially encoding the signals and a computer decodes these signals to produce a digitised image.

Prior to continuing, it is appropriate at this stage to review the NMR relaxation processes.

1.5.2 Relaxation Processes in NMR Spectroscopy

Relaxation of magnetic resonance signals generally results from the presence of local fluctuating magnetic fields. Spin relaxation, in general, is caused by the exchange of energy between one spin and another and between spins and their surroundings. These interactions give rise to two types of decay of M (the magnetisation) and are classified as *spin-lattice* (or T_1) and *spin-spin* (or T_2) relaxations. The result of relaxation is that the magnetisation vector (M_z) returns to its equilibrium state parallel to the magnetic field (B_0) (Figs. 1.13 and 1.14). This takes place when the radiofrequency has been stopped, *i.e.* at the end of the pulse.^[58,59]

1.5.2.1 Spin-lattice Relaxation

Spin-lattice relaxation causes the precessing magnetic moments to re-align gradually with B_0 . Thus the component of M parallel to B_0 (the longitudinal component) decays towards its equilibrium value of M , in a time characterised by the spin-lattice or longitudinal relaxation time, T_1 (Fig. 1.13). The term spin-lattice is derived since the energy is transferred to the surroundings of the nucleus.

1.5.2.2 Spin-spin Relaxation

This type of relaxation is caused by interactions between nuclear magnetic moments. The instantaneous magnetic field experienced by any nucleus is dominated by the externally-applied field, B_0 . However, there is also a contribution to the local field from any other nucleus in the vicinity. This dipole-dipole interaction causes the precession rates of individual nuclei to vary slightly. The result is that they lose phase coherence, so that the transverse component of M (perpendicular to B_0) is steadily reduced to zero. The time constant of the decay of M_{xy} is given by the spin-spin or transverse relaxation time, T_2 (Fig. 1.14).

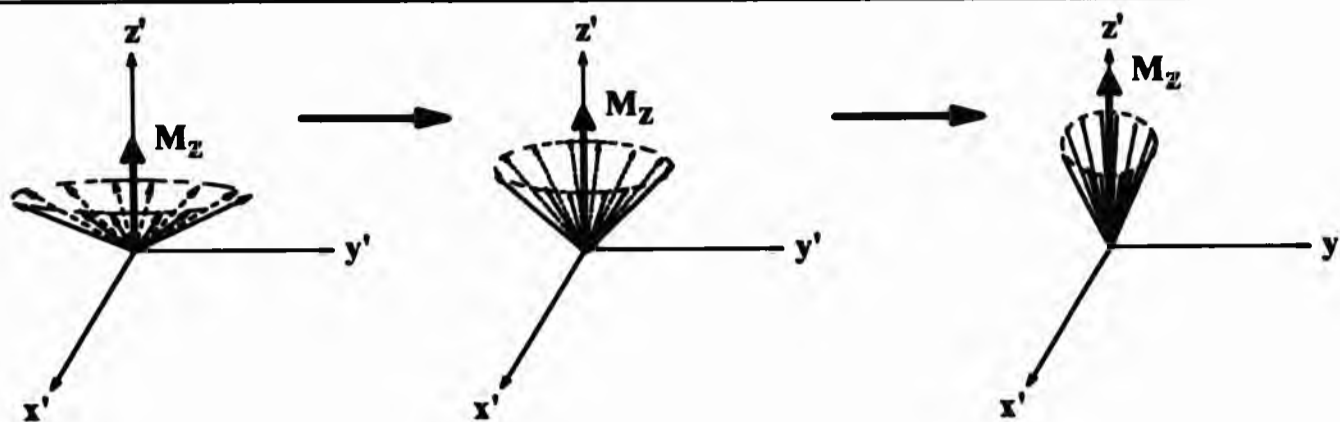


Fig. 1.13 Spin-Lattice Relaxation Causes the Longitudinal Component of the Magnetisation Vector to Return to its Equilibrium Value of M_0 with a Time Constant T_1

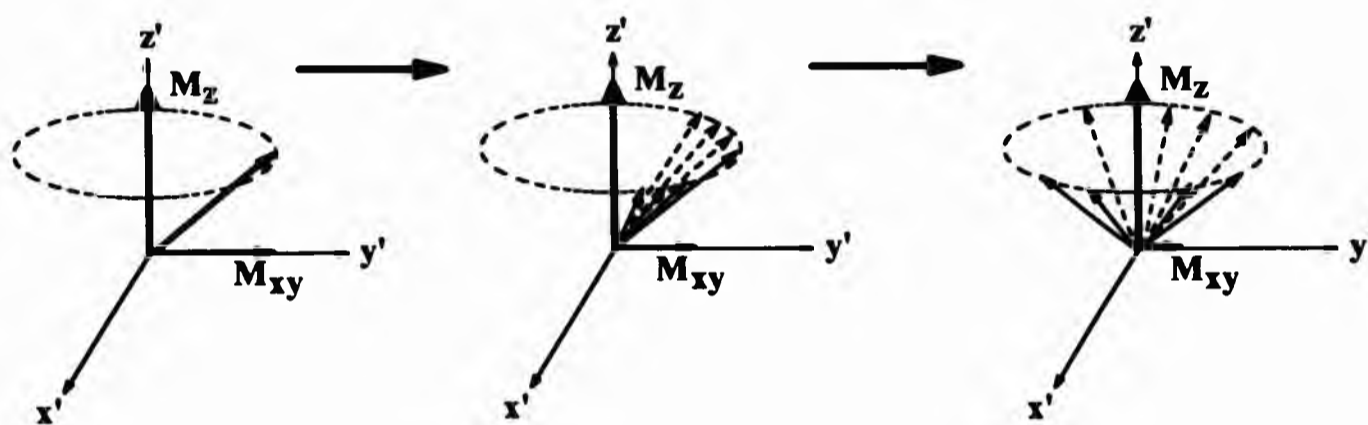


Fig. 1.14 Spin-Spin Relaxation Causes the Nuclear Magnetic Moments to Precess at Slightly Different Rates at any Instant. The Resulting Loss of Phase Coherence Causes an Exponential Decay of the Transverse Magnetisation with a Time Constant T_2

(reproduced from ref. 60)

1.5.3 Applying the Mechanism of Relaxation to MRI

The T_1 and T_2 relaxation processes of an excited proton may be considered as being secondary to the random magnetic and electric fields generated from the magnetic moments of other protons and unpaired electrons in the vicinity. The interaction of an excited proton undergoing relaxation with a nearby magnetic field of a proton in the molecular environment is known as a *dipole-dipole interaction*. Dipole-dipole interactions may be intramolecular or intermolecular, occurring between protons in

the same molecule or two different molecules respectively.^[61] The magnitude of the field experienced by the neighbouring proton fluctuates randomly thus producing relaxation. The relaxation times, T_1 and T_2 , are dependent not only on the magnitude of these fields but also on the time scale of the fluctuations. In fact, T_1 and T_2 depend in different ways on the time scale (expressed in terms of the correlation time, τ_c) and this causes the differences between T_1 and T_2 under conditions where the average mobility of water is reduced, as it is in tissues.^[62]

Relaxation times may also be influenced by *scalar (through bonds) interactions* of a nearby unpaired electron with a proton. This requires the unpaired electron and the proton nucleus to come within finite distance of each other.

The image intensity, therefore, is dependent on the nuclear relaxation times of protons as they exist in various tissues. Damadian stated that cancerous tissue has substantially longer proton relaxation times than in corresponding normal tissue as a result of an increase in motional freedom of tissue water, this in itself suggesting a decrease in the degree of ordering of intracellular water molecules.^[63]

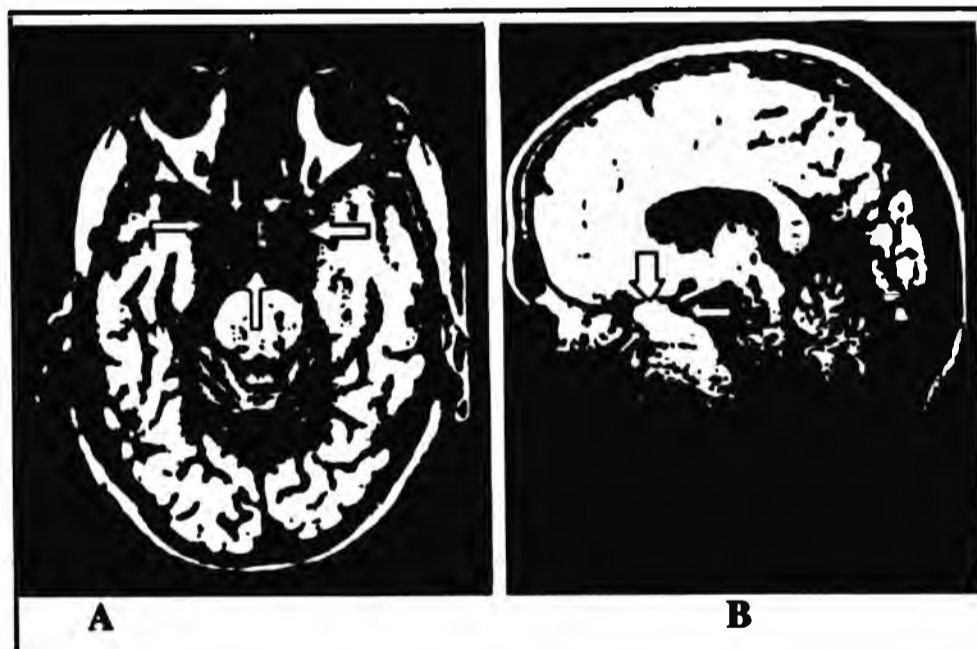


Fig. 1.15 Pituitary tumour (arrows) (A) T_1 weighted and (B) T_2 weighted. (reproduced from ref. 64)

Consequently, tissues with short T_1 values generally yield greater image intensity than those with longer values since the steady-state magnetisation along the z-axis is greater in the tissue with the shortest relaxation time. Conversely, short T_2 values are associated with lower signal intensity as these diminish the net transverse magnetisation available for detection. Fig. 1.15 shows images through the brain depicting the pituitary tumour,^[64] where a T_2 weighted image (B) results in better tissue contrast than the T_1 weighted image (A).

Paramagnetic ions have magnetic dipole moments that are of the order 1000 times as large as that of protons. These large magnetic moments produce correspondingly large local fields and can therefore enhance or shorten the relaxation rates of the water protons that are in the proximity of the ions. The closest protons are those of the water molecules that co-ordinate to the paramagnetic ion in aqueous solution. The relaxation of these bound water protons is actually communicated to the free water. That paramagnetic species can alter signal intensity has resulted in their development as contrast agents for MRI.

1.5.4. The Development of Contrast Agents

The development of MRI as a clinical diagnostic modality has prompted the need and discovery of a new class of pharmaceuticals, the contrast agents.^[65] The need arose when it was revealed that the distinction between tumour and oedema was better with enhanced CT than with unenhanced MRI.^[66] The drug would be administered to a patient in order to enhance the image contrast (Fig. 1.16). This renders the MRI technique as invasive.

There are currently three types of medical imaging where contrast agents are used in diagnosis, namely, X-ray imaging,^[67] nuclear imaging,^[68,69] and MRI.^[70] Paramagnetic contrast agents for the use in the latter technique will be the major issue for discussion.

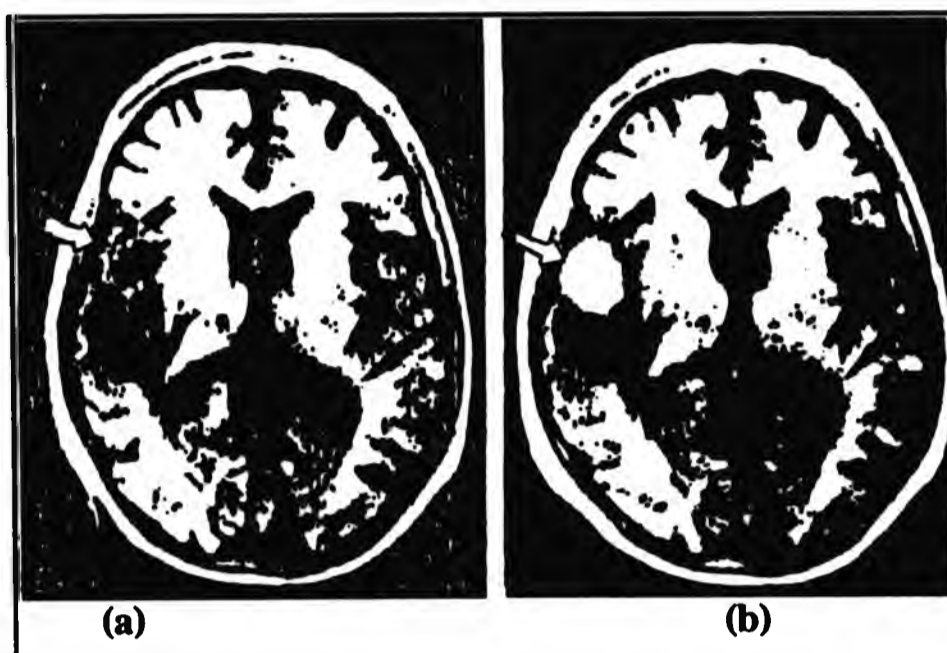


Fig. 1.16 *Metastatic lesion from the brain (a) before and (b) after the administration of a contrast agent, $[Gd(DTPA)H_2O]^+$. The lesion is highlighted with strong signal in (b). (reproduced from ref. 64)*

1.5.4.1 Mode of Action of Contrast Agents

The relaxation times of water protons are decreased dramatically by a factor of about 10^6 when the oxygen atom of the water molecule is co-ordinated to a highly paramagnetic metal ion such as gadolinium(III). It should be noted that with enhanced MR images it is the effect of the contrast agent on the water protons that is detected not the agent itself.

In contrast to the dipole-dipole and scalar relaxation processes in unenhanced MRI, the proton relaxation enhancement induced by paramagnetic compounds is much stronger resulting in more efficient T_1 and T_2 relaxation (Fig. 1.16). Scalar relaxation does not play a major rôle with some paramagnetic ions such as Gd^{3+} . However, it can result in significant contribution to relaxation enhancement with other ions, such as Mn^{2+} where T_2 relaxation effects can predominate over T_1 relaxation.

Paramagnetic compounds possess at least one unpaired electron thus creating a net magnetic moment in the species due to unpaired electron spins. The net magnetic moment of an unpaired electron spin is 657 times that of a proton. Therefore, an

electron is 500,000 times more effective at inducing relaxation than a proton, as $I = \mu^2$. Gadolinium(III), having seven unpaired electrons, has dramatic relaxation efficiency.

The magnitude of relaxation enhancement induced by paramagnetic metals depends on the proximity of the nuclear and electronic spins and on the correlation time of their interaction, *i.e.* the interaction between the magnetic moment of a nucleus and that of the paramagnetic species where the tumbling and rotation of unpaired electron spins induce randomly fluctuating electromagnetic fields at nearby protons. Some of the electron-induced electromagnetic fields match the nuclear precessional frequency of the protons thus facilitating T_1 relaxation. Similarly, T_2 relaxation is induced as the greater magnetic moment of the unpaired electron spins increase loss of phase coherence of these protons.^[71]

The observed relaxation rate is proportional to the concentration of the paramagnetic ion.^[72] Koenig^[73] used this characteristic to define *relaxivity*, the change in relaxation rate (in s^{-1}) produced by unit change in concentration ($mol\ dm^{-3}$). The relaxivity, denoted by R , describes the relaxation effectiveness of an ion and depends on the temperature and the NMR frequency and is normally quoted at $1\ dm^3\ mmol^{-1}\ s^{-1}$. Relaxivity values of some common paramagnetic ions are given in Table 1.1.

Table 1.1 Relaxivity values of some common paramagnetic aqua ions at 80 MHz and 30°C (data taken from ref. 74)		
ION	dm³ mmol⁻¹ s⁻¹	
	R_1	R_2
copper(II)	0.63	0.71
nickel(II)	0.70	0.78
manganese(II)	5.69	71.6
gadolinium(III)	10.38	11.7

Due to its high relaxivity, the complexes of the gadolinium(III) ion are generally used as contrast agents for MRI.

1.5.4.2 Essential Properties of Contrast Agents

To be successful as a contrast agent the metal complex must satisfy the criteria listed below.^[75,76]

1. To produce strong relaxation effects, the paramagnetic ion should preferably have a high electron spin number, S , and a long electron spin relaxation time, τ_s .
2. The distance between the paramagnetic ion and the protons that it is relaxing should be minimal, *i.e.* the ion, whether complexed or not, should bind directly to the water molecules. It is important, therefore, that when designing paramagnetic complexes to ensure that metal coordination sites are available and accessible to water molecules.
3. Toxicity is an important feature to be considered since the use of free ions is extremely hazardous. However, complexes of ions with chelating agents such as DTPA are safer than the aqua ion because the metal ion is held strongly and is prevented from interacting with enzymes and disrupting metabolic processes. Water solubility is also important. Administering the metal in the form of a chelate has a second advantage in that the chelating ligand can be used to overcome problems associated with poor solubility of some free metal ions at physiological pH.
4. The chelate must be neutral, stable *in vivo* and have low osmolality.
5. It would be desirable to target a contrast agent to specific sites of interest. Again, the nature and chemistry of the ligand is of importance. The simple chelate, $[\text{Gd}(\text{DTPA})\text{H}_2\text{O}]^{2-}$ is non-specific.

Fig. 1.17 summarises the above criteria. Once the chelate has met with most of the above criteria, it must then undergo pharmacological tests, followed by *in vivo* examination.

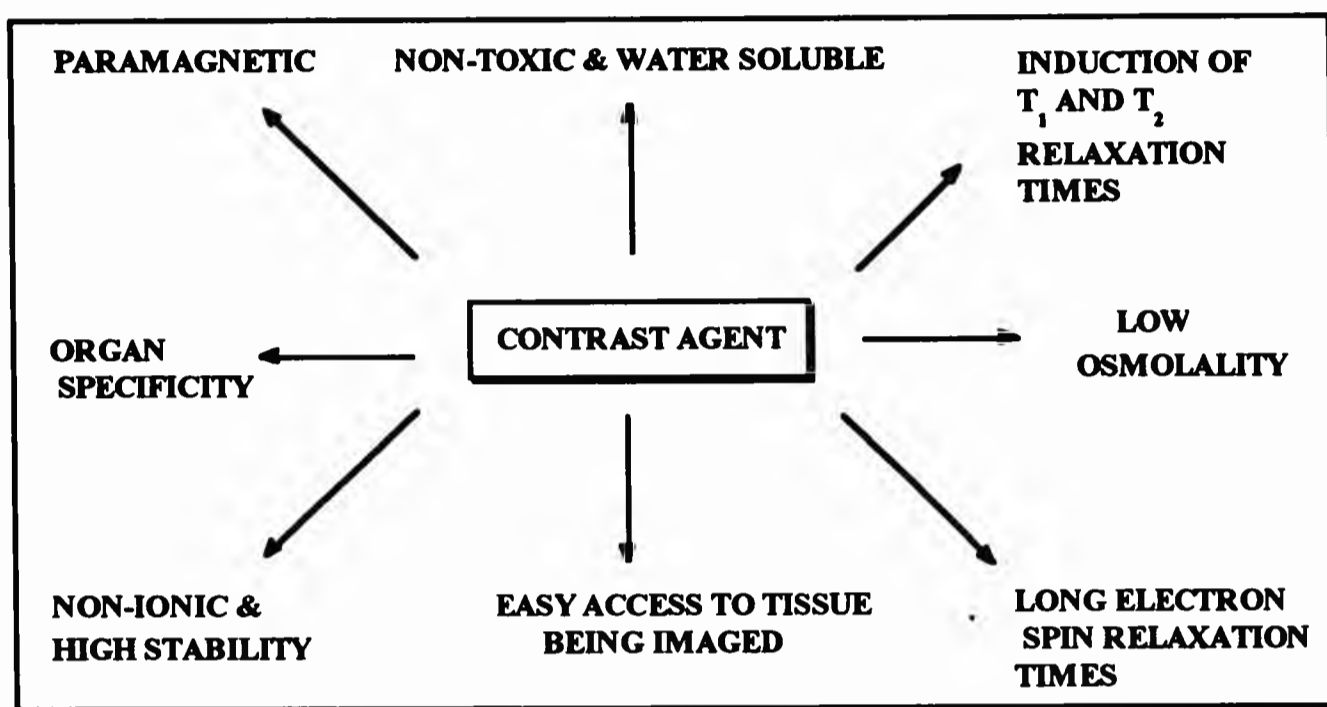


Fig. 1.17 The essential properties of contrast agents

1.5.4.3 Recent Advances on Contrast Agents For MRI

At present, $[\text{Gd}(\text{DTPA})\text{H}_2\text{O}]^{2-}$ and $[\text{Gd}(\text{DOTA})\text{H}_2\text{O}]^-$ and some of their derivatives are the only approved chelates for the use as MRI contrast agents although a number of compounds are undergoing trials, for example, metalloporphyrins,^[77-79] nitroxide stable free radicals,^[71] and oral agents.^[80] Research in this field is strong, competitive and thriving.

$[\text{Gd}(\text{DTPA})\text{H}_2\text{O}]^{2-}$ is currently marketed by Berlex Laboratories, New Jersey, as the N-methylglucamine (NMG) salt under the name **Magnevist®**. The large magnetic moment of the gadolinium(III) ion and the relatively low toxicity of the complex led to its successful use as a contrast agent. Its high *in vivo* stability ($\log K = 22.5$) reduces the toxic effects of the Gd^{3+} ion by lowering the concentration of the free metal ion.^[81] The LD_{50} in rats is 10 mmol/ kg as the complex is excreted intact *via* the renal system (83% in 6 h, 91% in 24 h), and it is well tolerated with few side effects. $[\text{Gd}(\text{EDTA})\text{H}_2\text{O}]^-$ has toxicity comparable to that of GdCl_3 (LD_{50} in rats

0.5 mmol/ kg) irrespective of its high thermodynamic stability ($\log K = 17.4$).^[81] The conclusion is that the latter complex dissociates *in vivo*, yielding the toxicity of the free ion^[82] and, consequently the toxicity of the free ligand. Free Gd^{3+} can bind to Ca^{2+} binding sites, often with higher affinity, due to its greater charge/radius ratio.

One factor limiting the effectiveness of $[Gd(DTPA)H_2O]^{2-}$ as a relaxation agent is the availability of only one co-ordination site for water^[76] resulting in the average relaxation rate of $R_1 = 4.1 \text{ dm}^3 \text{ mmol}^{-1} \text{ s}^{-1}$ at 35°C and 20 MHz, a value 3-4 lower than that of the aqua ion, $GdCl_3 \cdot 9H_2O$.^[65] The non-planarity attained by the ligand on metal co-ordination does not allow for maximum co-ordination of water to the Gd^{3+} ion (co-ordination number of Gd^{3+} in $[Gd(DTPA)H_2O]^{2-}$ is 9, the maximum co-ordination number of Gd^{3+} is 10). The relaxation ability of the chelate can be increased by the conjugation of $[Gd(DTPA)H_2O]^{2-}$ with a macromolecule such as albumin.^[83] Furthermore, the chelate is not organ-specific. Achieving specificity, *i.e.* the contrast agent is able to concentrate in one particular organ or area of the body, will reduce the amount of pharmaceutical administered (dosage of $NMG_2[Gd(DTPA)H_2O]^{2-}$ is 0.1 mmol/ kg which is 20 cm^3 for a typical adult) and at the same time reduce the cost and imaging time and therefore increase patient throughput. Tumour specificity can be achieved by attaching the complex to a monoclonal antibody but studies in this field have shown that covalent bonding of one or several of the acetate groups of DTPA to the antibody decrease the overall stability of the complex.^[84] For such important reasons there is significant room for improvement in the development of contrast agents.

In continuing the search for neutral, non-ionic gadolinium chelates, neutral functionalities have been used to replace two of the anionic carboxylate donors of DTPA. These functionalities include amides, esters, alcohols, phenols, amines, ethers, thiols and ketones which, with the exception of amines, are uncharged in water at pH 7 and all have electron pairs suitable for co-ordination to the metal.^[85] Examples of DTPA diamide derivatives are shown in Fig. 1.18.

	R ¹	R ²	Ref.
		CH ₃	CH ₂ CHO(H)CH ₂ OH
	H	CH ₂ CHO(H)CH ₂ OH	85
	H	CH ₂ Ph	86
	H	CH ₃	87

Fig. 1.18 Examples of DTPA-diamide derivatives

The gadolinium complexes of these diamides have relaxivities ($R_1 \approx 4 \text{ dm}^3 \text{ mmol}^{-1} \text{ s}^{-1}$) comparable to that of $[\text{Gd}(\text{DTPA})\text{H}_2\text{O}]^{2-}$ at the same temperature and spectrometer frequency,^[65] suggesting that the amide groups are binding to the metal and preventing the metal co-ordination of > 1 water molecule. Sanofi Winthrop Pharmaceuticals, New York (1992), marketed OMNISCAN_® (Gadodiamide Injection) based on the structure in Fig. 1.18; $R^1 = \text{H}$, $R^2 = \text{Me}$, *i.e.* GdDTPA-BMA.

The advantage of GdDTPA-BMA is that it has a higher LD_{50} (34.4 mmol/kg) than $[\text{GdDTPA}(\text{H}_2\text{O})]\text{NMG}_2$ credited to the enhanced thermodynamic selectivity^[88] and also to the presence of NaCaDTPA-BMA (caldiamide sodium) in the overall formulation of the gadodiamide injection. Further clinical studies confirmed the extra stability of GdDTPA-BMA over $[\text{GdDTPA}(\text{H}_2\text{O})]\text{NMG}_2$ in that the former complex is excreted intact in the urine $> 95\%$ in 72 h.

It was expected that some macrocyclic ligands could exhibit even stronger ligating properties than DTPA as a result of the macrocyclic effect (§ 1.2.3.1). Preliminary studies based on the lanthanide, hexaaza Schiff-base macrocycle, {XVII} indicated that these complexes are kinetically inert and do not decompose by well known precipitating agents such as oxalate.^[89] The disadvantages are that these compounds are poorly soluble in water, have high osmolality and form hydroxo species. Nevertheless, the backbone structure became a model to much more favourable structures as given in Fig. 1.19.^[90,91] Data on *in vivo* toxicity, stability or relaxivities of the gadolinium complexes of these ligands have not, to date, been reported.

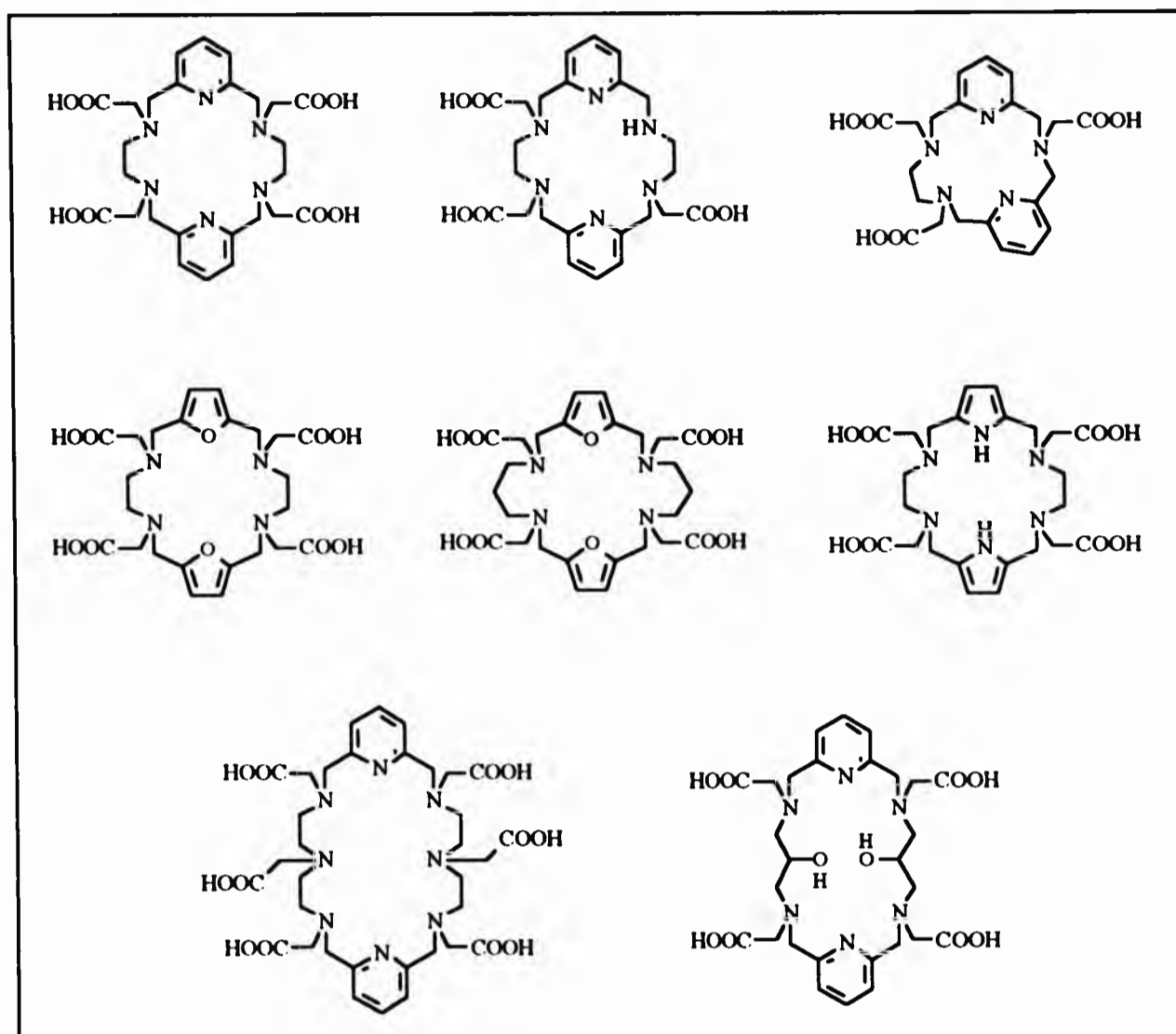
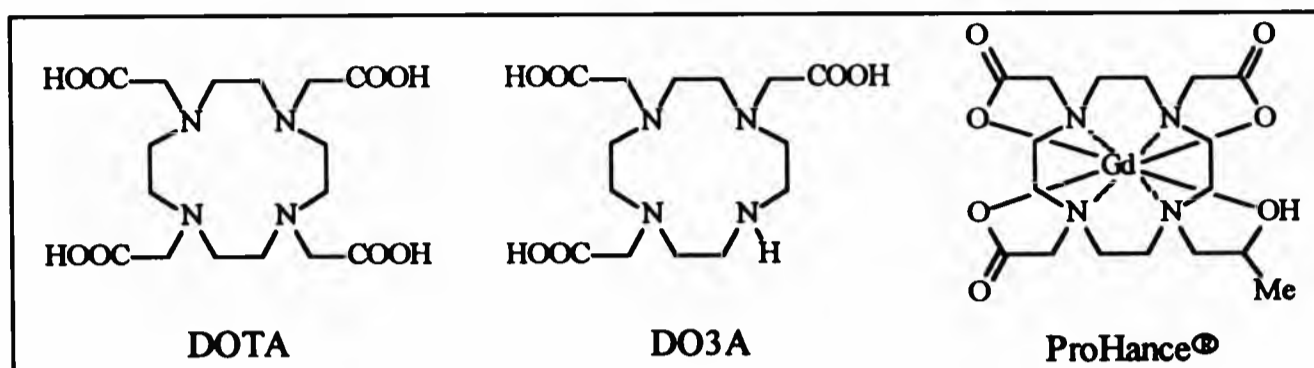


Fig. 1.19 Aromatic-ring-based macrocyclic ligands containing carboxylate pendant arms

Increasing the stability of gadolinium(III) complexes beyond that of DTPA was achieved by the introduction of non-aromatic macrocyclic ligands, again substituted with ionisable pendant arms (§ 1.4.3). Gadolinium complexes of H_3 NOTA, H_4 DOTA, and H_4 TETA were taken into account, these chelates being water soluble and exhibiting relaxation properties similar to those of $[Gd(DTPA)H_2O]^{2-}$.

H_4 DOTA forms the most stable Gd^{3+} complex known, with a stability constant of 10^{28} , compared to the complexes of H_3 NOTA and H_4 TETA with stability constants of 10^{17} and 10^{18} respectively.¹⁹²¹ The dissociation of $[Gd(DOTA)H_2O]^-$ is extremely slow ($k_d = 10^{-5} \text{ mol}^{-1} \text{ s}^{-1}$) due to its conformational stability and macrocyclic nature. **DOTAREM**[®], $NMG[Gd(DOTA)H_2O]$, became the second contrast agent on the pharmaceutical market, in 1989, as an alternative to **Magnevist**[®], due to its high

tolerance, low toxicity, high *in vivo* stability and comparable relaxivity. In 1992 ProHance® (Gadoteridol Injection), also a DOTA derivative, was released by Squibb Diagnostics, USA.



Most research groups today are concentrating on DO3A and its derivatives.^[93] The high stability, low osmolality and with a relaxivity matching that of $[\text{Gd}(\text{DTPA})\text{H}_2\text{O}]^{2-}$ render the gadolinium complexes of DO3A and its derivatives as favourable contrast agents. Work in this area is still in progress.

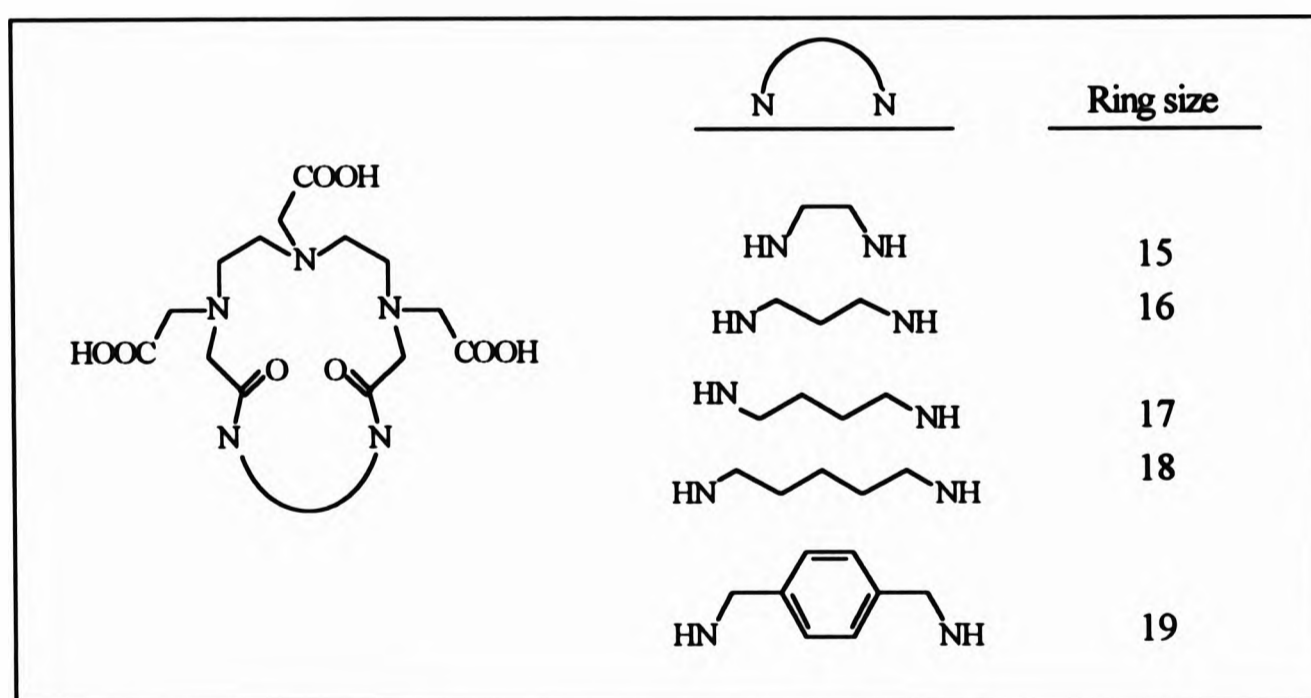


Fig. 1.20 Macrocyclic DTPA-bis(amide) Ligands

Most recently, structures combining DTPA-diamides as macrocyclic derivatives were prepared (Fig. 1.20).^[94] An increase in ring size, from 15 to 18-membered, led to

an increase in kinetic inertness, reflecting the enhanced participation of the amide carbonyl oxygen to the Gd^{3+} ion co-ordination. The 19-membered macrocycle, incorporating the aromatic ring, caused a significant decrease in the kinetic inertness.

1.6 References

1. G. A. Melson, in *Co-ordination Chemistry of Macrocyclic Compounds*, G. A. Melson (Ed.), Plenum, New York, 1979, p2.
2. L. F. Lindoy and D. H. Busch, in *Preparative Inorganic Reactions*, W. L. Jolly (Ed.), 1971, **6**, p1-63.
3. R. Hoss and F. Vögtle, *Angew. Chem. Int. Ed. Engl.*, 1994, **33**, 375.
4. S. M. Nelson, C. V. Knox, M. McCann and M. G. B. Drew, *J. Chem. Soc., Dalton Trans.*, 1981, 1669.
5. B. Dietrich, P. Viout and J.-M. Lehn, *Macrocyclic Chemistry, Aspects of Organic and Inorganic Supramolecular Chemistry*, VCH Verlagsgesellschaft mbH and Weinheim VCH publishers, Inc., New York, 1993.
6. M. G. B. Drew, A. H. B. Othman, P. D. A. McIlroy and S. M. Nelson, *J. Chem. Soc., Dalton Trans.*, 1977, 1173.
7. D. H. Cook, D. E. Fenton, M. G. B. Drew, A. H. B. Othman, S. G. McFall and S. M. Nelson, *J. Chem. Soc. Dalton Trans.*, 1977, 446.
8. M. G. B. Drew, J. Nelson, and S. M. Nelson, *J. Chem. Soc., Dalton Trans.*, 1981, 1678.
9. M. G. B. Drew, J. Nelson and S. M. Nelson, *J. Chem. Soc., Dalton Trans.*, 1981, 1685.
10. M. G. B. Drew, J. Nelson and S. M. Nelson, *J. Chem. Soc., Dalton Trans.*, 1981, 1691.
11. N. A. Bailey, D. E. Fenton, I. T. Jackson, R. Moody and C. R. de Barbarin, *J. Chem. Soc., Chem. Commun.*, 1983, 1463.
12. V. McKee and J. Smith, *J. Chem. Soc., Chem. Commun.*, 1983, 1465.
13. S. Brooker, V. McKee, W. B. Shepard and L. K. Pannell, *J. Chem. Soc., Dalton Trans.*, 1987, 2555.
14. H. C. Aspinall, J. Black, I. Dodd, M. M. Harding and S. J. Winkley, *J. Chem. Soc., Dalton Trans.*, 1993, 709.
15. H. Adams, N. A. Bailey, D. E. Fenton, R. J. Good, R. Moody and C. O. R. de Barbarin, *J. Chem. Soc., Dalton Trans.*, 1987, 207.
16. M. C. Thompson and D. H. Busch, *J. Am. Chem. Soc.*, 1964, **86**, 3561.

17. H. Jadamus, Q. Fernando and H. Freiser, *Inorg. Chem.*, 1964, **3**, 928.
18. L. F. Lindoy and D. H. Busch, *Inorg. Chem.*, 1974, **13**, 2494.
19. D. K. Cabbiness and D. W. Margerum, *J. Am. Chem. Soc.*, 1969, **91**, 6540.
20. M. Kodama and E. Kimura, *J. Chem. Soc., Dalton Trans.*, 1976, 2341.
21. F. P. Hinz and D. W. Margerum, *J. Am. Chem. Soc.*, 1974, **96**, 4993.
22. F. P. Hinz and D. W. Margerum, *Inorg. Chem.*, 1974, **13**, 294.
23. F. P. Hinz and D. W. Margerum, *Inorg. Chem.*, 1974, **13**, 2941.
24. A. Anichini, L. Fabrizzi, P. Paoletti and R. M. Clay, *Inorg. Chim. Acta.*, 1977, **22**, L25.
25. L. Y. Martin, L. J. DeHayes, L. J. Zompa and D. H. Busch, *J. Am. Chem. Soc.*, 1974, **96**, 4046.
26. L. Fabrizzi, P. Paoletti and R. M. Clay, *Inorg. Chem.*, 1978, **17**, 1042.
27. See for example M. Micheloni and P. Paoletti, *Inorg. Chim. Acta.*, 1980, **43**, 109.
28. J. D. Curry and D. H. Busch, *J. Am. Chem. Soc.*, 1964, **86**, 592.
29. R. L. Rich and G. L. Stucky, *Inorg. Nucl. Chem. Lett.*, 1965, **1**, 61.
30. S. M. Nelson and D. H. Busch, *Inorg. Chem.*, 1969, **8**, 1859.
31. E. Fleischer and S. Hawkinson, *J. Am. Chem. Soc.*, 1967, **89**, 720.
32. M. G. B. Drew, A. H. bin Othman, P. D. A. McIlroy and S. M. Nelson, *J. Chem. Soc., Dalton Trans.*, 1975, 2507.
33. E. Constable, *Metals and Ligand Reactivity*, J. Burgess (Ed.), Ellis Horwood Series in Inorganic Chemistry, Ellis Horwood, New York, 1991.
34. J. de O. Cabral, M. F. Cabral, M. G. B. Drew, A. Rodgers and S. M. Nelson, *Inorg. Chim. Acta.*, 1978, **30**, L313.
35. M. G. B. Drew, J. de O. Cabral, M. F. Cabral, F. S. Esho and S. M. Nelson, *J. Chem. Soc., Chem. Commun.*, 1979, 1033.
36. S. M. Nelson, F. S. Esho, M. G. B. Drew and P. Bird, *J. Chem. Soc., Chem. Commun.*, 1979, 1035.

37. S. M. Nelson, *Pure and Appl. Chem.*, 1980, **52**, 2461.
38. S. M. Nelson, C. V. Knox, M. MacCann and M. G. B. Drew, *J. Chem. Soc., Dalton Trans.*, 1981, 1669.
39. J. de O. Cabral, M. F. Cabral, M. G. B. Drew, F. S. Esho, O. Haas and S. M. Nelson, *J. Chem. Soc., Chem Commun.*, 1982, 1062.
40. J. de O. Cabral, M. F. Cabral, M. G. B. Drew F. S. Esho and S. M. Nelson, *J. Chem. Soc., Chem Commun.*, 1982, 1068.
41. R. E. Sievers, in *Inorganic Compounds With Unusual Properties*, R. B. King (Ed.), Advances in Chemistry Series, No. 150, American Chemical Society, Washington, D. C., 1976, p222-231.
42. C. C. Hinckley, *J. Am. Chem. Soc.*, 1969, **91**, 5160.
43. A. D. Sherry and C. F. G. C. Geraldes, in *Lanthanide Probes in Life, Chemical and Earth Sciences*, J.-C. G. Bünzli and G. R. Choppin (Eds.), Elsevier, Amsterdam, 1989, Chapter 4, p93-126.
44. K. S. Pitzer, *Acc. Chem. Res.*, 1979, **12**, 271.
45. F. S. Richardson, *Chem. Rev.*, 1982, **82**, 542.
46. G. Schwarzenbach, in *Advances in Inorganic Chemistry and Radiochemistry*, H. J. Emeléus and A. G. Sharpe (Eds.), vol. 3, Academic Press, New York, N. Y., 1961.
47. T. Moeller, D. F. Martin, L. C. Thompson, R. Ferrus, G. R. Feistel and W. J. Randal, *Chem. Rev.*, 1965, **65**, 1 and refs. therein.
48. G. R. Choppin, in *Lanthanide Probes in Life, Chemical and Earth Sciences*, J.-C. G. Bünzli and G. R. Choppin (Eds.), Elsevier, Amsterdam, 1989, Chapter 1, p1-32.
49. M. F. Loncin, J. F. Desreux and E. Merciny, *Inorg. Chem.*, 1986, **25**, 2646.
50. W. P. Cacheris, S. K. Nickle and A. D. Sherry, *Inorg. Chem.*, 1987, **26**, 958.
51. E. R. Andrew, *Acc. Chem. Res.*, 1983, **16**, 114.
52. P. Mansfield and P. G. Morris, *NMR Imaging in Biomedicine*, J. S. Waugh (Ed.), Academic Press, New York, 1982.
53. R. A. Komoroski, *Anal. Chem.*, 1993, **65**, 1068 and refs therein.

54. P. F. Renshaw, P. M. Joseph, R. M. Summers and H. L. Kundel, *Magn. Reson. Med.*, 1985, 2, 512.
55. J. R. Alger and R. G. Shulman, *Br. Med. Bull.*, 1984, 40, 160.
56. T. Nakada, I. L. Kwee, B. V. Griffey and R. H. Griffey, *Magn. Reson. Med.*, 1988, 6, 307.
57. I. R. Young, in *Practical NMR Imaging*, M. A. Foster and J. M. S. Hutchison (Eds.), 1987, IRL Press, Oxford, Chapter 8, p199-248.
58. G. K. Radda, P. J. Bore and B. Rajagopalan, *Br. Med. Bull.*, 1984, 40, 155.
59. S. W. Young, *Nuclear Magnetic Resonance Imaging, Basic principles*, Raven Press, New York, Chapter 5, p25-56.
60. D. Lurie, in *The Physical Basis of Magnetic Resonance Imaging*, Seventh Aberdeen NMR Summer School, University of Aberdeen, 1991, p21.
61. K. L. Nelson and V. M. Runge, in *Enhanced Magnetic Resonance Imaging*, V. M. Runge (Ed.), C. V. Mosby Co., St. Louis, 1989, Chapter 6, p57-75.
62. J. M. S. Hutchison and M. A. Foster, in *Practical NMR Imaging*, J. M. S. Hutchison and M. A. Foster (Eds.), IRL Press, Oxford, 1987, chapter 1, p1-48.
63. R. Damadian, *Science*, 1971, 171, 1151.
64. R. E. Steiner, *Am. J. Roentgenol.*, 1985, 145, 883.
65. R. B. Lauffer, *Chem. Rev.*, 1987, 87, 901.
66. G. M. Bydder, R. E. Steiner, I. R. Young, A. S. Hall, D. J. Thomas, J. Marshall, C. A. Pallis and N. J. Legg, *Am. J. Roentgenol.*, 1982, 139, 215.
67. J. E. Potchen, P. R. Koehlen and D. O. Davis, *Principles of Diagnostic Radiology*, 1971, McGraw-Hill, New York.
68. A. R. Fritzberg, *Radiopharmaceuticals: Progress and Clinical Perspectives*, 1986, CRC Press BOCA Raton, Fl.
69. J. G. Hardy, in *Radiopharmaceuticals and Medicine*, A. E. Theobald (Ed.), Ellis Horwood Series in Biomedical Sciences, Ellis Horwood Ltd, Chichester, 1989, p57
70. *Magnetic Resonance Imaging*, D. D. Stark, and W. G. Bradley (Eds.), C.V. Mosby Co., St. Louis, 1988.

71. B. L. Engelstad and G. L. Wolf, in *Magnetic Resonance Imaging*, D. D. Stark and W. G. Bradley (Eds.), C.V. Mosby Co., St. Louis, 1988, p163.
72. N. Bloembergen, E. M. Purcell and R. V. Pound, *Phys. Rev.*, 1948, **73**, 679.
73. S. H. Koenig and R. D. Brown, *Magn. Reson. Med.*, 1984, **1**, 478.
74. M. A. Foster, Personal Communication, Seventh Aberdeen NMR Summer School, 1991, Aberdeen.
75. D. G. Gadian, J. A. Payne, D. J. Bryant, I. R. Young, D. H. Carr and G. M. Bydder, *J. Comp. Assist. Tomogr.*, 1985, **9**, 242.
76. H. Gries and H. Miklautz, *Physiol. Chem. Phys. Med.*, 1984, **16**, 105.
77. J. L. Sessler, T. D. Mody, G. W. Hemmi and V. Lynch, *Inorg. Chem.*, 1993, **32**, 3175.
78. J. L. Sessler, T. D. Mody, G. W. Hemmi, V. Lynch, S. W. Young and R. A. Miller, *J. Am. Chem. Soc.*, 1993, **115**, 10368.
79. J. L. Sessler, G. Hemmi, T. D. Mody, T. Murai, A. Burrell and S. W. Young, *Acc. Chem. Res.*, 1994, **27**, 43.
80. R. F. Mattrey, *Am. J. Roentgenol.*, 1987, **148**, 1259.
81. R. C. Brasch, H.-J. Weinmann and G. E. Wesbey, *Am. J. Roentgenol.*, 1984, **142**, 625.
82. H.-J. Weinmann, R. C. Brasch, W. R. Press and G. E. Wesbey, *Am. J. Roentgenol.*, 1984, **142**, 619.
83. R. B. Lauffer and T. J. Brady, *Magn. Reson. Imaging*, 1985, **3**, 11.
84. W. T. Anderson-Berg, M. Strand, T. E. Lempert, A. E. Rosebaum and P. M. Joseph, *J. Nucl. Med.*, 1986, **27**, 829.
85. G. Gaughan, in *Enhanced Magnetic Resonance Imaging*, V. M. Runge (Ed.), C. V. Mosby Co., St. Louis, 1989, Chapter 9, p105-115.
86. A. Chowdhury, Unpublished results, University of North London.
87. M. Van Wagoner, M. O'Toole, D. Worah, P. T. Leese and S. C. Quay, *Invest Radiol.*, 1991, **26**, 980.
88. W. P. Chacheris, S. C. Quay and S. M. Rocklage, *Magn. Res. Imaging*, 1990, **8**, 467.

89. L. De Cola, D. L. Smailles, L. M. Vallarino, *Inorg. Chem.*, 1986, **25**, 1729.
90. S. C. Jackels and D. Meyers, *PCT Int. Pat. Appl.* WO 90/11282, CLA61 K49/00, 1990.
91. J. F. Carvalho, S. P. Crofts and S. M. Rocklage, *PCT Int. Pat. Appl.* WO 91/10645, CLA61 K49/00, 1991.
92. M. Magerstadt, *Magn. Reson. Med.*, 1986, **3**, 808.
93. C. A. Chang, L. C. Francesconi, M. F. Malley, K. Kumar, J. Z. Gougoutas, M. F. Tweedle, D. W. Lee and L. J. Wilson, *Inorg. Chem.*, 1993, **32**, 3501.
94. K.-Y. Choi, K. S. Kim and J. C. Kim, *Polyhedron*, 1994, **13**, 567.

CHAPTER 2

Chapter 2: SYNTHESIS AND CHARACTERISATION OF 18-MEMBERED HEXAAZA TETRAIMINE MACROCYCLES AND THEIR LANTHANIDE METAL COMPLEXES

(References to this Chapter are listed on pages 103-107)

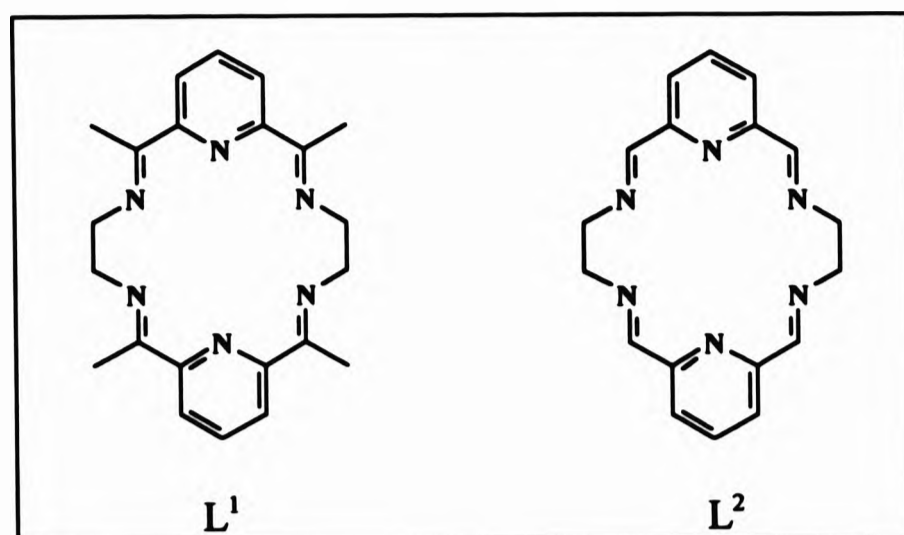
2.1 Introduction

The macrocycles discussed in this thesis were all derived from the [2+2] condensation of an amine (1,2-diaminoethane, 1,2-diaminobenzene or (\pm)-*trans*-1,2-diaminocyclohexane) and a dicarbonyl (2,6-pyridinedialdehyde or 2,6-diacetylpyridine) resulting in rigid 18-membered symmetrical cyclisation products. Cyclo-oligomerisation products of primary diamines with dicarbonyls may be controlled with metal templates where as polymeric species are usually obtained in the absence of the metal.

The chapter begins by repeating some earlier work in this area already carried out by others but the syntheses were essential in developing potentially novel macrocyclic ligands. In this study, where the macrocyclic complex was to be reduced and demetallated, the alkali earth barium(II) was used as a template agent, although other alkali metals such as Ca^{2+} and Sr^{2+} ,^[1] the transition metal, Pb^{2+} , and the lanthanide metals^[2-8] have also been previously employed for the template synthesis of macrocycles of this nature.

2.2 Synthesis and Characterisation of $\text{BaL}^1(\text{NO}_3)_2$

The metal template synthesis and characterisation of L^1 and L^2 has been well documented.^[11-17] It must be stressed that although the isolation of $\text{BaL}^1(\text{NO}_3)_2$ is not novel its synthesis was necessary for the isolation of the corresponding reduced and demetallated macrocyclic ligand (Chapter 3). The characterisation discussed here is comparable to that reported previously.^[18]



$BaL^1(NO_3)_2$ was isolated as large, white prismatic crystals from methanol on reacting 2,6-diacetylpyridine and 1,2-diaminoethane in the presence of barium(II) nitrate. Two distinctive strong, sharp bands in the IR spectrum at 1640 and 1586 cm^{-1} represent the co-ordinated imine, $\nu(C=N)$, and the high energy stretching modes of $\nu(C=N)$ of the pyridyl group respectively.^[19] The low energy pyridine band observed at 630 cm^{-1} confirmed the co-ordination of the pyridine nitrogen to the metal.^[20] The absence of bands due to unreacted or uncyclised amine (*ca.* 3500 - 3200 and 1610 - 1590 cm^{-1}) or dicarbonyl (*ca.* 1720 - 1670 cm^{-1}) supported the integrity of the tetraimine macrocyclic complex. Vibrations at 1360 and 821 cm^{-1} were indicative of non-co-ordinating, ionic, nitrate groups^[21] but co-ordinated nitrate groups cannot be ruled out completely since the region where these absorb is obscured by the ligand vibrations.

The EI mass spectrum showed a molecular ion of m/z 498, this being consistent with the formulation of $L^1(NO_3)_2$. The 1H NMR in D_2O and at 270 MHz consisted of a complex multiplet at δ_H 7.5 - 8.2 which integrated for six protons representing the six pyridine protons. Two *singlets* at δ_H 2.65 and 3.35 accounted for the twelve methyl and eight methylene protons respectively.

The metal counter-ion plays an important rôle in the isolation of metal complexes in particular where the template agent is a lanthanide. The perchlorate and nitrate counter-ions are most favourable. The complexes formed tend to be insoluble in most

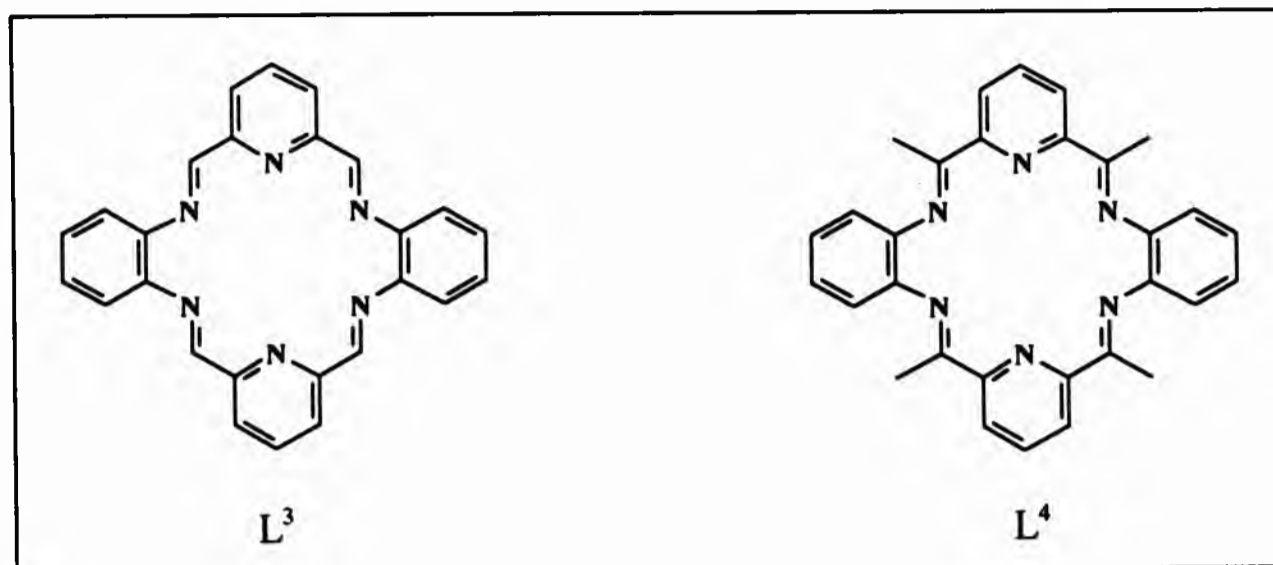
common solvents and usually precipitate out of solution. Macrocyclic complexes of metal chlorides, on the other hand, have relatively high solubility in most solvents and tend to remain in solution. Vallarino^[22] has developed a work-up method of isolating such yttrium and lanthanide metal acetate complexes of 18-membered macrocyclic ligands successfully. Where lanthanide metals are concerned, the ease as well as the yield of the metal template synthesis appear to depend on the counter-ion present as well as on the metal ion;^[6] good oxygen donor anionic ligands such as acetate and nitrate favour the reaction much more efficiently than do chloride. The former counter-ions greatly facilitate the metal template synthesis of the macrocycle. It has been suggested that substitution by the non-co-ordinating counter-ions is feasible once the macrocyclic cations have been formed.^[15]

The above *counter-ion theory* stood its ground when the synthesis of $[\text{BaL}^1]^{2+}$ was attempted using barium(II) chloride. Only when the nitrate salt was used was a product corresponding to $\text{BaL}^1(\text{NO}_3)_2$ isolated. This does not mean that macrocyclic metal complexes have not been isolated with chloride anions and indeed three are being reported here.

2.3 The Template Synthesis of L^3 with Gadolinium(III)

The macrocycle L^3 has received much attention over the past decade, initially its synthesis being the template [2+2] condensation of 2,6-pyridinedialdehyde and 1,2-diaminobenzene, the metals facilitating its synthesis being the alkali earths,^[23] Ca^{2+} , Sr^{2+} and Ba^{2+} and also Pb^{2+} where the stoichiometries are $[\text{ML}^3]^{2+}$ ($\text{M} = \text{Ca}, \text{Sr}$ and Pb) and for the sandwich structure $[\text{ML}^3_2]^{2+}$, where $\text{M} = \text{Ba}$. Complexes of L^3 with lanthanide metals were isolated by transmetallation of $[\text{BaL}^3_2](\text{ClO}_4)_2$ ^[24] in very high yields and also by the template method.^[7] The isolation of L^3 in the absence of a metal failed,^[25] the ligand alone was isolated by the decomplexation of its potassium complex using 18-crown-6 as a scavenger.^[26,27]

Whereas all the lanthanide complexes of L^3 reported to date have been isolated as the metal perchlorate, nitrate, acetate, thiocyanate, or triflate, in this work $[\text{GdL}^3]^{3+}$



was isolated as the chloride when 2,6-pyridinedialdehyde was reacted with 1,2-diaminobenzene and gadolinium(III) chloride hexahydrate. The main aim for this preparation was in the hope of isolating crystals for structure determination since the arrangement adopted by L^3 in the presence of gadolinium(III) is yet to be reported. However, several attempts at recrystallising the yellow solid yielded crystals which were unsuitable diffractors. Table 2.1 summarises the major IR bands of $[GdL^3]^{3+}$ and compares these bands to those of related lanthanide, actinide and alkali earth metal complexes of L^3 and L^4 .

The spectrum of $[GdL^3]Cl_3$ showed typical characteristics of a tetraimine macrocycle of this kind. The medium absorbance at 1630 cm^{-1} with a shoulder at 1650 cm^{-1} corresponded to $\nu(C=N)$ of the imine bonds and no evidence of solvolytic addition to this double bond is observed as such additions have been well documented for Schiff base complexes prepared under such reaction conditions.^[10,28,29] The strong bands at 1589 , 1482 and 1458 cm^{-1} correspond to pyridine and phenyl ring absorbances, the former being due to $\nu(C=N)$ of pyridine and the latter two arose from the C-C stretching modes of pyridine and the phenyl rings. The series of bands at 816 , 775 and 746 cm^{-1} arise from the benzene C-H out of plane deformations and this pattern is usually indicative of 1,2-substituted rings.^[30,31] The sharp, strong bands at 3063 and 3016 cm^{-1} were due to $\nu(C-H)$ stretching modes of the pyridine and phenyl rings. The weak band at 2933 cm^{-1} is probably due to the imine $\nu(C-H)$ stretch. A broad band at $3385 - 3393\text{ cm}^{-1}$ was assigned to lattice water and another broad band at 3195 cm^{-1} was assigned to co-ordinated water.^[5]

Table 2.1 Infrared^a and magnetic data of [GdL³]³⁺ and selected L³ and L⁴ metal complexes

COMPLEX	$\nu(\text{C}=\text{N})$ imine	$\nu(\text{C}=\text{N})$ pyridine	$\nu(\text{OH})$	$\mu_{\text{B}}^{\text{d}}$	Ref
[GdL ³ Cl ₂ (MeOH)(H ₂ O)]Cl.1½H ₂ O	1630m	1589s	3385s	7.9	*
[GdL ³ (NO ₃) ₃]	1630	1590	-	c	7
[LaL ³ (NO ₃) ₃]	1633	1593	-	b	24
[LaL ⁴ (H ₂ O) ₂](NO ₃) ₃	1609	1590	3330	b	20
[NdL ³ (NO ₃) ₃]	1634	1594	-	c	24
[BaL ³] ₂ (ClO ₄) ₂	1620	1585	-	b	1
[SrL ³](CF ₃ SO ₃) ₂	1655m	1580s	-	b	27
[UO ₂ L ⁴](ClO ₄) ₂	1615m	1595s	-	b	14

* this work, ^a in cm⁻¹, ^bdiamagnetic, ^cnot reported, ^d at 299 K

LSIMS and elemental analyses led to the formulation [GdL³(Cl)₂(MeOH)(H₂O)]Cl.1½H₂O. The fragmentation, as shown in Table 2.2 shows the direct co-ordination of methanol, one molecule of water and two chloride anions.

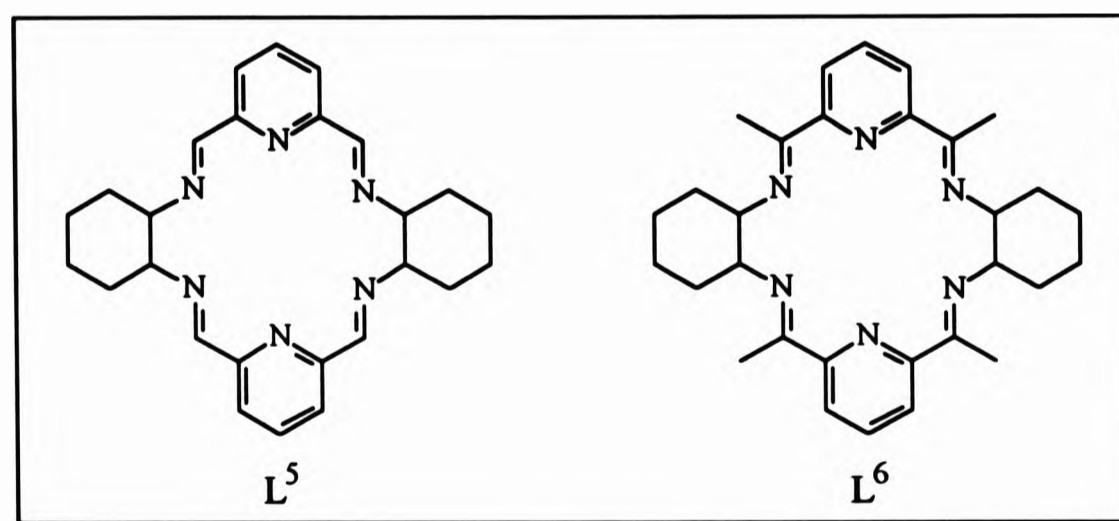
This indicates that the third counter-ion and the remaining one and a half water molecules, as predicted by the elemental analysis, are in the second co-ordination sphere. That the gadolinium ion has seven unpaired f-electrons was determined by the magnetic moment 7.9 BM at 299 K.

Table 2.2 The LSIMS fragmentation pattern of $[GdL^3(Cl)_2(MeOH)(H_2O)]^+$

FRAGMENTATION	m/z	ABUNDANCE (%)
$[GdL^3(Cl)_2(MeOH)(H_2O)]^+$	692	2
$[GdL^3Cl_2]^+$	642	25
$[GdL^3Cl]^+$	607	31
$[GdL^3]^+$	571	9
$[L^3]^+$	414	4

**2.4 Synthesis, Characterisation and Metal Complexation of L^5 and L^6
Incorporating the Cyclohexyl Unit**

The substitution of the phenyl rings in L^3 and L^4 with the cyclohexyl rings yielding L^5 and L^6 was expected to produce similar results to those already reported for L^3 and L^4 . Ligand arrangement and conformation on complexation, was expected to differ due to the chirality of the 1,2-substituted cyclohexane.



2.4.1 The Template Synthesis of L^5

The reaction of 2,6-pyridinedialdehyde and (\pm)-*trans*-1,2-diaminocyclohexane in the absence of a metal, both at low and at high dilution resulted in the isolation of the

pure ligand, L^5 and the reaction of 2,6-diacetylpyridine and (\pm)-*trans*-1,2-diaminocyclohexane yielded L^6 (§ 2.4.2). Isolation of the metal complexes of L^5 by reacting the ligand directly with a lanthanide metal salt was inconclusive. The next step in obtaining metal complexes of L^5 was through metal templates, *i.e.* the preparation of L^5 *in situ*, which proved successful in particular with barium(II), yttrium(III) and the trivalent lanthanide metals.

Metal chloride, nitrate and perchlorate L^5 macrocyclic complexes were isolated, those of the nitrate counter-ion being easier to isolate, with much higher yields, as they precipitated during reflux, yet were restricted in solubility to warm water and DMSO. The metal chloride complexes were soluble in warm water, methanol and DMSO, the yield being low relative to the metal nitrate analogues. The analyses indicate that with metal chloride complexes hydration, or water or solvent coordination, was to be expected. Complexation was concentrated mainly on barium(II), yttrium(III), lanthanum(III), neodymium(III), gadolinium(III) and dysprosium(III). All the complexes were isolated as white and amorphous solids. Recrystallisation from methanol yielded crystals in all cases, those of $[GdL^5]^{3+}$ were suitable for crystallographic analysis.

Whereas the template synthesis of L^3 yielded the sandwich structure, $[BaL^3_2](ClO_4)_2$, the same reaction, in this study, for the template synthesis of L^5 , formed the monomer, $[BaL^5](ClO_4)_2$. Furthermore, the template synthesis of L^3 with yttrium and the lanthanide metals yields exclusively monomeric species. In this work, the template synthesis of L^5 with barium(II) perchlorate, yttrium(III) chloride, lanthanum(III) nitrate, gadolinium(III) chloride and nitrate and dysprosium(III) nitrate also afforded monomeric species. In contrast, dimeric species were characterised when yttrium(III)- and neodymium(III)-nitrate were employed as templates. The general formula derived for these dimers is $[\{LnL^5(NO_3)_2\}_2(NO_3)(OH)]MeOH.xH_2O$, where $Ln = Y$ ($x = 1/2$) and Nd ($x = 1$). In both cases, five nitrate counter-ions were detected suggesting that a hydroxyl group is present to counter-balance the positive charge on the metal. That the nitrate complexes of yttrium(III) and

neodymium(III) are dimeric is supported by NMR and magnetic moments. A preliminary crystal structure for the yttrium(III) dimer, not reported here, indicates two yttrium metals in very close proximity.

2.4.1.1 Infrared Studies

Table 2.3 shows the major imine bands in the region 1630 - 1660 cm^{-1} proving the formation of [2+2] cyclisation. In conjunction, Fig. 2.1 shows the IR spectra of the free ligand L^5 and $[YL^5Cl_2(H_2O)_2]^+$. Suffice is to say that on complexation the band due to the C=N of the imine shifts to higher wavenumbers to 1640 - 1660 cm^{-1} compared to that of L^5 at 1639 cm^{-1} . The same applies for the co-ordinated C=N of the pyridyl group. Sharp bands due to unco-ordinated nitrate anions were observed for all the nitrate complexes at 1384 cm^{-1} and in the range 813 - 817 cm^{-1} .

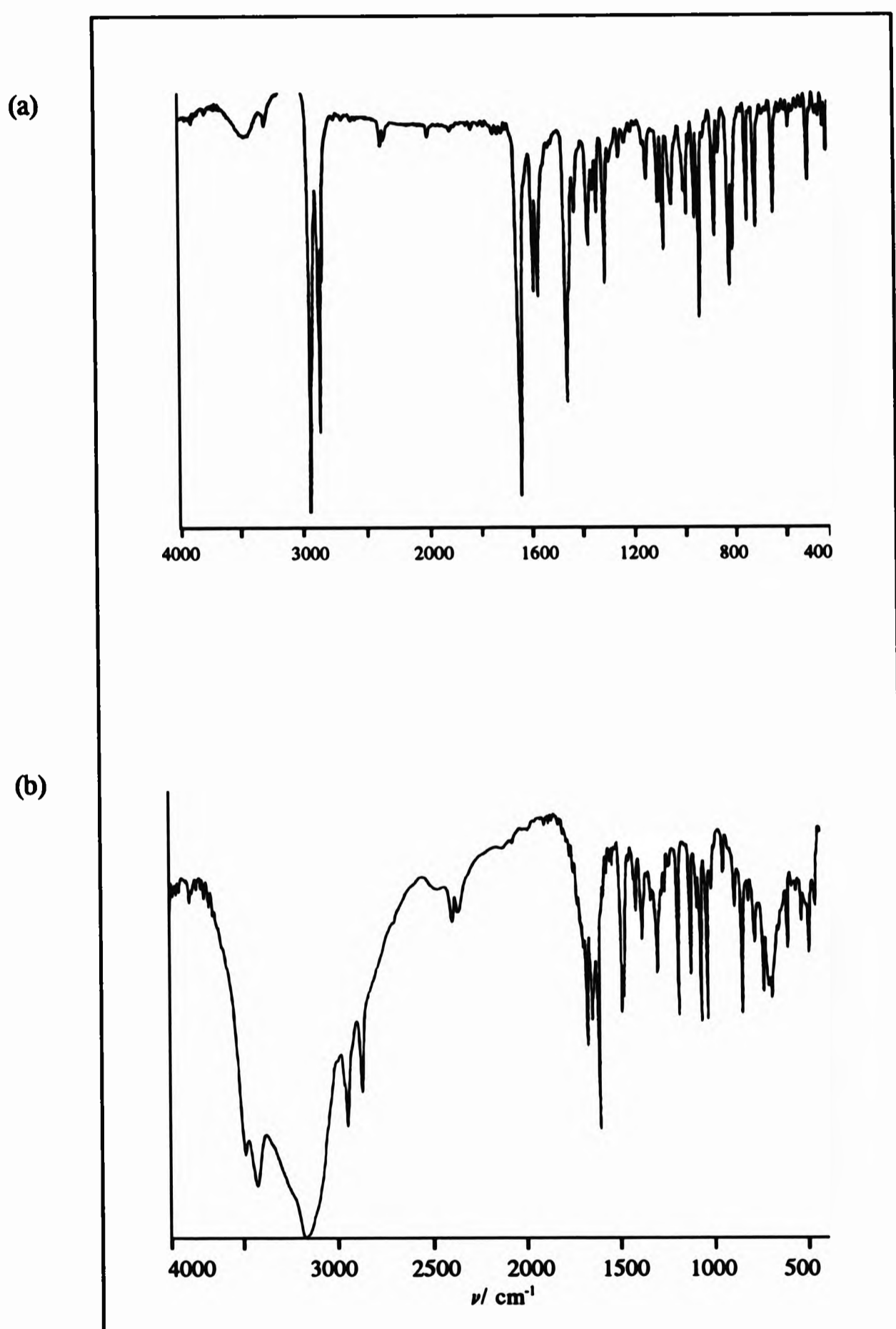
For $[BaL^5](ClO_4)_2$ both of the perchlorate counter-ions are not co-ordinating to the metal due to the broad intense absorption centred at 1096 cm^{-1} and more evidently due to the sharp band at 626 cm^{-1} .^[32]

The yttrium and neodymium nitrate complexes presented some form of asymmetry in the nitrate absorption bands. Elemental analysis and magnetic moments indicated that dimeric compounds existed, the two monomers being held together by a bridging co-ordinating nitrate group. Ionic, unco-ordinated, nitrate groups are also present and depicted at 1384 and 813 cm^{-1} . Although, by its non-equivalence, the bridging nitrate group complicates the IR analysis, with regards to the symmetry of the nitrate groups themselves, it does in fact act as a bidentate ligand if it is to hold the two monomers together. Nitrate absorption bands are also observed at 710 (ν_5), 740 (ν_3), 1023 (ν_2), 1286 (ν_4) and 1495 cm^{-1} (ν_1) but distinguishing between monodentate and bidentate chelation is rather ambiguous. The splitting $|\nu_1 - \nu_4| = 209 \text{ cm}^{-1}$ suggests bidenticity.^[32]

Table 2.3 Infrared^a and magnetic^b data of L⁵ and its Ba²⁺, Y³⁺, La³⁺, Nd³⁺, Gd³⁺ and Dy³⁺ complexes

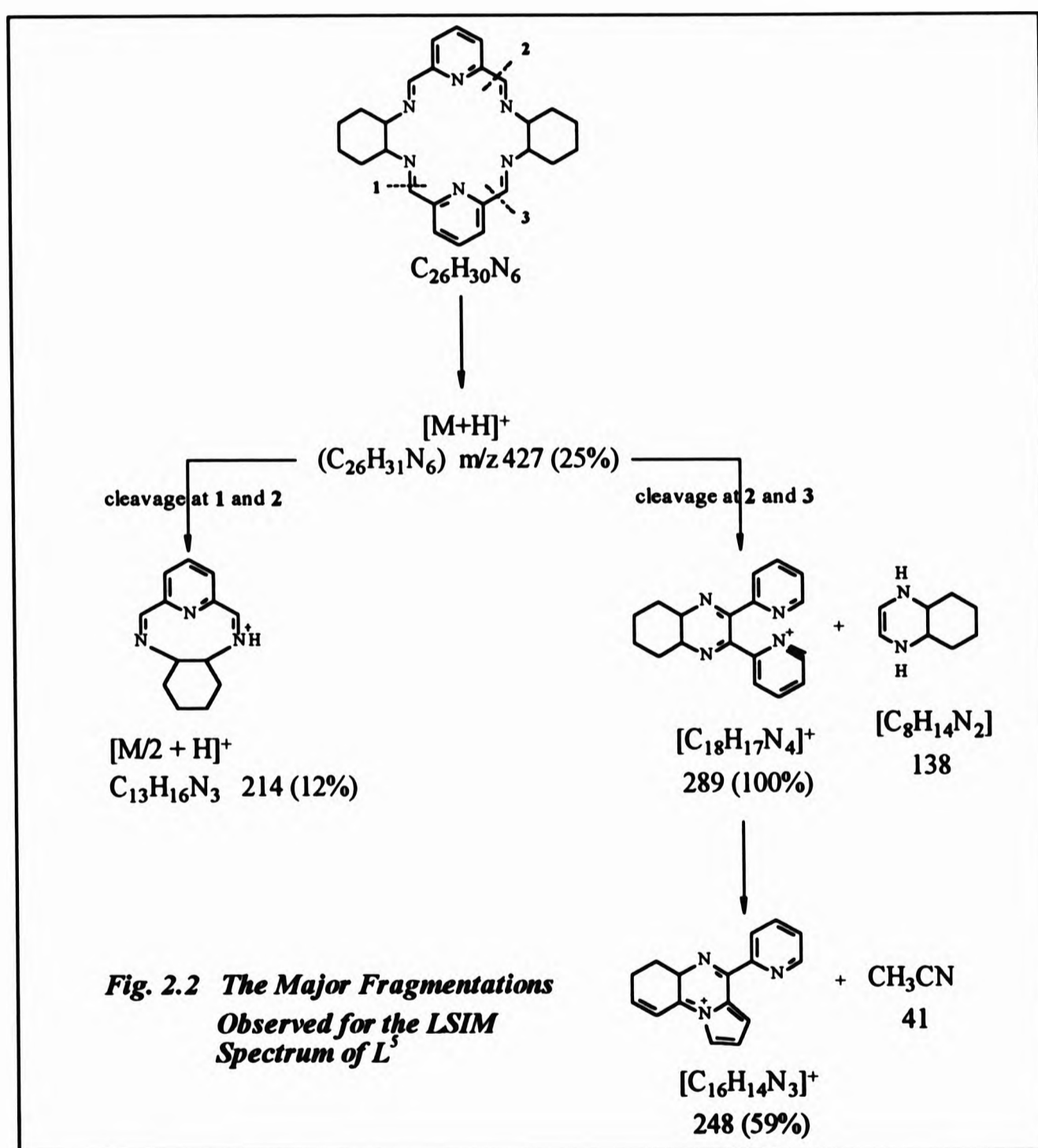
COMPOUND	$\nu(\text{C}=\text{N})_{\text{imine}}$	$\nu(\text{C}=\text{N})_{\text{py}}$	$\nu(\text{OH})$ of water	$\nu(\text{counter-ion})$	μ_{B}
L ⁵	1639s	1585m	-	-	-
[BaL ⁵] (ClO ₄) ₂	1643m	1584s	3505, 3402	1096	c
[LaL ⁵ (NO ₃) ₂]NO ₃	1644m	1590s	3423, 3140b	1384s, 817m	c
[YL ⁵ Cl ₂ (H ₂ O) ₂]Cl.3½H ₂ O	1656s	1593s	3481s, 3416s, 3166b	-	c
[{YL ⁵ (NO ₃) ₂ }] ₂ (NO ₃)(OH) MeOH.½H ₂ O	1651w	1594w	3443b	1384s, 813m, 710w, 710w 1023m, 1286s, 1495s	c
[{NdL ⁵ (NO ₃) ₂ }] ₂ (NO ₃)(OH) MeOH.H ₂ O	1649w	1593m	3423s	1384s, 816m 710w, 740w, 1011m, 1278s, 1457s	5.2 ^d
[GdL ⁵ (H ₂ O) ₃ Cl ₂]Cl	1650s	1591s	3478b, 3363b	-	7.4
[GdL ⁵ (NO ₃) ₂]NO ₃	1649w	1594m	-	1384s, 813w	7.8
[DyL ⁵ (NO ₃) ₂]NO ₃	1661w	1594m	-	1384s, 815w	10.4
^a in cm ⁻¹ , ^b at 294 K, ^c diamagnetic, ^d expected for two Nd metals = 5.1 BM					

Fig. 2.1 The infrared spectra of (a) L^5 and (b) $[YL^5Cl_2(H_2O)_2]^+$
(% transmittance is arbitrary)



2.4.1.2 Liquid Secondary Ionisation Mass Spectrometry of L^5 and its Metal Complexes

Due to characteristic low volatility, the mass spectra of both ligands and their metal complexes were recorded using liquid secondary ionisation. A parent ion at m/z 427, $[M+H]^+$ for $C_{26}H_{30}N_6$, was detected for the free ligand, L^5 . Two modes of fragmentation were predicted (Fig. 2.2). A band at m/z 214, from the symmetrical cleavage at 1 and 2 represents $[M/2 + H]^+$. The unsymmetrical cleavage at 2 and 3 leads to the second fragmentation route. The structures given in Fig. 2.2 are not necessarily the only possible configurations of the fragments.



The spectra of the metal complexes (Table 2.3) are consistent with the formation of [2+2] condensation. In all the complexes the most intense band represented the mass of the complex minus one counter-ion, in the case of $[\text{BaL}^5](\text{ClO}_4)_2$, $[\text{LaL}^5(\text{NO}_3)_2]\text{NO}_3$ and $[\text{DyL}^5(\text{NO}_3)_2]\text{NO}_3$ this band was the most stable at 100% abundance. The loss of the remaining two counter-ions consecutively followed by the loss of the metal was a fragmentation pathway followed by almost all the complexes with the exception of $[\text{DyL}^5(\text{NO}_3)_2]\text{NO}_3$, where fragmentation beyond the $[\text{DyL}^5(\text{NO}_3)_2]^+$ was inconclusive. As with the spectrum of L^5 two bands at m/z 248 and 289, both of relatively high abundance account for the structures in Fig. 2.2.

A parent ion was not observed for the dimeric species, $[\{\text{YL}^5(\text{NO}_3)_2\}_2(\text{NO}_3)(\text{OH})]$ and $[\{\text{NdL}^5(\text{NO}_3)_2\}_2(\text{NO}_3)(\text{OH})]$. In both cases, species of the type $[\text{LnL}^5(\text{NO}_3)_2]^+$ and $[\text{LnL}^5(\text{NO}_3)_2\text{OH}]^+$ were detected. The former species dissociates in the same manner as with the monomeric structures. No order of preference of dissociation of the counter-ions was observed in the fragmentation of the latter species. Three ways of losing the counter-ions were found; first: the consecutive loss of the two nitrate ions followed by the loss of the hydroxyl group, second: the loss of the hydroxyl group followed by the consecutive loss of the two nitrate groups and third: the loss of one nitrate, the hydroxyl group and finally the remaining nitrate group. The pattern is summarised in Table 2.3.

With the exception of the metal chloride complexes, all the yttrium and lanthanide metal complexes showed the correct isotopic pattern for each metal, the mass and abundance of each isotope being shown in Table 2.4. The isotopic patterns of the chloride complexes were too complicated to be analysed.

An interesting observation was that the barium L^5 complex had a molecular ion and base peak at m/z 663 suggesting that the compound has a 1:1 metal : ligand ratio as opposed to $[\text{BaL}^3](\text{ClO}_4)_2$ which contains a 1 : 2 metal : ligand ratio.^[1]

Table 2.3 *Liquid secondary mass spectrometry of L⁵ and its Ba²⁺, Y³⁺, La³⁺, Nd³⁺, Gd³⁺ and Dy³⁺ complexes*

COMPOUND	FRAGMENT	MASS (m/z)	RELATIVE ABUNDANCE (%)
L ^{5*}	[L ⁵ + H] ⁺	427	25
	[M/2 + H] ⁺	214	12
	*	289	100
	*	248	59
[BaL ⁵](ClO ₄) ₂	[BaL ⁵ (ClO ₄) ₂] ⁺	663	100
	[BaL ⁵] ⁺	563	13
[LaL ⁵ (NO ₃) ₂] ₂ NO ₃	[LaL ⁵ (NO ₃) ₂ + H] ⁺	690	100
	[LaL ⁵ (NO ₃) ₂] ⁺	689	77
	[LaL ⁵ (NO ₃)] ⁺	627	10
[YL ⁵ Cl ₂ (H ₂ O)]Cl.3½H ₂ O	[YL ⁵ Cl ₂] ⁺	587	7
	[YL ⁵ Cl] ⁺	550	21
[{{YL ⁵ (NO ₃) ₂ }} ₂ (NO ₃)(OH)] .MeOH.½H ₂ O	[YL ⁵ (NO ₃) ₂ + H] ⁺	640	96
	[YL ⁵ (NO ₃)] ⁺	577	2
	[L ⁵ - 2H] ⁺	424	6
[{{NdL ⁵ (NO ₃) ₂ }} ₂ (NO ₃)(OH)] MeOH.H ₂ O	[NdL ⁵ (NO ₃) ₂ OH] ⁺	711	32
	[NdL ⁵ (NO ₃) ₂] ⁺	694	86
	[NdL ⁵ (NO ₃)OH] ⁺	649	19
	[NdL ⁵ NO ₃] ⁺	632	15
	[NdL ⁵] ⁺	570	12
[GdL ⁵ (H ₂ O)Cl ₂]Cl	[GdL ⁵ Cl ₂] ⁺	654	12
	[GdL ⁵ Cl] ⁺	619	7
	[GdL ⁵] ⁺	584	4
[GdL ⁵ (NO ₃) ₂] ₂ NO ₃	[GdL ⁵ (NO ₃) ₂] ⁺	707	80
	[GdL ⁵ (NO ₃)] ⁺	645	16
	[L ⁵ + H] ⁺	427	9
[DyL ⁵ (NO ₃) ₂] ₂ NO ₃	[DyL ⁵ (NO ₃) ₂] ⁺	714	100

*See Fig. 2.2

Table 2.4 *Naturally occurring isotopes of barium, yttrium and some lanthanide metals^[33]*

METAL	ISOTOPE MASS	ABUNDANCE (%)
Barium	130	0.1
	132	0.1
	134	2.4
	135	6.6
	136	7.8
	137	11.3
	138	71.7
Yttrium	89	100
Lanthanum	138	0.1
	139	99.9
Neodymium	142	27.1
	143	12.2
	144	23.9
	145	8.3
	146	17.6
	148	5.7
	150	5.6
Europium	151	47.8
	153	52.2
Gadolinium	152	0.2
	154	2.2
	155	14.8
	156	20.5
	157	15.7
	158	24.8
	160	21.8
Dysprosium	156	0.1
	158	0.1
	160	2.3
	161	18.9
	162	25.5
	163	24.9
	164	28.2

2.4.1.2 Nuclear Magnetic Resonance Spectroscopy

The investigation of the solution structures of the diamagnetic metal complexes of L^5 was carried out as far as solubilities would allow. The free ligand, L^5 , was too insoluble for NMR spectroscopy, both in $CDCl_3$ and d_6 -DMSO. $[LaL^5(NO_3)_2]^+$ was also too insoluble for the collection of ^{13}C NMR spectra. This discussion will be based on the spectra of $[YL^5Cl_2(H_2O)_2]^+$ and $[{YL^5(NO_3)_2}_2NO_3(OH)]$ and compared to those of $[LaL^5(NO_3)_2]^+$ and $[BaL^5]ClO_4$ (Table 2.5).

The 1H NMR spectra of $[YL^5Cl_2(H_2O)_2]^+$ (Fig. 2.3) and $[{YL^5(NO_3)_2}_2NO_3(OH)]$ (Fig. 2.4) in D_2O were expected to have similar solution structures. NMR studies have indicated that whereas $[YL^5Cl_2(H_2O)_2]^+$ proved to be symmetrical (more evident in the ^{13}C NMR spectrum, Table 2.6), the $[{YL^5(NO_3)_2}_2NO_3(OH)]$ showed asymmetry both in the 1H - and ^{13}C -NMR spectra. The asymmetry in the latter arises not from the individual L^5 units in the dimer, as this asymmetry would have also been observed in the NMR spectra of $[YL^5Cl_2(H_2O)_2]^+$, but from the differing counterions on each monomer. In other words, the monomeric unit, $[YL^5(NO_3)_2OH]$, of the dimeric species, resonates at different chemical shifts to the unit $[YL^5(NO_3)_3]$. Such asymmetry can only occur if the nitrate group is causing the bridging between the two units. Hydroxyl group bridging would render both units symmetrical and hence the NMR spectra of the dimer would have followed a similar pattern to those of $[YL^5Cl_2(H_2O)_2]^+$.

The *singlet* most downfield in the spectrum of $[YL^5Cl_2(H_2O)_2]^+$ (Fig. 2.3) at δ_H 9.12 is assigned to the imino protons H^4 [4H, s, $C(H)=N$]. The *triplet* and *doublet* at δ_H 8.63 and 8.31 respectively are due to H^1 [2H, t, $^3J(H^1 - H^2) = 7.7$ Hz] and H^2 [4H, d, $^3J(H^2 - H^1) = 7.7$ Hz] resonances respectively as a result of AB_2 coupling.^[34]

Yttrium ($I = 1/2$) coupling to protons is obvious in two cases. The first is due to coupling with the imino protons, H^4 indicating three bond coupling through the imine nitrogen atoms. The coupling constant cannot be determined since the second band of the yttrium *doublet* is overlapped by the imine proton resonance. The second form

of yttrium coupling observed is a four-bond coupling with the *doublet* H², through the pyridine nitrogen atom, splitting into a *doublet of doublets* of equal intensities (naturally occurring ⁸⁹Y is 100% abundant) resulting in the coupling constant ${}^4J({}^{89}\text{Y}-\text{H}^2) = 7.4 \text{ Hz}$. The latter coupling indicates co-ordination of yttrium to the pyridyl nitrogen and the former indicates yttrium-to-imine co-ordination. Since the spectrum shows the structure to be symmetrical this concludes that in solution the yttrium in $[\text{YL}^5\text{Cl}_2(\text{H}_2\text{O})_2]^+$ is hexa-co-ordinated by the six nitrogen atoms from the macrocyclic ligand. This is supported by X-ray characterisation of $[\text{YL}^1(\text{OAc})_2]\text{ClO}_4$ and $[\text{YL}^1(\text{H}_2\text{O})(\text{OAc})](\text{OAc})(\text{ClO}_4)$.^[13]

Fig. 2.3 ¹H NMR spectrum of $[\text{YL}^5\text{Cl}_2(\text{H}_2\text{O})_2]^+$ in D₂O and at 250 MHz

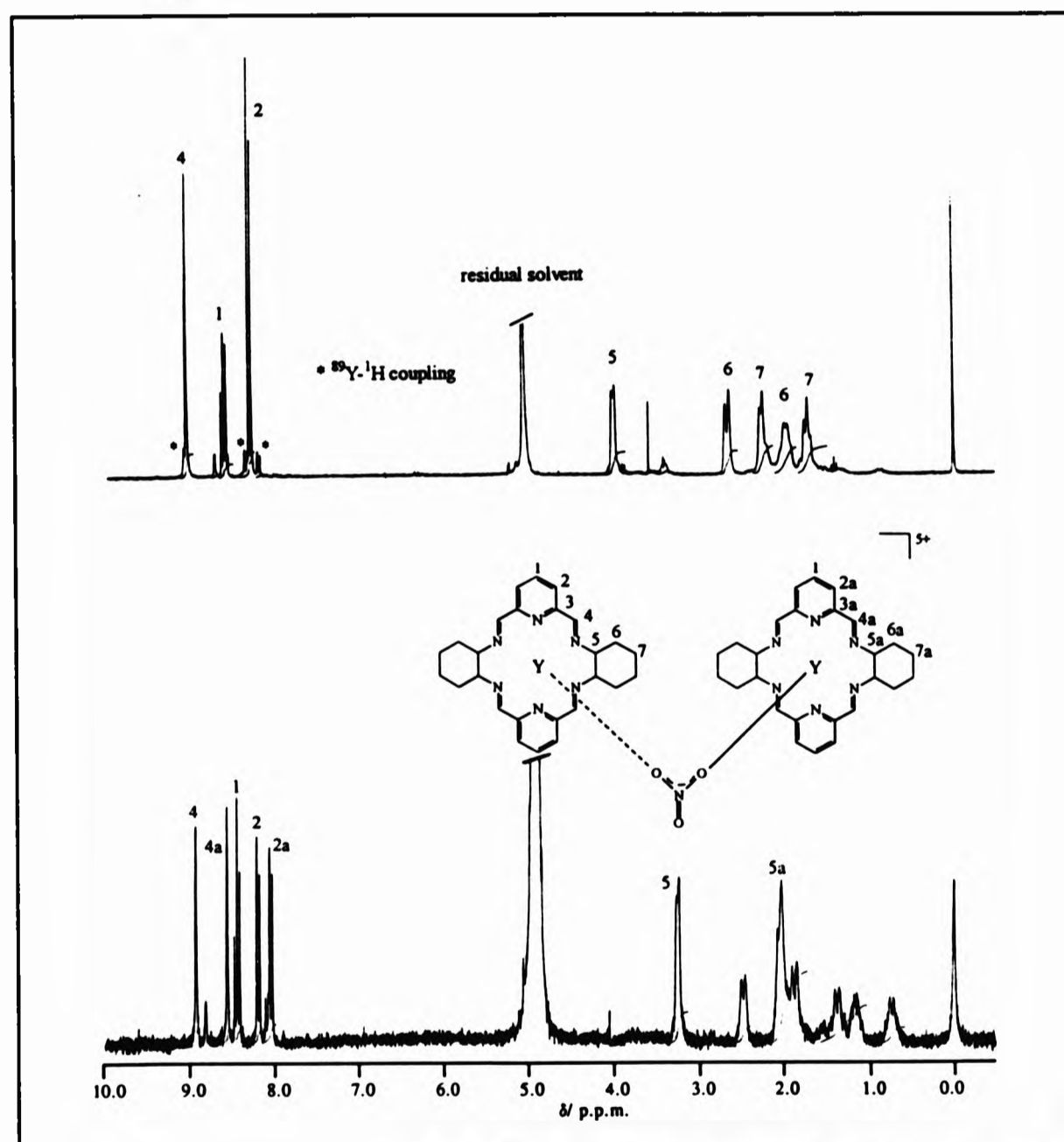
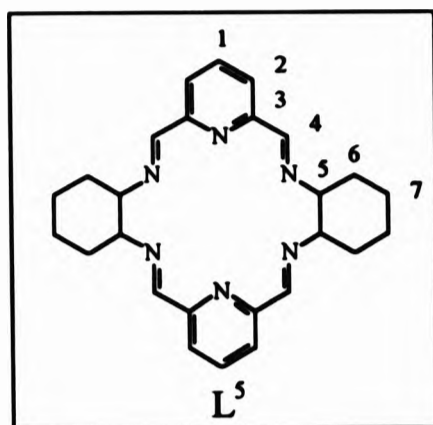


Fig. 2.4 ¹H NMR spectrum of $[\{\text{YL}^5(\text{NO}_3)_2\}_2\text{NO}_3(\text{OH})]$ in D₂O and at 250 MHz

Table 2.5 ^1H NMR^{a,b} data of $\text{BaL}^5(\text{ClO}_4)_2$,^c $[\text{LaL}^5(\text{NO}_3)_2]\text{NO}_3$,^d $[\text{YL}^5\text{Cl}_2(\text{H}_2\text{O})_2]^+$,^e and $[\{\text{YL}^5(\text{NO}_3)_2\}_2\text{NO}_3(\text{OH})]^+$ at 250 MHz
(^a represents signals from the asymmetric unit of $[\{\text{YL}^5(\text{NO}_3)_2\}_2\text{NO}_3(\text{OH})]^+$)



^1H assignment	$[\text{BaL}^5]^{2+}$	$[\text{LaL}^5(\text{NO}_3)_2]^+$	$[\text{YL}^5\text{Cl}_2]^+$	$[\{\text{YL}^5(\text{NO}_3)_2\}_2\text{NO}_3(\text{OH})]^+$
1	8.14 (t)	8.61 (t)	8.63 (t)	8.45 (t)
2	7.72 (d)	8.32 (d)	8.31 (d)	8.21 (d)
2a	-	-	-	8.06 (d)
4	8.45 (s)	9.02 (s)	9.12 (s)	8.94 (s)
4a	-	-	-	8.57 (s)
5	3.52 (m)	4.0 (m)	3.98	3.23
5a	-	-	-	e
6	1-2 (m)	1.5-2.5 (m)	2.6 and 1.9	e
6a	-	-	-	e
7	1-2 (m)	1.5-2.5 (m)	2.2 and 1.7	e
$^3J(\text{H}^1-\text{H}^2)/\text{Hz}$	7.5	7.8	7.7	7.6
$^3J(\text{H}^1-\text{H}^{2a})/\text{Hz}$	-	-	-	7.7

^ain p.p.m., ^brelative to SiMe_4 , ^cin d_6 -DMSO, ^din D_2O , ^eComplete assignment cannot be achieved

Table 2.6 The off resonance proton decoupled ^{13}C NMR^{a,b} data of $\text{BaL}^5(\text{ClO}_4)_2$,^c $[\text{YL}^5\text{Cl}_2(\text{H}_2\text{O})_2]^+$,^d and $[\{\text{YL}^5(\text{NO}_3)_2\}_2\text{NO}_3(\text{OH})]$.^d

('a' represents signals from the asymmetric unit of $[\{\text{YL}^5(\text{NO}_3)_2\}_2\text{NO}_3(\text{OH})]$)

^{13}C assignment	$[\text{BaL}^5]^+$	$[\text{YL}^5\text{Cl}_2]^+$	$[\{\text{YL}^5(\text{NO}_3)_2\}_2\text{NO}_3(\text{OH})]$
1	139.88	145.92	144.74
2	127.61	132.51	132.43
2a	-	-	131.25
3	153.37	154.59	155.00
3a	-	-	153.21
4	160.53	165.81	163.52
4a	-	-	163.43
5	67.63	70.69	70.74
5a	-	-	68.48
6	30.46	32.91	32.26
6a	-	-	31.27
7	24.25	26.90	26.16

^ain p.p.m., ^brelative to SiMe_4 , ^cin d_6 -DMSO, ^din D_2O

The region ranging from δ_{H} 1.5 - 4.0 of the spectrum due to C-H or CH_2 resonances of the cyclohexyl protons was assigned with the aid of correlated spectra (^1H -COSY). As a result of bands overlapping the multiplicities could not be accounted for. Detailed NMR characterisation of this region is given in Chapter 3. The bands are assigned in Fig. 2.3.

The ^{13}C -broad band proton decoupled NMR spectrum of $[\text{YL}^5\text{Cl}_2(\text{H}_2\text{O})_2]^+$ (Table 2.6) supports the suggestion of symmetry in the structure in that seven bands were observed which implies the presence of seven different environments, in other words, one quarter of the structure. Yttrium coupling is also observed in this

spectrum, occurring at four carbon sites, C² - C⁵. The coupling constants are listed in Table 2.7.

Table 2.7 Coupling constants arising from yttrium-89 - carbon-13 coupling in $[YL^5Cl_2(H_2O)_2]^+$

Coupling	$^nJ(^{89}Y - C)$ (Hz)	n
$^{89}Y - C^2$	286.3	3
$^{89}Y - C^3$	190.7	2
$^{89}Y - C^4$	320.0	2
$^{89}Y - C^5$	542.3	2

The 1H NMR of $[Y(L^5(NO_3)_2)_2NO_3(OH)]$ (Fig. 2.4 and Table 2.5) shows the presence of two imine proton *singlets* (H⁴ and H^{4a}) at δ_H 8.94 and 8.57 both integrating for four protons each. Two *doublets* centred at δ_H 8.21 and 8.06, integrating for four protons each, are assigned to the pyridine β -protons (H² and H^{2a}). The presence of two *singlets* for the imino protons and two *doublets* for the β -protons on the pyridine ring suggest some form of asymmetry about the dimer. The asymmetry is about the dimer itself *i.e.* both monomeric units are asymmetric with respect to each other.

Interestingly, the γ -protons on the pyridine arise only as one *triplet* (H¹) and integrate for four protons at δ_H 8.45. The coupling constants are $^3J(H^1 - H^2) = 7.6$ Hz and $^3J(H^1 - H^{2a}) = 7.7$ Hz.

It is impossible to pin-point which protons of 2 or 2a to assign to the two *doublets* at δ_H 8.21 and 8.06. H² can be assigned to the *doublet* at δ_H 8.21 and therefore H^{2a} is assigned to δ_H 8.06. But *vice-versa* is equally acceptable. The same applies for the two *singlet* bands of the imino protons H⁴ and H^{4a} for the two bands at δ_H 8.94 and 8.57. Due to noise, broadness of bands and possibly the low concentration under which the spectrum was ran, satellites from yttrium-proton coupling were not

observed.

The region 0.5 - 3.5 p.p.m due to the alkyl resonances of the cyclohexane also indicates the asymmetry in the dimer compared to the spectrum of $[\text{YL}^5\text{Cl}_2(\text{H}_2\text{O})_2]^+$ in the same region. The same band at δ_{H} 3.23 integrating for four protons due to H^5 is seen for $[\text{YL}^5\text{Cl}_2(\text{H}_2\text{O})_2]^+$ at δ_{H} 3.98. Complete assignments of this region of the spectrum of $[\{\text{YL}^5(\text{NO}_3)_2\}_2\text{NO}_3(\text{OH})]$ cannot be accomplished.

In agreement with the ^1H NMR spectrum, the ^{13}C -broad band proton decoupled spectrum of $[\{\text{YL}^5(\text{NO}_3)_2\}_2\text{NO}_3(\text{OH})]$ (Table 2.6) has two bands at δ_{C} 163.52 and 163.43 due to the imine carbon atoms C^4 and C^{4a} , two bands at δ_{C} 132.43 and 131.25 due to C^2 and C^{2a} , the β -carbon atoms on the pyridine ring, C^1 , at δ_{C} 144.74. Two bands are also observed for the α -carbon atom, C^3 and C^{3a} at δ_{C} 155.00 and 153.21. The alkyl region follows a similar pattern with two bands at δ_{C} 70.74 and 68.48 for C^5 and C^{5a} , two bands at δ_{C} 32.26 and 31.27 for C^6 and C^{6a} and a band at δ_{C} 26.16 for C^7 . Again, due to excess noise, satellites were not observed due to yttrium - carbon coupling in the ^{13}C -NMR spectrum.

The NMR spectra of $[\text{BaL}^5](\text{ClO}_4)_2$ and $[\text{LaL}^5(\text{NO}_3)_2]^+$ were similar to the spectra of $[\text{YL}^5\text{Cl}_2(\text{H}_2\text{O})_2]^+$. The chemical shifts are compared in Tables 2.5 and 2.6.

Whilst this work was being carried out, Tsubomura^[35] published complexes of the type $\text{LnL}^5(\text{NO}_3)_3.n\text{H}_2\text{O}$ (where $\text{Ln} = \text{La}, \text{Eu}$ and Tb and $n = 0-2$). Whereas these workers used specifically 1(*R*), 2(*R*)-1,2-diaminocyclohexane, in this work (\pm)-*trans*-1,2-diaminocyclohexane was employed. These workers also used nitrate metal salts but observed only monomeric species. This may postulate that not only does the μ -bridging occur with co-ordinating counterions but also involves the larger lanthanide metals (Ce - Eu) as far as the system L^5 is concerned. Possibly, the ionic radii of these metals play a rôle and therefore the resulting dihedral angle of the diimino pyridine section of each monomer (Section 2.4.1.3) also contributes. $[\{\text{EuL}^1(\text{OAc})\}_2(\mu\text{-CO}_3)](\text{OH})_2.7\text{H}_2\text{O}$ ^[36] adopts a similar arrangement,

the bridging of two monomers being completed by a bis-chelating carbonato group.

Tsubomura also showed, using CD and circularly polarised luminescence, that the macrocyclic complexes, $\text{LnL}^5(\text{NO}_3)_3 \cdot n\text{H}_2\text{O}$, possess a D_2 symmetry and their structure to be twisted and oriented at counterclockwise positions^[35] (Fig. 2.5). The crystal structure of $[\text{GdL}^5\text{Cl}_2(\text{H}_2\text{O})]\text{Cl}$ (section 2.4.1.3), as determined by this work, justifies their prediction.

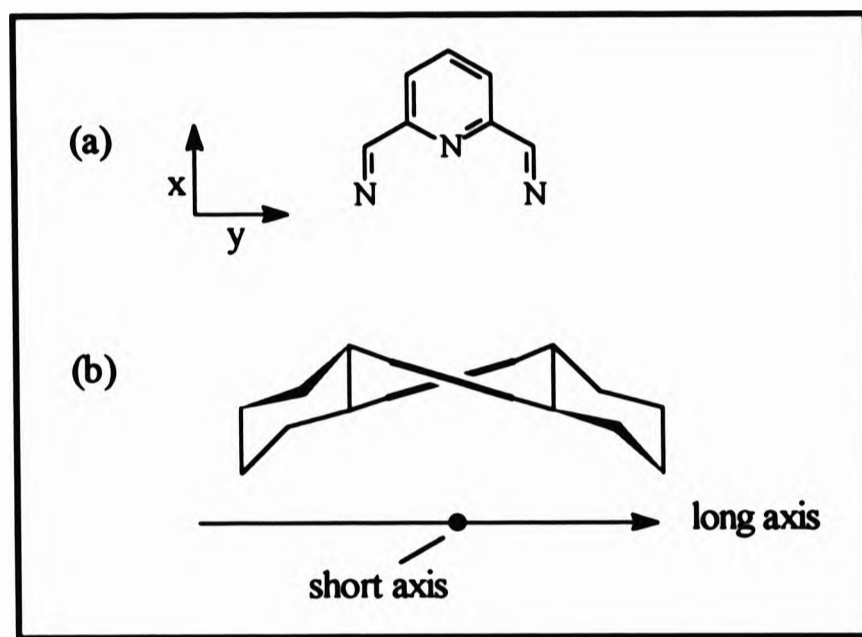


Fig. 2.5 (a) Structure of the chromophore and (b) twisted-structure model of the R,R - L^5 ligand (reproduced from ref. 35)

Fig. 2.6 shows representations of some of the arrangements which can be adopted by linear chain 1,2-diaminocyclohexane complexes.^[37] These arrangements depend on the conformation of the amine substituents on the substituted cyclohexane ring. *Trans*- R,R -isomers only adopt the metal complexation c (Fig. 2.6). *Cis*-ligands result in the structures b, d and e. For a given chirality of a *trans*-1,2-diaminocyclohexane, the conformation of the chelate ring is defined and no conformational inversions are possible in the complex as is the case for the complex $[\text{LnL}^5]^{3+}$. If both of the cyclohexane *trans*-derivatives are (+) or (-) (*i.e.* R,R) a $\lambda\lambda$ or $\delta\delta$ conformation is obtained (Fig 2.5a). However, if one is (-) and the other (+) a $\lambda\delta$ (*meso*) conformation is expected (Fig. 2.6a). *Cis*-isomers cannot be resolved so $\lambda\lambda$, $\delta\delta$ and $\lambda\delta$ are all possible.

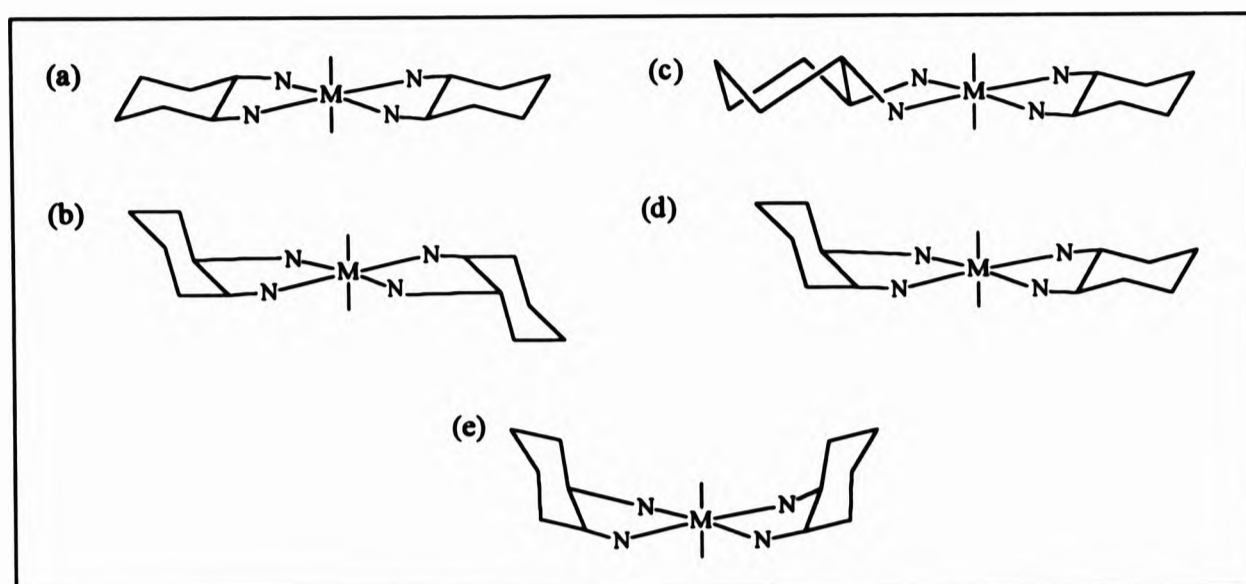


Fig. 2.6 Representations of some of the possible structures of linear chain 1,2-diaminocyclohexane complexes (reproduced from ref. 37)

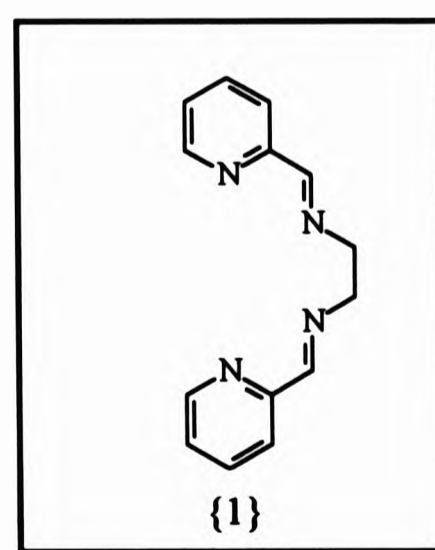
2.4.1.3 The Solid State Characterisation of $[\text{GdL}^5(\text{H}_2\text{O})_3]\text{Cl}_3 \cdot 3\text{H}_2\text{O}$

Recrystallisation of $[\text{GdL}^5\text{Cl}_2(\text{H}_2\text{O})]\text{Cl}$ from methanol afforded colourless crystals suitable for crystallographic analysis (Fig. 2.7).

The asymmetric unit of the crystal consisted of a complex cation, three chloride counter-ions, three co-ordinated water molecules and three molecules of water of crystallisation leading to the formulation $[\text{GdL}^5(\text{H}_2\text{O})_3]\text{Cl}_3 \cdot 3\text{H}_2\text{O}$. This is in contrast to the elemental and LSIMS analyses of the amorphous solid, where only one water molecule was found to co-ordinate to the metal ion.

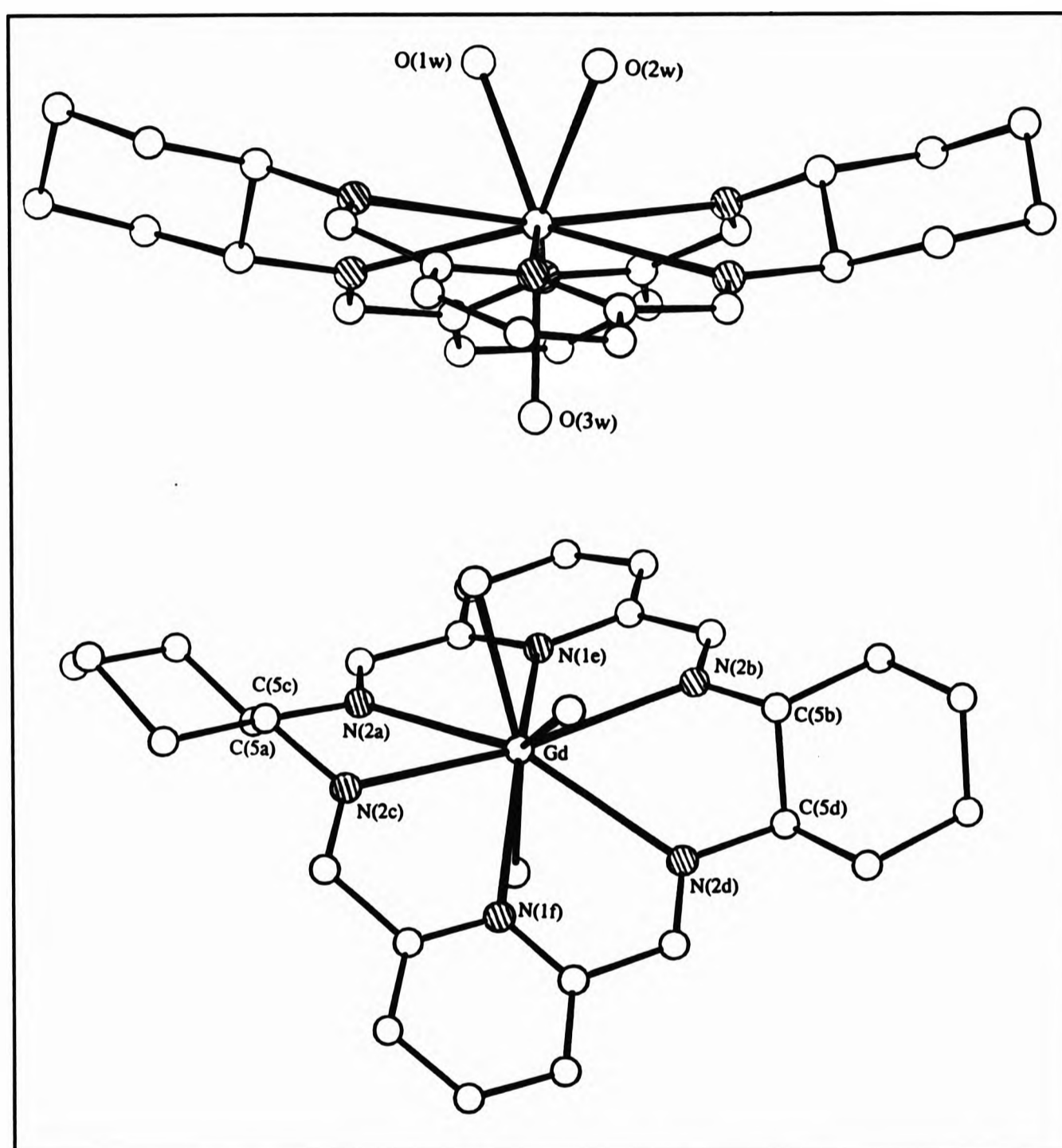
The structure of $[\text{GdL}^5(\text{H}_2\text{O})_3]\text{Cl}_3 \cdot 3\text{H}_2\text{O}$, consisting wholly of non-co-ordinating counter-ions, is the first to be reported.^[38]

The gadolinium ion has an irregular nine co-ordinate geometry, the donor atoms being six nitrogen atoms from the macrocycle and three oxygen atoms from the co-ordinated water molecules. Selected bond lengths are shown in Table 2.8 and compared to the



only other crystal structure of a gadolinium 18-membered macrocycle, $[\text{GdL}^1(\text{OAc})_2]\text{Cl}\cdot 4\text{H}_2\text{O}$,^[39] to have been documented and also to $\text{Gd}\{1\}(\text{NO}_3)_3$,^[40] a related open chain diimino structure.

Fig. 2.7 *The perspective views of $[\text{GdL}^5(\text{H}_2\text{O})_3]^{3+}$*



Because the gadolinium ion in $[\text{GdL}^5(\text{H}_2\text{O})_3]\text{Cl}_3\cdot 3\text{H}_2\text{O}$ is nine co-ordinate and in $[\text{GdL}^1(\text{OAc})_2]\text{Cl}\cdot 4\text{H}_2\text{O}$ and $\text{Gd}\{1\}(\text{NO}_3)_3$ are both ten co-ordinate, a comparison of bond lengths can be quite misleading. The average metal-nitrogen atom bond length in the acyclic analogue is 2.54 Å, that of $[\text{GdL}^1(\text{OAc})_2]\text{Cl}\cdot 4\text{H}_2\text{O}$ being 2.62 Å and

in the case of $[\text{GdL}^5(\text{H}_2\text{O})_3]\text{Cl}_3 \cdot 3\text{H}_2\text{O}$ also 2.62 Å. The Gd - N bond lengths are longer in both of the macrocycles compared to the acyclic analogue. The reason for this is that the Gd - N distances in $\text{Gd}\{1\}(\text{NO}_3)_3$ are a result of non-constrained Gd-N bond lengths, the much longer distances in the macrocycles being due to a mismatch in cavity and metal size. Whereas the acyclic ligand can get as close to the metal as it can, the rigidity imposed on the macrocycle restricts the donor atoms from approaching just as close.

The two water ligands in the structure of $[\text{GdL}^5(\text{H}_2\text{O})_3]^{3+}$, O(1w) and O(2w), are *cis* to each other and are in sufficiently close contact to indicate hydrogen bonding interaction [O(1w)...O(2w) 2.17 Å]. The co-ordinated oxygen atom of the third water ligand, O(3w), is within hydrogen bonding distance from one of the three water molecules of crystallisation, O(3w)...O(5w) 2.65 Å. The closest contact between the water molecules of crystallisation and the gadolinium metal is Gd...O(5w) 4.49 Å.

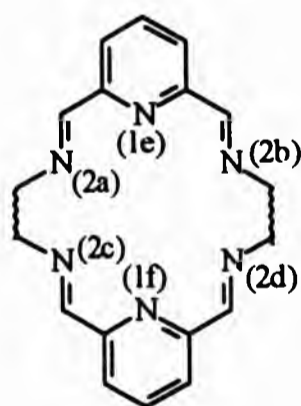
The inner great ring of the macrocyclic ligand may be divided into two sections each of which is almost planar. The first section comprises the nine atoms from C(5a) through N(1e) to C(5b) [maximum deviation from the least squares mean plane of 0.137 Å for C(5a)] and the second section comprises the nine atoms from C(5c) through N(1f) to C(5d) [maximum deviation from the least squares mean plane of 0.126 Å for C(5d)]. The dihedral angle between the two planes is 42.83°; these approximately planar sections are consistent with the regions of extended conjugation, broken by the cyclohexane rings. The two sections are folded away from the two *cis*-water molecules O(1w) and O(2w), towards the third co-ordinated water, O(3w).

Similar yttrium and lanthanide structures of symmetrical 18-membered hexaaza macrocycles have been reported including those of L^1 ,^[4,5,8,11-13,15-17,36] L^3 and L^4 ^[8,14] and the two diimino-pyridine sections in these structures also exhibit characteristic non-coplanarity.

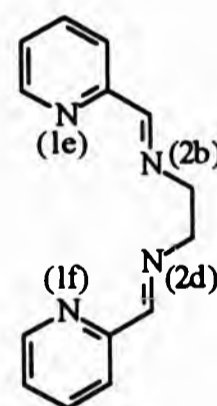
Table 2.8 Selected bond distances^{a,b} of the metal co-ordination sphere of [GdL^S(H₂O)₃]Cl₃·3H₂O, [GdL^L(OAc)₂]Cl·4H₂O and Gd{1}(NO₃)₃

BOND	[GdL ^S (H ₂ O) ₃] ³⁺	[GdL ^L (OAc) ₂] ⁺	[Gd{1}(NO ₃) ₃]
Gd - O(1w)	2.385(9)	-	-
Gd - O(2w)	2.330(9)	-	-
Gd - O(3w)	2.319(10)	-	-
Gd - N(2a)	2.632(11)	2.563(6)	-
Gd - N(2b)	2.583(12)	2.654(6)	2.513(8)
Gd - N(2c)	2.571(11)	2.643(6)	-
Gd - N(2d)	2.692(11)	2.602(6)	2.500(9)
Gd - N(1e)	2.618(11)	2.642(6)	2.606(8)
Gd - N(1f)	2.638(10)	2.627(6)	2.546(7)

^ain Å, ^bESDs shown in parentheses



L^L/L^S



{1}

The deviation of folding was initially believed to have been dictated by the *R,R*-, *R,R*-configuration of the cyclohexane ring carbon atoms C(5a), C(5c), C(5b) and C(5d) but although this is a contributing factor in the case of $[\text{GdL}^5(\text{H}_2\text{O})_3]^{3+}$ similar *butterfly* folding arrangements are adopted by other 18-membered macrocyclic ligands chelated to lanthanide metals such that the size of the metal as well as counter-ions or other co-ordinating ligands need to be taken into account. In all cases the macrocyclic ligand folds away from the hemisphere containing the two co-ordinating ligands as a result of steric interaction. This relieves the strain in the macrocycle and minimises repulsion between the heteroatoms and therefore allows optimum co-ordination at the metal.

Progressing along the lanthanide metal series, complexes of L^1 or L^2 show a decrease in co-ordination number of the metal irrespective of counter-ion,^[41] La = 12, Ce = 11, Nd = 10, Sm = 10, Lu = 9 (Table 2.9).

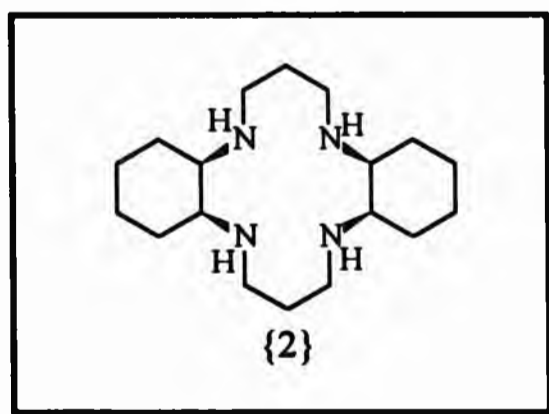
The dihedral angle between the *wing* planes containing the two pyridine rings generally increases with decreasing ionic radius of the metal (*i.e.* along the lanthanide series) but with no apparent trend as it also depends on the size/bulk of the counter-ion or the non-macrocyclic co-ordinating ligand. The side-chain also plays an important part, *i.e.* "the presence of aromatic side-chains reduces the flexibility of the structure relative to ligands of L^1 and L^2 where the aliphatic $-\text{CH}_2-\text{CH}_2-$ side-chain function as adjustable hinges."^[42] As a result, the dihedral angle for the structures of L^1 , L^2 and L^5 has two components associated with it: a bending at the diamine bridges and a twisting about an axis through the pyridine nitrogen atoms as observed by solutions studies^[35] (Fig. 2.5). The conformation of the macrocycles along the lanthanide series ranges from being almost purely twisted for the lanthanum complexes to primarily bent for the lutetium complexes. The gadolinium macrocycles of L^1 and L^5 are a combination of these two extremes, the dihedral angle for $[\text{GdL}^1(\text{OAc})_2]\text{Cl}4\text{H}_2\text{O}$ being 48° . "These distortions would be expected to decrease the cavity size of the macrocycle relative to a planar form. However, there appears to be no simple correlation between the degree of bend/ twist

character and the ionic radii of the metal, since the cerium (dihedral angle = 59.0°) and neodymium (dihedral angle = 63.9°) complexes appear to be more like the lutetium (dihedral angle = 65.6°) than the lanthanum complex (dihedral angle = 26.7°)^[39] (Table 2.9).

With large lanthanide ions, such as lanthanum, three nitrate groups can be bidentate on the metal, again the macrocycle bending towards the less hindered side. On decreasing the ionic radii, as with praseodymium (dihedral angle = 69.7°), one nitrate position is replaced by the less hindered methanol and with samarium (dihedral angle not reported), two nitrate ligands are substituted by a hydroxy group and a water molecule. With the less hindering thiocyanato anions, NCS, the resulting complexes are $ML^1(NCS)_3$ ($M = Y, Eu$) with relatively large dihedral angles of *ca.* 68.9° .

To summarise, the trend of folding of the macrocyclic ligand towards the single coordinating ligand is more dependent on steric requirements of the macrocyclic ligand and less dependent on the metal size yet the degree of non-coplanarity of the macrocycle increases as the co-ordination number (and the metal size) decreases. So it can be said that as the metal size increases the ligand buckles to accommodate and maintain hexadentate contact.

$Ni\{2\}(NO_3)_2$, a nickel(II) cyclam derivative also adopts the *butterfly* fold but this is expected since *cis*-1,2-diaminocyclohexane was the reactant in its synthesis.



The cross-over bonding (Fig. 2.5b) is evident in the crystal structure of $[GdL^5(H_2O)_3]Cl_3 \cdot 3H_2O$ due to the *trans*- (locked) conformation of the 1,2-diaminocyclohexane. This also occurs for acyclic complexes.^[43]

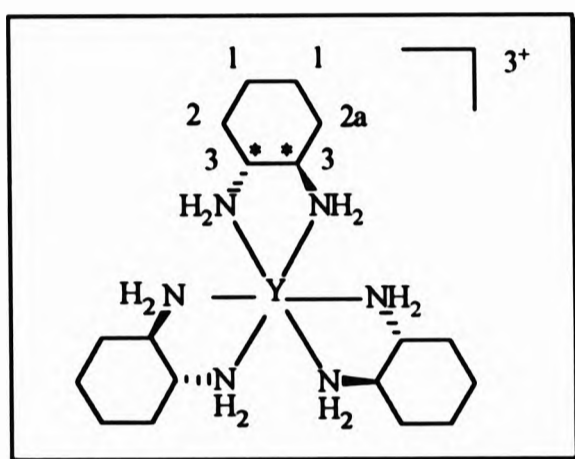
Table 2.9 The dihedral angles of L¹, L², L⁴, and L⁵ macrocyclic ligands along the lanthanide series and yttrium

COMPLEX	CN	IONIC RADIUS ^a (Å)	DIHEDRAL ANGLE (°)	Ref.
[LaL ¹ (NO ₃) ₃]	12	1.016	26.7	12
[LaL ² (OAc)(NCS) ₂]	10		32.7	42
[CeL ¹ (NO ₃) ₂ (H ₂ O)]NO ₃ ·H ₂ O	11	1.034	59.0	12
[PrL ⁴ (NO ₃) ₂ (MeOH)]ClO ₄	11	1.013	69.7	14
[NdL ¹ (OAc) ₂]Cl·4H ₂ O	10	0.995	47.2	16
[{NdL ¹ (NO ₃ (H ₂ O) ₂ }] ₂]NO ₃ (ClO ₄) ₃ ·4H ₂ O	10		61.6, 63.9	12
[SmL ² (NO ₃) ₂ (OH)(H ₂ O)]NO ₃ ·2MeOH	10	0.964	-	11
[EuL ¹ (OAc) ₂]Cl·4H ₂ O	10	0.950	47.6	16
[EuL ¹ (OAc) ₂](AOC)·9H ₂ O	10		57.5	17
[EuL ¹ (NCS) ₃]	9		77.9, 68.7	15
[GdL ¹ (OAc) ₂]Cl·4H ₂ O	10	0.938	48.0	39
[GdL ³ (H ₂ O) ₃]Cl ₃ ·3H ₂ O	9		42.8	38*
[LuL ¹ (OAc)(H ₂ O)](MeOH)(OH)(ClO ₄)	9	0.848	65.6	5
[YL ¹ (OAc) ₂](ClO ₄)(MeOH)	9	0.893	64.3	13
[YL ¹ (NCS) ₃]	9		68.9	15

*this work, ^aionic radii quoted from ref. 44

2.4.2 The Non-Template Synthesis of L⁶

As reported previously,^[35] and also observed in this work, the reaction of 2,6-diacetylpyridine and (\pm)-*trans*-1,2-diaminocyclohexane in the presence of $GdX_3 \cdot nH_2O$ ($X = OAc, Cl, NO_3; n = 6$) as a template did not yield any macrocyclic products as in the case of $[GdL^3Cl_2(MeOH)(H_2O)]^+$ and $[GdL^5(H_2O)_3]^{3+}$. On repeating the procedure at low methanolic dilution with yttrium(III) nitrate pentahydrate a white solid precipitated instantly which analysed for tris[(\pm)-*trans*-1,2-diaminocyclohexane] nitrate yttrium(III).



*Tris[(\pm)-*trans*-1,2-diaminocyclohexane] yttrium(III) with NMR assignments. (nitrate groups are omitted for clarity)*

This structure is supported by the IR spectrum (Fig. 2.8) which shows no imine bands (*ca.* 1650 - 1620 cm^{-1}) which are characteristic of the macrocycles discussed in this chapter.

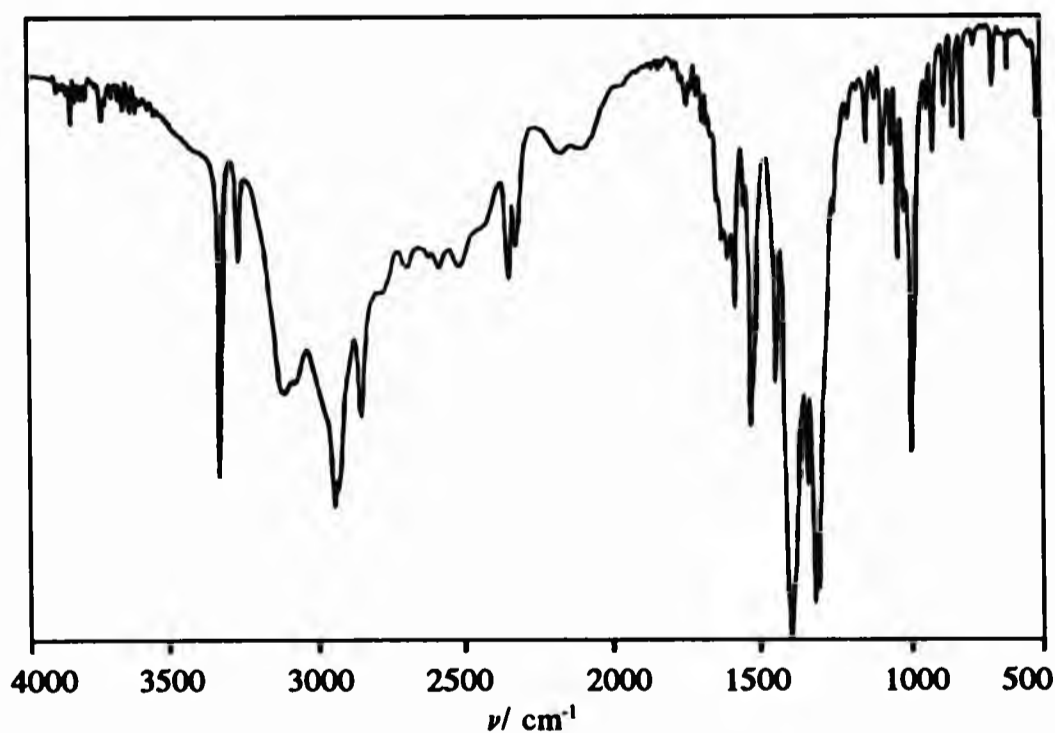
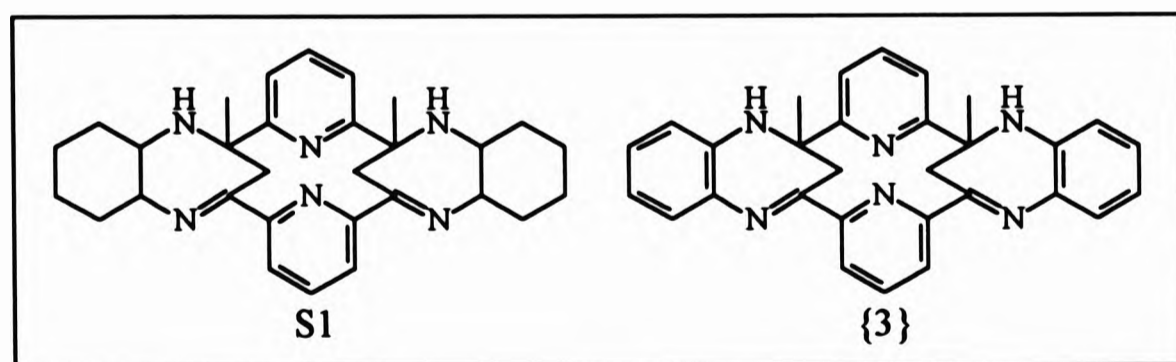


Fig. 2.8 *The infrared spectrum of tris[(\pm)-*trans*-1,2-diaminocyclohexane] nitrate yttrium(III)*

Instead, two sharp bands at 3337 and 3278 cm^{-1} represent the co-ordinated secondary amine of (\pm)-*trans*-1,2-diaminocyclohexane and a medium band at 1590 cm^{-1} due to the secondary amine stretching frequencies. All three of these bands have moved to lower frequencies as a result of metal co-ordination compared to the IR spectrum of the uncomplexed amine.

The ^1H NMR spectrum of tris[(\pm)-*trans*-1,2-diaminocyclohexane] nitrate yttrium(III) in D_2O and at 250 MHz showed four relatively broad resonances, their centres being at δ_{H} 1.32, 1.76, 1.99, 2.78 and integrating for 2 (H^1), 1 (H^2), 1 ($\text{H}^{2\text{a}}$) and 1 (H^3) protons respectively. The acidic, amino protons were not observed due to exchange with deuterium. In the ^{13}C -off resonance broad band proton decoupled NMR spectrum three bands were observed at δ_{C} 26.74 (C^1), 34.69 (C^2 and $\text{C}^{2\text{a}}$) and 57.39 (C^3). No bands were present due to 2,6-diacetylpyridine in the aromatic regions of both the ^1H - and ^{13}C -NMR spectra.

Tsubomura *et al.*^[35] claimed that electrostatic repulsion between the methyl groups and the hydrogen atoms on the cyclohexane rings prevent the cyclisation and therefore the synthesis of L^6 from proceeding. As far as the template synthesis of L^6 , using optically pure 1,2-diaminocyclohexane, is concerned, this is justified by molecular models.



When GdX_3 and $\text{Y}(\text{NO}_3)_3 \cdot 5\text{H}_2\text{O}$ were replaced by $\text{BaQ}_2 \cdot n\text{H}_2\text{O}$ ($\text{Q} = \text{Cl}$, $n = 2$; $\text{Q} = \text{ClO}_4$, $n = 0$) the reaction followed a similar pattern as documented by Benetollo *et al.*^[7] during the template synthesis of $[\text{EuL}^3]^{3+}$ and $[\text{CeL}^3]^{3+}$ (Fig. 2.9).

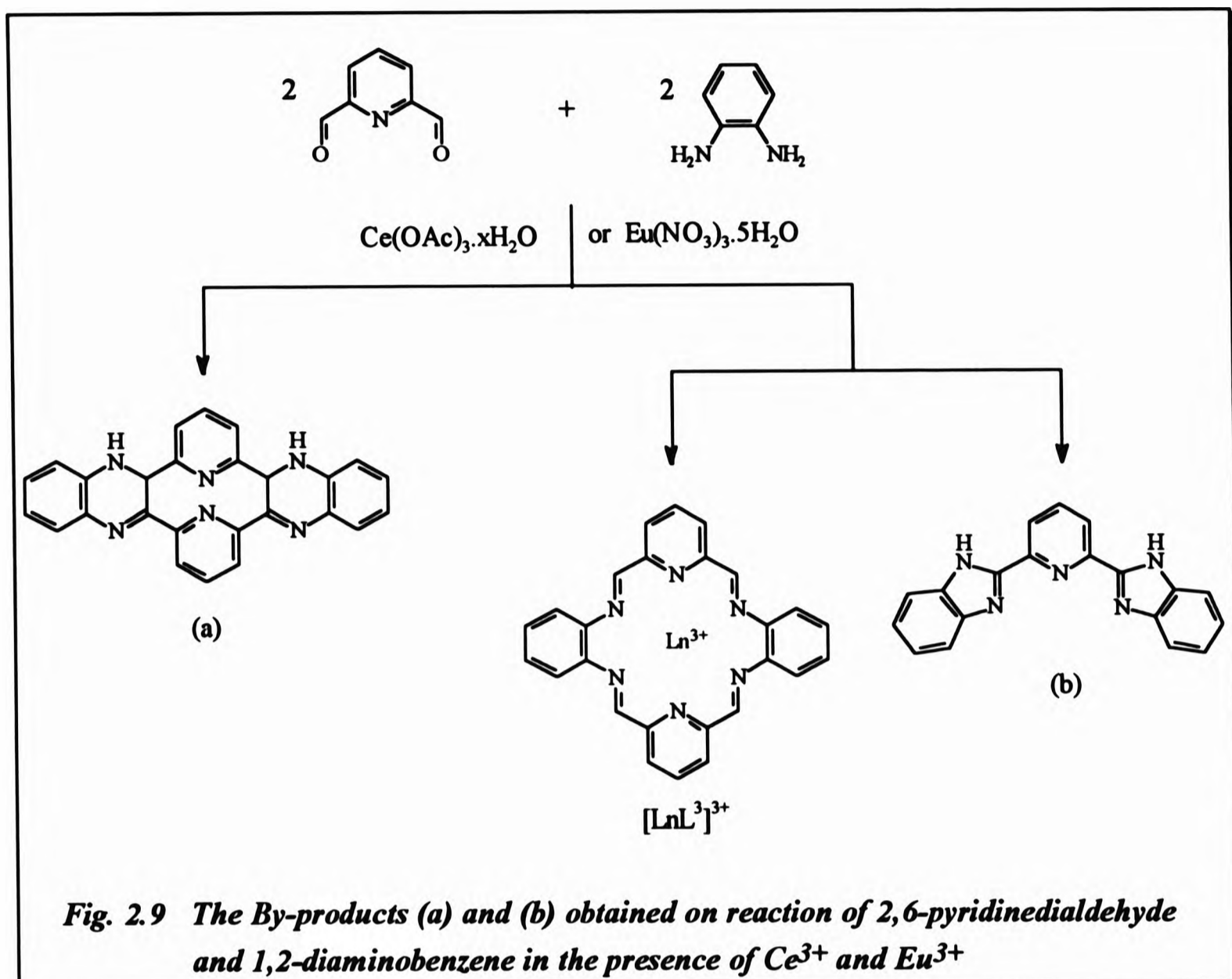
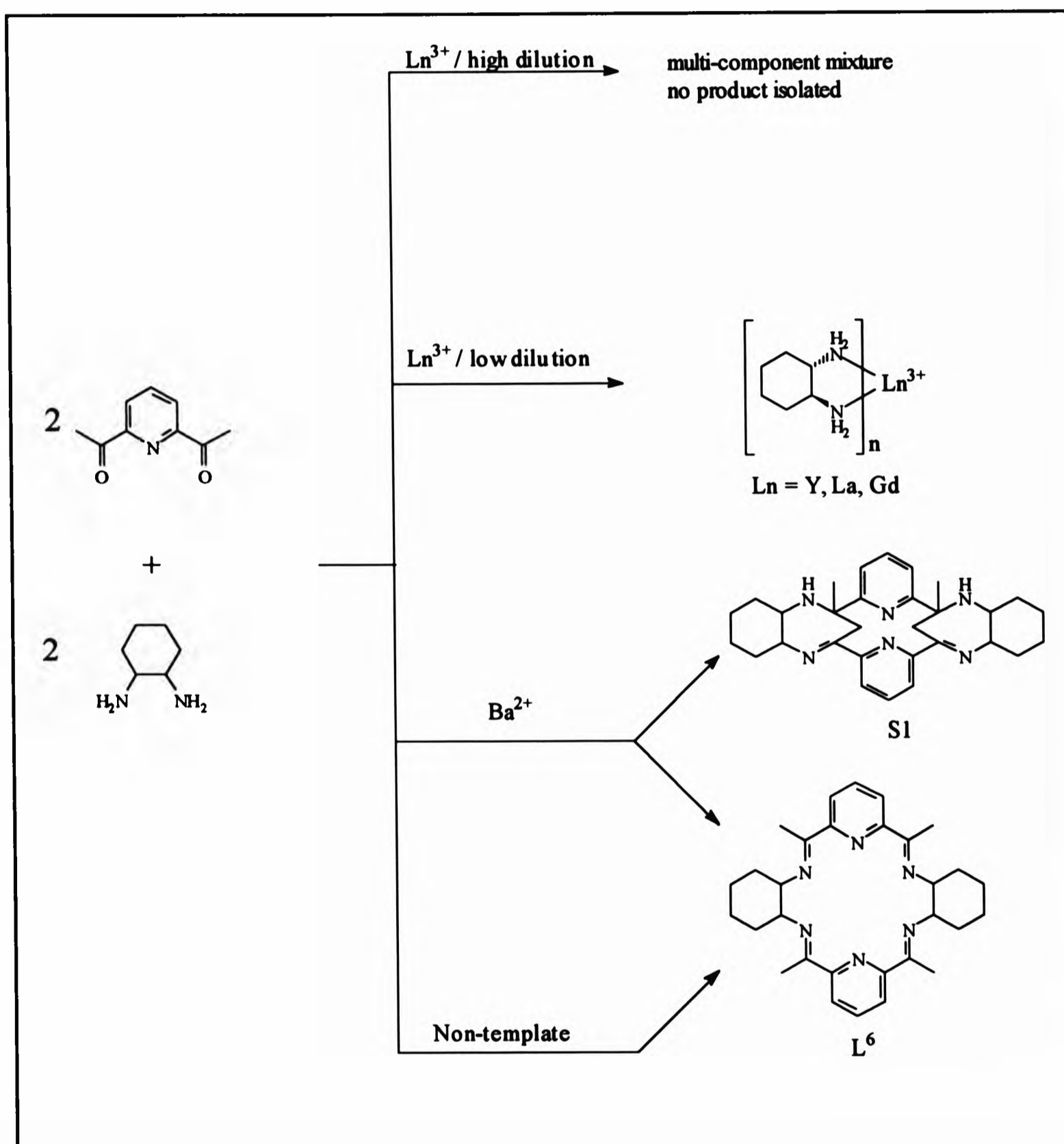


Fig. 2.9 The By-products (a) and (b) obtained on reaction of 2,6-pyridinedialdehyde and 1,2-diaminobenzene in the presence of Ce^{3+} and Eu^{3+}

A white solid, S1, separated first from the reaction mixture during reflux. On filtering hot and allowing the filtrate to stand a white solid having the same composition as S1, $\text{C}_{30}\text{H}_{38}\text{N}_6$, but different IR and NMR spectra, was also isolated. The latter solid analysed for the macrocyclic ligand, L^6 , alone with no trace of the metal. This suggested that L^6 could be formed in the absence of the metal and indeed this proved to be the case. To determine whether this product was L^6 or the structure adopted by the phenyl derivative, {3}, as discovered by Nelson,^[45] a crystallographic analysis was undertaken and concluded that an 18-membered macrocycle was formed (section 2.4.2.2). Fig. 2.10 summarises the various results obtained in the attempt to isolate L^6 .

Fig. 2.10 The results obtained in the attempts to isolate L^6



2.4.2.1 Spectroscopic Characterisation of L⁶ and S1

The IR spectra of L⁶ and S1 (Fig. 2.11) show some contrasting differences. The spectrum of L⁶ is similar to that obtained for L⁵ (Fig. 2.1) with the major bands in the spectrum of L⁶ shifting by *ca.* 10-20 cm⁻¹ compared to those of L⁵ (Table 2.10).

Table 2.10 The assignments of the infrared^a spectra of L⁵, L⁶ and S1 and {3}

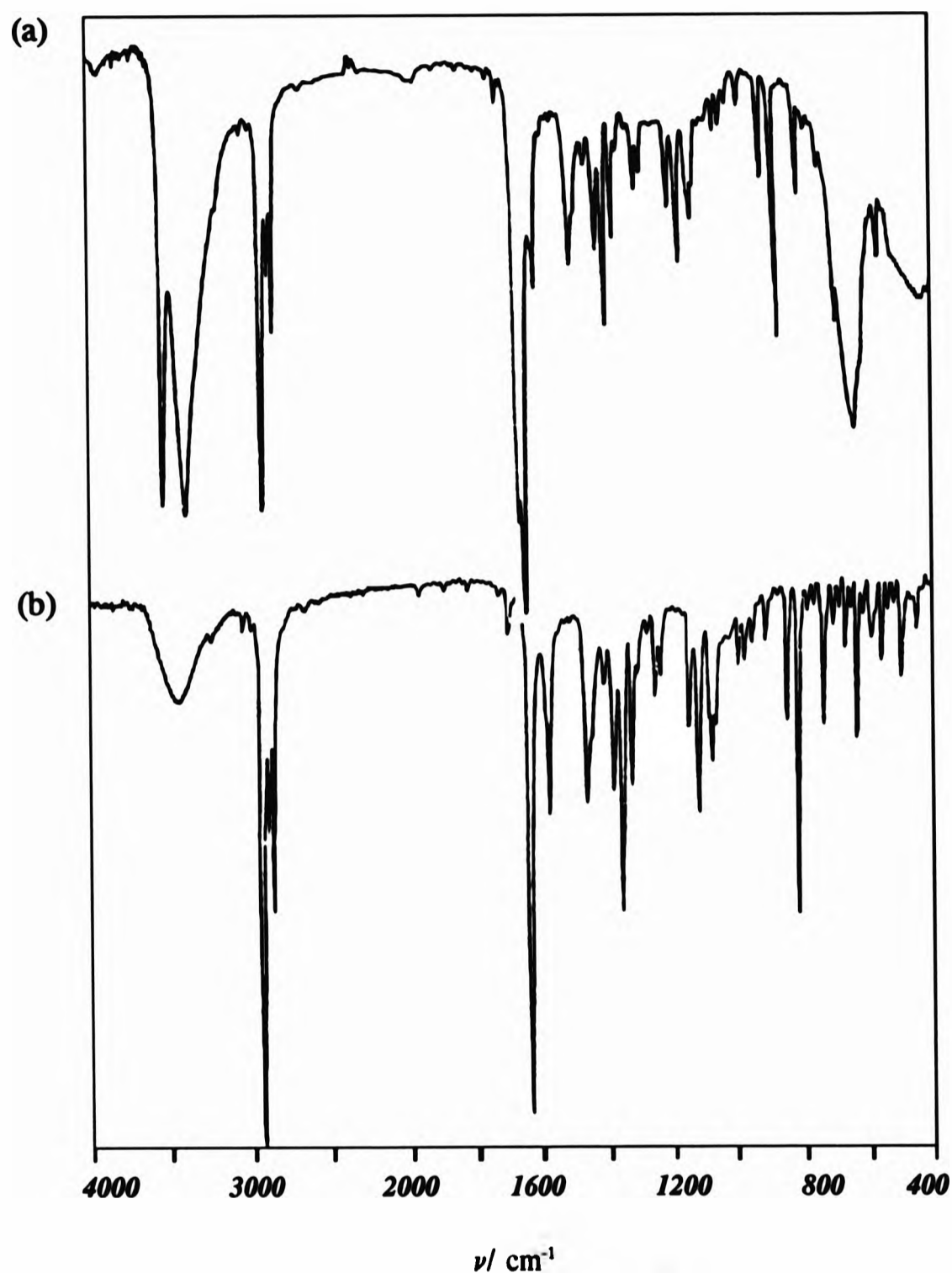
COMPOUND	$\nu(\text{C}=\text{N})_{\text{imine}}$	$\nu(\text{C}=\text{N})_{\text{py}}$	$\nu(\text{N}-\text{H})$	$\nu(\text{C}-\text{H})_{\text{CH,CH}_2}$	$\nu(\text{C}-\text{H})_{\text{Me}}$
L ⁵	1639s	1585m	-	2936s, 2836s	-
L ⁶	1629s	1567m	-	2926s, 2854m	2885m
S1	1627s,	1567m	3540s, 3399s, 1612s	2926s, 2854m	2885m
{3}	b	b	3336	b	b

^ain cm⁻¹, ^bnot reported

The presence of methyl groups in L⁶ causes the imine bonds to absorb at 1629 cm⁻¹, 10 cm⁻¹ lower than that observed for L⁵ due to the inductive effect. The same applies for the $\nu(\text{C}=\text{N})$ of the pyridine ring and the two $\nu(\text{C}-\text{H})$ absorption bands of the cyclohexane rings. For both L⁶ and S1 the medium absorption band at 2885 cm⁻¹ is assigned to C-H stretch of the methyl substituent as this is absent in the spectrum of L⁵.

The contrasting bands found in the spectrum of S1 are two strong, sharp bands at 3540 cm⁻¹ and 3399 cm⁻¹ and are assigned to N-H stretching modes of a secondary amine. Although these bands appear to be at extremely high wavenumbers, the normal range of the N-H stretching modes of solid samples being 3350 - 3200 cm⁻¹ and especially that two bands are observed instead of just one that is normally seen, such unexplained high frequencies and extra bands have been previously reported.^[46]

Fig. 2.11 The infrared spectra of (a) S1 and (b) L⁶ (% transmittance is arbitrary)



This also explains the strong, sharp band at 1610 cm⁻¹ as a result of $\nu(\text{N-H})$ bending vibrations. Alongside this band and of equal strength and sharpness is a band absorbing at 1627 cm⁻¹ and is assigned to $\nu(\text{C}=\text{N})$ of the imine function. The N-H out of plane bend is typically depicted as a broad band in the region 630 - 450 cm⁻¹.

The LSIM spectra of both L⁶ and S1 were identical having a molecular ion of $[\text{M} + \text{H}]^+$, m/z 483, this being consistent with $\text{C}_{30}\text{H}_{38}\text{N}_6$. The spectra were very simple in that three main bands were present at m/z 483, 405 and 248 with relative

abundances of 100, 95 and 80% respectively. That L^6 does not fragment in the same manner as L^5 (§ 2.4.1.2, Fig. 2.2) suggests that the former rearranges to S1 before fragmenting. This would explain the identical fragmentation pattern of L^6 and S1. To support the argument of rearrangement it is evident that metal-free structures containing the hexaaza backbone, such as $L^1 - L^5$, have the characteristic fragment $M/2$. This was observed for all the metal-free ligands characterised in this study (See Chapters 3-5), L^6 being the only exception. The latter fragmentation, with m/z 248, cannot be assigned. The proposed fragmentation upon rearrangement is shown in Fig. 2.12.

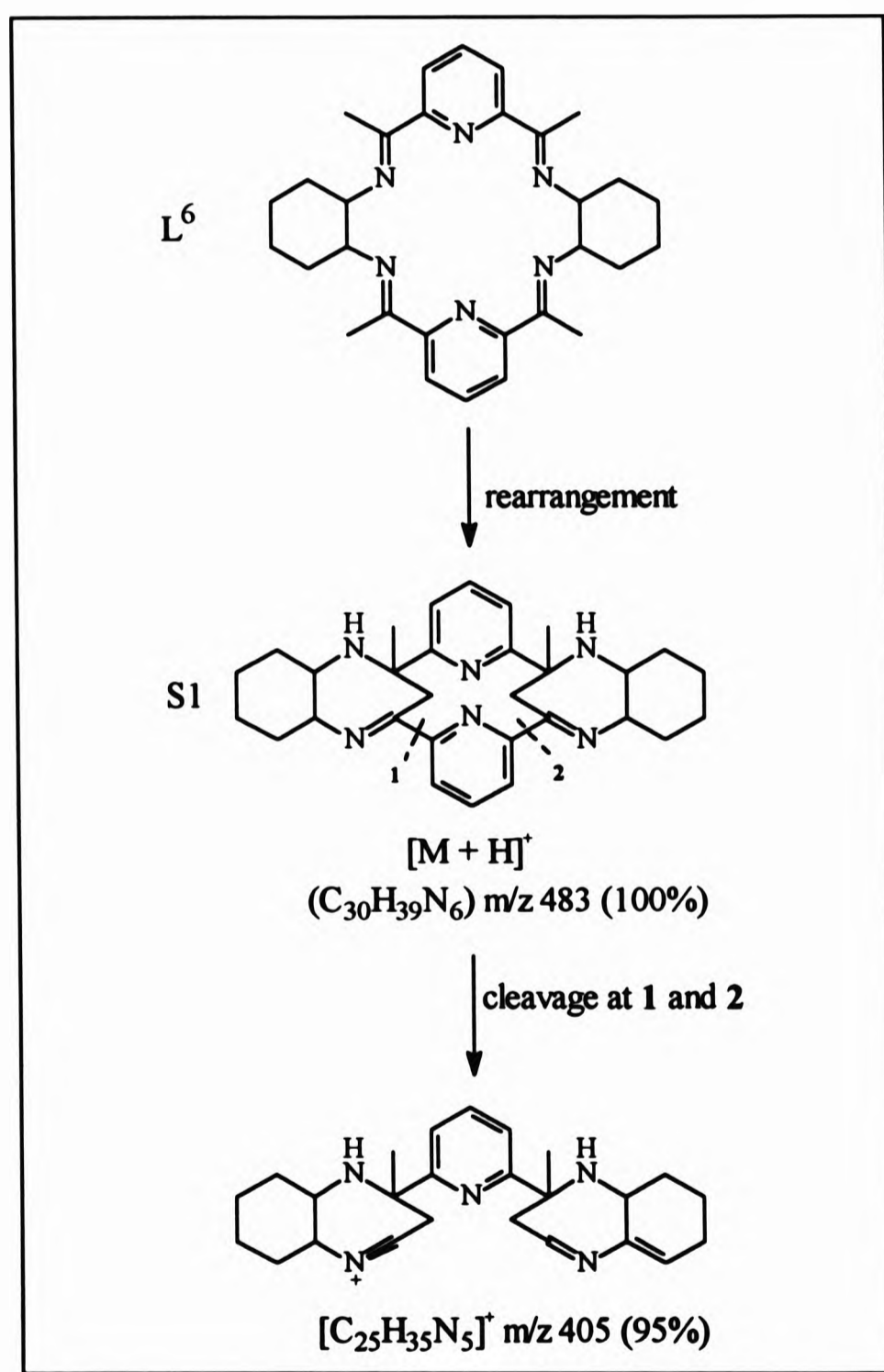


Fig. 2.12 The LSIMS Induced Fragmentation of L^6 and S1

Both L⁶ and S1 were insoluble in common solvents though partial solubility in hot CDCl₃ enabled the collection of NMR spectra (Table 2.11 and 2.12, Figs. 2.13 and 2.14). The insolubility of L⁵ prevented the comparison of L⁵ with L⁶ although a comparison is made of S1 and {3} and also of L⁶ and S1 (Table 2.11).

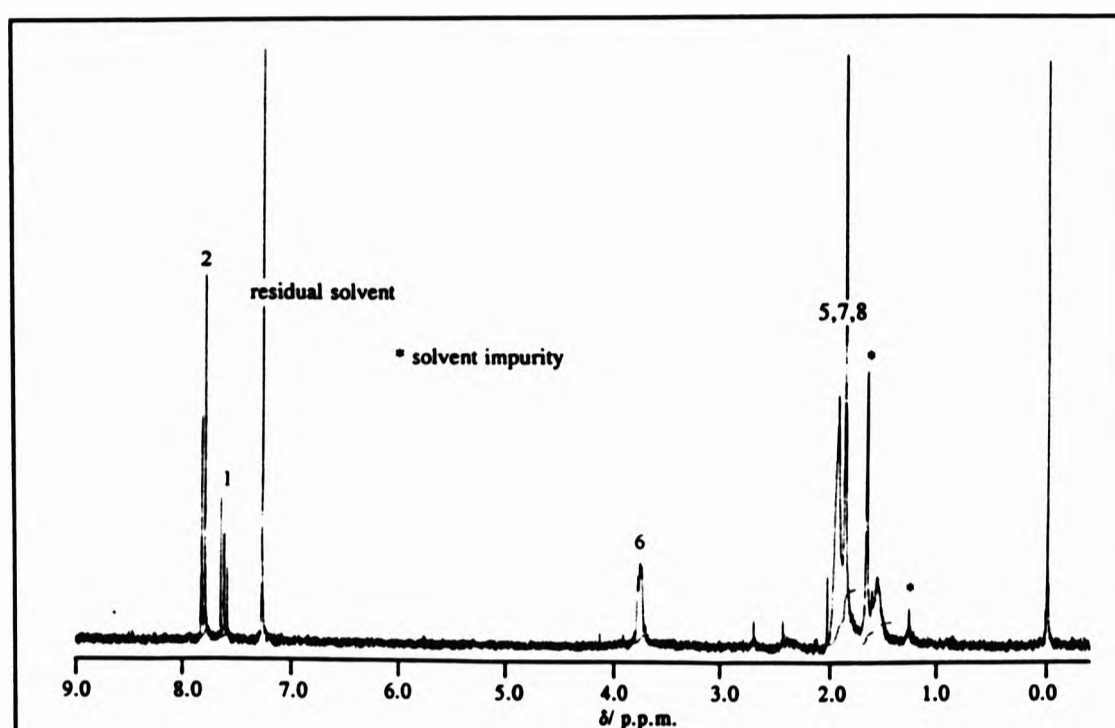


Fig. 2.13 The ¹H NMR spectrum of L⁶ in CDCl₃ and at 250 MHz (refer to Table 2.11 for numbering scheme)

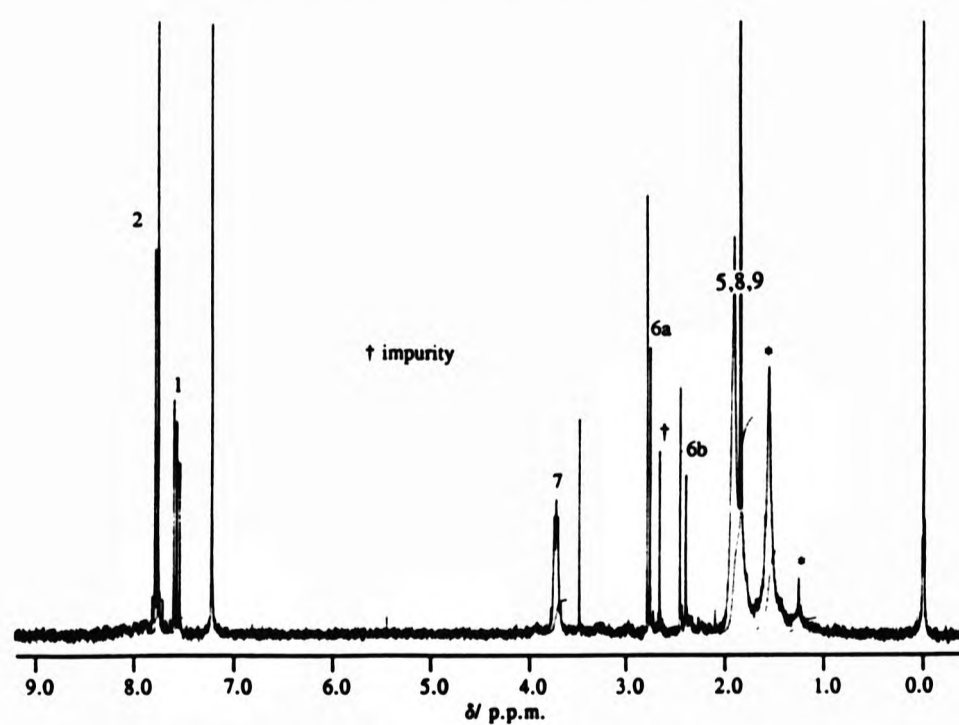
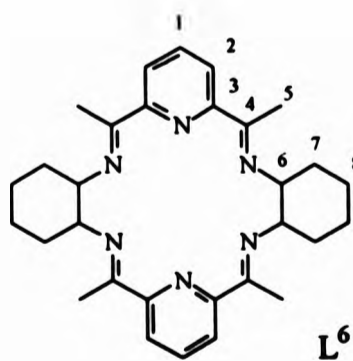
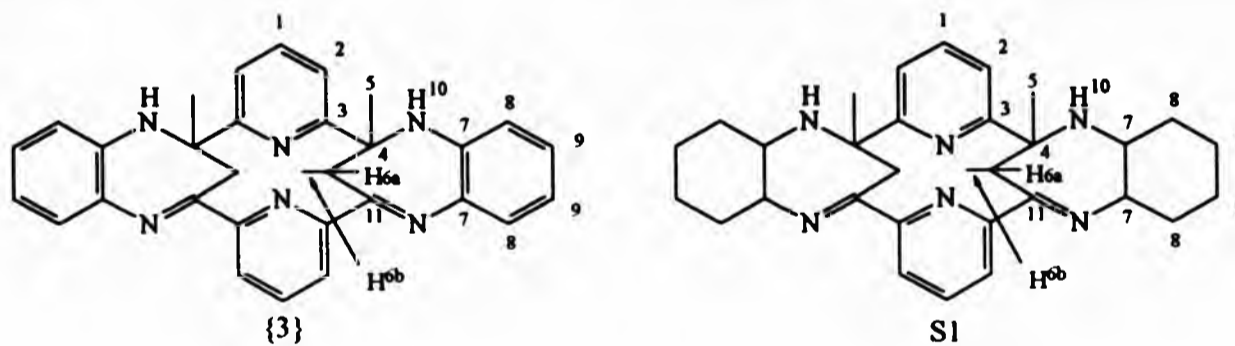


Fig. 2.14 The ¹H NMR spectrum of S1 in CDCl₃ and at 250 MHz

Table 2.11 The ^1H NMR assignments^a of S1 in CDCl_3 , {3} in d_5 -pyridine and L⁶ in CDCl_3

^1H ASSIGNMENT	S1	Hz	{3} ^[45]	Hz	L ⁶	Hz
1	7.60(t)	$^3J_{1,2} = 7.15$	b	b	7.60(t)	$^3J_{1,2} = 7.48$
2	7.82(d)	$^3J_{1,2} = 7.15$	b	b	7.81(d)	$^3J_{1,2} = 7.48$
5	1.85(s)	-	1.95(s)	-	1.86(s)	-
6a	2.78(d)	$^2J_{6a,6b} = 14.5$	4.72(d of d)	$^2J_{6a,6b} = 12$ $J_{6a,10} = 2$	3.74(m)	-
6b	2.43(d)	$^2J_{6a,6b} = 14.5$	2.60(d)	$^2J_{6a,6b} = 12$		-
7	3.73(m)	-	-	-	1.92(m)	-
8	1.92(m)	-	b	-	1.92(m)	-
9	1.92(m)	-	b	-	-	-
10	c	-	5.57(s)	-	-	-

^a in p.p.m, ^b not reported, ^c NH not observed



One interesting feature of the ^1H NMR spectra of the L^6 and S1 is the position of the AB_2 bands, H^1 [2H, t, $^3J(\text{H}^1-\text{H}^2) = 7.48_{\text{L}^6}, 7.15_{\text{S1}}$ Hz] and H^2 [4H, d] with respect to each other compared to the ^1H NMR spectra of $[\text{YL}^5\text{Cl}_2(\text{H}_2\text{O})_2]^+$ and $[\{\text{YL}^5(\text{NO}_3)_2\}_2\text{NO}_3(\text{OH})]$ (Figs. 2.5 and 2.6 respectively). Whereas for the spectra of L^6 and S1 the *doublet*, H^2 , is downfield to the *triplet*, H^1 , for the yttrium complexes of L^5 the reverse occurs and the *doublet* is upfield from the *triplet*.

Taking upfield shifts into account and the use of 1,2-diaminocyclohexane instead of 1,2-diaminobenzene, the ^1H NMR spectrum of S1 matches that described by Nelson^[45] in the synthesis of {3} (Table 2.11).

In both the ^1H NMR spectra of L^6 and S1 the bands at δ_{H} 1.85 and 1.92 are assigned to the methyl (former), H^5 , and the methylene protons, H^8 and H^9 (latter). Although not a singlet, the methylene band at δ_{H} 1.92 is not split as with the spectra of $[\text{YL}^5\text{Cl}_2(\text{H}_2\text{O})_2]^+$ and $[\{\text{YL}^5(\text{NO}_3)_2\}_2(\text{OH})]$ indicating that S1 and L^6 are fluxional on the NMR timescale. Common to L^6 , S1, $[\text{YL}^5\text{Cl}_2(\text{H}_2\text{O})_2]^+$ and $[\{\text{YL}^5(\text{NO}_3)_2\}_2(\text{OH})]$ is the *multiplet*, arising from the methine protons on the cyclohexane ring, at δ_{H} 3.73 and 3.74 for L^6 and S1 and at δ_{H} 3.98 and 3.23 for the yttrium complexes of L^5 respectively.

The distinguishing features between S1 and L^6 is the methylene bridging, CH_2^6 . For the ^1H NMR spectrum of {3}, Nelson^[45] reported a singlet band at δ_{H} 5.57 for the *NH* resonance. (A signal for the *NH* proton was not observed for S1.) The bridging methylene carbon atoms were reported to be prochiral such that the methylene protons resonated as two *doublets*, the *doublet* most downfield, being itself a *doublet of doublets*, collapsing to a *doublet* on D_2O addition. In other words, one of the methylene protons is coupled to the *NH* proton. Two doublets are also observed for the ^1H NMR spectrum of S1, the bands being not of equal intensity, although they do integrate for four protons.

With regards to the ^{13}C -off resonance broad band proton decoupled NMR spectra,

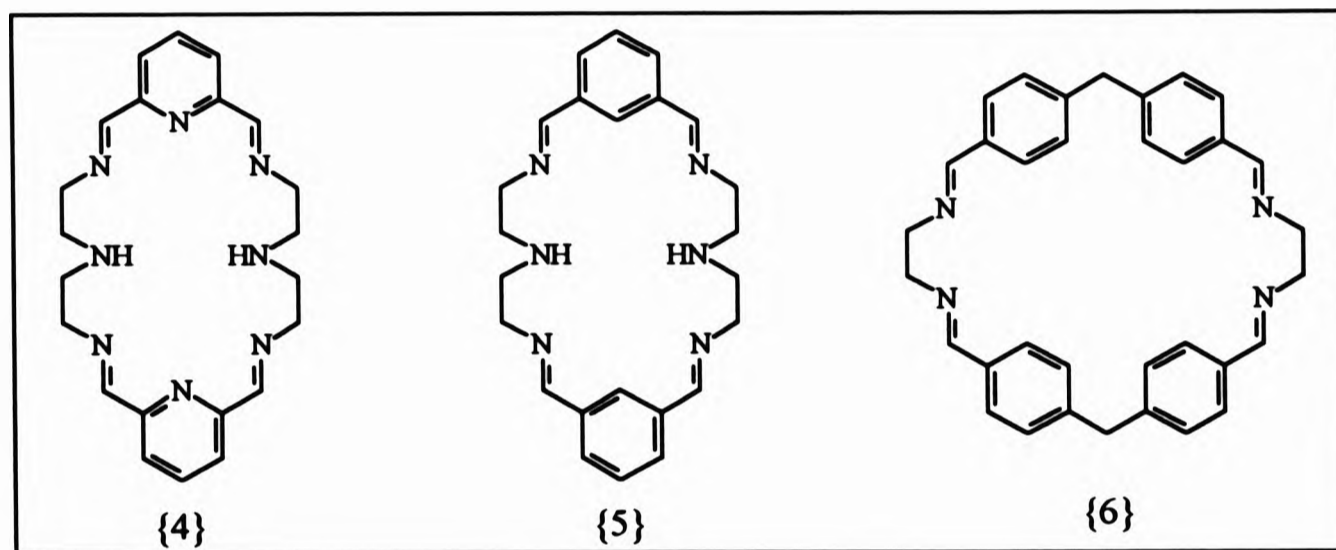
S1 has ten different carbon atom environments, as depicted by Table 2.12, as opposed to eight carbon atom environments for L⁶. DEPT-135 ¹³C NMR spectroscopy identified three methylene carbon atoms in different environments and also three quaternary carbon atoms. L⁶ has only two methylene carbon atoms in different environments and also two such quaternary carbon atoms. This is supporting evidence that S1 adopts the *Nelson-type*, {3}, arrangement.

Table 2.12 Assignment of the ¹³C NMR spectrum of S1 and L⁶

¹³ C Assignment	δ_c	
	S1	L ⁶
1	135.86	135.84
2	119.66	119.65
3	156.63	156.62
4	77.22	166.45
5	14.96	14.95
6	67.9	66.63
7	66.64	32.06
8	31.07	24.68
9	24.67	-
11	166.47	-

This work has shown that the free 18-membered macrocyclic ligand, L⁶, can be isolated in the absence of a metal template in both methanol and acetonitrile irrespective of the dilution factor necessary for the non-template synthesis of ligands such as {4},^[47,48] {5}^[49] and {6}.^[50]

L^5 can also be prepared by the direct method (section 2.4.1) but not L^3 . L^3 was isolated in the metal-free form by the demetallation of its potassium complex.^[27] Whereas macrocyclic products were not isolated with lanthanide metal templates, the use of barium(II) assists in the formation of the seven-membered structure, S1, as this compound was not isolated in the non-template experiments. Excluding the two pyridine rings, two of the remaining rings are seven-membered and the central one being twelve-membered.



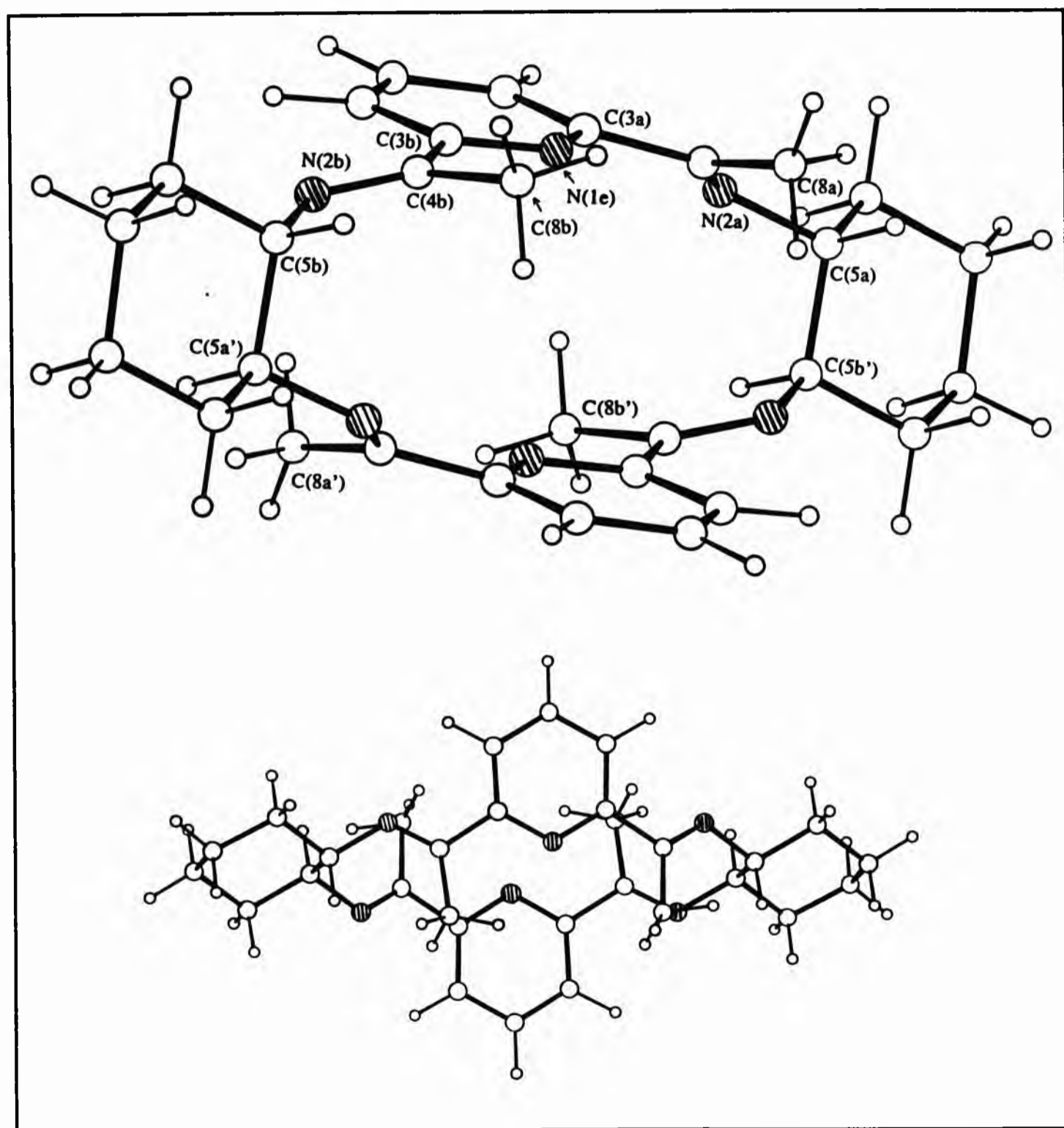
2.4.2.2 The X-Ray Crystal Structure of L^6

To determine the conformation adopted by L^6 a single crystal X-ray crystallographic analysis was undertaken. The white solid of L^6 could not be recrystallised due to restricted solubility. The non-template reaction was repeated at extremely high dilution in acetonitrile. The solvent was changed to dichloromethane and slow diffusion of diethyl ether yielded colourless square plate crystals suitable for analysis.

The analysis showed the structure to be of an 18-membered macrocycle (Fig. 2.15). The asymmetric unit of the crystal contains only half of the ligand with an inversion

about the centre of the molecule. The diiminopyridine section, comprising the seven atoms from C(8a) through N(1e) to C(8b), is almost coplanar, consistent with the region of extended conjugation. Overall the ligand adopts a stepped conformation, the direction of folding being dictated by the *R,R*-conformation of the cyclohexane ring atoms C(5a) and C(5b') *S,S*-conformation at C(5a') and C(5b).

Fig. 2.15 The solid state structure of *L*⁶



The crystal structure of metal-free L^3 has been reported^[27] and adopts a different arrangement to L^6 when the positions of four methyl groups and the four imino protons are compared. The conformation adopted by L^6 in the solid state is believed to be the energy minimum where the two methyl groups, C(8a) and C(8b), are pointing out of the plane of the pyridine ring and the two methyl groups, C(8a') and C(8b'), are pointing behind the plane of the paper. This arrangement minimises repulsion between the methyl hydrogen atoms and the hydrogen atoms on the cyclohexane rings which is evident from molecular models. For L^3 , on other hand (Fig. 2.16), where the methyl groups are replaced by protons and the cyclohexane rings by phenyl rings, a *trans* conformation is adopted by the imino groups which ensures the maximum distance between the lone pair of electrons of the imino nitrogen atoms N^f and N^g and also between N^h and N^m (Fig. 2.16). On metal complexation the respective electron lone pairs do face towards each other and the imine bonds become *cis*.^[27]

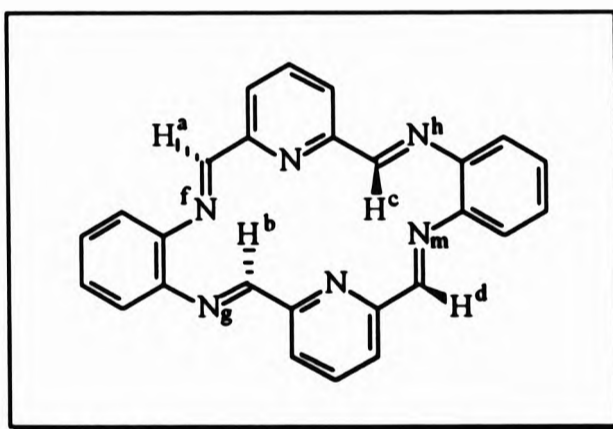
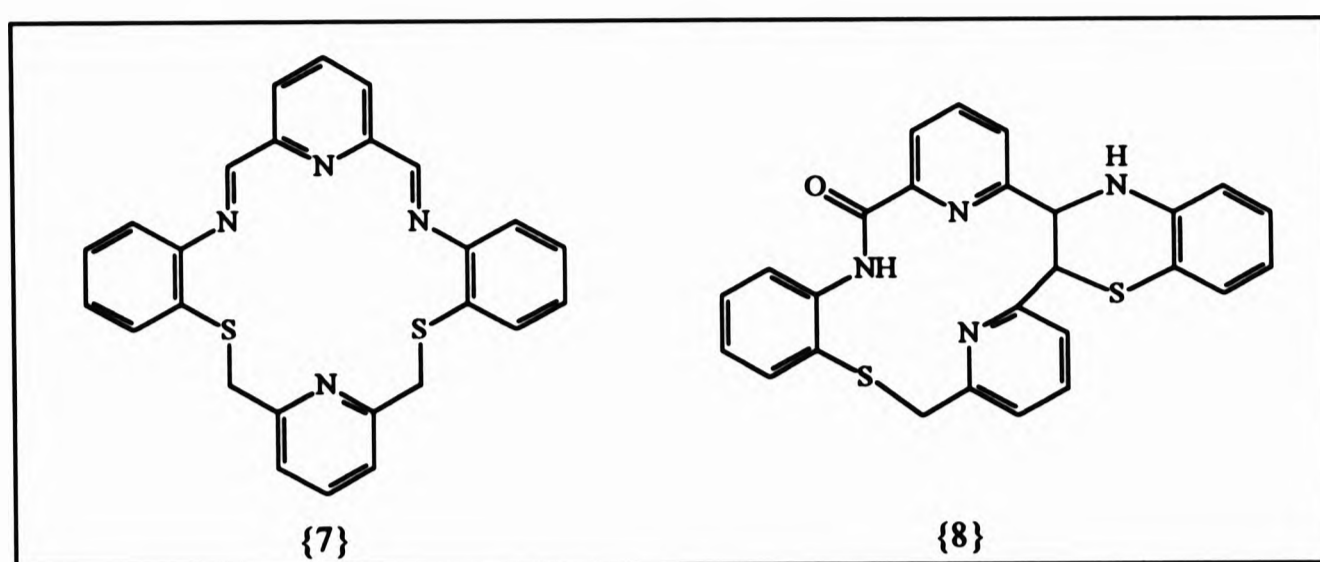


Fig. 2.16 The conformation adopted by L^3

Rearrangements forming S1 or {3} (refer to page 72) also occur during the synthesis of $[Zn\{7\}](ClO_4)_2$ where {8} is formed (metal-free) as a by-product via internal cyclisation which was analysed crystallographically.^[51] This rearrangement is also believed to be metal assisted resulting in a six-ring structure, two new rings being formed during the rearrangement, the inner great ring being fourteen-membered and the smaller external ring being six membered. The inclusion of an amide bond was also noted.



2.4.3 Metal Complexation of L⁶

As described in Section 2.4.2, the template synthesis of L⁶, and indeed of L⁴, was unsuccessful but the isolation of the metal-free [2+2] ligand, L⁶, *via* the direct method proved relatively simple. The next step was to complex the ligand, initially with lanthanide metals.

2.4.3.1 Complexation of L⁶ with Lanthanide Metals

The complexation of L⁶ with lanthanum nitrate was attempted both in methanol and in dichloromethane, L⁶ being insoluble in methanol, yet partially soluble in dichloromethane. No interaction between the ligand and the metal took place in methanol and the unreacted ligand was recovered.

On dropwise addition of the metal salt to the suspension of the ligand in dichloromethane, a white solid was obtained which did not analyse for an imine complex or a complex of a L⁶ related or rearranged macrocycle. The infrared spectrum was similar, not say identical, to that of tris[(±)-*trans*-1,2-diaminocyclohexane] nitrate yttrium(III) (§ 2.4.2 and Fig. 2.8) with the exception

of one sharp band at 3547 cm⁻¹ with a shoulder at 3525 cm⁻¹. These are attributed to a co-ordinated hydroxyl group^[10,11] or a co-ordinated water molecule.^[12] In conclusion, the reaction of La³⁺ with L⁶ causes the dissociation of L⁶ forming hydroxy-tris[(±)-*trans*-1,2-diaminocyclohexane] nitrate lanthanum(III). Further analyses or attempts to complex L⁶ with lanthanide metals were discontinued.

2.4.3.2 Complexation of L⁶ with Copper(II)

Failing to obtain lanthanide metal complexes of L⁶, the next stage was to attempt the complexation with transition metals. The same procedure was adopted as described by Nelson^[52] on complexation of {3}. A dark brown microcrystalline solid precipitated from a dark green viscous solution which analysed for [CuL⁶(H₂O)](ClO₄)₂(MeOH)(H₂O).

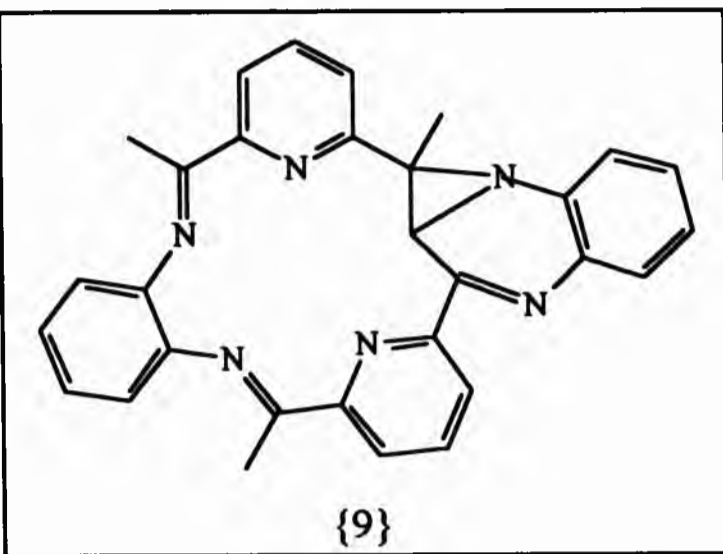
The IR spectrum was dominated by the strength of the split perchlorate band in the region 1087 - 1144 cm⁻¹ accompanied by the sharp band at 627 cm⁻¹. A medium band at 1636 cm⁻¹ is due to the co-ordinated imine and another of equal absorbance at 1594 cm⁻¹ is due to the ν(C=N) of the pyridine rings.

The LSIM spectrum (Table 2.13) indicates the co-ordination of a water molecule to the metal resulting in a band at m/z 564 and on its loss a fragment at m/z 546 is observed corresponding to the metal-ligand co-ordination. The non-detection of the two perchlorate counter-ions suggests that both are ionic in nature. The magnetic moment of 2.1 BM at 299 K is in the range expected (μ_{so} 1.8 - 2.2)^[53] for the spin-only moment of Cu²⁺, d⁹, with one unpaired d-electron.

Table 2.13 The major fragmentations detected in the LSIM spectrum of [CuL⁶(H₂O)](ClO₄)₂(MeOH)(H₂O)

FRAGMENT	MASS (m/z)	RELATIVE ABUNDANCE (%)
[CuL ⁶ (H ₂ O)] ⁺	564	16
[CuL ⁶] ⁺	546	90

When Nelson complexed {3} with Cu^{2+} a rearrangement had taken place forming $[\text{Cu}\{9\}(\text{H}_2\text{O})](\text{ClO}_4)_2 \cdot \text{H}_2\text{O}$ which was proved crystallographically.^[52] The advantage in the rearrangement to the structure {9} containing a [15 + 6 + 3] inner ring system, with the loss of two hydrogen atoms, is that extra stability is gained by providing a suitably sized macrocycle cavity for the copper(II) ion (Chapter 1, section 1.3, Fig. 1.11).



It is believed that on complexation {3} reverts to the original 18-membered product, L^4 , but due to the small ionic radius of the Cu^{2+} , relative to the macrocyclic cavity of L^4 , the ligand has to rearrange to the 15-membered ring in order to accommodate and satisfy the co-ordination properties of the metal. Due to conjugation throughout the whole structure, the rigidity in L^4 does not allow for the 18-membered ring to contract and therefore the system has to partially rearrange. The co-ordination geometry of the structure is best described as a distorted square pyramid. It is suspected that the copper complex of L^6 adopts a similar arrangement but the inability to obtain suitable crystals will leave this mystery unsolved.

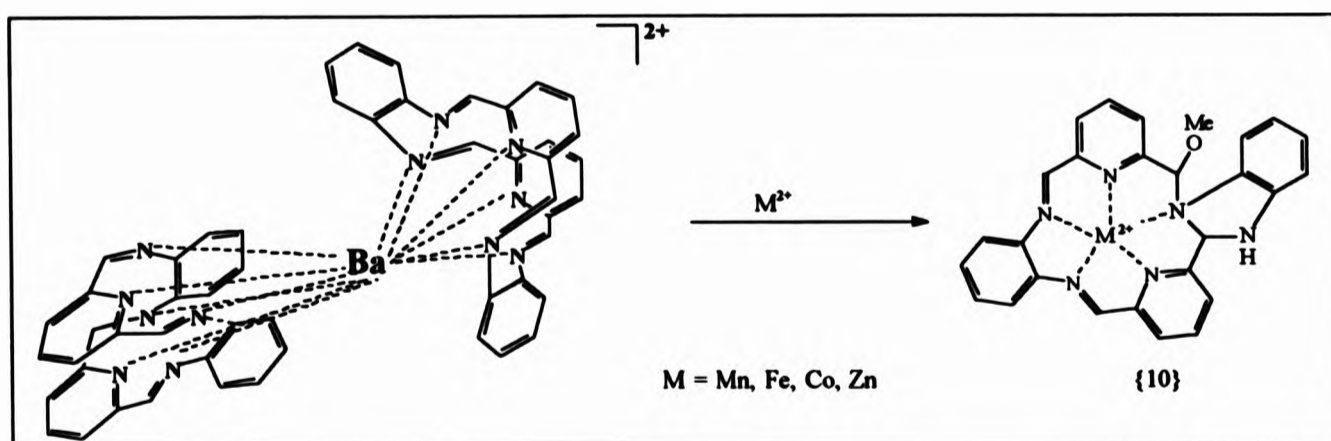


Fig. 2.17 Transmetalation of $[\text{BaL}^3_2](\text{ClO}_4)_2$ with first row transition metals

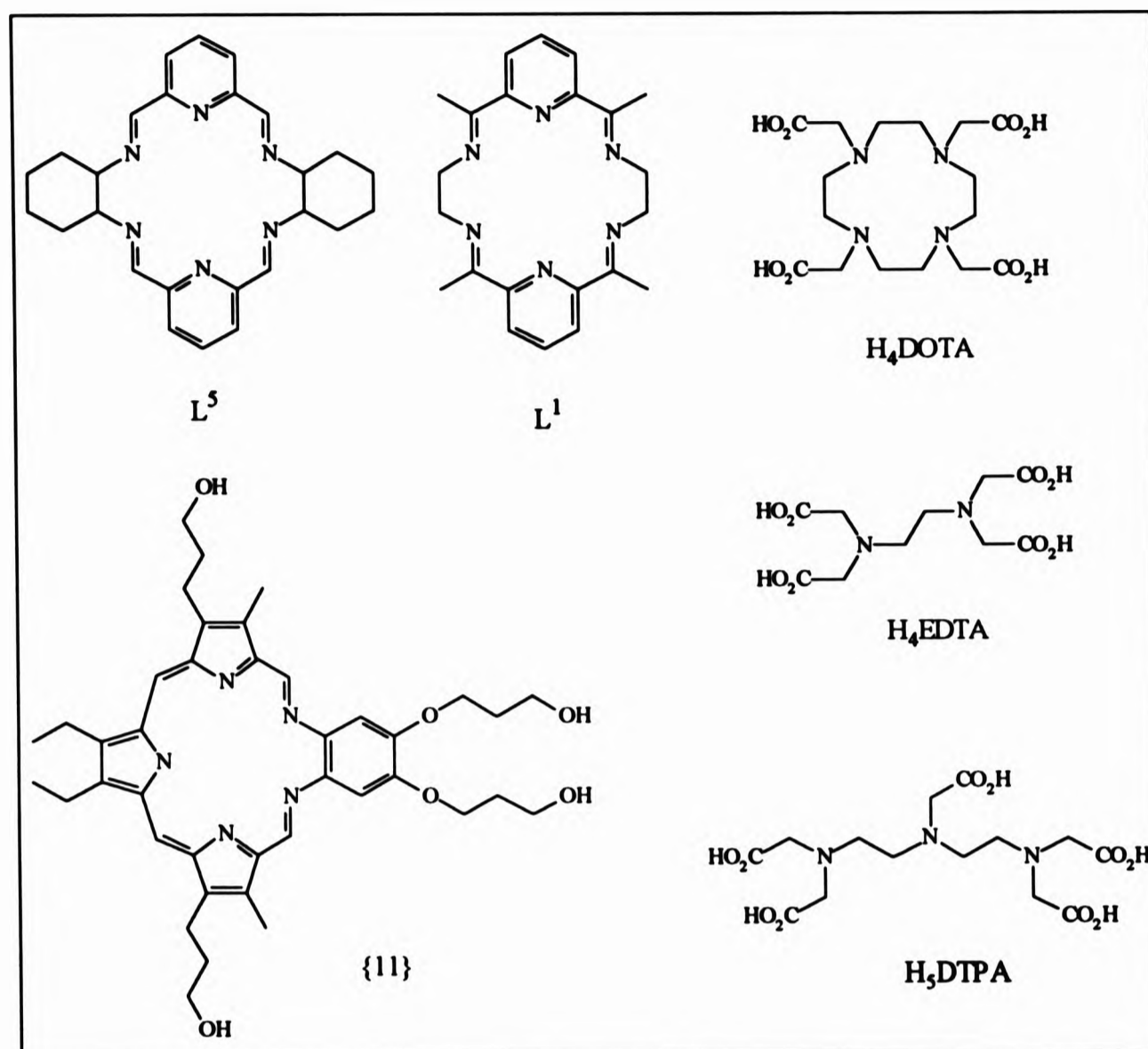
The transmetalation of $[\text{BaL}^3_2](\text{ClO}_4)_2$ with first row transition metals led to a

similar ring contraction (Fig. 2.17). The 18-membered ring contracts to one with a 15-membered cavity due to the relatively small ionic radius of the transition metal relative to the macrocyclic cavity, the radius of the hole size being *ca.* 2.7 Å and those of the first row transition metals being in the range 1.8 - 1.92 Å.^[54,55] Thus the first row transition metals are too small to be co-ordinated by all six nitrogen donor atoms of the macrocycle and this also accounts for their inability to act as templates. [Co{10}(H₂O)(MeOH)](ClO₄)₂ has been solved crystallographically^[54] and the Co²⁺ metal adopts a pentagonal pyramidal geometry bonding to five nitrogen atoms. The addition of a methoxy group across one C=N bond increases the flexibility of the macrocycle as a result of the conversion of a double bond to a single bond. The presence of the methyl groups in L⁴ or L⁶ does not allow for solvolytic attack.

2.4.4 Relaxation Rate Studies of [GdL⁵(H₂O)₃]Cl₃·3H₂O

Relaxation rate measurements are the initial trials when a new compound is to be considered as a contrast agent for MRI. Properties of contrast agents were discussed in Chapter 1, the two major aspects being that the metal ion has the most unpaired electrons possible and a maximum number of water molecules co-ordinated to it or in very close proximity. Gadolinium(III) with seven unpaired electrons fits the former criterion relatively well.

The relaxation rate of [GdL⁵(H₂O)₃]Cl₃·3H₂O was determined both in water and phosphate buffer at pH 6, 37°C and at 20 MHz. The resulting relaxation rates are listed in Table 2.14 and compared to other gadolinium-related macrocycles such as [GdL¹(OAc)₂]Cl·4H₂O and also to the currently used contrast agents, [Gd-DTPA(H₂O)]²⁻ and [Gd-DOTA(H₂O)]⁻.



The presence of water molecules is well documented at inducing relaxation and a trend can also be observed in Table 2.14. When q , the number of co-ordinated water molecules, increases, the relaxation rate increases. But ideal comparisons can only be made if the measurements are made at the same temperature and the same frequency of the spectrometer since the relaxation time is dependent on these factors. Proton relaxation time is also dependent on the concentration of the paramagnetic species and it is the norm to quote the relaxation at 1 mmol dm^{-3} .

The gadolinium(III) ion can attain a maximum co-ordination number of ten. Six of these co-ordination sites in $[\text{GdL}^5(\text{H}_2\text{O})_3]\text{Cl}_3 \cdot 3\text{H}_2\text{O}$ are taken by the six nitrogen atoms from the macrocyclic ligand. The non-co-ordinating chloride ions, therefore, allow 3 - 4 free co-ordination sites on the gadolinium ion for solvent co-ordination

and three of these are being taken by water molecules as depicted by X-ray crystallography (§ 2.4.1.3). As a result of these three co-ordinated water molecules ($q = 3$), $[\text{GdL}^5(\text{H}_2\text{O})_3]\text{Cl}_3 \cdot 3\text{H}_2\text{O}$ has a relatively high relaxation rate, $R_1 = 11.0 \text{ dm}^3 \text{ mmol}^{-1} \text{ s}^{-1}$, at 37°C and at 20 MHz when compared to the aqua ion, GdCl_3 , $R_1 = 16.1 \text{ dm}^3 \text{ mmol}^{-1} \text{ s}^{-1}$, $q = 9$, and $[\text{Gd-DTPA}(\text{H}_2\text{O})]^{2-}$, $R_1 = 4.5 \text{ dm}^3 \text{ mmol}^{-1} \text{ s}^{-1}$ ^[56] and $[\text{Gd-DOTA}(\text{H}_2\text{O})]^-$, $R_1 = 3.4 \text{ dm}^3 \text{ mmol}^{-1} \text{ s}^{-1}$ ^[57] at the same temperature and frequency. For the latter two compounds the low relaxation rate is due to only one water molecule^[58] being found to co-ordinate to the metal.

Table 2.14 Relaxation rates^{a,d} of some gadolinium complexes

Gd^{3+} Complex	q^c	medium	Freq. (MHz)	Temp. ($^\circ\text{C}$)	R_1	R_2	Ref.
$[\text{GdL}^5]\text{Cl}_3$	3	water	20	37	11.0	14.4	38*
	3	phosphate	20	37	4.6	7.9	38*
$[\text{GdL}^1(\text{OAc})_2]\text{Cl}$	0 ^b	water	20	30	9.7	-	39
GdCl_3	9	water	20	35	9.1	-	59
	9	water	10	25	16.1	-	60
$[\text{Gd-EDTA}]^-$	1	water	20	37	6.9	-	57
$[\text{Gd-DTPA}]^{2-}$	1	water	20	37	4.5	-	57
	1	water	10	23	5.6	-	61
$[\text{Gd-DOTA}]^-$	1	water	20	37	3.4	-	56
	1	water	10	23	7.2	-	57
$[\text{Gd}\{11\}(\text{NO}_3)_2]$	0 ^b	water	20	25	19.0	-	62

^athis work, ^bin $\text{dm}^3 \text{ mmol}^{-1} \text{ s}^{-1}$, ^cno water molecules co-ordinated to the metal but 4-5 molecules of water are in the outer sphere, ^ddetermined by X-ray crystallography, q = number of co-ordinated water molecules, ^e $R = 1/T$ where T is the relaxation time in s.

Additionally, the solid state structure of the gadolinium complex of L^5 showed three more water molecules in the outer sphere which would decrease the distance between the water molecules in the vicinity and the metal and thus increasing the communication of the relaxation.

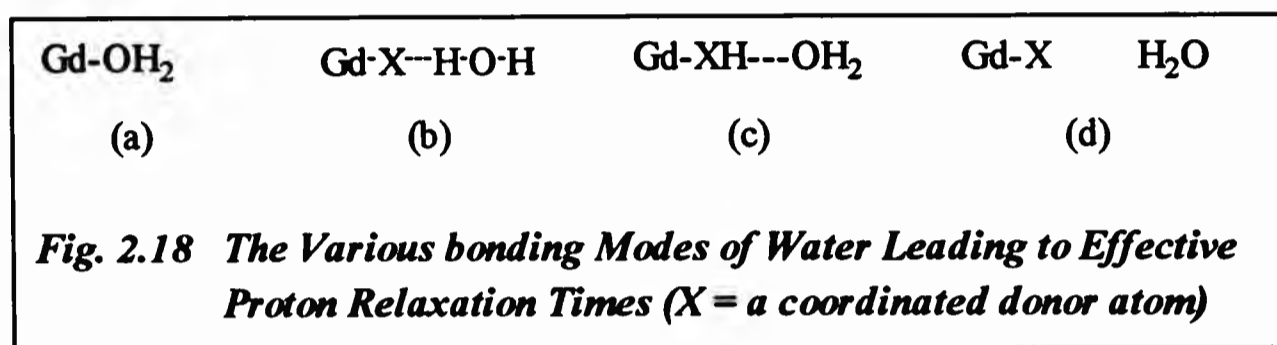
In most cases the value of q is determined by X-ray crystallography though solution, luminescence and NMR,^[63,64] studies are just as adequate when crystals cannot be obtained.

In gadolinium complexes of EDTA, DTPA and DOTA the metal has a co-ordination number of six, eight and eight respectively so there are co-ordination sites available for water, a maximum of three for $[Gd-EDTA]^-$, and two for both $[Gd-DTPA]^{2-}$ and $[Gd-DOTA]^-$. The overcrowding of the methylene carboxylate pendant arms limits water co-ordination to $q = 1$, in particular for $[Gd-DTPA]^{2-}$ and $[Gd-DOTA]^-$, restricting their ability at inducing the relaxation times of water protons in the vicinity.

$[GdL^1(OAc)_2]Cl \cdot 4H_2O$, a structurally related macrocycle to L^5 , has a relaxation rate of $9.7 \text{ dm}^3 \text{ mmol}^{-1} \text{ s}^{-1}$ at 30°C and at 20 MHz.^[39] The relaxation rate afforded by $[Gd\{11\}(NO_3)_2]$ is $19.0 \text{ dm}^3 \text{ mmol}^{-1} \text{ s}^{-1}$ at 25°C and at 20 MHz.^[62] The R_1 values given by both of the latter gadolinium complexes are extremely high, considering that $q = 0$ in both cases, and are comparable or much higher than the relaxation rate of the aqua ion, $GdCl_3$, $R_1 = 9.0 \text{ dm}^3 \text{ mmol}^{-1} \text{ s}^{-1}$,^[39] at the same temperature and frequency. If the relaxation rate is directly dependent on q then the relaxation rate produced by the aqua ion, compared to other gadolinium complexes at the same temperature and frequency, should be the maximum. This not being the case for $[GdL^1(OAc)_2]Cl \cdot 4H_2O$ and $[Gd\{11\}(NO_3)_2]$ suggests that the value of q is not the only parameter contributing to the relaxation rates of these two complexes.

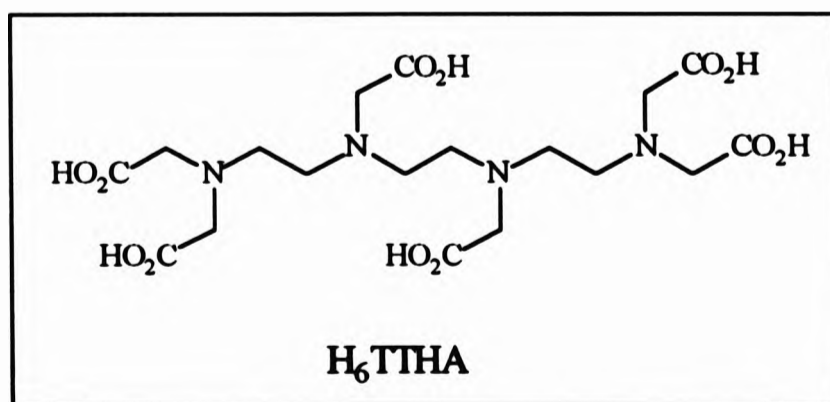
Increase in electron spin relaxation time, τ_s , and also various spin orbital interactions have been suggested to contribute to the increase in relaxation rates. Another

possibility is that the water molecule may not be co-ordinated to the metal but a hydrogen bond between the lone pair of electrons of the co-ordinated oxygen atom of a water molecule and the co-ordinated nitrogen atoms in the macrocycle may force a high tilt angle and lead to a shorter through-space Gd---H distance and therefore higher relaxivities. Fig. 2.18 shows the relationship between the protons on co-ordinated water and the gadolinium metal.^[56]



Water can be hydrogen-bonded to co-ordinated carboxylate oxygen atoms^[65] so it is reasonable to assume this occurs for nitrogen donors also. The hydrogen-bonded water molecules would have hydrogen atoms pointing towards the metal (Fig. 2.18b) which is close relative to water molecules hydrogen-bonded to co-ordinated water (Fig. 2.18c, $X = \text{O}$) or water molecules diffusing past in the outer sphere (Fig. 2.18d) but still distant relative to inner sphere water molecules (Fig. 2.18a).

The gadolinium complex of H_6TTHA , where $q = 0$, has a relaxivity, $R_1 = 2.0 \text{ dm}^3 \text{ mmol}^{-1} \text{ s}^{-1}$ at 39°C and at 20 MHz. This value is half that found for gadolinium complexes with $q = 1$, such as $[\text{Gd-DTPA}(\text{H}_2\text{O})]^{2-}$ and $[\text{Gd-DOTA}(\text{H}_2\text{O})]^-$. This concludes that the outer sphere relaxivity, in this case, is equal to the relaxivity contributed by a single inner sphere water molecule.



To create an *in-vivo* environment the relaxation rates of $[\text{GdL}^5(\text{H}_2\text{O})_3]\text{Cl}_3 \cdot 3\text{H}_2\text{O}$ were determined in a phosphate buffer at pH 6, 37°C and at 20 MHz. An increase in T_1 and T_2 meant a decrease in R_1 and R_2 from 11.0 and 14.4 $\text{dm}^3 \text{mmol}^{-1} \text{s}^{-1}$ in water to 4.6 and 7.9 $\text{dm}^3 \text{mmol}^{-1} \text{s}^{-1}$ in phosphate respectively. This sharp decrease indicates that the three co-ordinated water molecules are being displaced by phosphate groups as the gadolinium binds strongly to phosphate^[66] and the relaxivity recorded is purely due to outer sphere water protons.

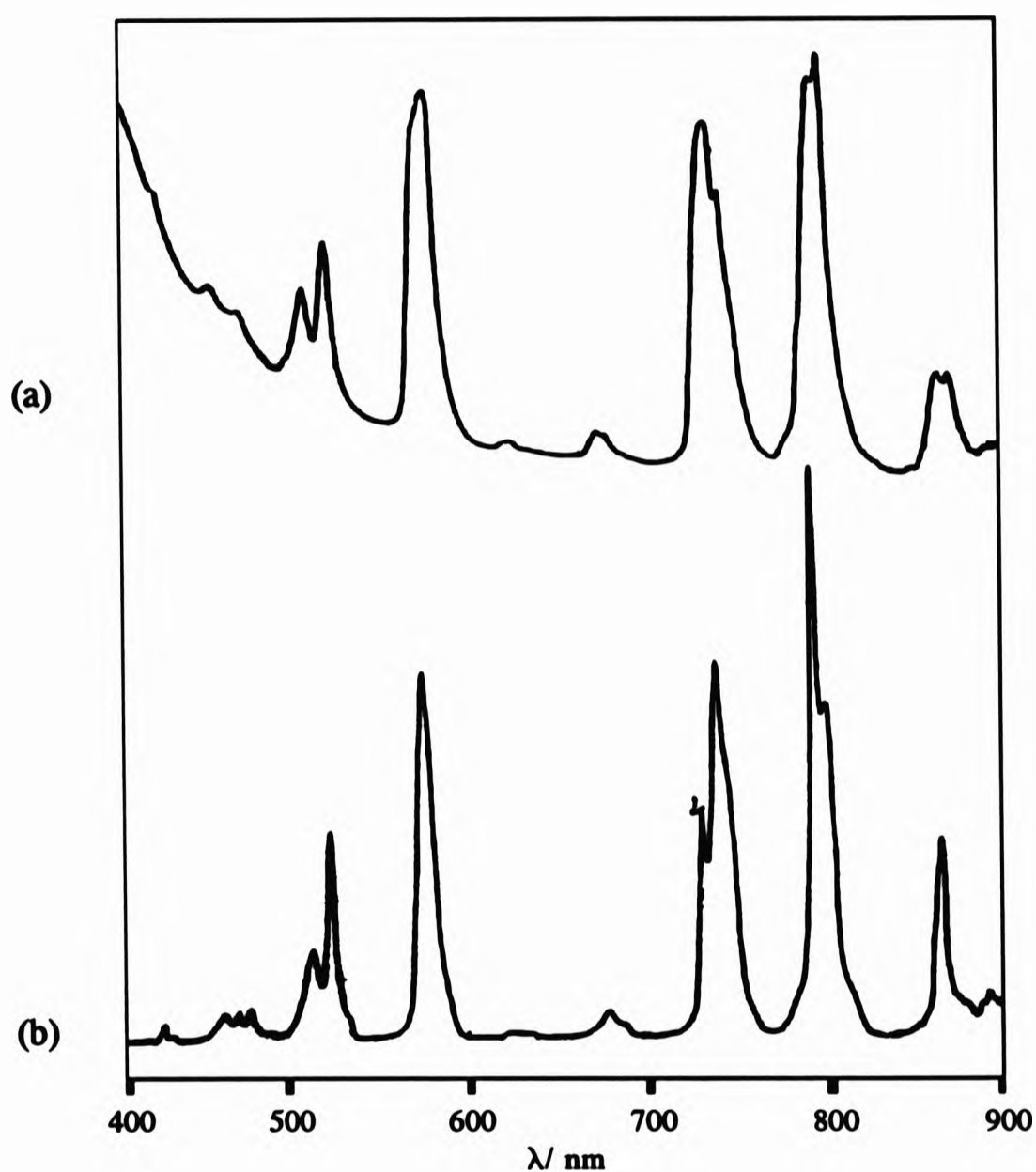
2.4.5 Electronic Spectroscopy of $[\{\text{NdL}^5(\text{NO}_3)_2\}_2\text{NO}_3(\text{OH})]$

Due to the insolubility in water of the paramagnetic complexes of L^5 at a relatively high concentration, electronic spectroscopy studies were only possible for $[\{\text{NdL}^5(\text{NO}_3)_2\}_2\text{NO}_3(\text{OH})]$.

At 0.2 mmol dm^{-3} and pH 7, the observed absorption bands at 230 nm ($\epsilon = 1860 \text{ mol}^{-1} \text{ m}^2$) and 246 nm ($\epsilon = 1700 \text{ mol}^{-1} \text{ m}^2$) are assigned to $\pi \rightarrow \pi^*$ of the pyridine rings whilst the bands at 305 nm ($\epsilon = 722 \text{ mol}^{-1} \text{ m}^2$) with a shoulder at 320 nm ($\epsilon = 400 \text{ mol}^{-1} \text{ m}^2$) are assigned to the $n \rightarrow \pi^*$ transitions of the imine chromophore.^[20,67,68]

At 25 mmol dm^{-3} , and again at pH 7, the weak yet sharp $f \rightarrow f$ transitions typical of lanthanide metals were observed (Fig. 2.19a) in contrast to the broad $d \rightarrow d$ absorptions of transition elements. This is due to the 4f orbitals being buried and shielded within the atom by the d-orbitals, thus minimising the broadening effect of ligand vibrations.^[69,70] The bands in the electronic spectra of lanthanide metals are not affected by complexation as much as those of transition metals which lead to ligand field effects.^[53,71] The little effect inflicted by the ligand is noted by certain *hypersensitive bands*,^[72,73] since their intensities depend on the co-ordinated ligands,^[72,74] and this assists in producing the fine structure, changes in shape and intensity in these bands.^[75] The changes in the hypersensitive bands allow for characterisation and estimation of the co-ordination in lanthanide ions.

Fig. 2.19 The electronic absorption spectra of (a) $[\{\text{NdL}^5(\text{NO}_3)_2\}_2\text{NO}_3(\text{OH})]$ and (b) $\text{Nd}(\text{NO}_3)_3 \cdot 6\text{H}_2\text{O}$ in water at pH 7 and 25 mmol dm^{-3}



The bands are assigned^[68,76,77] in Table 2.15, the ground state level of Nd^{3+} being $^4\text{I}_{9/2}$. The hypersensitive bands in the electronic spectrum of $[\{\text{NdL}^5(\text{NO}_3)_2\}_2\text{NO}_3(\text{OH})]$, compared to $\text{Nd}(\text{NO}_3)_3 \cdot 6\text{H}_2\text{O}$ (Fig. 2.19a and b) are centred at 872, 798, 738, 581 and 512 nm and these are generally the ^4F and ^4G bands. These bands are affected by the complexation of L^5 by increasing in intensity ($^4\text{G}_{7/2}$), becoming much broader ($^2\text{G}_{7/2}$ and $^4\text{F}_{7/2}$) or by splitting ($^4\text{F}_{3/2}$). The transitions

${}^4I_{9/2} \rightarrow {}^4G_{7/2}$, ${}^4I_{9/2} \rightarrow {}^4F_{7/2}$, ${}^4I_{9/2} \rightarrow {}^4F_{5/2}$ and ${}^4I_{9/2} \rightarrow {}^4F_{3/2}$ are not hypersensitive but in certain chemical environments, such as in this case, where changes in co-ordination ability and denticity take place, they have become hypersensitive.^[78] The general similarity between the spectrum of $Nd(NO_3)_3 \cdot 6H_2O$ and that of $[NdL^5(NO_3)_2]_2NO_3(OH)$ suggests that the electrons responsible for the absorption bands are not directly involved in the complex formation.^[79]

Table 2.15 The assignment of the $f \rightarrow f$ transition bands of Nd^{3+} in the electronic spectrum of $[NdL^5(NO_3)_2]_2NO_3(OH)$ and $Nd(NO_3)_3 \cdot 6H_2O$ between 900 - 400 nm

$Nd(NO_3)_3 \cdot 6H_2O^a$			$[NdL^5(NO_3)_2]_2NO_3(OH)^a$		
λ (nm)	Transition	ϵ ($mol^{-1} m^2$)	λ (nm) ^b	Transition	ϵ ($mol^{-1} m^2$)
512	${}^4I_{9/2} \rightarrow {}^2G_{9/2}$	0.172	512	${}^4I_{9/2} \rightarrow {}^2G_{9/2}$	0.404
522	${}^4I_{9/2} \rightarrow {}^4G_{7/2}$	0.380	524	${}^4I_{9/2} \rightarrow {}^4G_{7/2}$	0.472
538	${}^4I_{9/2} \rightarrow {}^2K_{13/2}$	0.012			
575	${}^4I_{9/2} \rightarrow {}^2G_{7/2}, {}^4G_{5/2}$	0.672	581	${}^4I_{9/2} \rightarrow {}^2G_{7/2}, {}^4G_{5/2}$	0.716
623	${}^4I_{9/2} \rightarrow {}^2H_{11/2}$	0.020			
679	${}^4I_{9/2} \rightarrow {}^4F_{9/2}$	0.052	675	${}^4I_{9/2} \rightarrow {}^4F_{9/2}$	0.152
732	${}^4I_{9/2} \rightarrow {}^4S_{3/2}$	0.420			
740	${}^4I_{9/2} \rightarrow {}^4F_{7/2}$	0.688	738	${}^4I_{9/2} \rightarrow {}^4F_{7/2}$	0.644
794	${}^4I_{9/2} \rightarrow {}^2H_{9/2}$	1.068			
800	${}^4I_{9/2} \rightarrow {}^4F_{5/2}$	0.616	798	${}^4I_{9/2} \rightarrow {}^4F_{5/2}$	0.770
864	${}^4I_{9/2} \rightarrow {}^2F_{3/2}$	0.364	872	${}^4I_{9/2} \rightarrow {}^2F_{3/2}$	0.240

^aat 25 mmol dm⁻³, ^bvalue given indicates the band centre

The spectrum of the macrocyclic complex shows a slight shift of the spectral bands towards lower energy (longer wavelengths) as compared with those of the aqua ion^[80] due to the nephelauxetic effect which is regarded as a measure of covalency between the metal and ligand interactions^[75] or related to a shift in the ground state level.^[77] Overall the changes in the hypersensitive bands are not that great when compared to, say, carboxylate co-ordination to a lanthanide metal, implying that nitrogen donor chelation is not affecting the 4f-electrons to a dramatic extent. The reason being that the nitrate ligands in $\text{Nd}(\text{NO}_3)_3 \cdot 6\text{H}_2\text{O}$ are co-ordinating to the Nd^{3+} ion through the oxygen donor atoms and according to the lanthanide nephelauxetic series^[81] oxygen is the most basic (hard base) ligand, F^- being the least basic, resulting in greater covalency. Therefore, the hypersensitive bands are also affected by the basicity of the ligand. L^5 , consisting of six nitrogen donor atoms, nitrogen being neither a hard nor a soft base as far as the HSAB^[82] theory is concerned, will not affect the hypersensitive bands a great deal as shown in Fig. 2.19.

In order to determine the ability of L^5 to hold on to the metal the solution of $[\{\text{NdL}^5(\text{NO}_3)_2\}_2\text{NO}_3(\text{OH})]$ was challenged quantitatively with 4-fold excess of DTPA solution in water at pH 7. The electronic spectrum was recorded at intervals of 0, 5, 10 and 15 minutes of mixing the two solutions, paying particular attention to the hypersensitive bands. The procedure was repeated with the solutions in the ratios of 1 : 1 with regards to $[\{\text{NdL}^5(\text{NO}_3)_2\}_2\text{NO}_3(\text{OH})] : \text{DTPA}$. The resulting spectra were identical in the region 900 - 400 nm irrespective of time and ratio of reactants. The spectrum discussed here was ran at time = 0 minutes, the ratio of reactants being 1 : 4. Fig. 2.20 shows this spectrum at $12.5 \text{ mmol dm}^{-3}$ and the spectra of $\text{Nd}(\text{NO}_3)_3 \cdot 6\text{H}_2\text{O}/\text{DTPA}$ ($12.5 \text{ mmol dm}^{-3}$) and $[\{\text{NdL}^5(\text{NO}_3)_2\}_2\text{NO}_3(\text{OH})]$ (25 mmol dm^{-3}). On adding the excess DTPA solution to the solution of $[\{\text{NdL}^5(\text{NO}_3)_2\}_2\text{NO}_3(\text{OH})]$ the hypersensitive bands of the resulting spectrum afforded the same pattern as that given by the neat solution of $\text{Nd}(\text{NO}_3)_3 \cdot 6\text{H}_2\text{O}/\text{DTPA}$ almost immediately. The hypersensitive bands most affected by the DTPA complexation are the splitting of the ${}^2\text{G}_{7/2}$ and ${}^4\text{F}_{7/2}$ bands and the almost complete unison of the bands ${}^2\text{H}_{9/2}$ and ${}^4\text{F}_{5/2}$. The splitting of the ${}^4\text{F}_{3/2}$ has become more defined.

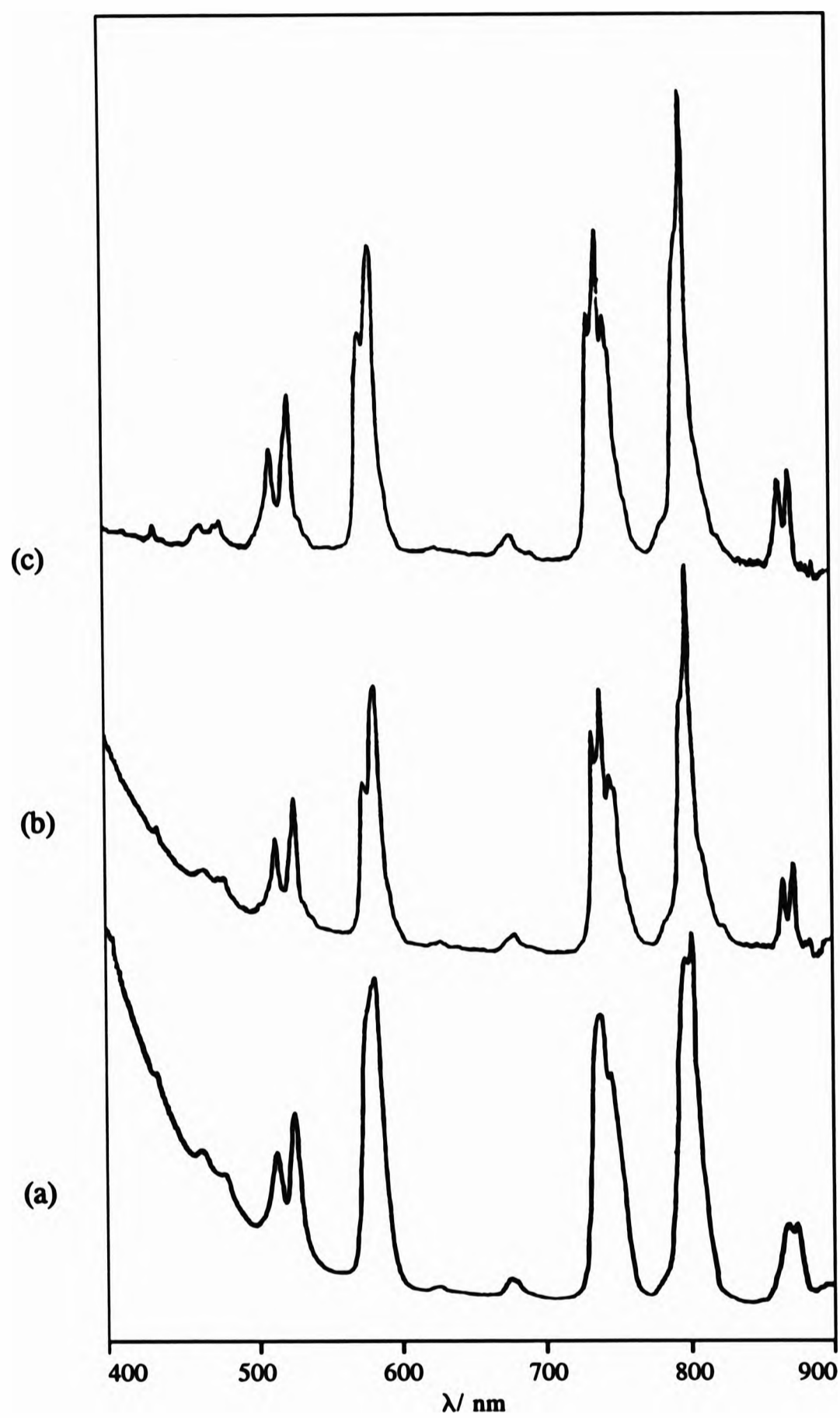


Fig. 2.20 *Electronic absorption spectra of (a) $[\text{NdL}^5(\text{NO}_3)_2]\text{NO}_3$, (b) $[\{\text{NdL}^5(\text{NO}_3)_2\}_2\text{NO}_3(\text{OH})]/\text{DTPA}$ and (c) $\text{Nd}(\text{NO}_3)_3 \cdot 6\text{H}_2\text{O}/\text{DTPA}$ in Water at pH 7*

These more obvious changes in the hypersensitive bands are conclusively related to the stronger covalent bonding (electron donating power) of the DTPA ligand as opposed to L^5 . So, oxygen donor atoms with increased basicity result in increased hypersensitivity. The results were similar when DTPA was replaced with EDTA, a slightly weaker ligand than DTPA.^[79]

2.4.6 Instant Thin Layer Chromatography of $[YL^5Cl_2(H_2O)]^+$

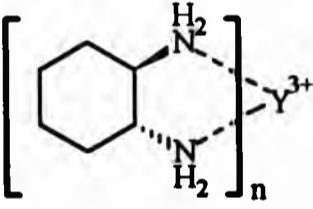
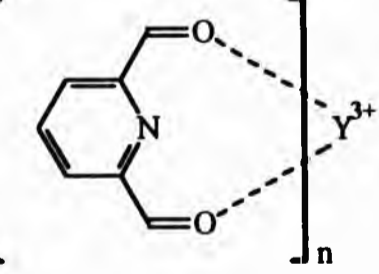
The technique of ITLC is one analogous to TLC which monitors only radioactive species such that any non-radioactive material is not detected. The technique was used to monitor the template synthesis of $[YL^5Cl_2(H_2O)]^+$ with radioactive yttrium-90, a pure β^- emitter, in 0.04 mol dm^{-3} hydrochloric acid.

Initially, the idea was to spike *cold* samples of $[YL^5Cl_2(H_2O)]^+$ and $[\{YL^5(NO_3)_2\}_2NO_3(OH)]$ with Y^{3+} but this was prevented by their insolubility at room temperature in solvents such as water, methanol, saline (NaCl, 0.9% w/v), methyl ethyl ketone and 10% acetic acid in water when TLC was carried out on ITLC-SG, cellulose, aluminium plates and Whatman filter paper, so a suitable solvent system was not found to run the ITL chromatograms.

The alternative was to prepare the macrocyclic complex in solution, spike with $^{90}Y^{3+}$ and perform the ITL chromatograms without pre-isolating the complex. In order to increase the dose and therefore the detection of the radioactive material by the ITLC scanner, the dilution under which the experiment was carried out needed to be relatively low. As a result, on spiking, due to the presence of excess $^{90}Y^{3+}$ ions, a white precipitate formed which was assumed to be $[YL^5Cl_2(H_2O)]^+$. This was confirmed by a *cold* synthesis under similar conditions. When the template reaction was repeated with the same weights and volumes of reagents and solvent (methanol) in the absence of *cold* $^{89}Y^{3+}$ but in the presence of $^{90}Y^{3+}$ as a template, a precipitate was not formed and ITL chromatograms were carried out in methanol after 1 h and 24 h later. This is termed labelling rather than spiking.

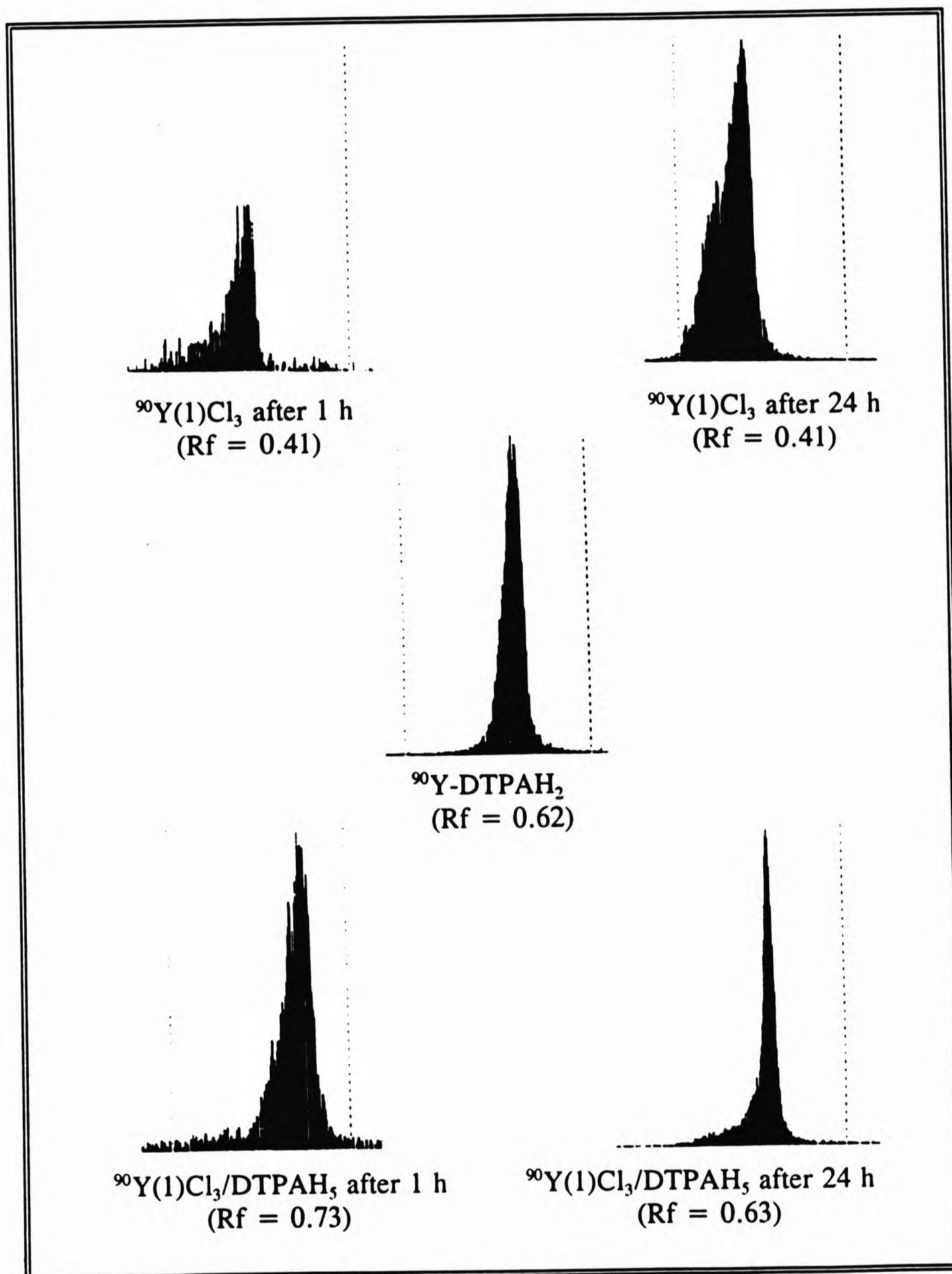
The solution was then challenged with 10-fold excess DTPA at pH 7 and the ITL chromatograms were re-ran, again 1 h after the experiment and also after 24 h. ITL chromatograms were also recorded of ^{90}Y -DTPA and also of the reaction between $^{90}\text{Y}^{3+}$ and (\pm)-*trans*-1,2-diaminocyclohexane and of $^{90}\text{Y}^{3+}$ and 2,6-pyridinedialdehyde. This catered for most of the possibilities which could occur during the template labelling process. The determination of the R_f value of the latter two complexes was necessary to prove the formation of the 18-membered macrocycle and not open chain products. The ITL chromatograms are presented in Fig. 2.21 and the R_f values in Table 2.16.

Table 2.16 *The R_f values obtained in methanol for various complexes of yttrium-90 at 1 h and 24 h.*

Y-COMPLEX ^a	R_f
$\text{YCl}_3 \cdot n\text{H}_2\text{O}$	0.0
Y-DTPA	0.62
	0.0
	0.0 - 1.0 ^b

^a n is not known in solution, ^bin methanol the complex dragged along the plate

Fig.2.21 The ITL Chromatograms of the template labelling of $[YL^5Cl_2(H_2O)]^+$, ^(a) in methanol after 1 h and 24 h [(1) = L⁵]



^(a)the actual composition is not known but is expected to be similar to the solid state

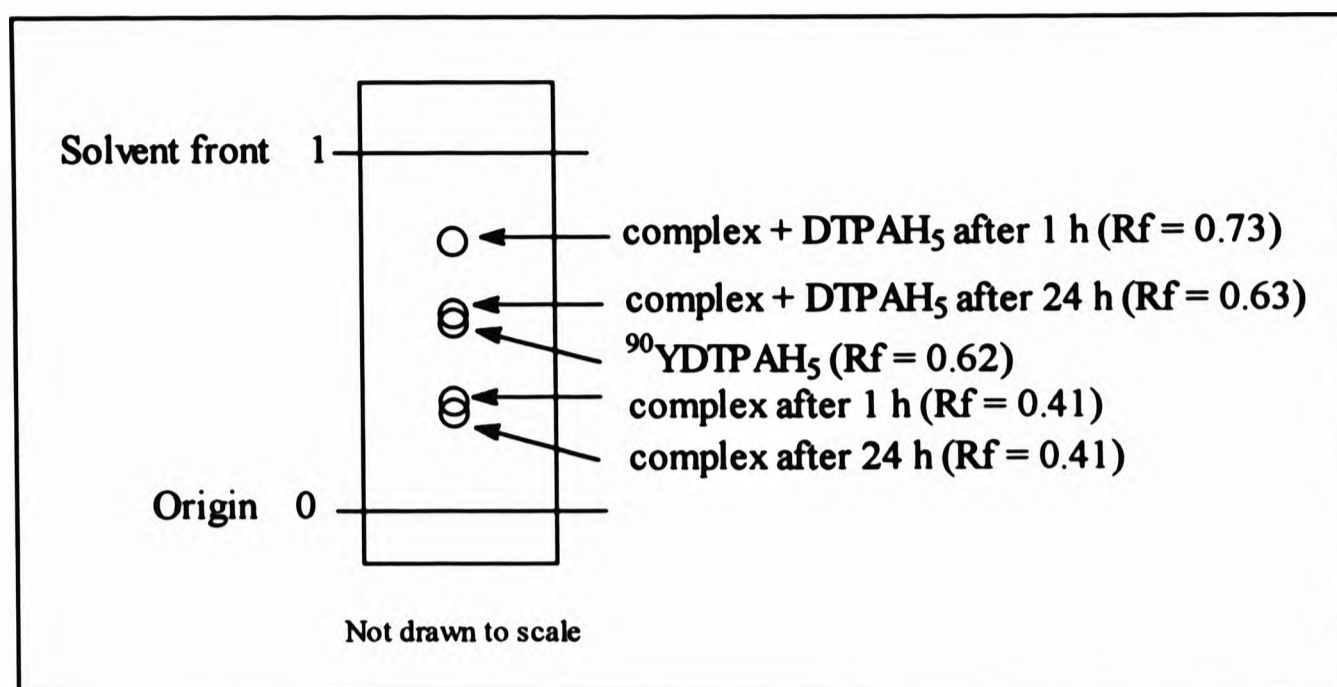


Fig. 2.22 A summary of the ITLC chromatograms

The good separation observed for the R_f values indicates that methanol is a good solvent system for monitoring the template synthesis and the challenge. The results from Fig. 2.21 are summarised diagrammatically in Fig. 2.22. The consistency in the R_f values obtained for $[YL^5Cl_2(H_2O)]^+$ ($R_f = 0.41$) after 1 and 24 h indicates that the complex is kinetically inert in solution. (The varied intensities of the chromatograms is not important as it is the position of the highest band that is of importance not its intensity.) When this solution was challenged with 10-fold excess of DTPA at pH 7, R_f values of 0.73 and 0.63 were obtained 1 and 24 h later respectively. The latter value matched that of Y-DTPA ($R_f = 0.62$) suggesting that after 24 h DTPA scavenges the metal from the macrocycle. The component with a R_f value of 0.73 is believed to be a ternary complex where the DTPA co-ordinates to the yttrium whilst the metal is still within the macrocyclic cavity. In contrast to the challenge carried out and detected by electronic spectroscopy the ITLC results suggest that it takes longer than 1 h for the DTPA to completely "grab" the metal for itself. After 24 h the scavenging is complete and the metal is completely dissociated from the macrocyclic cavity.

2.5 Conclusion

This work has shown that, in contrast to $L^1 - L^4$, L^5 and L^6 can be isolated *via* direct methods in the absence of metal templates. The presence of barium(II), in the synthesis of L^6 , also yields the rearranged product, S1. Direct complexation of L^5 was not possible, although template procedures were successful in obtaining complexes of L^5 and co-ordination of L^6 was achieved only with copper(II). In $[\text{GdL}^5(\text{H}_2\text{O})_3]^{3+}$ the methine carbon atoms on the cyclohexane rings have the configurations RR,RR and for the free ligand, L^6 , RR,SS (or SS,RR). These configurations may be the reason for the inability to obtain lanthanide metal complexes of the tetramethyl derivative, L^6 ; in order to complex, the ligand, as shown by the crystal structure of $[\text{GdL}^5(\text{H}_2\text{O})_3]^{3+}$, needs to adopt the RR,RR configurations at the methine carbon atoms, a rearrangement which is impossible without the macrocycle breaking and reforming. This reasoning also explains why Tsubomura *et al.*,^[35] could not isolate the ligand or metal complexes of tetramethyl derivative, L^6 , as they specifically used 1(*R*), 2(*R*)-diaminocyclohexane. The use of a racemic mixture 1(*R*), 2(*R*) and 1(*S*), 2(*S*)-diaminocyclohexane, in this study, enabled the isolation of the macrocycle L^6 .

$[\text{GdL}^5(\text{H}_2\text{O})_3]^{3+}$ has relatively high relaxivities when compared to those of $[\text{Gd-DTPA}]^{2-}$ and $[\text{Gd-DOTA}]^-$ and is therefore a potential contrast agent for MRI. But the stability of $[\text{GdL}^5(\text{H}_2\text{O})_3]^{3+}$ may be lower than that of $[\text{Gd-DTPA}]^{2-}$ as the former ligand loses the metal to DTPA as shown by solution competition studies of $[\text{LnL}^5\text{X}_q]^{n+}/\text{DTPA}$ ($\text{Ln} = \text{Nd}$, $\text{X} = \text{NO}_3$, $q = 2$, $n = 1$; $\text{Ln} = \text{Y}$, $\text{X} = \text{Cl}_2(\text{H}_2\text{O})$, $q = 1$, $n = 1$). Hence, it would be misleading for $[\text{GdL}^5(\text{H}_2\text{O})_3]^{3+}$ to be considered as a contrast agent based solely on its merits at inducing water proton relaxation times. Solubility restrictions need to be taken into account also and, more importantly, *in vivo* stability.

2.6 References

1. L. De Cola, D. L. Smailes and L. M. Vallarino, *Inorg. Chim. Acta*, 1985, **110**, L1.
2. J. de O. Cabral, M. F. Cabral, W. J. Cummins, M. G. B. Drew, A. Rogers and S. M. Nelson, *Inorg. Chim. Acta*, 1978, **30**, L313.
3. N. Sabatini, L. De Cola, L. M. Vallarino and G. Blasse, *J. Phys. Chem.*, 1987, **91**, 4681.
4. J. D. J. Backer-Dirks, J. C. Gray, A. F. Hart, M. B. Hursthouse and B. C. Schoop, *J. Chem. Soc., Chem. Commun.*, 1979, 774.
5. G. Bombieri, F. Benetollo, A. Polo, L. De Cola, D. L. Smailes and L. M. Vallarino, *Inorg. Chem.*, 1986, **25**, 1127.
6. L. De Cola, D. L. Smailes and L. M. Vallarino, *Inorg. Chem.*, 1986, **25**, 729.
7. F. Benetollo, G. Bombieri, K. K. Fonda, A. Polo, J. R. Quagliano and L. M. Vallarino, *Inorg. Chem.*, 1991, **30**, 1345.
8. G. Bombieri, *Inorg. Chim. Acta*, 1987, **139**, 21.
9. W. Radecka-Paryzek, *Inorg. Chim. Acta*, 1980, **45**, L147.
10. K. K. Abid and D. E. Fenton, *Inorg. Chim. Acta*, 1984, **95**, 119
11. K. K. Abid, D. E. Fenton, U. Casselato, P. A. Vigato and R. Graziani, *J. Chem. Soc., Dalton Trans.*, 1984, 351.
12. A. M. Arif, J. D. J. Backer-Dirks, C. J. Gray, F. A. Hart and M. B. Hursthouse, *J. Chem. Soc., Dalton Trans.*, 1987, 1665.
13. G. Bombieri, F. Benetollo, W. T. Hawkins, A. Hawkins, A. Polo and L. M. Vallarino, *Polyhedron*, 1989, **8**, 1923.
14. F. Benetollo, G. Bombieri, L. De Cola, A. Polo, D. L. Smailes and L. M. Vallarino, *Inorg. Chem.*, 1989, **28**, 3447.
15. G. Bombieri, F. Benetollo, A. Polo, L. De Cola, W. T. Hawkins and L. M. Vallarino, *Polyhedron*, 1989, **8**, 2157.
16. F. Benetollo, A. Polo, G. Bombieri, K. K. Fonda and L. M. Vallarino, *Polyhedron*, 1990, **9**, 1411.

17. K. K. Fonda, D. L. Smailes, L. M. Vallarino, G. Bombieri, F. Benetollo, A. Polo and L. De Cola, *Polyhedron*, 1993, **12**, 549.
18. S. Hewett. MPhil Thesis, Birkbeck College, University of London 1990.
19. L. J. Bellamy, *The Infra-red Spectra of Complex Molecules*, Muthuen, London, 1969.
20. W. Radecka-Paryzek, *Inorg. Chim. Acta*, 1981, **54**, L251.
21. N. Nakamoto, *Infrared Spectra of Inorganic and Co-ordination Compounds*, Wiley-Interscience, New York, 2nd edn., 1970.
22. L. M. Vallarino and R. C. Leif, *Int. PCT Pat. Appl.*, WO89 11868 CLA61 K43/00, 1989.
23. M. G. B. Drew, J. De O. Cabral, M. F. Cabral, F. S. Esho and S. M. Nelson, *J. Chem. Soc., Chem. Commun.*, 1979, 1033.
24. C. J. Gray and F. A. Hart, *J. Chem. Soc., Dalton Trans*, 1987, 2289.
25. F. Guzzo, M. S. Thesis, State University of New York, Stony Brook, 1985.
26. T. W. Bell and F. Guzzo, *J. Chem. Soc., Chem Commun.*, 1986, 769.
27. T. W. Bell, F. Guzzo and M. G. Drew, *J. Am. Chem. Soc.*, 1991, **113**, 3115.
28. D. C. Liles, M. McPartlin and P. A Tasker, *J. Chem. Soc., Dalton Trans.*, 1987, 1631.
29. Z. P. Haque, M. McPartlin and P. A. Tasker, *Inorg. Chem.*, 1979, **18**, 2920.
30. R. M. Silverstein, G. C. Bassler and T. C. Morrill, *Spectrometric Identification of Organic Compounds*, Wiley, Singapore, 4th edn., 1981.
31. D. H. Williams and I. Flemming, *Spectroscopic Methods in Organic Chemistry*, McGraw-Hill, London, 4th edn., 1987.
32. J.-C. G. Bünzli and D. Wessner, *Coord. Chem. Rev.*, 1984, **60**, 191.
33. *Handbook of Chemistry and Physics*, CRC Press, 63rd edn., 1982-1983, B-255.
34. H. Günther, *NMR Spectroscopy, An Introduction*, Wiley, Malta, 1980.

35. T. Tsubomura, K. Yasaki, T. Sato and M. Morita, *Inorg. Chem.*, 1992, **31**, 447.
36. G. Bombieri, F. Benetollo, A. Polo, K. K. Fonda and L. M. Vallarino, *Polyhedron*, 1991, **10**, 1385.
37. R. J. H. Clark, M. Kurmoo and D. N. Mountney, *J. Chem. Soc., Dalton Trans.*, 1982, 1851.
38. S. W. A. Bligh, N. Choi, W. J. Cummins, E. G. Evagorou, J. D. Kelly and M. McPartlin, *Polyhedron*, 1992, **11**, 2571.
39. P. H. Smith, J. R. Brainard, D. E. Morris, G. D. Jarvinen and R. R. Ryan, *J. Am. Chem. Soc.*, 1989, **111**, 7437.
40. G. D. Smith, C. N. Caughlan, Mazhar-Ul-Haque and F. A Hart, *Inorg. Chem.*, 1973, **12**, 2654.
41. D. E. Fenton and P. A Vigato, *Chem. Soc. Rev.*, 1988, **17**, 69.
42. F. Benetollo, G. Bombieri, L. M. Vallarino, *Polyhedron*, 1994, **13**, 573.
43. M. Morooka and S. Ohba, *Acta Crystallogr., Sect. A*, 1992, **B48**, 667.
44. *Handbook of Chemistry and Physics*, CRC Press, 63rd edn., 1982-1983, F-179.
45. J. De Cabral, M. F. Cabral, M. G. B. Drew, F. S. Esho, O. Haas and S. M. Nelson, *J. Chem. Soc., Chem. Commun.*, 1982, 1066.
46. M. Davies, *Discuss. Faraday Soc.*, 1950, **9**, 325.
47. J. F. Carvalho, S. P. Crofts and S. M. Rocklage, *Pat. PCT Int. Appl.*, WO91/10 645, CLA61 K49/00, 1991.
48. K. I. Dhont, W. Lippens and A. M. Goeminne, *Bull. Soc. Chim. Belg.*, 1992, **101**, 1061.
49. R. Menif and A. Martell, *J. Chem. Soc., Chem. Commun.*, 1989, 1521.
50. J. Jazwinski, J.-M. Lehn, R. Méric, J.-P. Vigneron, M. Cesario and C. Pascard, *Tetrahedron Lett.*, 1987, **28**, 3489.
51. S. Waiker, PhD Thesis, University of North London, 1992.
52. J. de O. Cabral, M. F. Cabral, M. G. B. Drew, F. S. Esho and S. M. Nelson, *J. Chem. Soc., Chem Commun.*, 1982, 1068.

53. N. N. Greenwood and A. Earnshaw, *Chemistry of the Elements*, Pergamon Press, Oxford, 3rd edn., 1986, p1386.
54. S. M. Nelson, F. S. Esho, M. G. B. Drew and P. Bird, *J. Chem. Soc., Chem. Comm.*, 1979, 1035.
55. S. M. Nelson, *Pure and Appl. Chem.*, 1980, **52**, 2461.
56. M. F. Tweedle in *Lanthanide Probes in Life, Chemical, and Earth Sciences: Theory and Practice*; J.-C. G. Bünzli, G. R. Choppin (Eds.), Elsevier, New York, 1989, Chapter 5.
57. H.-J. Weinmann, R. C. Brasch, W.-R. Press and G. E. Wesbey, *Am. J. Roentgenol.*, 1984, **142**, 619.
58. H. Gries and H. Miklautz, *Physiol. Chem. Phys. Med. NMR*, 1984, **16**, 105.
59. R. B. Lauffer, *Chem. Rev.*, 1987, **87**, 909.
60. S. H. Koenig and M. J. Epstein, *Chem. Phys.*, 1975, **63**, 2279.
61. M. Magerstaadt, O. A. Gansow, M. W. Brechbiel, D. Colcher, L. H. Baltzer, R. H. Knop, M. E. Girton and M. Naegele, *Magn. Reson. Med.*, 1986, **3**, 808.
62. J. L. Sessler, T. D. Mody, G. W. Hemmi and V. Lynch, *Inorg. Chem.*, 1993, **32**, 3175.
63. M. C. Alpoim, A. M. Urbano, C. F. G. C. Gerlades and J. A. Peters, *J. Chem. Soc., Dalton Trans.*, 1992, 463.
64. K. Micskei, L. Helm, E. Brücher and A. Merbach, *Inorg. Chem.*, 1993, **32**, 3844.
65. J. Oakes and E. Smith, *J. Chem. Soc., Faraday Trans. 2*, 1981, **77**, 299.
66. J. R. Morrow, L. A. Buttrey, V. M. Shelton and K. A Berback, *J. Am. Chem. Soc.*, 1992, **114**, 1903.
67. S.-M. Peng, G. C. Gordon and V. L. Goedken, *Inorg. Chem.*, 1978, **17**, 119.
68. M. K. Muraleedharan Nair and P. K. Radhakrishnan, *Polyhedron*, 1993, **12**, 1227.
69. J. E. Huheey, *Inorganic Chemistry, Principles of Structure and Reactivity*, Harper and Row, Cambridge, 3rd Edn., 1983, p803.

70. W. T. Carnal and P. R. Fields, in *Lanthanide/ Actinide Chemistry*, P. R. Fields and T. Moeller (Eds.), Advances in Chemistry Series, 71, American Chemical Society, Washington D. C., 1967.
71. J.-C. Bünzli in *Handbook on the Physics and Chemistry of the Rare Earths*, K. A. Gschneider, Jr. and L. Eyring (Eds.), Elsevier, New York, 1987, Chapter 60.
72. E. M. Stephens, K. Schoene and F. S. Richardson, *Inorg. Chem.*, 1984, 23, 1641.
73. D. E. Henrie, R. L. Fellows and G. R. Choppin, *Coord. Chem. Rev.*, 1976, 18, 199.
74. G. R. Choppin in *Lanthanide Probes in Life, Chemical, and Earth Sciences: Theory and Practice*; J.-C. G. Bünzli, G. R. Choppin (Eds.), Elsevier, New York, 1989, Chapter 1.
75. R. Reisfeld and C. K. Jørgensen, *Lasers and the Excited States of the Rare Earths*, Inorganic Chemistry Concepts 1, Springer-Verlag, Berlin, 1977, Chapter 3.
76. W. T. Carnall, P. R. Fields and K. Rajnak, *J. Chem. Phys.*, 1968, 49, 4425.
77. L. I. Katzin and M. L. Barnett, *J. Phys. Chem.*, 1964, 68, 3379.
78. S. N. Misra and S. O. Sommerer, *Rev. Inorg. Chem.*, 1993, 12, 157.
79. T. Moeller and J. C. Brantley, *J. Am. Chem. Soc.*, 1950, 72, 5447.
80. W. T. Carnall, P. R. Fields and K. Rajnak, *J. Chem. Phys.*, 1961, 34, 477.
81. S. P. Sinha, *Complexes of the Rare Earths*, Pergamon Press, Oxford, 1966, p106.
82. C. F. Bell, *Principles and Applications of Metal Chelation*, Clarendon Press, Oxford, 1977.

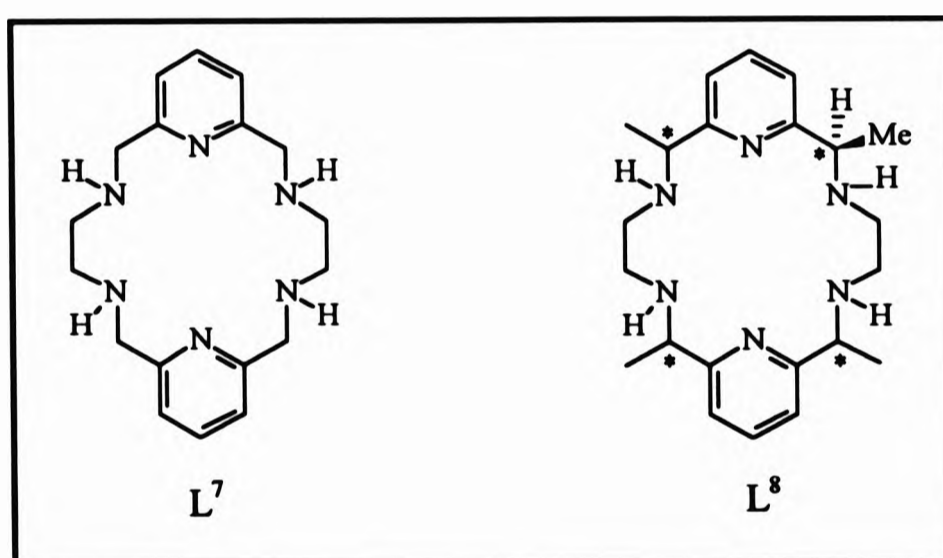
CHAPTER 3

Chapter 3: REDUCTION, DEMETALLATION AND METAL COMPLEXES OF 18-MEMBERED HEXAAZA MACROCYCLIC LIGANDS

(References to this Chapter are listed on pages 161 -163)

3.1 Introduction

The reaction of 2,6-diacetylpyridine or 2,6-pyridinedialdehyde with 1,2-diaminoethane in the presence of barium(II) resulted in the isolation of the 18-membered hexaaza tetraimine macrocycles $[\text{BaL}^1]^{2+}$ and $[\text{BaL}^2]^{2+}$ respectively (Chapter 1). Reduction of the imine, $\text{C}=\text{N}$, bonds with sodium borohydride resulted in the demetallation of L^1 and L^2 , leading to the corresponding hexaaza tetraamine macrocycles, L^7 and L^8 respectively.



Barium(II) was used as a template for the syntheses of the tetraimine macrocycles not only due to its relative size, resulting in [2+2] condensation, but where reduction and demetallation is concerned, it is favoured over other metals due to its lability. On reduction the lability of the barium(II) ion is increased which leads to its spontaneous dissociation from the macrocycle.^[1] The use of second and third row transition, lanthanide or actinide metals as templates, although as described in Chapter 2, is possible with excellent results and high yields, due to the strong bonding interactions (HSAB) between these metals with nitrogen and oxygen donor

atoms, demetallation is prevented in most cases under the applied borohydride conditions.^[2] One possibility is that demetallation does occur but the metal complexes back during the process.

In some cases where transition metals have been used as templates, the use of hydrogen chloride (Fig. 3.1a),^[3] dilute sulphuric acid (Fig. 3.1b),^[4] sodium or potassium cyanide (Fig. 3.1c)^[5] or EDTA (Fig. 3.1b)^[4] resulted in the demetallation and isolation of many macrocyclic ligands.

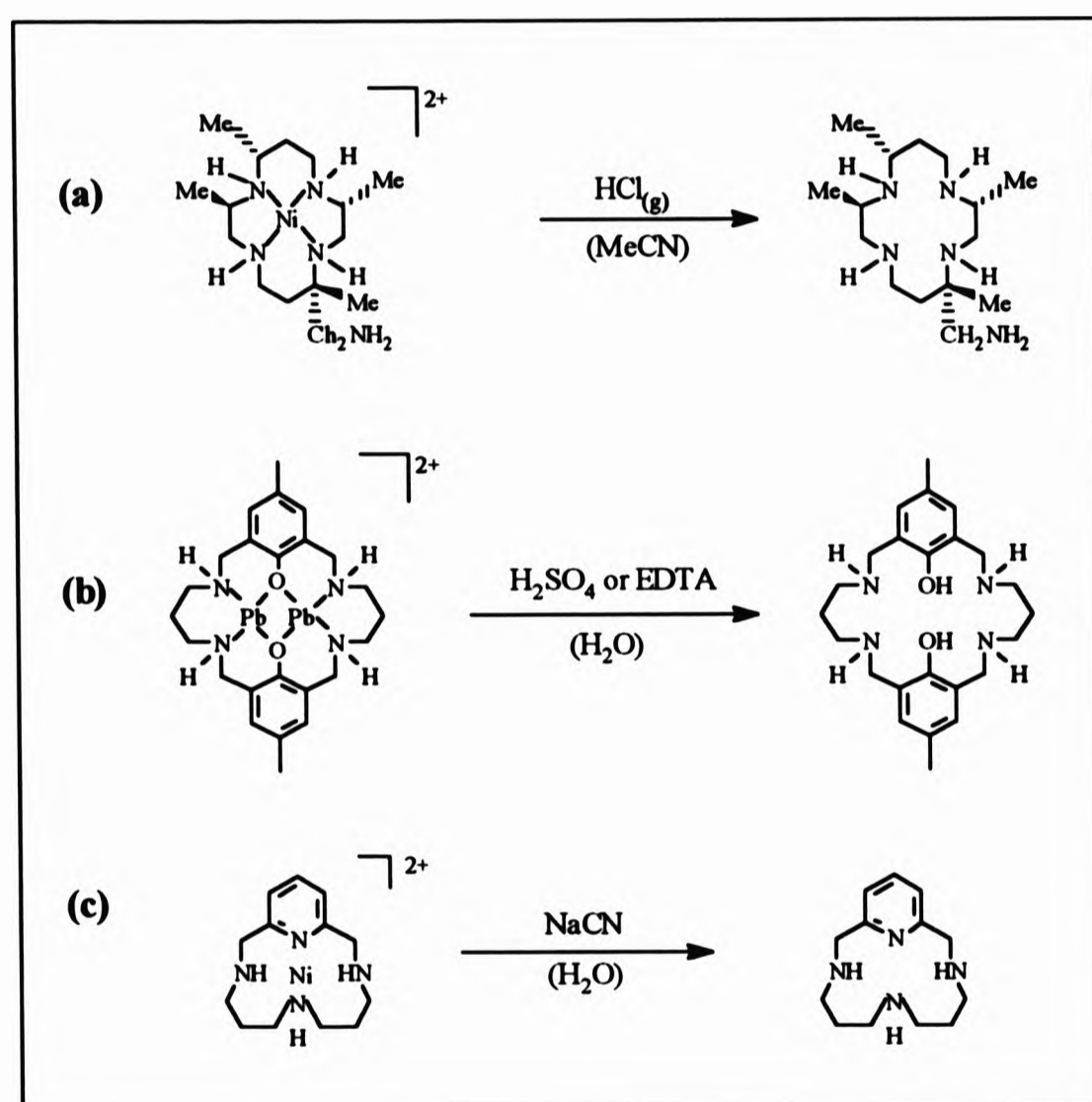


Fig. 3.1 Examples of demetallation of reduced transition metal complexes (refer to text for refs.)

Reduction and demetallation of 18-membered tetraamine macrocycles with sodium borohydride was achieved via a procedure that is well documented.^[6-11] The only difference in this work was that the barium(II) tetraamine was not isolated but

reduced *in-situ* and this is where the solubility of barium(II) chloride complexes have an advantage over those of barium(II) nitrate. This technique was used to isolate all of the reduced and demetallated macrocycles, L⁷ - L¹⁰, except where the tetraimine could be isolated metal-free.

One advantage of the free ligand over the metal template imine complexes, apart from being much more soluble in common solvents, was its selectivity towards metal ions, which may allow them to serve as therapeutic agents in metal detoxification or overload disorders particularly with metals which are unsuitable templates. This chapter discusses the characterisation of these ligands and their complexation with transition and lanthanide metals.

3.2 The Macroyclic Ligands L⁷ and L⁸

The ligands L⁷ and L⁸ were isolated in a pure form as the tetrahydrobromide salts by a published procedure and will be referred to as [L⁷H₄]Br₄ and [L⁸H₄]Br₄.^[7,12]

3.2.1 Infrared Spectrophotometry

Evidence that reduction of [BaLⁿ]Cl₂ (where n = 1, 2) had taken place was inferred by the sharp medium band at 1595 cm⁻¹ in the IR spectrum (Table 3.1) replacing the C=N band of the imine group at 1640 cm⁻¹. Although a strong sharp band at 3257 cm⁻¹ due to ν(NH) was occasionally present this was not always the case repeatedly. Its absence is attributed to the formation of the hydrobromide salt as a result of hydrogen bonding which was always observed as a series of strong sharp bands ranging from 2350 - 2800 cm⁻¹.^[13] The IR spectrum of the non-hydrobrominated amine, L⁸-free, (isolated as an oil, prior to purification as the hydrobromide salt) showed the presence of two bands at 3289 and 3319 cm⁻¹. The sharp band in the region 1573 -1578 cm⁻¹ of the ν(C=N) of the pyridyl groups has shifted to lower wavenumbers from 1585 -1595 cm⁻¹, as seen for the imine complexes in Chapter 2, suggesting that demetallation had occurred. The broad band in all L⁷ and L⁸ ligands at *ca.* 3500 and *ca.* 3430 cm⁻¹ is due to ν(OH) of lattice water. Table 3.1 summarises the major IR bands in the ligands L⁷ and L⁸.

Table 3.1 Some common bands in the infrared spectra of L^7 - L^8 ligands, in cm^{-1} .

LIGAND	$\nu(NH)$ str.	$\nu(NH)$ bend	$\nu(C=N)$ of py
$[L^7H_4]Br_4$	a	1596m	1578s
$[L^8H_4]Br_4$	3257s ^b	1595m	1573s
L^8 -free ^c	3319, 3289s	1591m	1578s
L^8 -meso	3264s	1603m	1577s

^anot observed but a series of bands due to $-NH_2Br$ observed in the region 2350 - 2800 cm^{-1} ,
^bnot observed in all cases, ^cFree indicates the amine prior to hydrobromination.

3.2.2 Mass Spectral Analyses

The EI mass spectra of $[L^7H_4]Br_4$ and $[L^8H_4]Br_4$ were consistent with the reduction and, in particular, demetallation. The spectrum of $[L^8H_4]Br_4$ has a molecular ion at m/z 706 (1%), $[(L^8H_4)Br_4]^+$, which fragments by losing initially three HBr groups followed by the loss of the final HBr group leaving a band at m/z 382 (6%). A molecular ion was not detected for $[L^7H_4]Br_4$ but a band at m/z 326 (1%) corresponding to $[(L^7H_4)Br_4 - 4HBr]^+$ was observed. The fragmentation of L^7 and L^8

follows a mechanism typical of amines by means of alpha-cleavage. Fig. 3.2 shows the alpha-cleavage sites (a, b, c and d).

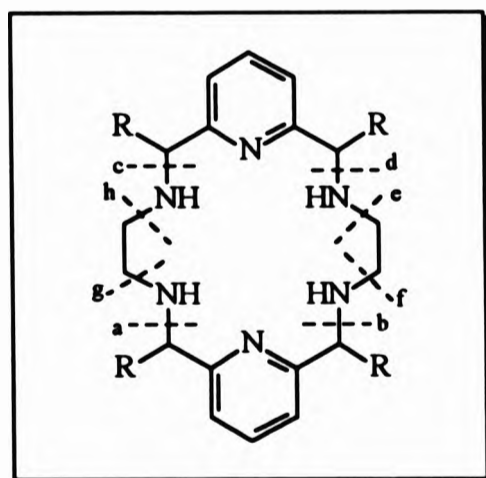


Fig. 3.2 Cleavage sites for L^7 ($R=H$) and L^8 ($R=Me$)

For macrocyclic structures, two or more bonds need to be cleaved for the formation of a fragment ion. There are four major possibilities for the initial fragmentation of the macrocycle; cleavage at a and b (or c and d), a and c (or b and d), a and d (or b and c), e and g (or f and h) and e and f (or g and h). The fragmentation

which was prominent was formed from the cleavage at sites a and d which

corresponds to $[L^n/2]^+$ where $n = 7, 8$ (Fig. 3.3).

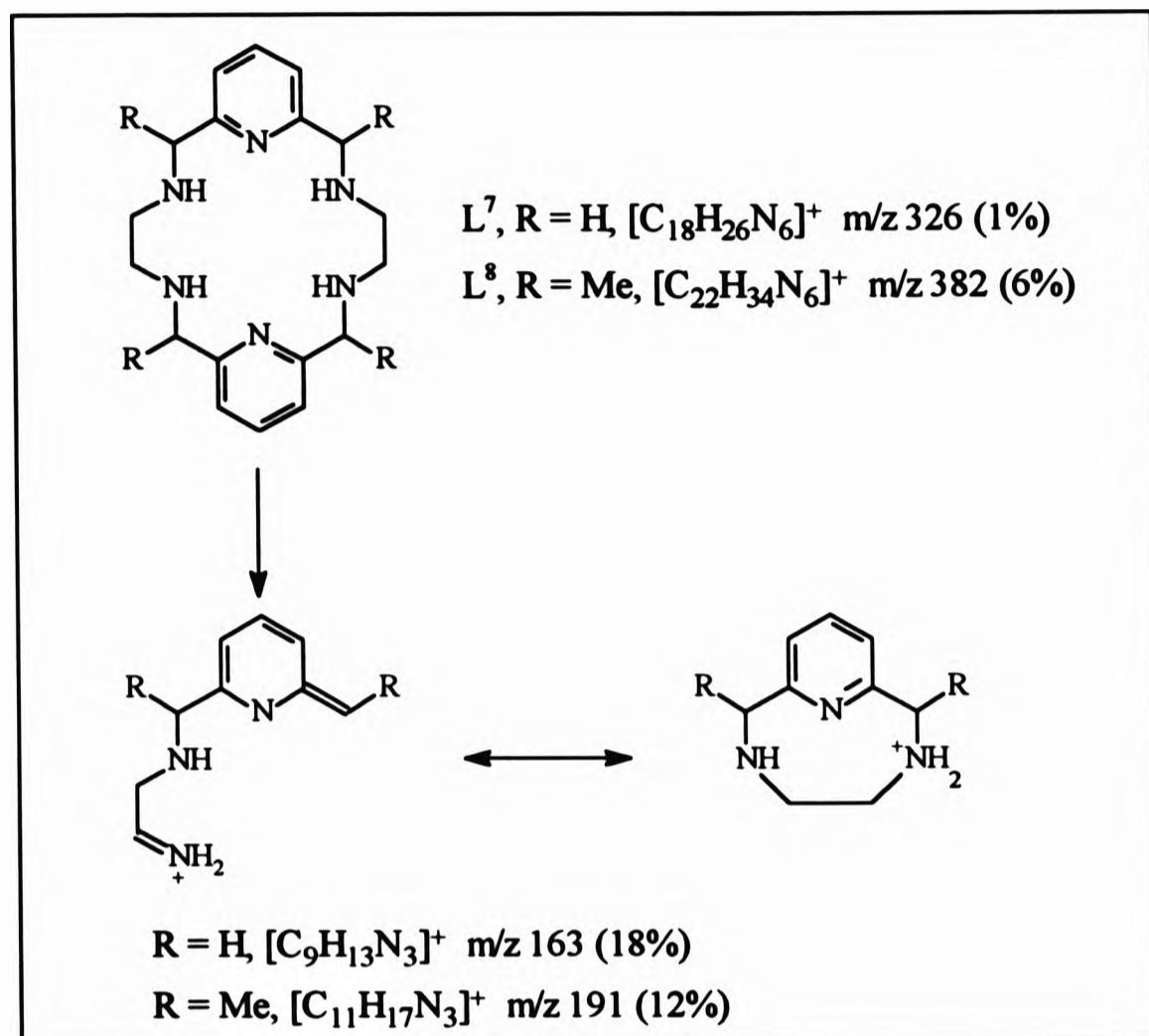
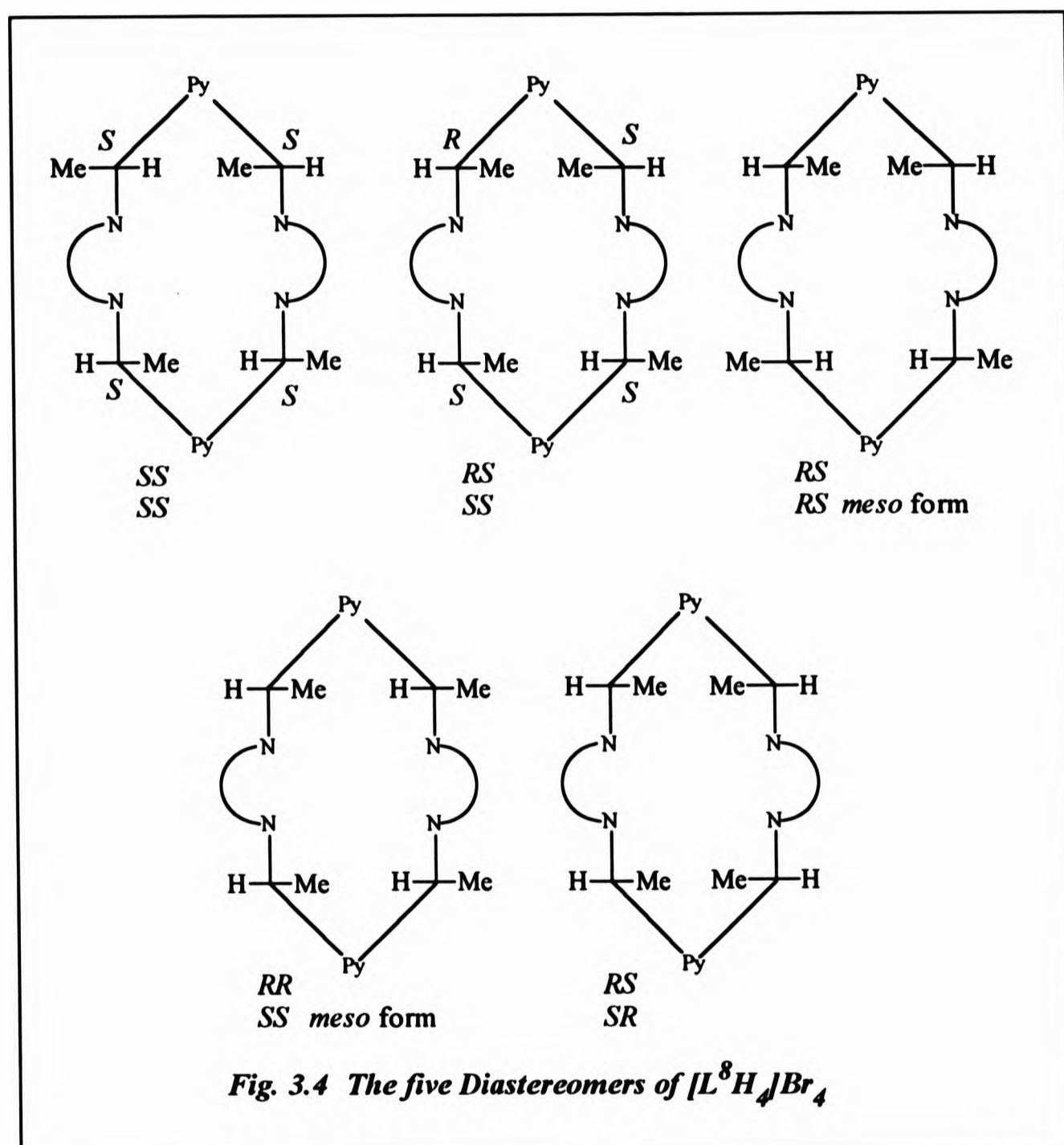


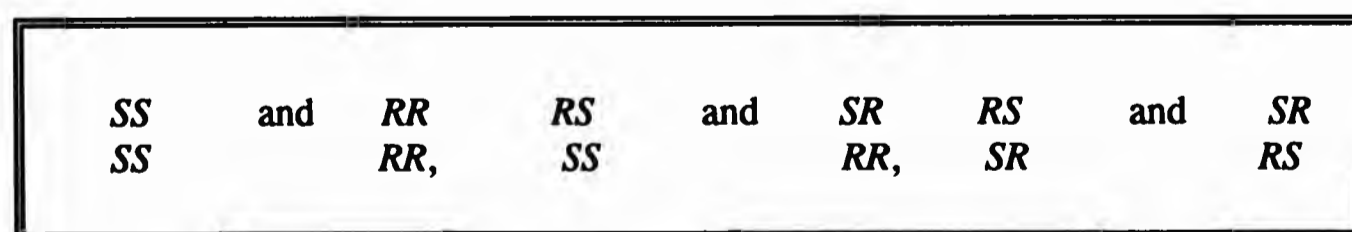
Fig. 3.3 The formation of $[L^n/2]^+$ ($n = 7, 8$)

3.2.3 NMR and Circular Dichroism Spectroscopy of $[L^7H_4]Br_4$ and $[L^8H_4]Br_4$
 $[L^8H_4]Br_4$ exists as many enantiomeric forms due to the methine carbon centres (*) being chiral. Each chiral centre may have either the configuration *R* or *S* according to the Cahn-Ingold-Prelog rules or the *RS* convention.^[14,15] The number of possible enantiomers expected would be sixteen. But due to all four chiral carbon centres being identical, as far as the substituent groups are concerned, this indicates that the number of possible enantiomers should be less than sixteen and hence there is the presence of *meso* forms and diastereoisomerism.^[16] Additionally, there would also be less than sixteen enantiomers to be considered from the stereochemistry of the four identical secondary amine nitrogen centres. But the formation of the NH_2^+ salt implies

that these nitrogen atoms are no longer chiral and that the two protons are symmetrically equivalent. The actual number of diastereomers, as shown in Fig. 3.4, is five, two of which are *meso* forms, hence six enantiomers.



The enantiomers are paired as follows:



The two diastereomers, *RSRS* and *RRSS*, represent the *meso* forms and the plane of symmetry about their structures does not allow for them to have an enantiomeric counterpart.

Although $[L^8H_4]Br_4$ was isolated as a pure white solid with the expected elemental and mass spectral analyses, these analyses could not indicate the presence of enantiomeric species. That the compound was a mixture of diastereomers was evident from the 1H NMR (Fig. 3.6a). In other words, the resonances and the chemical shifts could be assigned to a particular structural group of the macrocycle but the multiplicities of each band could not be accounted for. The same is also true for the coupling constants. The complexity can be observed by regarding the methyl protons centred at δ_H 1.55. If only one enantiomer could be considered, the methyl protons would *probably* resonate at *ca.* δ_H 1.6 but only one band would be expected depending on whether all the chiral centres had the same configuration and on the planarity or symmetry of the macrocycle as a whole. By observing a complex multiplet in the 1H NMR spectrum this indicates that the methyl protons are in different environments, and since there are more than four bands in the multiplet, and the mass spectral and elemental analyses agree with the required formulation, this would suggest the presence of a number of different isomers. The same reasoning applies for methylene protons centred at δ_H 3.0, the aromatic protons at δ_H 7.4 and 7.9 and the methine protons at δ_H 4.35. Irrespective of the complexity, the integration of the bands corresponded to the number of protons in the macrocyclic structure.

Recrystallisation of the white solid of $[L^8H_4]Br_4$ in water/concentrated hydrochloric acid (1 : 1) and allowing the mixture to stand at room temperature afforded colourless crystals which dulled on isolation indicating the loss of solvent. When analysed these proved to be the *meso* form of $[L^8H_4]Br_4$. From here onwards the *meso* form will be referred to as the L^8 -*meso*.

The crystals were determined to be the *meso* form by circular dichroism (CD) spectroscopy.^[17,18] The spectrum in Fig. 3.5 shows that the sample was not optically active since it did not interact with polarised light indicating it could be the *meso* form. This in itself is not directly conclusive since any one diastereomer, other than the *meso*, in other words a 50:50 mixture of two non-superimposable mirror image enantiomers (a racemic mixture), would also not affect polarised light as they would cancel each other out. ¹H NMR and X-ray crystallography discussed from here onwards will prove that the compound is the *meso* form alone.

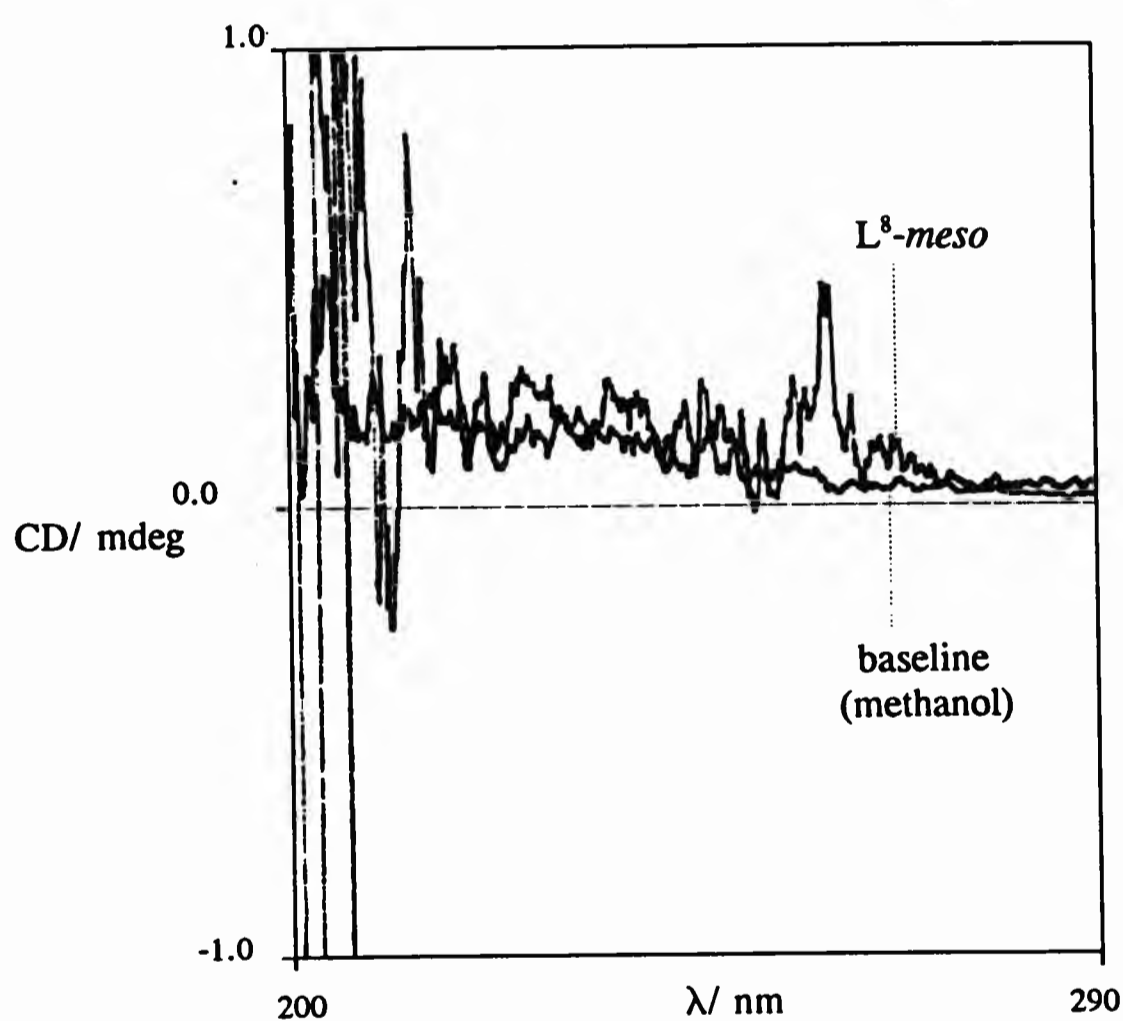
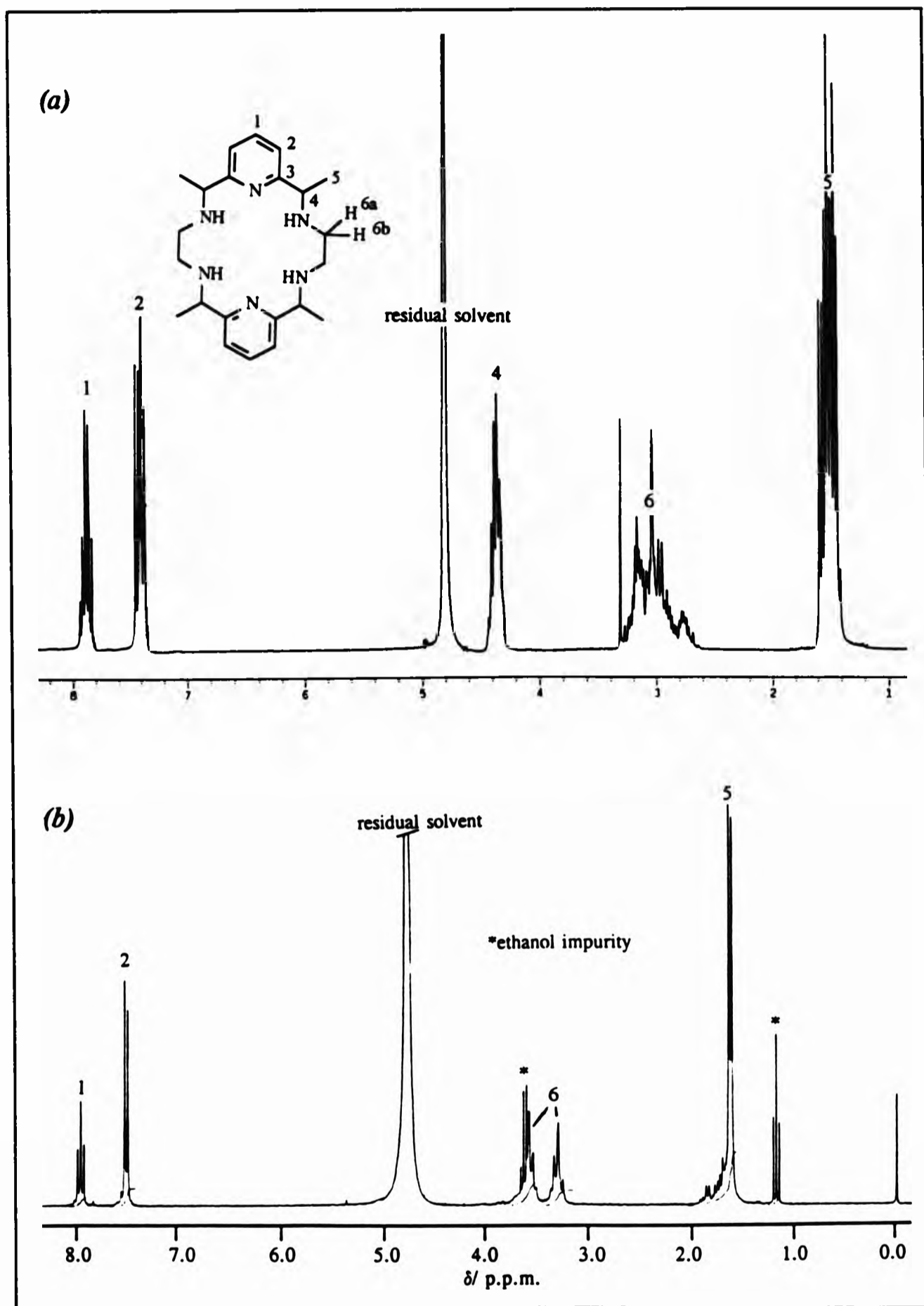


Fig. 3.5 Circular dichroism spectrum of *L⁸-meso*

Fig. 3.6 The ^1H NMR of (a) $[\text{L}^8\text{H}_4]\text{Br}_4$ in D_2O and at 500 MHz - a mixture of diastereomers and (b) $\text{L}^8\text{-meso}$ in D_2O and at 250 MHz - one diastereomer (relative to SiMe_4 as internal standard at 0.0 p.p.m.)



The ^1H NMR spectrum of the crystals of $\text{L}^8\text{-meso}$ in D_2O and at 250 MHz (Fig.3.6b) was so less complicated, in that there were no complex multiplets, such that the multiplicities could be accounted for. There were no changes in the integral values compared to those of $[\text{L}^8\text{H}_4]\text{Br}_4$. Broad bands were not available due to the acidic NH protons from their exchange with deuterium but these acidic protons were also not observed when the spectrum was recorded in $\text{d}_6\text{-DMSO}$.

The typical *triplet-doublet* arrangement of an AB_2 coupled system, as observed for the ^1H NMR of the tetraimine compounds (Chapter 2), is also seen here centred at δ_{H} 8.06 and 7.59 and is assigned to H^1 and H^2 respectively, the coupling constant, $^3J(\text{H}^1, \text{H}^2)$, typically, being 7.8 Hz. Two *singlets* at δ_{H} 1.73 and 1.70 arise from the methyl protons being in two different environments, typical of methyl groups close to a chiral centre.¹¹³⁾ The methine protons were not observed since they resonate at the same chemical shift as DOH , the NMR solvent, at δ_{H} 4.8. These became apparent when the spectrum was ran in $\text{d}_6\text{-DMSO}$. Two *singlets* were observed for these also, at δ_{H} 4.83 and 4.88. Proton coupling between CH^4 and CH^5 or NH^6 does not occur.

The spectrum also shows an A_2B_2 system, a *doublet of quartets*, centred at δ_{H} 3.55 which is assigned to the bridging methylene groups, H^{6a} and H^{6b} [$^3J(\text{H}^{6a}, \text{H}^{6b}) = 10.6$ Hz]. The *quartet* most downfield is shadowing a *doublet*. This *doublet* is, in fact, also a *quartet*, from a methylene group coupled to a methyl group, the *triplet* shown upfield at δ_{H} 1.17. These bands are typical of ethanol, an impurity in the NMR tube. That these two bands are coupled was concluded by their coupling constant, $^3J(\text{CH}_2, \text{CH}_3) = 7.1$ Hz

The broad band proton decoupled ^{13}C NMR spectrum of $\text{L}^8\text{-meso}$ (Table 3.2) was also relatively simple. The pyridine carbon atoms resonated at δ_{C} 157.82 (C^3), 143.49 (C^1) and 126.71 (C^2). Two bands were observed for the methyl carbon atoms (C^5) at δ_{C} 22.97 and 19.73 the former being more intense than the latter. The two bands at δ_{C} 60.32 and 44.65, characterised by DEPT-135 ^{13}C NMR spectra, are

assigned to the methylene carbon atom, C⁶, the band downfield being less intense than the band upfield. Only one band resonating at δ_c 62.54 was due to the methine carbon atoms, C⁴.

Fig. 3.7 *L'* showing the two planes of symmetry

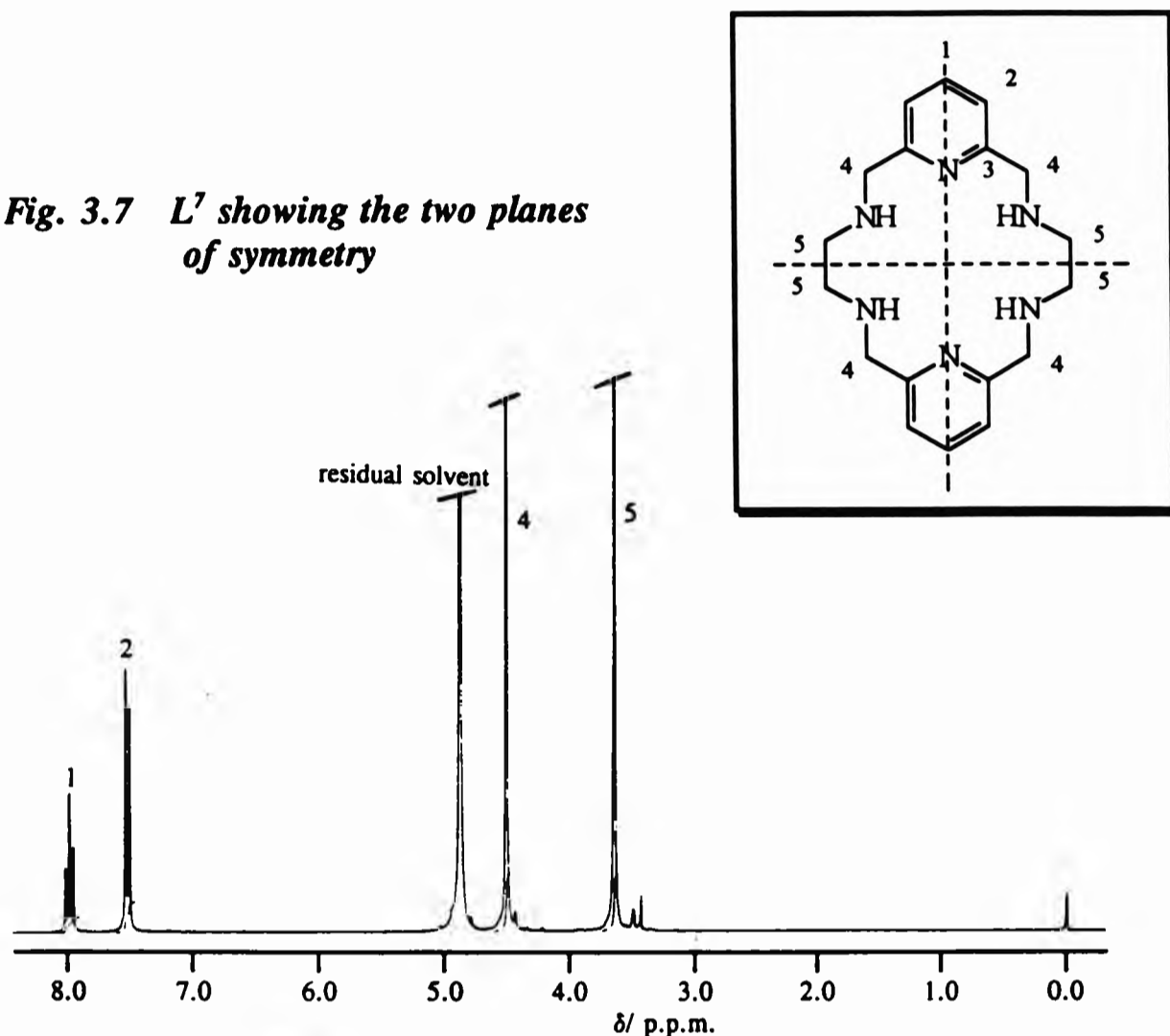


Fig. 3.8 The ¹H NMR of [L⁷H₄]Br₄ in D₂O and at 250 MHz (relative to SiMe₄ as internal standard at 0.0 p.p.m.)

For comparison purposes the experiment was repeated with 2,6-pyridinedialdehyde instead of 2,6-diacetylpyridine yielding [L⁷H₄]Br₄. In this case there are no chiral carbon centres and only one conformation is possible, as was detected by the ¹H NMR (Fig. 3.8). The spectrum shows the molecule to have two planes of symmetry (Fig. 3.7), indicating that the bridging methylene protons, H⁵, are in the same environment. These appear as a *singlet* at δ_H 3.63 (H⁵). The *singlet* at δ_H 4.50 arises from the methylene groups, H⁴. One band was observed for each of the carbon atoms C⁴ and C⁵ at δ_H 54.43 and 48.11 respectively (Table 3.2) in the ¹³C NMR spectrum.

Table 3.2 The ^1H and ^{13}C NMR chemical shifts^a of L^8 -meso in D_2O

ASSIGNMENT	δ_{H}	Hz	δ_{C}
1	8.04 (t)	$^3J(\text{H}^1, \text{H}^2) = 7.78$	143.49
2	7.59 (d)	7.78	126.71
3	-	-	157.82
4	4.83(s), 4.88(s)	-	62.54
5	1.73(s), 1.70(s)	-	22.97, 19.73
6	3.55 (d of q)	$^3J(\text{H}^6, \text{H}^7) = 10.6$	60.32, 44.65
7	not detected	-	-

^ain p.p.m

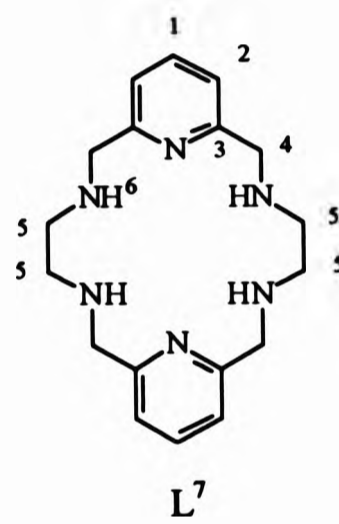
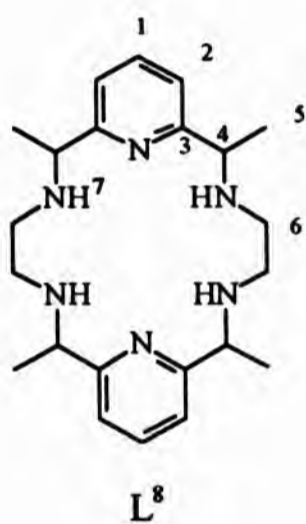


Table 3.3 ^1H - and ^{13}C -NMR Chemical Shifts^a of $[L^7\text{H}_4]\text{Br}_4$ in D_2O .

ASSIGNMENT	δ_{H}	δ_{C}
1*	8.00 (t)	142.01
2*	7.53 (d)	125.22
3	-	154.82
4	4.50 (s)	54.43
5	3.63 (s)	48.11
6	not detected	-

$^3J(\text{H}^1\text{H}^2) = 7.78 \text{ Hz}$

^ain p.p.m with SiMe_4 as internal standard

3.2.4 The Absolute Configuration of L^8 -meso

The absolute configuration of L^8 -meso, in the solid state, was achieved via X-ray crystallography. Colourless crystals were grown from water and the perspective views are shown in Fig. 3.9.

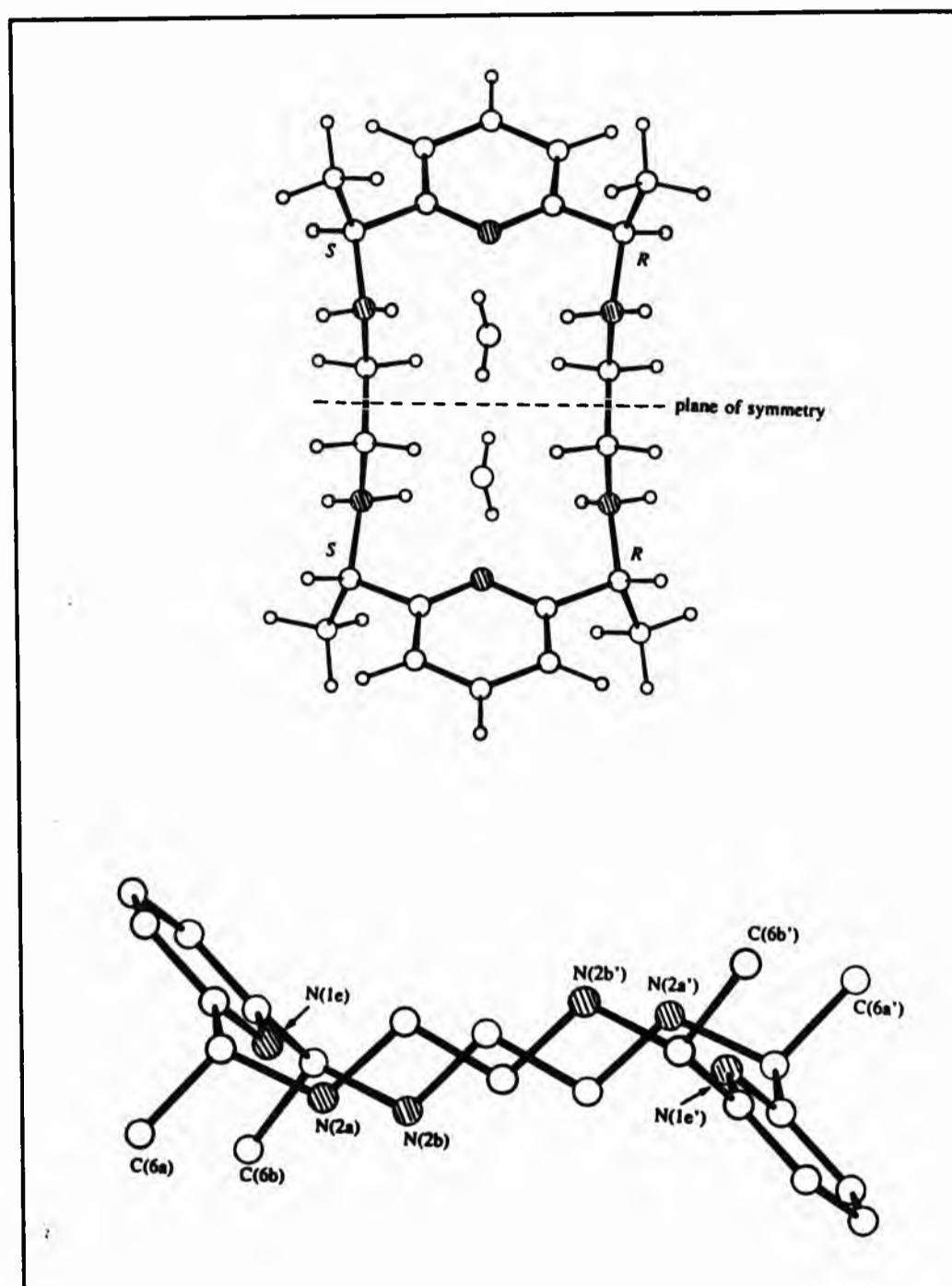


Fig 3.9 The perspective views showing the absolute configuration of L^8 -meso.2H₂O and the plane of symmetry about the molecule. (Bromine atoms are omitted from both structures and the water molecules from the second structure)

The unit of the crystal contained only half of the ligand with an inversion about the centre. This was the first indication that the molecule was centrosymmetric, *i.e.* it

had a plane of symmetry about itself. Assigning the chiral centres according to the X-ray crystal structure, there is only one position for the plane of symmetry (Fig. 3.9). The configuration adopted, *SRSR*, is in agreement with the configuration predicted for one of the *meso* forms in Fig. 3.4.

Finally, this concludes that this compound is the *meso* form of $[L^8H_4]Br_4$. The plane of symmetry results from the configuration of the chiral centres and this confirms that there are two methyl and two methylene environments as depicted by the 1H and ^{13}C NMR spectra.

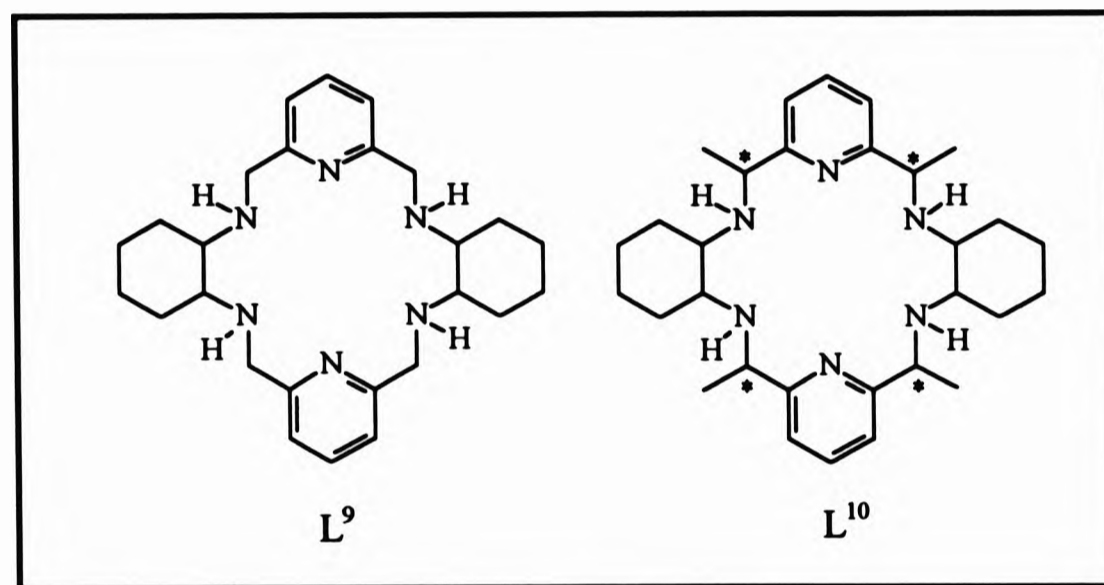
L^8 -*meso* crystallises with two molecules of water of crystallisation per unit. It too adopts a stepped conformation as L^6 (Chapter 2) but the co-planarity of the diimino pyridine regions is lost when the $C=N$ double bond is reduced to a single bond, thus rendering the structure of the molecule much more flexible. The average $C=N$ bond length in L^6 is 1.271 Å. The length increases, on reduction, to an average of 1.513 Å for $[L^8H_4]Br_4$. One similarity of the two structures is that the two methyl groups C(6a) and C(6b) are both pointing behind the plane of the adjacent pyridine ring and the two methyl groups C(6a') and C(6b') are pointing out of the plane of their adjacent pyridine ring.

From the crystal structure and from models the conformation adopted by the *meso* form, *RSRS*, is the energy minimum as no indication of steric interaction between the methyl groups and the methylene or the pyridyl protons is evident.

Metal complexation of these ligands was not carried out as this was not the purpose for the syntheses of $[L^7H_4]Br_4$ or $[L^8H_4]Br_4$. Stability constants with $[L^7H_4]Br_4$ have been reported^[12] with alkali earth, transition and lanthanide metals and the solid state structure of $ZnL^7(CF_3SO_3)_2$ was only very recently published^[19] where the structure adopted by the ligand involves the ligand octahedrally wrapping itself around the metal in a hexa-co-ordinated manner. Metal co-ordination will be discussed further in Section 3.4.1.4 and 3.4.2.4.

3.3 The Macrocyclic Ligands L⁹ and L¹⁰ Incorporating the Cyclohexyl Group

Reduction of the free ligands L⁵ and L⁶ yielded the cyclohexane amine derivatives L⁹ and L¹⁰ respectively. Isolation of these products as the tetrahydrobromide salts proved impossible as unstable hygroscopic materials were obtained which were not analysed. Both products were initially isolated as brown-yellow oils which were purified *via* silica based column chromatography,^[9] the eluents containing the pure tetraamine being a 5:1 mixture of methanol/ammonia solution.



L⁹ was obtained as a pure white solid which was recrystallised to colourless crystals. The powdered form became off-white on prolonged standing but this change in colour did not alter the composition of the compound. In contrast, L¹⁰ was isolated as an oil.

3.3.1 Infrared and Mass Spectrometry

The IR spectra (Table 3.4) of L⁹ and L¹⁰ confirmed the synthesis of the tetraamine compounds. One medium sharp band at 3305 cm⁻¹ for L⁹ and two at 3358 and 3288 cm⁻¹ for L¹⁰ were assigned to the $\nu(\text{NH})$ stretch. Not considering the band at

3288 cm⁻¹, the bands at 3305 and 3358 cm⁻¹ are at higher wavenumbers than those observed for [L⁸H₄]Br₄. This is suggested to be due to the absence of the hydrogen bonded HBr group, the series of bands in the region 2800 - 2350 cm⁻¹ also being absent. The ν(NH) bend vibrations resonate at 1592 cm⁻¹ for both L⁹ and L¹⁰ and these values are in agreement with [L⁷H₄]Br₄, [L⁸H₄]Br₄ and L⁸-free. For L⁹, a series of medium bands at 714, 742, 792, 828 and 862 cm⁻¹ arose due to the ν(NH) out of plane bend. In the L¹⁰ spectrum this is depicted by relatively broad band centred at 732 cm⁻¹ and a medium band at 814 cm⁻¹. The medium band at 1576 cm⁻¹ and the strong band at 1451 cm⁻¹ correspond to the pyridine ring absorbances, the former being due to ν(C=N) and the latter due to the ν(C-C) stretching modes.

Table 3.4 Some common bands in the infrared spectra of L⁹, L¹⁰ and [L⁹H₄](ClO₄)₄

LIGAND	ν(NH) str.	ν(NH) bend	ν(C=N) of py
L ⁹	3305m	1592m	1577s
[L ⁹ H ₄](ClO ₄) ₄	3337m	1595m	1581m
L ¹⁰	3358, 3288m	1592m	1577s

The most intense bands in both spectra are due to the ν(C-H) stretches of the cyclohexyl group at 2853 and 2927 cm⁻¹. The band at 2970 cm⁻¹, resonating only in the IR spectrum of L¹⁰, is assigned to the ν(C-H) stretch of the methyl groups.

A parent ion was detected for both ligands in the EI and LSIM spectra. The fragmentations of L⁹ and L¹⁰ (Table 3.5) follow the same pattern as that described for [L⁷H₄]Br₄ and [L⁸H₄]Br₄. The LSIM spectrum of L⁹ has a parent ion at 100% abundance. In contrast, the parent ion of L¹⁰ is 5% abundant, the ion with the composition [C₇H₆N₃]⁺ and m/z 132 being the most stable having an intensity of 100%. The characteristic fragment, [Lⁿ/2], where n = 9, 10, was observed for both ligands, irrespective of the ionisation type employed.

Table 3.5 Common fragmentations* of L⁹, via LSIMS, and L¹⁰, via EI

L ⁹		L ¹⁰	
FRAGMENT	m/z	FRAGMENT	m/z
[C ₂₆ H ₃₈ N ₆ + H] ⁺	435 (100)	[C ₃₀ H ₄₆ N ₆] ⁺	490 (5)
[C ₁₃ H ₁₉ N ₃ + H] ⁺	218 (26)	[C ₁₅ H ₂₃ N ₃] ⁺	245 (29)
[C ₇ H ₅ N ₃ + H] ⁺	132 (9)	[C ₇ H ₆ N ₃] ⁺	132 (100)

* Relative abundances(%) given in parentheses

3.3.2 Nuclear Magnetic Resonance Spectroscopy

The ¹H NMR spectrum of L⁹ (Fig. 3.10) in CDCl₃ and at 250 MHz confirms the integrity of this compound. The assignments are made on the spectrum. The *triplet* at δ_H 7.53 is coupled to the *doublet* at δ_H 7.03, the two bands forming an AB₂ system. These arose due to the pyridyl protons, H¹ and H², the coupling constant being ³J(H¹,H²) = 7.65 Hz. Compared to the spectra of the amines [L⁷H₄]Br₄, [L⁸H₄]Br₄ and L⁸-*meso*, these two bands have shifted upfield by *ca.* 0.5 p.p.m.

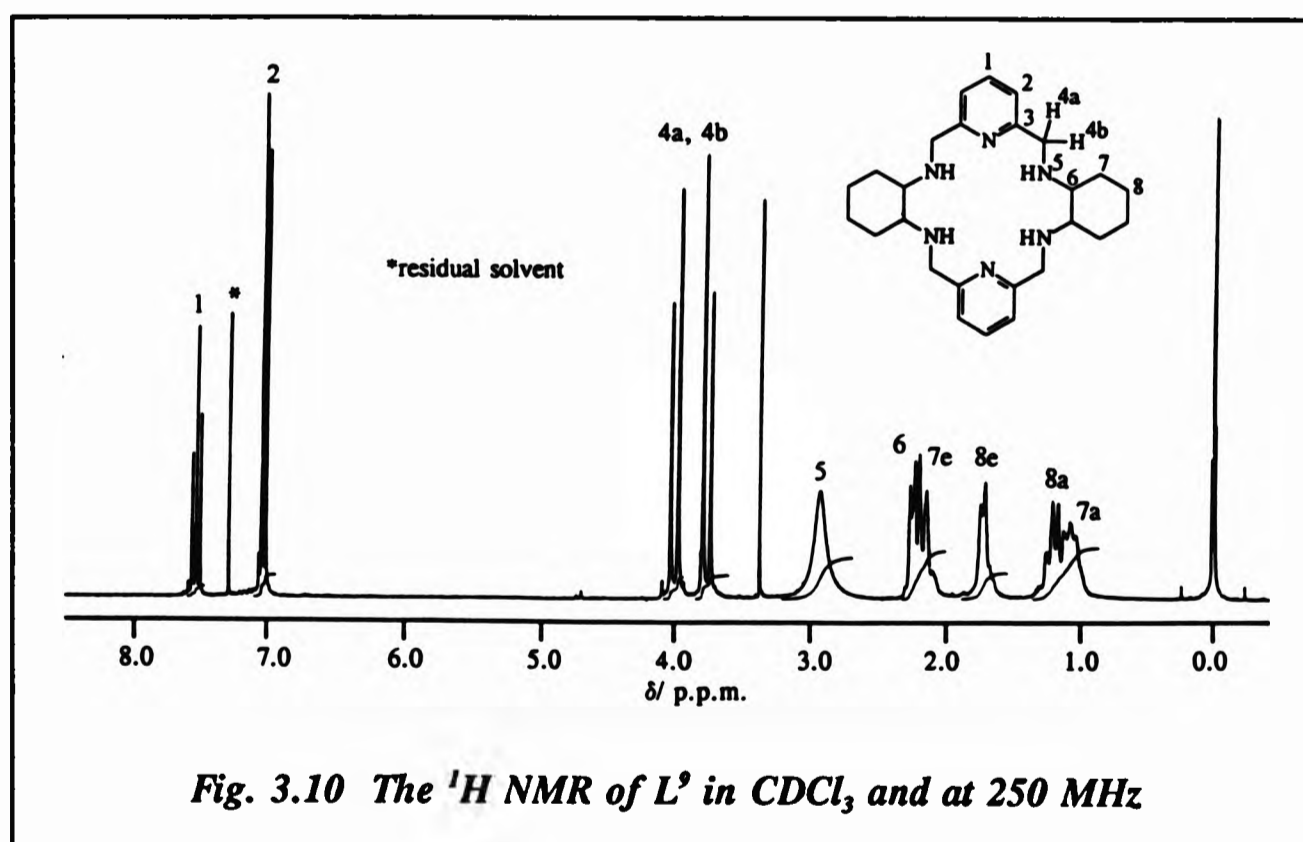


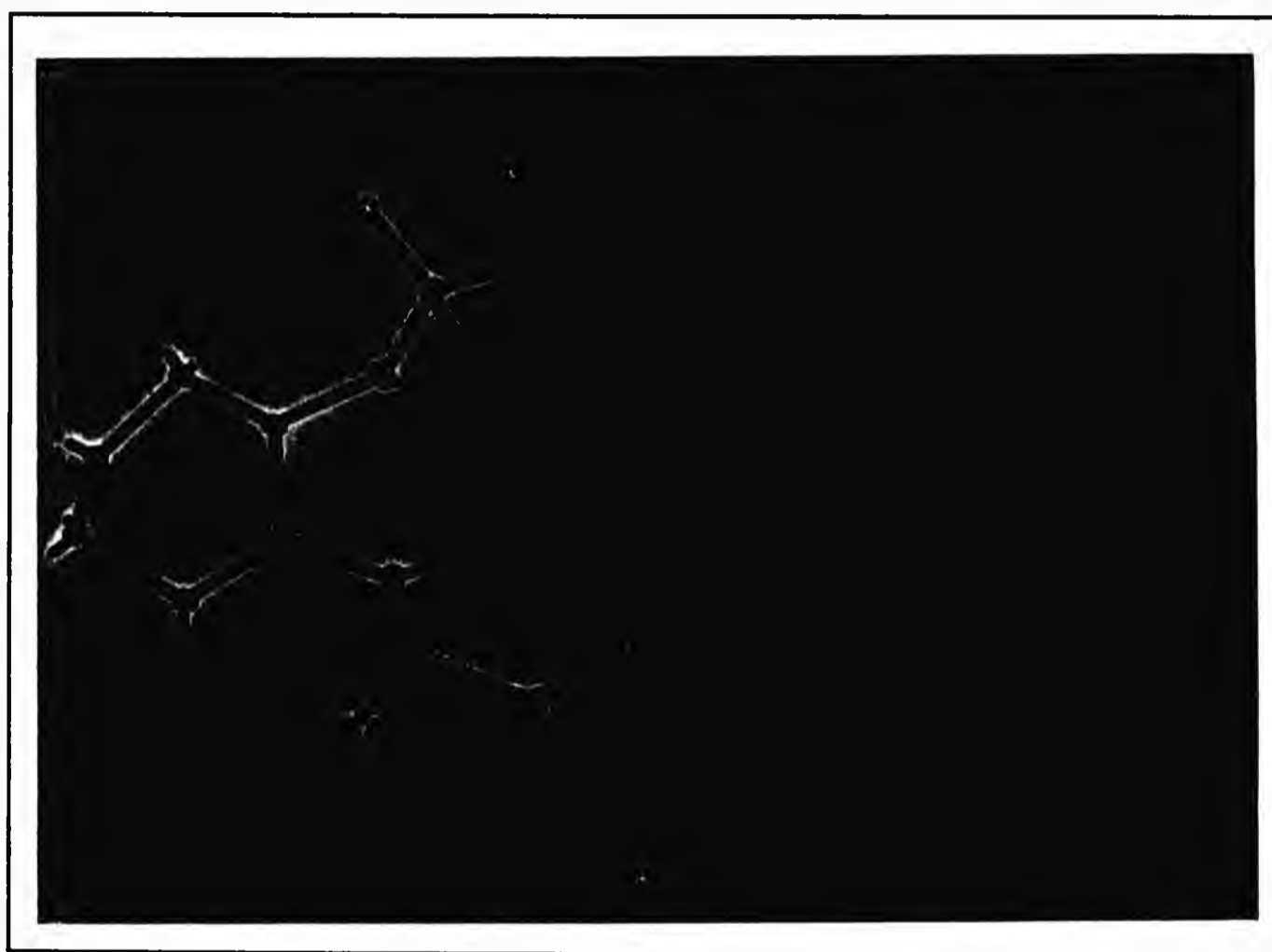
Fig. 3.10 The ¹H NMR of L⁹ in CDCl₃ and at 250 MHz

The broad band at δ_{H} 2.93 is due to the *NH* functionality as this proton exchanged with deuterium on addition of D_2O to the CDCl_3 solution of the sample. The only anomaly was that this band integrated for 7.5 protons whereas only four of these protons are available in the structure of L^9 . Accounting for the two water molecules of crystallisation, as predicted by the elemental analysis, this value is no longer an anomaly. Also, a *singlet* due to the methyl protons of methanol resonates at δ_{H} 3.4.

The methylene protons, H^4 , give rise to a band of doublet of doublets centred at δ_{H} 3.88 as a result of geminal, 2J , coupling of the protons on the same carbon atom. This is representative of an AB pattern with a typical coupling constant, $^2J(\text{H}^{4\text{a}}, \text{H}^{4\text{b}}) = 13.7$ Hz suggesting that the two methylene protons are non-equivalent (anisochronous on the NMR timescale) and that the methylene carbon atoms, C^4 , are prochiral.^[20,21] The large coupling constant is consistent with the methylene protons being adjacent to the electronegative nitrogen atom and overlapping with the π -bonds of the pyridine rings.^[13] Furthermore, the chiral nitrogen centres contribute to the methylene protons being non-equivalent.^[22] These protons would still be non-equivalent even if fast rotation about the $\text{C}^3 - \text{C}^4$ or $\text{C}^4 - \text{N}^5$ bonds is assumed. The remaining other bulky substituents on C^4 also play a rôle in the non-equivalence of $\text{H}^{4\text{a}}$ and $\text{H}^{4\text{b}}$ when viewed as Newman projections. As only four signals are observed due to these methylene protons the structure lacks a symmetry plane through the prochiral carbon atoms. But the structure as a whole does have a centre of symmetry, alternatively eight bands would have been expected for these protons. Therefore, all four C^4 carbon centres are in the same environment since only one band is depicted in the ^{13}C spectrum for these carbon atoms, yet two protons are found to correspond to this band as shown by the ^{13}C - ^1H -COSY spectrum. A prediction to the stereochemistry of the C^4 carbon centres, through molecular models, is that one proton, $\text{H}^{4\text{b}}$, is directed towards the centre of the macrocycle whilst the other proton coupled to it, $\text{H}^{4\text{a}}$, is directed away from the macrocycle altogether, as depicted by the photograph in Fig. 3.11. This arrangement does not alter the symmetry as far as the carbon skeleton structure is concerned, hence in the broad band proton decoupled ^{13}C NMR spectrum, a quarter of the molecule is

observed, in other words, the structure contains two planes of symmetry, these being the same as for $[L^7H_4]Br_4$ (Fig. 3.7).

Fig. 3.11 *The structural arrangement adopted by L^9 (hydrogen atoms other than H^1 , which are shown in red, are omitted for clarity)*



A prediction calculated by the molecular modelling package, Alchemy III, supports this reasoning and Fig. 3.12 shows two views of the minimised structure of L^9 . Interestingly, the structures (Fig. 3.12) show both the cyclohexyl groups to be folded towards each other.

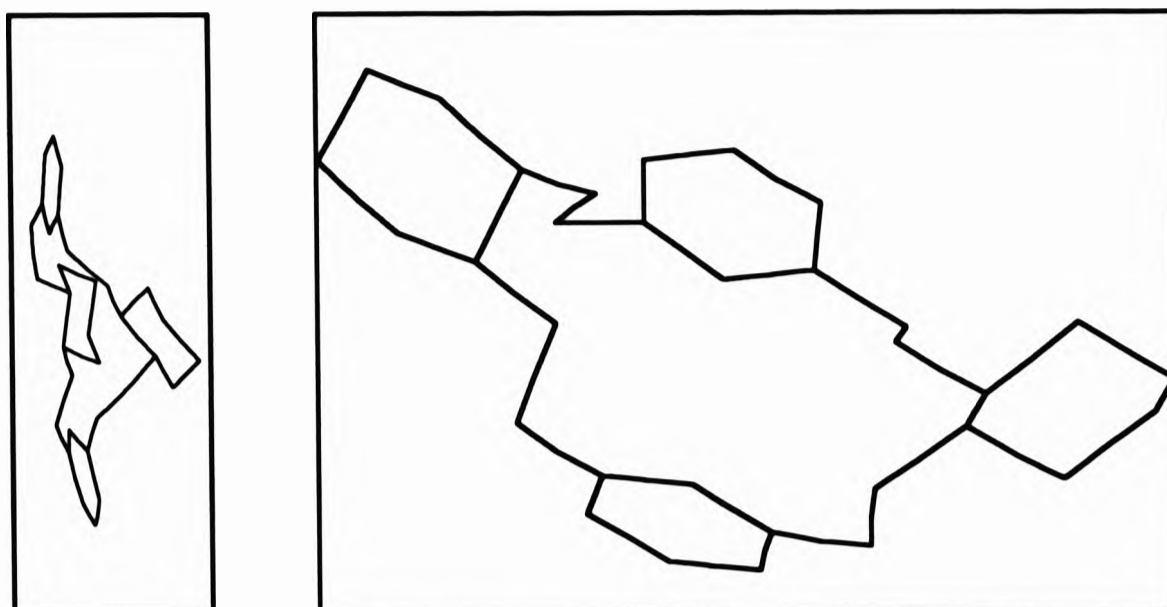
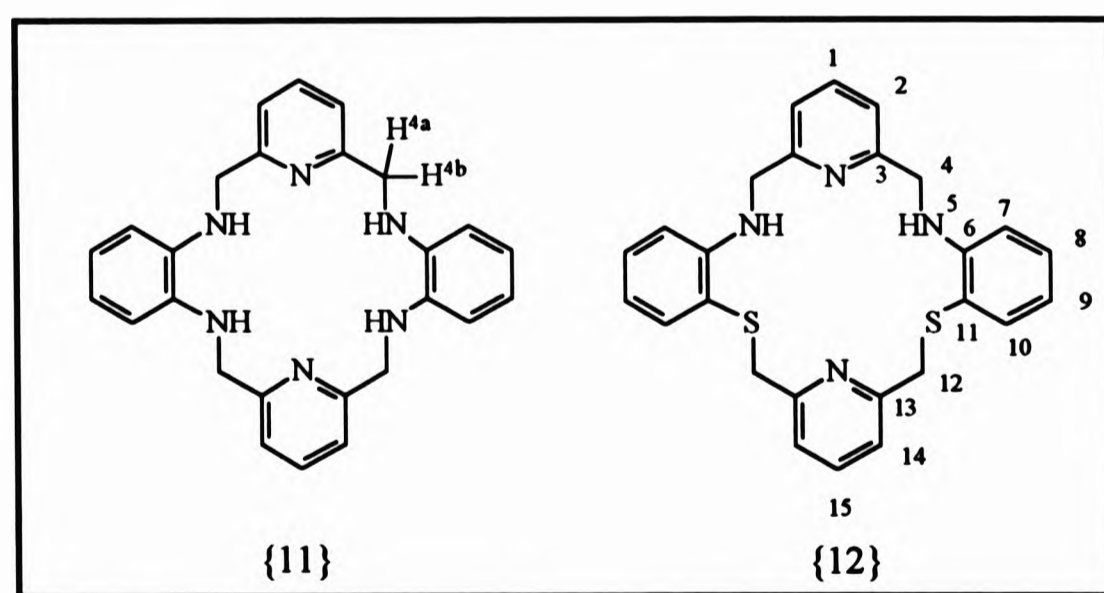


Fig. 3.12 The minimized structures of L^9 as calculated by the Alchemy III package

Likewise, an 18-membered hexaaza analogue $\{11\}^{[23]}$ also exhibits prochirality about C^4 suggesting that protons H^{4a} and H^{4b} are also non-equivalent. In contrast a *doublet* with a smaller band on either side for the methylene protons and a *multiplet* for the amino proton suggests they are coupled, the *doublet* resulting from the collapse of an AB system, the whole system being one of the type ABX. On D_2O addition, the amino protons exchange with deuterium leaving a *triplet* with the intensities 1:16:1, for the methylene protons, the two inner bands having coalesced.

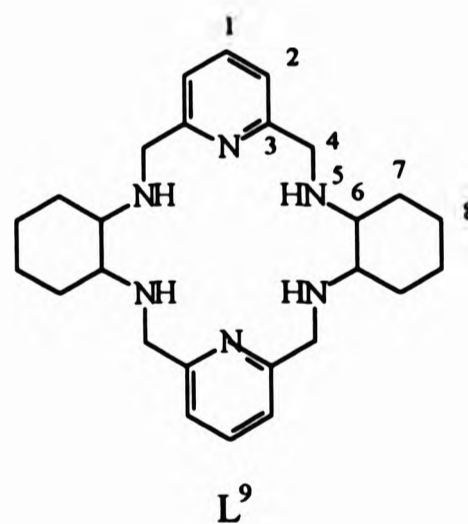


To further contrast, the methylene protons H^4 and H^{12} , for the N_4S_2 macrocycle {12},^[24] resonate as a *doublet* and a *singlet* at δ_H 4.36 and 4.04 respectively. The *doublet* for H^4 is due to coupling with the acidic amino proton, H^5 , and collapses to a *singlet* on D_2O addition. Free rapid rotation about the C-S and C-N bands in solution makes the methylene protons magnetically equivalent on the NMR timescale.

The chiral centres at C^6 in the structure of L^9 are locked and no rotation is possible, so only one configuration is adopted by each centre and no alternatives are likely. The off resonance broad band proton decoupled ^{13}C NMR spectrum (Table 3.6) was solved with the aid of a DEPT - 135 spectrum, seven bands resonating in all, representing a quarter of the structure, thus confirming the two planes of symmetry discussed above. Solving the ^{13}C NMR spectrum enabled the elucidation of the region 1.0 - 2.5 p.p.m. of the 1H NMR spectrum, *via* a ^{13}C - 1H - and 1H -COSY spectra (Fig. 3.13), which represents the protons of the cyclohexane rings.

Table 3.6 The chemical shifts^a of the ^{13}C NMR spectrum of L^9 in $CDCl_3$,

ASSIGNMENT	δ_c
1	136.42
2	120.96
3	159.44
4	51.22
5	-
6	59.83
7	30.72
8	25.02



^ain p.p.m relative to $SiMe_4$ as internal standard at 0.0 p.p.m.

The ^{13}C - ^1H -COSY spectrum indicated that the cyclohexyl carbon atoms are also prochiral such that the two protons of each methylene group bonded to the carbon atoms C^7 and C^8 are inequivalent, *i.e.* one is axial and the other equatorial. The multiplet band centred at δ_{H} 1.15 is, in fact, from protons H^7 and H^8 . This multiplet represents the four axial protons of H^7 (δ_{H} 1.1) and the four axial protons of H^8 (δ_{H} 1.2). The four equatorial protons of H^8 resonate alone, the band being centred at δ_{H} 1.72.

The distinction between axial and equatorial protons could be made as it is well known that axial protons generally come to resonate at higher field than their equatorial counterparts.^[13] The multiplet band at δ_{H} 2.19 was assigned to the four methine protons, H^6 and the four equatorial protons, $\text{H}^{7\text{e}}$, H^6 being downfield to $\text{H}^{7\text{e}}$. The ^1H -COSY spectrum concluded that vicinal and geminal coupling is occurring; $\text{H}^{8\text{a}}$ is coupled to $\text{H}^{8\text{c}}$ which is also coupled to $\text{H}^{7\text{e}}$. In turn, $\text{H}^{7\text{e}}$ is coupled to $\text{H}^{7\text{a}}$ and H^6 .

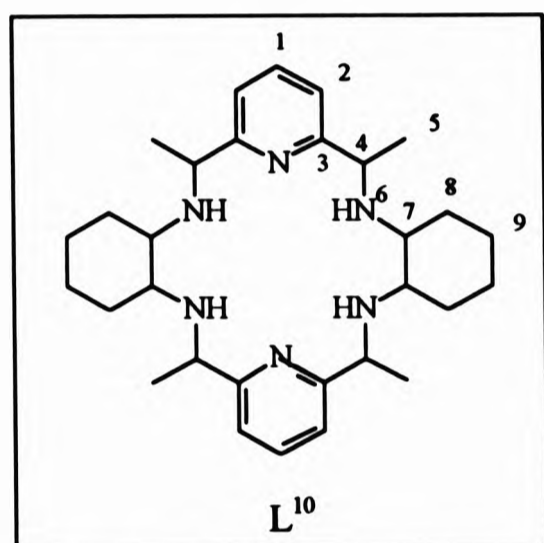
As for $[\text{L}^8\text{H}_4]\text{Br}_4$, the NMR spectrum of L^{10} showed the compound to be diastereomeric and complex multiplet bands were characteristic. In addition to the four chiral centres at C^4 , the four nitrogen chiral centres, N^6 , would further complicate the spectrum, but similar to L^9 and the transition metal complexes of L^9 , it is assumed that these latter chiral centres do not affect the NMR spectra, *i.e.* these chiral centres always adopt one configuration. The number of diastereomers would be five in this case also, Fig. 3.4 being applicable here too. The chemical shifts referred to here for the ^1H and ^{13}C NMR spectra are either the mean or a range of values of the bands (Table 3.7).

Two multiplet bands in the ranges δ_{H} 7.69 - 7.54 and 7.27 - 7.10 are assigned to H^1 and H^2 respectively. These appear to have the same chemical shifts as for L^9 . The *multiplet* in the region δ_{H} 4.94 - 4.82 and another in the range δ_{H} 4.1 - 3.9 arise from the methine protons, H^4 , integrating for two protons each. Likewise the methyl protons, H^5 , resonate as two distinct multiplets at δ_{H} 1.52 - 1.47 and 1.38 - 1.34.

Coupling between the methyl and the methine protons, H⁴, is not evident but it is also not observed in the L⁸-meso spectrum.

The methyl protons, H⁵, resonate amidst the cyclohexyl protons, H⁷, H⁸ and H⁹, in the region 2.5 - 0.8 p.p.m. Distinguishing between H⁷, H⁸ and H⁹ is impossible as is the discrimination between axial and equatorial protons. The acidic, H⁶, proton centred at δ_{H} 2.7 exchanged with deuterium on addition of D₂O.

Table 3.7 The chemical shifts* of the ¹H- and ¹³C-NMR spectra of L¹⁰ in CDCl₃ (Values in parentheses indicate the number of bands in the region)

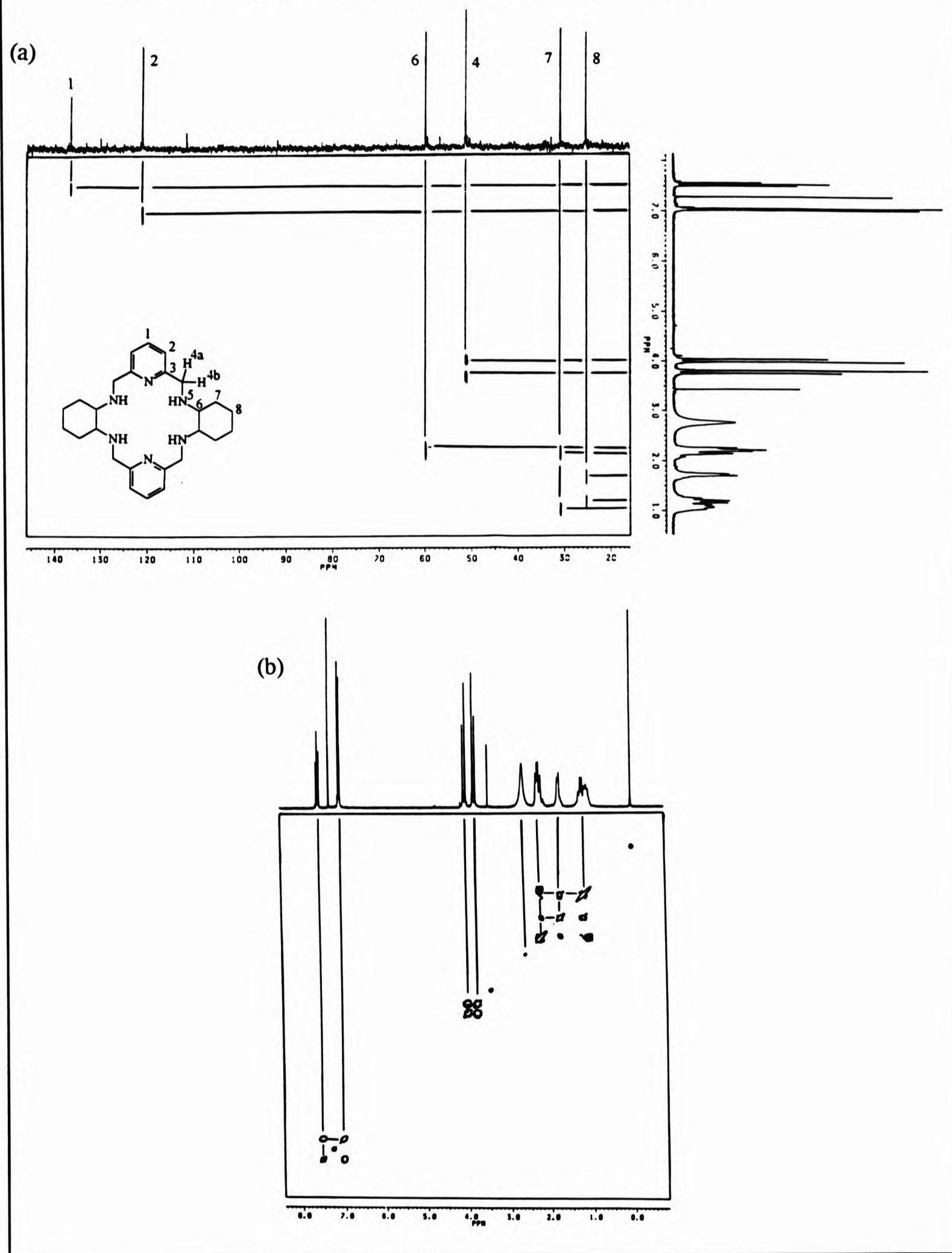


ASSIGNMENT	δ_{H}	INTEGRATION	δ_{C}
1	7.69 - 7.54	2	137 - 136 (2)
2	7.27 - 7.10	4	120 - 118 (6)
3	-	-	164 - 163 (5)
4	4.94 - 4.82, 4.1 - 3.9	4	69 - 55 (11) ^b
5	1.52 - 1.47, 1.38 - 1.34	c	25 - 22 (11) ^a
6	2.86 - 2.57	4	-
7	see below	see below	69 - 55(11) ^b
8, 9	2.5 - 0.8 ^d	28 ^c	35 - 25 (7) ^a

*in p.p.m relative to SiMe₄ as internal standard at 0.0 p.p.m.

^aAssigned by DEPT-135 spectra, ^b C⁴ and C⁷ are indistinguishable without further NMR analyses, ^cincluded in the integral of H⁷, H⁸ and H⁹, ^dincludes resonance of H⁷ also, ^eintegral includes that of H⁵ and H⁷

Fig. 3.13 The (a) ^{13}C - ^1H -COSY and (b) the ^1H -COSY of L^9



3.3.3 Isolation and Characterisation of $[L^9H_4](ClO_4)_4$

Despite the deliberate attempts to obtain L^9 and L^{10} as the hydrobromide salts, the complexation of L^9 with lanthanide perchlorate salts in methanolic medium yielded $[L^9H_4](ClO_4)_4$ as a white crystalline solid.

The presence of the metal was initially questioned when, in the IR spectrum (Table 3.4), a split perchlorate band absorbed at 1146, 1115 and 1088 cm^{-1} and also at 628 cm^{-1} accompanied by a series of medium bands in the region 2870 - 2370 cm^{-1} . The latter series of bands were also observed in the spectrum of $[L^7H_4]Br_4$ and $[L^8H_4]Br_4$ and were assigned to the $-NH_2^+$ salt formation. A tetraperchlorate salt also forms for L^9 the result being $[L^9H_4](ClO_4)_4$. A medium sharp band at 3337 cm^{-1} from $\nu(NH)$ is a shoulder to a much more stronger sharp band at 3420 cm^{-1} assigned to lattice water, $\nu(OH)$.

The absence of the metal was also inferred by LSIM spectrometry where the molecular ion was not detected. The fragment with the highest mass was $[L^9H \cdot ClO_4 + H]^+$, m/z 535(26%) and the base peak corresponded to $[L^9 + H]^+$, m/z 435. The next common fragment was that representing $[L^9/2 + H]^+$ at m/z 218(33%).

A negative magnetic susceptibility reading, further suggested the absence of a metal, whereas in the presence of gadolinium(III) a positive reading in the range 800 - 1300 $erg\ gauss^{-2}\ vol^{-1}$ is the norm. To have recorded a good 1H NMR spectrum from a sample suspected of containing gadolinium(III), a highly paramagnetic metal, which should have led to the induction of proton relaxation and hence broad resonances, would also conclude that the metal is not present. The overall formulation is $[L^9H_4](ClO_4)_4 \cdot 3H_2O$.

The 1H NMR spectrum (Fig. 3.14) in D_2O and at 250 MHz was expected to resemble that of L^9 (Fig. 3.10) but this was not so. Generally, the signals in the spectrum of $[L^9H_4](ClO_4)_4$ were chemically shifted downfield from those of L^9 and

the multiplicity of certain bands had increased. The former could be as a result of using a different solvent, D_2O for $[L^9H_4](ClO_4)_4$, $CDCl_3$ for L^9 . The typical *triplet-doublet* arrangement is no longer such but two *quartets* centred at δ_H 8.00 (H^1) and 7.54 (H^2) respectively. This follows a similar pattern to the spectrum of $[{YL^5(NO_3)_2}_2NO_3(OH)]$ (Chapter 2, Fig. 2.3) but the two *doublets* at δ_H 7.54 are overlapping as determined by their coupling constant, $^3J(H^1, H^2) = 7.8$ Hz, the *doublet* most upfield of the two being less intense, the approximate ratios of the two *doublets* being 3:2. The *quartet* at δ_H 8.00 is, in fact, two *triplets*, the *triplet* most upfield of the two being overlapped by the one downfield. Conclusively, the AB_2 characteristics still apply.

The bands in the range δ_H 4.7 - 4.9 are artefacts from the irradiation of the solvent band, DOH, at δ_H 4.8. Opposing the *doublet of doublets* centred at δ_H 3.88 for L^9 (Fig. 3.10), a *triplet* resonates at δ_H 4.48 for the methylene protons, H^4 .

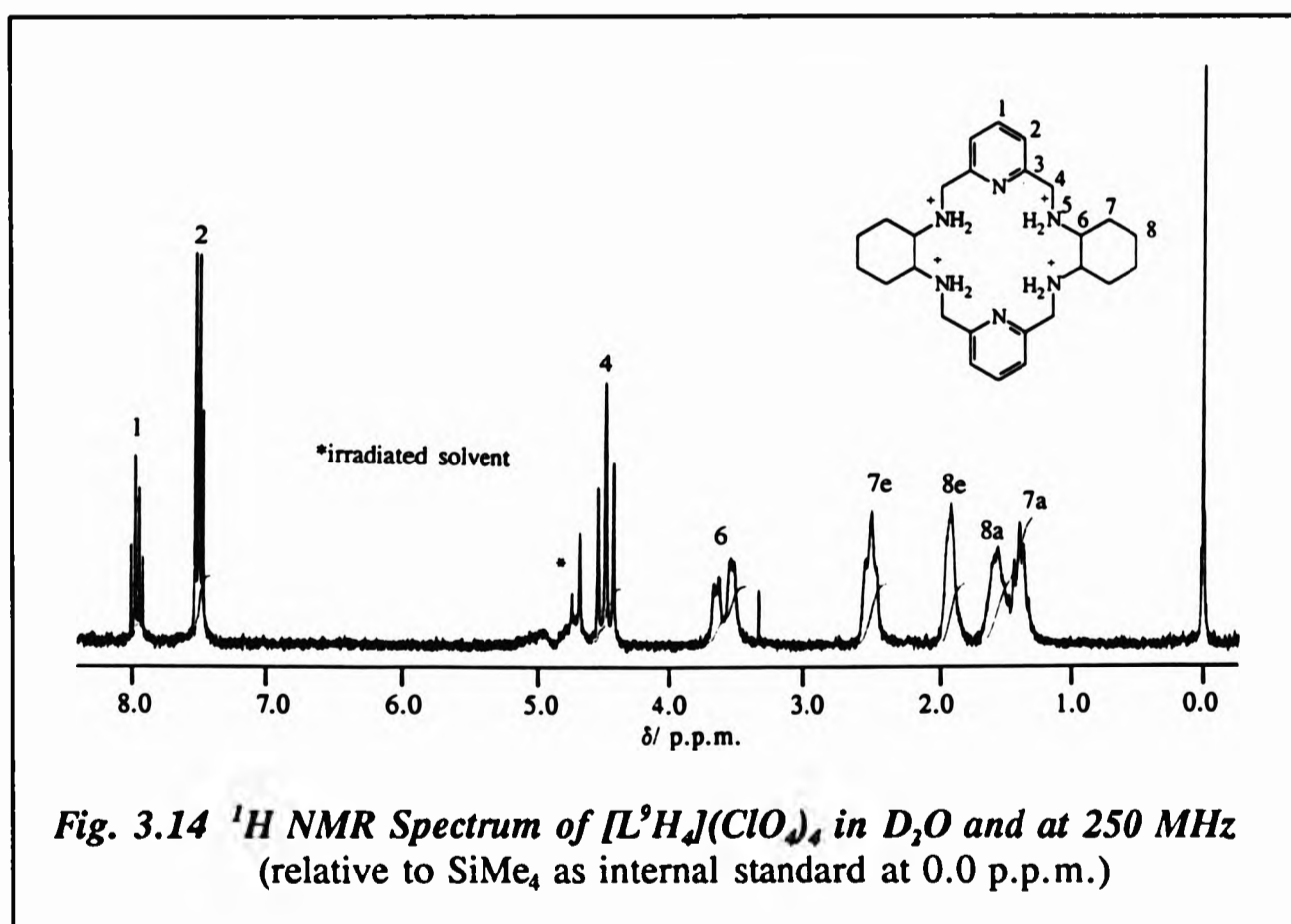


Fig. 3.14 1H NMR Spectrum of $[L^9H_4](ClO_4)_4$ in D_2O and at 250 MHz (relative to $SiMe_4$ as internal standard at 0.0 p.p.m.)

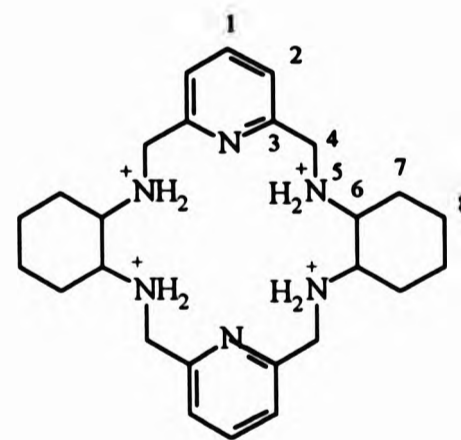
The formation of the NH_2^+ salt renders the amino nitrogen, N^5 , achiral but the methylene protons, H^4 , still show non-equivalence. The triplet band at δ_{H} 3.88 is representing an AB system where the two inner bands of the *doublet of doublets* have coalesced, suggesting that these protons are almost becoming equivalent on the NMR timescale. The coupling constant resembles that of L^9 , $^3J(\text{H}^{4a}, \text{H}^{4b}) = 13.3 \text{ Hz}$. The unaccountable anomaly is that this *triplet* integrates for four protons and not eight that are present in the structure. The remaining bands do integrate correctly. Due to their exchange with deuterium in D_2O the amino protons were not detected. The cyclohexyl proton bands follow a similar pattern to that observed for the ^1H NMR spectrum of $[\text{YL}^5\text{Cl}_2(\text{H}_2\text{O})_2]$ (Chapter 2, Fig. 2.4) and axial and equatorial protons are assigned as shown in Fig. 3.14.

Thirteen bands were detected in the broad band proton decoupled ^{13}C NMR spectrum as was expected, in agreement with the two environments depicted in the ^1H NMR spectrum; two bands for $\text{C}^1 - \text{C}^3$, $\text{C}^6 - \text{C}^8$ but only one band for the methylene carbon atoms, C^4 . These bands are listed in Table 3.8.

Table 3.8 Chemical shifts* of the ^{13}C NMR spectrum of $[\text{L}^9\text{H}_4](\text{ClO}_4)_4$ in D_2O

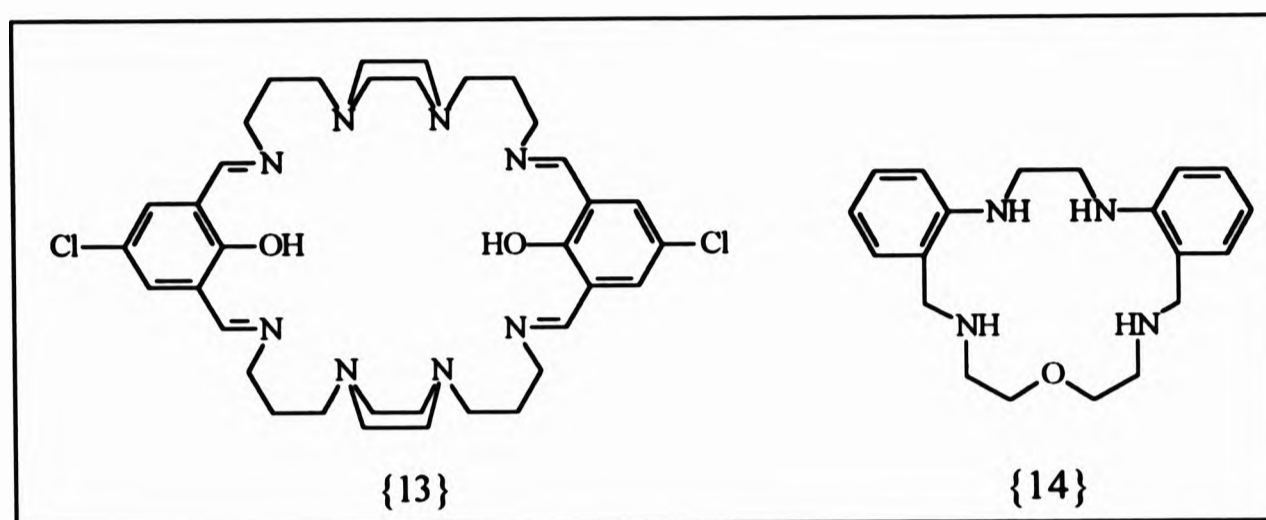
ASSIGNMENT	δ_{C}
1	143.35, 142.70
2	126.59, 125.93
3	153.87, 153.34
4	50.65
5	-
6	60.91, 60.59
7	30.10, 29.46
8	25.68, 25.57

* in p.p.m. relative to SiMe_4 as standard



$[\text{L}^9\text{H}_4](\text{ClO}_4)_4$

The absence of the metal from the structure is not a rarity. The template synthesis of {13} with lanthanum perchlorate yielded the structure $[\{13\}H_4](ClO_4)_4$, also in a methanolic medium and the metal being absent from the macrocyclic cavity.^[25]



Duckworth *et al.*^[26] very recently also reported the same occurrence when the complex formation of {14} was attempted with Mg^{2+} , Ca^{2+} and Sr^{2+} perchlorate salts. $[\{14\}H]ClO_4$ was isolated.

3.4 Metal Complexation of L^9 and L^{10}

Complexation of lanthanide metals with nitrogen donor based ligands was sceptical, after all, lanthanide metals being hard acids would chelate strongly to hard bases, in particular oxygen donor atoms. As discussed previously, the reaction of L^9 with $Gd(ClO_4)_3 \cdot 6H_2O$ in methanol yielded the salt $[L^9H_4](ClO_4)_4$ (§ 3.3.3). However, under the same reaction conditions, first and second row transition metals were found to complex L^9 and L^{10} with ease.

3.4.1 Transition Metal Complexes of L^9 and L^{10}

The reaction of L^9 or L^{10} with transition metals in a methanolic medium under reflux gave the corresponding complexes as amorphous solids in yields 55 - 70%. Repeating the procedure at room temperature afforded these chelates as crystalline materials some of which were suitable for X-ray crystallography. Complexes were

isolated of Mn^{2+} , Co^{3+} , Cu^{2+} , Zn^{2+} and Cd^{2+} for L^9 and of Mn^{2+} , Co^{3+} and Cu^{2+} for L^{10} . These were soluble in warm acetonitrile, dichloromethane, DMSO and methanol.

3.4.1.1 Infrared Spectrophotometry and Magnetic Data

The magnetic moments at 291 K are listed in Table 3.9 for the expected paramagnetic complexes. The manganese(II) complexes resulted in magnetic moments of 5.49 and 5.74 B.M. for the L^9 and L^{10} complexes respectively. These values are typical of d^5 high spin configuration where extra stability is associated with a half-filled shell.^[27,28] Although L^9 and L^{10} are potentially octahedral, the octahedral geometry favouring a high spin arrangement, the geometry adopted by $[\text{MnL}^9](\text{ClO}_4)_2$ cannot be determined with magnetic data alone, manganese(II) having, theoretically, a magnetic moment of 5.9 B.M. for a tetrahedral arrangement also.^[28]

The copper(II) complexes had effective magnetic moments of 2.06 and 1.97 B.M. for L^9 and L^{10} respectively and these are in agreement with d^9 ions possessing one unpaired electron. The magnetic moments of the cobalt complexes were virtually zero B.M. indicating that all the electrons in the d-orbitals are spin-paired and that oxidation from $\text{Co}^{2+}(d^7) \rightarrow \text{Co}^{3+}(d^6)$ had occurred. The magnetic moment of zero further suggests a low-spin arrangement in an octahedral environment; cobalt(II) is stable in aqueous solution, but in the presence of strong-field ligands it readily oxidises to cobalt(III).^[29]

The general features of the IR spectra of the transition metal perchlorate complexes were similar (Table 3.9) for both L^9 and L^{10} . Compared to the free ligands, the complexes displayed the $\nu(\text{NH})$ stretching modes at 3290 - 3160 cm^{-1} , in some cases two bands, at lower wavenumbers to the respective ligands. The weak band between 1600 - 1615 cm^{-1} was assigned to the $\nu(\text{NH})$ bending vibrations. The slight variation in the IR spectra of the complexes was in the symmetry and co-ordination of the perchlorate counterions, these absorbing generally around 1100 cm^{-1} (ν_3)

accompanied by a band in the region 600 - 660 cm^{-1} (ν_4). The variation and intensity of these bands can be used to determine the nature of the perchlorate groups. Broad bands centred at 1100 cm^{-1} , a sharp intense band at 625 - 628 cm^{-1} and a weak band at 930 cm^{-1} (ν_1) featured in the spectra of $[\text{MnL}^9]^{2+}$, $[\text{MnL}^{10}]^{2+}$, $[\text{CoL}^9]^{3+}$, $[\text{CoL}^{10}]^{3+}$, $[\text{CuL}^9]^{2+}$, $[\text{CuL}^{10}]^{2+}$, $[\text{ZnL}^9]^{2+}$ and $[\text{CdL}^9]^{2+}$ conclude that the perchlorate groups are all ionic.^[30-32]

Table 3.9 Infrared^a and magnetic data^b of $[\text{TML}^9]^{n+}$ and $[\text{TML}^{10}]^{n+}$
(when TM = Co, n = 3, else n = 2)

COMPLEX	$\nu(\text{NH})$ str.	$\nu(\text{NH})$ bend	$\nu(\text{ClO}_4)$			μ_{eff} (B.M)
			ν_3	ν_1	ν_4	
$[\text{MnL}^9](\text{ClO}_4)_2$	3280s, 3168b	1607m	1100b	937w	624s	5.49
$[\text{MnL}^{10}](\text{ClO}_4)_2 \cdot \text{MeOH} \cdot \text{H}_2\text{O}$	3246m	1604w	1090b	-	627s	5.74
$[\text{CoL}^9](\text{ClO}_4)_3 \cdot 2\frac{1}{2}\text{H}_2\text{O}$	3037b	1614w	1143 1114 1088	938w	628s	0.43 ^c
$[\text{CoL}^{10}](\text{ClO}_4)_3 \cdot 3\frac{1}{2}\text{MeOH} \cdot 3\frac{1}{2}\text{H}_2\text{O}$	3234m	1611w	1090b	928w	625s	0.59
$[\text{CuL}^9](\text{ClO}_4)_2 \cdot \text{MeOH}$	3290m	1612w	1092b	942	625s	2.06
$[\text{CuL}^{10}](\text{ClO}_4)_2 \cdot 1\frac{1}{2}\text{H}_2\text{O}$	3258m	1603w	1090b	-	625s	1.97
$[\text{ZnL}^9](\text{ClO}_4)_2$	3283s 3170b	1608w	1090b	941w	626s	-
$[\text{CdL}^9](\text{ClO}_4)_2$	3290m 3182b	1604w	1088b	936w	626s	-

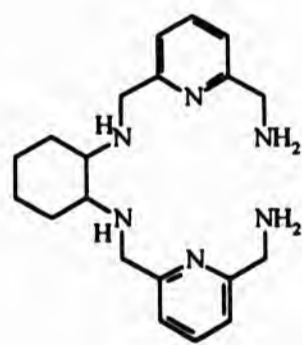
^ain cm^{-1} , ^bat 291 K unless other wise stated, ^cat 301 K

3.4.1.2 Liquid Secondary Ion Mass Spectrometry

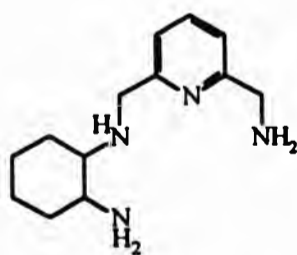
Mass spectrometry was consistent with 1:1 metal-to-ligand complexation. Typically the base peak in all the complexes was $[\text{TML}^n(\text{ClO}_4)_x]^{n+}$, (n = 9, 10, x = 1, 2).

Table 3.10 The fragmentation patterns of $[TML^9]^+$ and $[TML^{10}]^+$
 (when TM = Co, n = 3 else n = 2; the m/z of the most intense band is given)

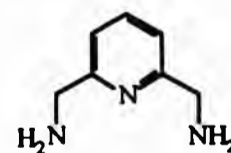
FRAGMENT	m/z	RELATIVE ABUNDANCE (%)
$[MnL^9(ClO_4)]^+$	588	100
$[MnL^9]^+$	488	23
$[MnL^{10}(ClO_4)]^+$	645	100
$[MnL^{10}]^+$	545	24
$[CoL^9(ClO_4)_2]^+$	691	22
$[CoL^9(ClO_4)]^+$	592	100
$[CoL^9]^+$	491	62
$[Co(A)]^+$	409	7
$[Co(B)]^+$	289	14
$[Co(E)]^+$	193	14
$[E]^+$	136	29
$[CoL^{10}(ClO_4)_2]^+$	748	45
$[CoL^{10}(ClO_4)]^+$	648	100
$[CuL^9(ClO_4)]^+$	596	59
$[CuL^9]^+$	497	100
$[Cu(A)]^+$	416	1
$[Cu(B)]^+$	295	9
$[CuL^{10}(ClO_4)]^+$	653	100
$[CuL^{10}]^+$	553	52
$[ZnL^9(ClO_4)]^+$	597	100
$[ZnL^9]^+$	497	49
$[Zn(A)]^+$	414	4
$[Zn(B)]^+$	307	7
$[CdL^9(ClO_4)]^+$	647	100
$[CdL^9]^+$	547	44
$[Cd(E)]^+$	433	11



(A)
 $C_{20}H_{30}N_6$



(B)
 $C_{13}H_{22}N_4$



(E)
 $C_7H_{11}N_3$

After the loss of all the perchlorate counter-ions (Table 3.10), the complexes dissociate by losing a quarter of the ligand at a time, first the loss of a cyclohexane ring forming [TM(A)]⁺, second the loss 2,6-dimethylenepyridine forming [TM(B)]⁺. Thirdly, the loss of the remaining cyclohexane ring yields [TM(E)]⁺. In Table 3.10, the most intense bands are given.

3.4.1.3 NMR Spectroscopy of [ZnL⁹](ClO₄)₂ and [CdL⁹](ClO₄)₂

¹H NMR spectra were ran of both of the diamagnetic complexes [CdL⁹](ClO₄)₂ and [ZnL⁹](ClO₄)₂ (Figs. 3.15c and 3.15d) and showed some differences between themselves and the free ligand, L⁹ (Fig. 3.15a), therefore conformational differences were expected of the ligand on co-ordination to a metal (Table 3.11).

There is no variation in the chemical shifts as far as the two complexes and the ligand are concerned for the protons H⁴ - H⁸ but the shift of *ca.* 0.4 p.p.m. downfield for the AB₂ triplet-doublet system, from that of the ligand is noted. The coupling constant, ³J(H¹,H²) = 7.8 Hz, has not altered and the integral values correspond to the correct number of protons in the complexes.

Two-dimensional ¹³C-¹H-COSY spectra aided in the assignment of the remaining portion of the proton spectra of both complexes and the distinction between axial and equatorial protons on the cyclohexane rings could be made. For the [CdL⁹]²⁺ spectrum two adjacent *multiplets* centred at δ_H 1.0 and 1.16 are assigned to the axial protons of H⁷ and H⁸ respectively with their equatorial counterparts at δ_H 2.43 and 1.72 respectively. The former two *multiplets* in the [ZnL⁹]²⁺ complex merge together, as do the two multiplets at δ_H 1.78 and 1.67 representing H⁶ and the equatorial protons of H⁸. The equatorial protons of H⁷ resonate at δ_H 2.29. Two-dimensional spectroscopy (¹H-COSY) revealed that H^{7a} is coupled to H^{7e} which is also coupled to H^{8e}, H^{8e} being also coupled to H^{8a}. To determine the coupling constants of these protons one would need to undertake irradiation or decoupling studies to reveal the exact multiplicities of the bands which are obscured by

overlapping. This was not felt necessary.

The methine protons, H^6 , in both complexes are coupled to a band which resonates at δ_H 2.93 for $[ZnL^9]^{2+}$ and at δ_H 2.87 for $[CdL^9]^{2+}$. The latter band, according to the ^{13}C - 1H -COSY, does not have a carbon counterpart, *i.e.* it is not attached to a carbon atom. This sharp multiplet is, therefore, assigned to the amino proton, NH^6 which does not collapse on D_2O addition to the sample as it is exchanging too rapidly.^[33,34] In the spectrum of the free ligand, these acidic protons also resonate at δ_H 2.93 but as a broad band and they do exchange with deuterium on *shaking* with D_2O which signifies the rate of exchange is neither fast nor slow but intermediate. The NH proton is partially decoupled resulting in a broad band and the adjacent CH^6 and CH^4 protons are not split by this proton.

The methylene carbon, C^4 , is still prochiral in the complexes, again the methylene protons, CH^4 forming an AB system. The NH^6 proton is coupled to these methylene protons and to the methine protons, CH^6 . In the spectrum of $[CdL^9]^{2+}$ the methylene protons appear as a *doublet* at δ_H 4.20 which has collapsed from the *doublet of doublets*, the AB system of the free ligand (Fig. 3.15a). For the free ligand, L^9 , $\Delta\nu/J = 0.02$ (*i.e.* < 10) hence the typical pattern of *doublet of doublets* resulting from the second order spectrum. For the $[CdL^9]^{2+}$ (Fig. 3.15c), $\Delta\nu/J$ becomes even smaller. The *doublets* have come much closer to themselves, the two inner peaks have increased in intensity and the two outer peaks decreased.^[35] Impurities lingering at the base of the inner bands prevent the identification of the smaller outer bands. In the same region of the spectrum of $[ZnL^9]^{2+}$ (Fig. 3.15d), a *singlet* resonates at δ_H 4.17. This, too, is part of the collapsed AB system, the two smaller outer bands being much clearer in this spectrum.

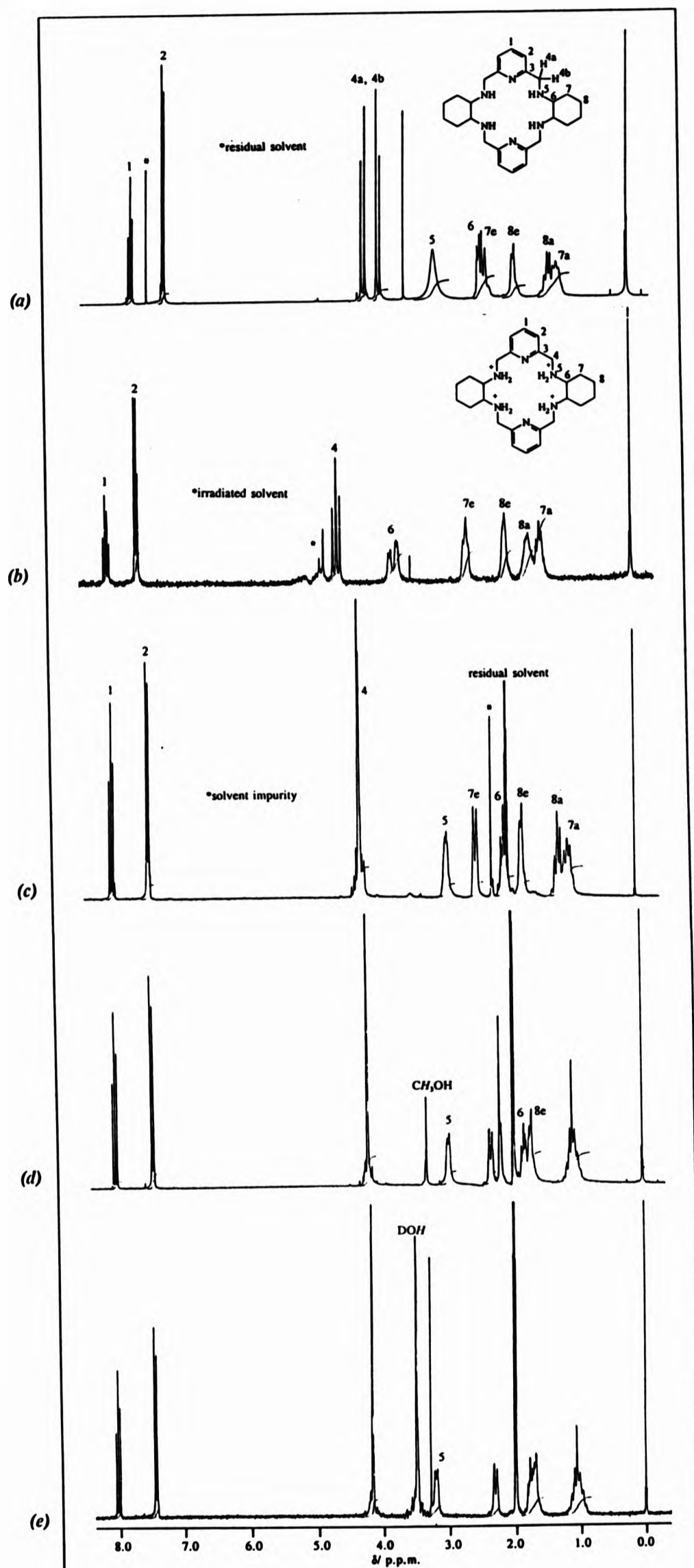


Fig. 3.15 The ^1H NMR spectra of (a) L^2 in CDCl_3 , (b) $[\text{L}^2\text{H}_4]^{2+}$ in D_2O , (c) $[\text{CdL}^2]^{2+}$ in CD_3CN , (d) $[\text{ZnL}^2]^{2+}$ in CD_3CN and (e) $[\text{ZnL}^2]^{2+}$ in $\text{CD}_3\text{CN}/\text{D}_2\text{O}$ at 250 MHz using SiMe_4 as internal standard

Table 3.11 ^1H NMR chemical shifts* of $[\text{ZnL}^9]^{2+}$ and $[\text{CdL}^9]^{2+}$ in CD_3CN , compared to the free ligand, L^9 , in CDCl_3 at 250 MHz (a = axial, e = equatorial)

ASSIGNMENT	δ_{H}		
	$[\text{ZnL}^9]^{2+}$	$[\text{CdL}^9]^{2+}$	L^9
1	8.05 (t)	7.98 (t)	7.53 (t)
2	7.47 (d)	7.42 (d)	7.03 (d)
3	-	-	-
4	4.17 (s)	4.20 (d)	3.88(d of d)
5	2.93 (m)	2.87 (m)	2.93 (br)
6	1.78	1.93***	2.2
7e	2.29	2.43	2.15
7a	**	1.00	1.08
8e	1.67	1.72	1.72
8a	**	1.16	1.14

*in p.p.m with SiMe_4 as internal standard **these protons resonate in the band at δ_{H} 1.06 but cannot be distinguished. ***this band was revealed upon irradiation of the residual solvent band.

Table 3.12 The chemical shifts* of the broad band proton decoupled ^{13}C NMR spectra of $[\text{ZnL}^9](\text{ClO}_4)_2$ and $[\text{CdL}^9](\text{ClO}_4)_2$ in CD_3CN

ASSIGNMENT	δ_{C}	
	$[\text{ZnL}^9]^{2+}$	$[\text{CdL}^9]^{2+}$
1	142.33	141.64
2	124.20	124.15
3	155.17	155.63
4	48.05	47.35
5	-	-
6	60.64	60.65
7	31.08	31.93
8	25.56	26.65

*in p.p.m with SiMe_4 as internal standard

On addition of D₂O this inner band becomes better resolved and is in fact also a *doublet*, the coupling constant being almost half that determined for the [CdL⁹]²⁺ complex, $^3J(\text{NH}^5, \text{CH}^4) = 2.32$ Hz. Three more changes were revealed when the spectra were ran in CD₃CN/ D₂O [Fig.3.15e]. The second was that the band labelled NH⁵ at δ_{H} 2.93 had chemically shifted downfield to δ_{H} 3.20. Thirdly, a strong band due to DOH appeared at δ_{H} 3.5 and finally a band at δ_{H} 2.14 had disappeared, this band being a common impurity in the solvent, CD₃CN. These changes also occur for the spectrum of [CdL⁹]²⁺ in this case the NH⁵ band became more defined such that its multiplicity could be interpreted as a sextuplet with ratios 1:4:5:5:4:1. This clearly agrees with the NH⁵ proton coupling to H⁴ and H⁶. This band also chemically shifted from δ_{H} 2.87 to δ_{H} 3.04.

The band at δ_{H} 3.48, present only in the [ZnL⁹]²⁺ complex, represents the methyl protons of lattice methanol and this was also detected in the X-ray crystal structure of this compound.

In contrast, the zinc(II) complex of {11}^[23] depicts the NH proton as a *doublet* indicating that it couples to only one of the methylene protons, CH⁴, such that instead of a *doublet of doublets* resonating for these protons, as for L⁹ (Fig. 3.15a), one of these *doublets* is itself further split into two more *doublets*. The addition of D₂O causes the amino signals to disappear and the methylene protons to adopt the typical AB, *doublet of doublets*, arrangement as for L⁹. A similar splitting pattern was observed for [ZnL⁷]²⁺ ^[19] (Fig. 3.16) but like [ZnL⁹]²⁺ and [CdL⁹]²⁺ the NH band did not exchange when the spectrum was ran in D₂O.

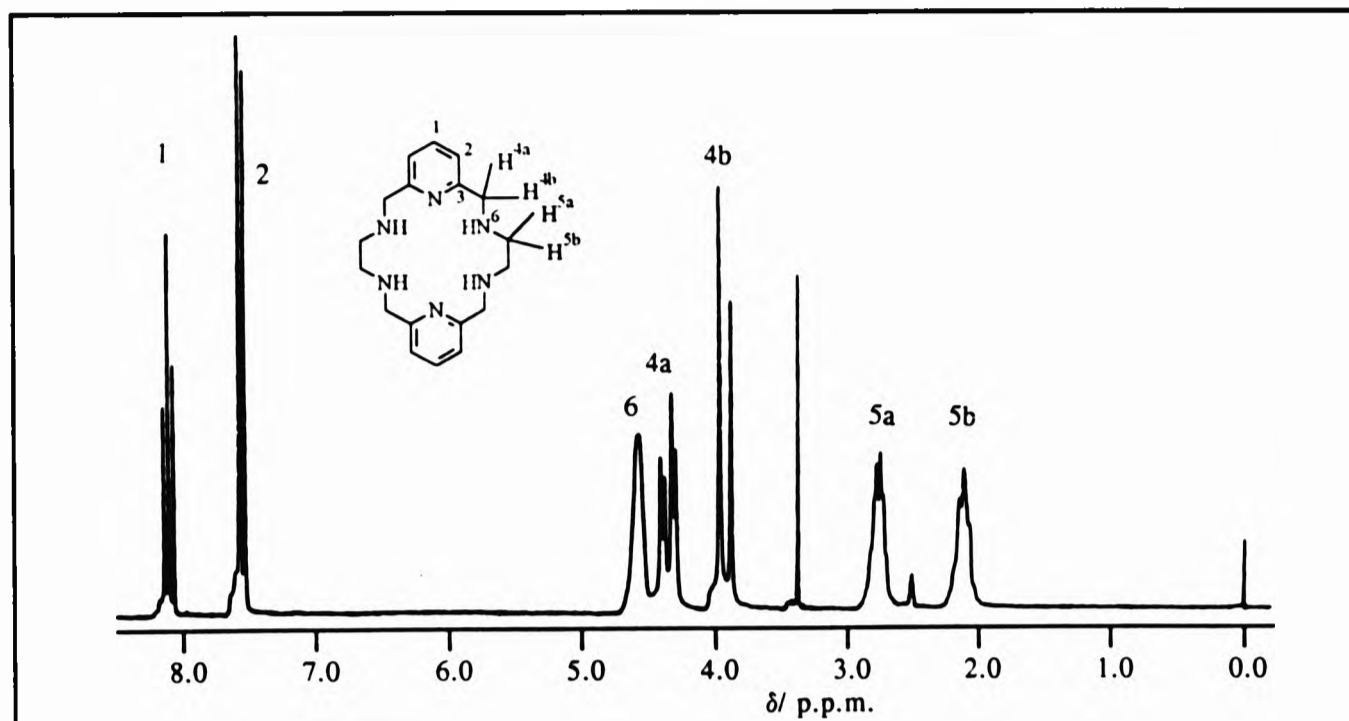


Fig. 3.16 The ^1H NMR spectrum of $[\text{ZnL}']^{2+}$ in d_6 -DMSO and at 200 MHz with SiMe_4 as internal standard (reproduced from ref. 19)

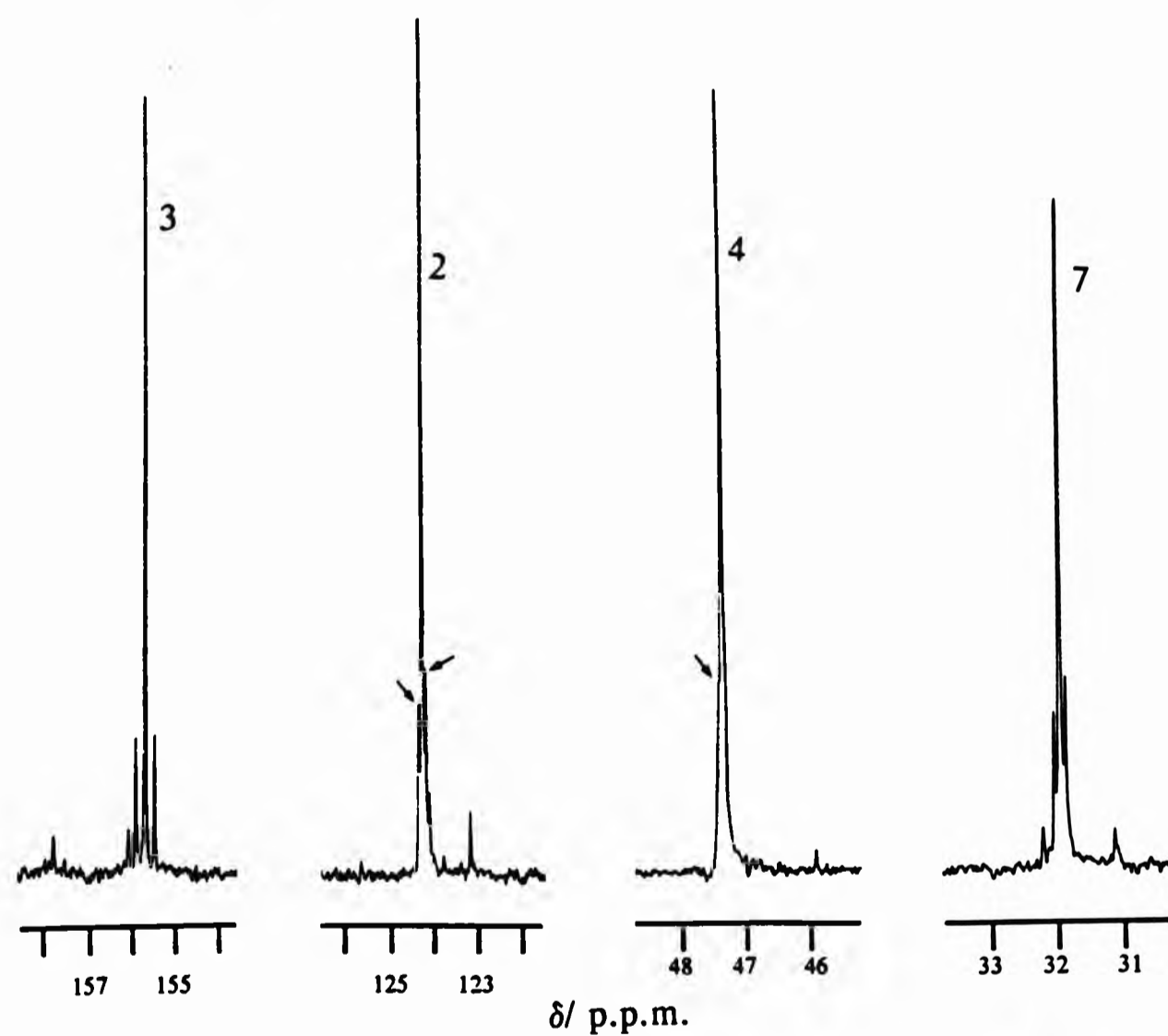


Fig. 3.17 ^{13}C NMR spectrum of $[\text{CdL}']^{2+}$ displaying the ^{112}Cd - ^{13}C coupling

The broad band proton decoupled ^{13}C NMR spectra of $[\text{ZnL}^9]^{2+}$ and $[\text{CdL}^9]^{2+}$ contained seven bands, again representing one quarter of the structure of the ligand (Table 3.12). The spectrum of $[\text{CdL}^9]^{2+}$ ($\text{Cd}, I = 1/2$) was further used to determine the co-ordination structure of the complex in solution. The bands corresponding to C^2 , C^3 , C^4 and C^7 possess satellites or spinning side bands associated with $^{112}\text{Cd} - ^{13}\text{C}$ coupling (Fig. 3.17). Table 3.13 shows the chemical shifts and the coupling constants of these satellites. Two- and three-bond coupling is taking place for cadmium coupling to C^3 and C^4 and C^2 and C^7 respectively. The coupling to C^2 and C^3 is through the pyridyl nitrogen and C^4 and C^7 through the amino nitrogen. Since the structure is symmetrical, as far as the carbon skeleton is concerned, the ligand can be thought to be hexa-co-ordinated to the metal in an octahedral arrangement. To achieve an octahedral arrangement, the ligand must twist, pucker or fold. Twisting is favoured as revealed by crystallographic studies.

Table 3.13 ^{13}C NMR data of the $^{112}\text{Cd} - ^{13}\text{C}$ coupling for $[\text{CdL}^9]^{2+}$

COUPLING	$^nJ(^{112}\text{Cd} - ^{13}\text{C}) / \text{Hz}$	n
Cd - C^2	37.5	3
Cd - C^3	102.5	2
Cd - C^4	*	2
Cd - C^7	92.5	3
*overlaps with the main ^{13}C band at $\delta_{\text{C}} 155.63$		

3.4.1.4 X-ray Crystallographic Studies of $[\text{ZnL}^9](\text{ClO}_4)_2 \cdot \text{MeOH}$ and $[\text{CdL}^9](\text{ClO}_4)_2$

Single crystal X-ray structure determination of $[\text{ZnL}^9]^{2+}$ (Fig. 3.18) and $[\text{CdL}^9]^{2+}$ (Fig. 3.19) revealed a distorted octahedral co-ordination about the transition metal where the ligand twists and wraps itself around the metal using the six nitrogen donor atoms available. The ligand is, thus, much more flexible and capable of

twisting to accommodate metals of various sizes including first row transition metals, which the imine analogues are prevented from mimicking without rearranging. The flexibility relates to the ease with which the ligand twists indicating that there is little or no interference from steric strain. Comparison of the metal ion co-ordination sphere dimensions are made in Table 3.14.

In both structures, the ligand adopts only one of the possible five diastereomeric forms involving the stereochemistry at the chiral amine nitrogen centres. As illustrated the ligand in $[\text{ZnL}^9]^{2+}$ has the *RRRR* configuration and in $[\text{CdL}^9]^{2+}$ the *SSSS* configuration. As far as transition metal co-ordination is concerned, the ligand always adopts equivalent conformation, as *SSSS* is the enantiomeric counterpart of *RRRR*. That only one diastereomer is present is also confirmed from the NMR spectra of these compounds (§ 3.4.1.3).

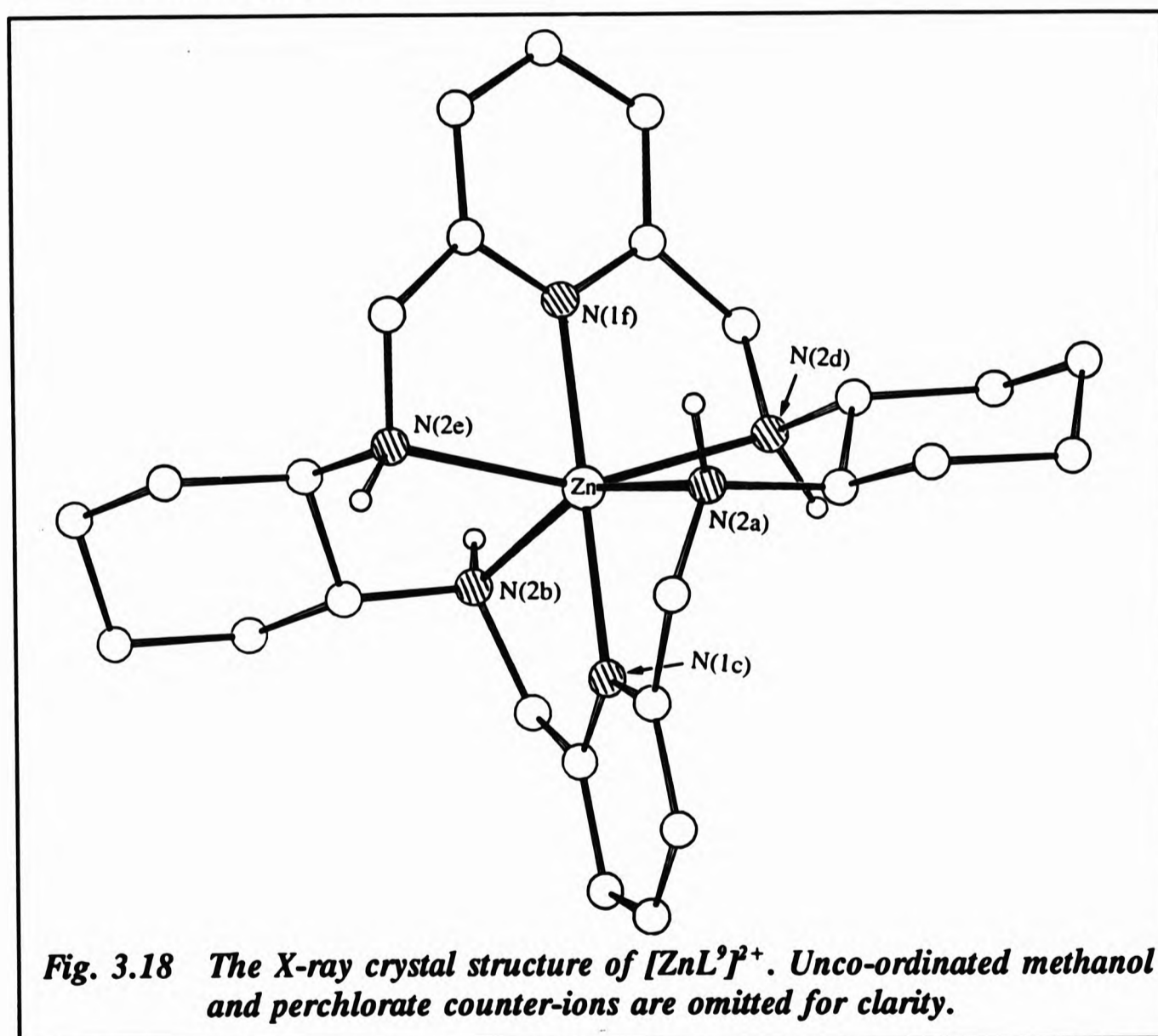


Table 3.14 Dimensions* of the metal ion co-ordination sphere of $[ZnL^7]^{2+}$ and $[CdL^7]^{2+}$

	$[ZnL^7]^{2+}$	$[CdL^7]^{2+}$
Bond Length (Å)		
N(2a) - M	2.220(11)	2.378(6)
N(2b) - M	2.210(10)	2.361(5)
N(1c) - M	2.066(11)	2.261(6)
N(2d) - M	2.266(11)	2.369(5)
N(2e) - M	2.175(10)	2.396(5)
N(1f) - M	2.096(11)	2.263(6)
Bond Angles (°)		
N(1f) - M - N(2a)	103.3(4)	103.8(2)
N(1f) - M - N(2b)	103.8(4)	109.8(2)
N(1f) - M - N(1c)	178.1(4)	174.8(2)
N(1f) - M - N(2d)	75.1(4)	71.3(2)
N(1f) - M - N(2e)	76.7(4)	72.1(2)
N(1c) - M - N(2b)	77.0(4)	73.7(2)
N(1c) - M - N(2a)	75.9(4)	72.8(2)
N(1c) - M - N(2d)	103.5(4)	106.4(2)
N(1c) - M - N(2e)	104.7(4)	110.3(2)
N(2e) - M - N(2a)	81.6(4)	76.0(2)
N(2e) - M - N(2b)	107.9(4)	114.5(2)
N(2e) - M - N(2d)	151.7(4)	143.3(2)
N(2d) - M - N(2b)	79.8(4)	75.9(2)
N(2d) - M - N(2a)	104.2(4)	115.7(2)
N(2a) - M - N(2b)	152.7(4)	146.4(2)

*Estimated standard deviations shown in parentheses

The same configurations were observed for related structures. $[TM\{11\}]^{2+}$ (where TM = Fe, Co, Ni, Cu)^[23] and $[ZnL^7]^{2+}$ ^[19] also exhibit the configuration *RRRR* or *SSSS*. Similarly, $[Ni\{12\}]^{2+}$ and $[Cu\{16\}]^{2+}$, where only two such amino chiral centres are available, the configuration, *RR* is displayed.^[24]

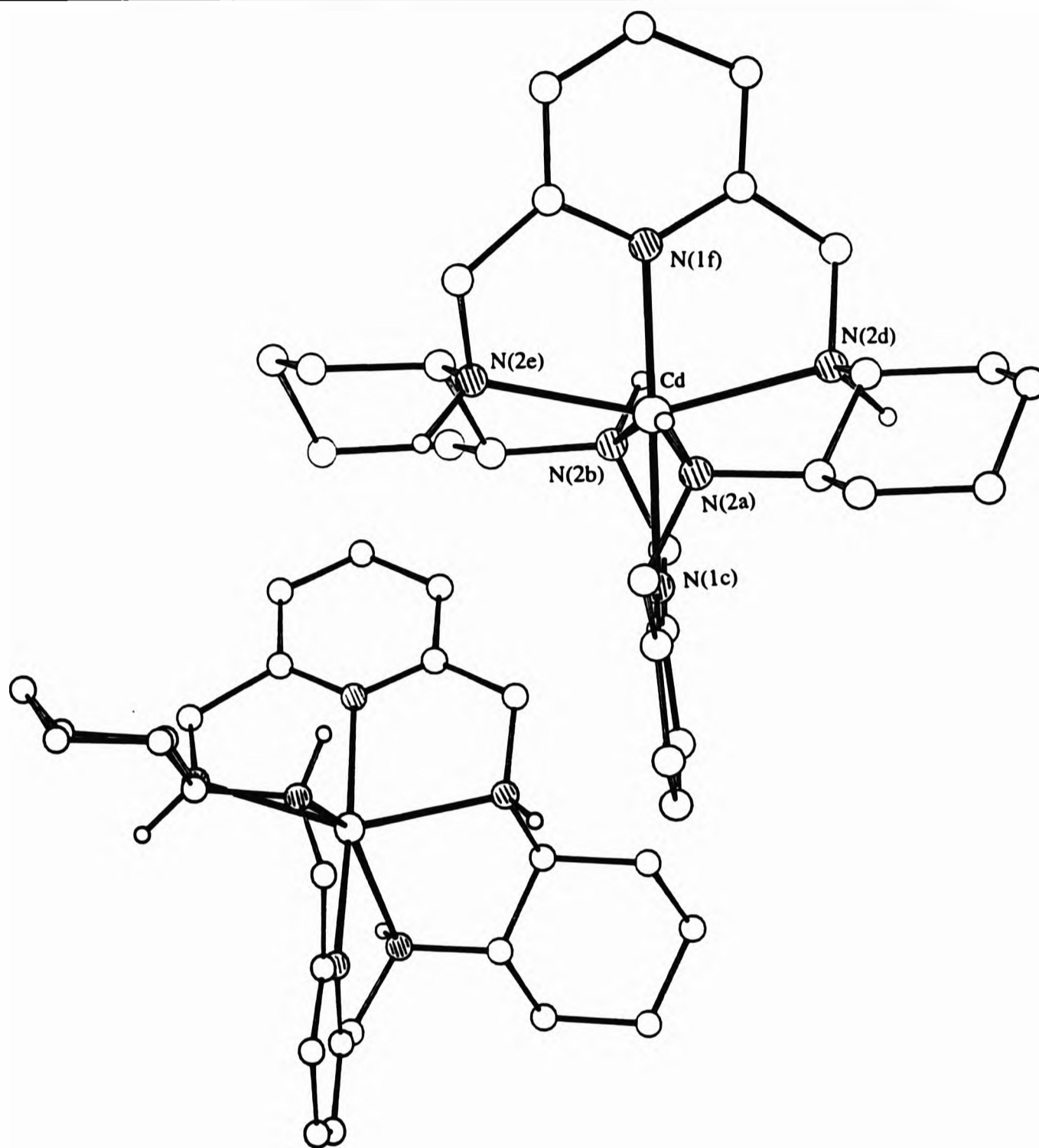
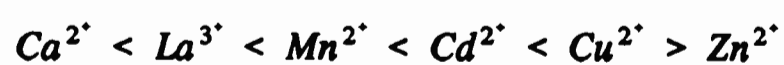


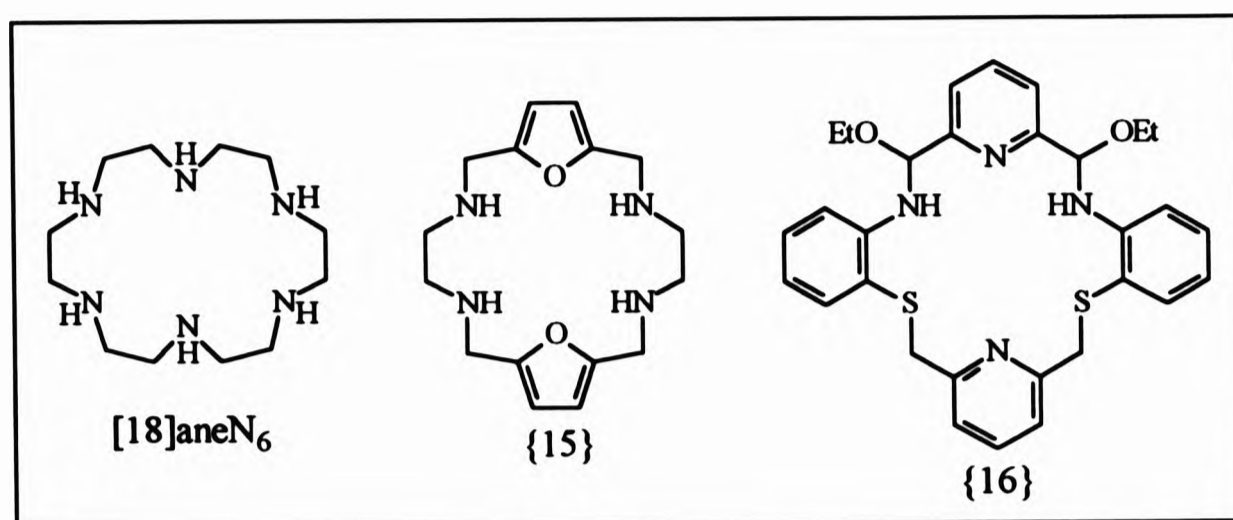
Fig. 3.19 The X-ray crystal structure of $[CdL^9]^{2+}$. Unco-ordinated perchlorate counter-ions are omitted.

Jackels and co-workers^[12] have determined the metal binding constants of $[L^7H_4]Br_4$ with various metals and deduced the order:



which follows the order of the Irving-Williams series. L^7 was found to bind to these metals as strongly as $[18]aneN_6$.^[36] L^7 complexes of Ca^{2+} , Zn^{2+} and La^{3+} are three

times more stable than the corresponding complexes of [18]aneN₆.



The enhanced stability of the metal complexes of L⁷ is owed to the increase in the enthalpy of binding due to the higher dipole moment of pyridine,^[37] compared to secondary amines. Furthermore, the rigidity of the pyridine and its ability to stabilise the free ligand in a conformation similar to that of the co-ordinated ligand reduces the entropy suggesting the *juxtapositional fixedness* of the ligand prior to co-ordination. In marked contrast, solution studies of {15} indicated that this ligand is a poor chelator, the instability being attributed to unfavourable enthalpic or entropic contributions. It has been suggested that "the increased rigidity of the furan ring system does not allow either one of the lone pair of electrons to overlap favourably with the metal ion orbitals."^[12] Also, the macrocycle, {15}, may "experience steric strain in twisting to accommodate the size of the metal ion due to smaller size of the furan ring and the larger angle between substituents, thus necessitating more twisting to accommodate a given size metal ion."^[12]

[18]aneN₆ is also capable of octahedrally wrapping itself about small metal ions. Whereas [18]aneN₆ can co-ordinate both in *meridional* and *facial* dispositions^[38] (Fig. 3.20a and 3.20b), L⁷, L⁸, L⁹, L¹⁰, {11}, {12} and {16} are restricted to the *meridional* mode due to the planarity and rigidity of the pyridine rings. Fig. 3.20c represents the *meridional* geometry of the ligands L⁷ - L¹⁰ where an idealised octahedron is given.

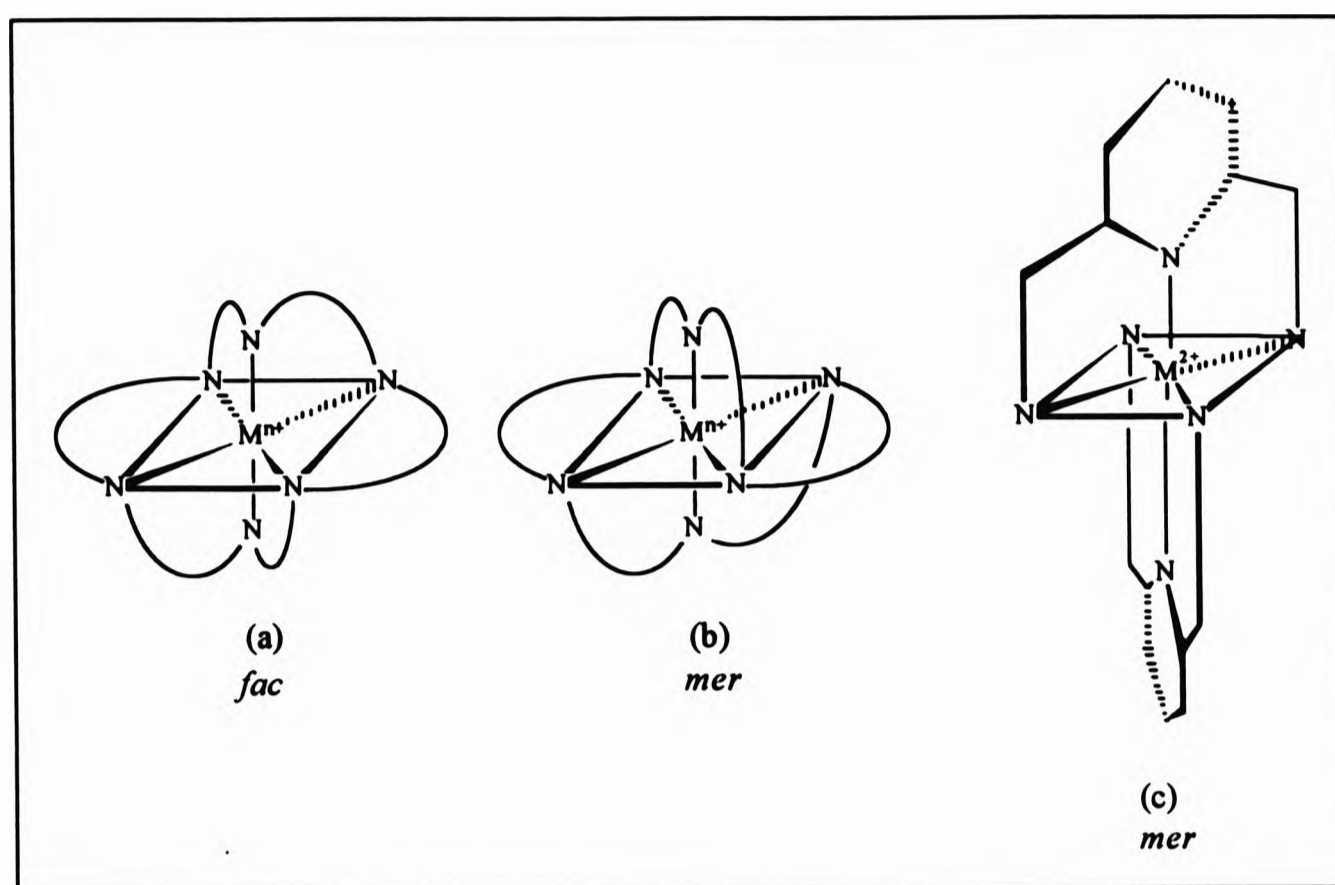
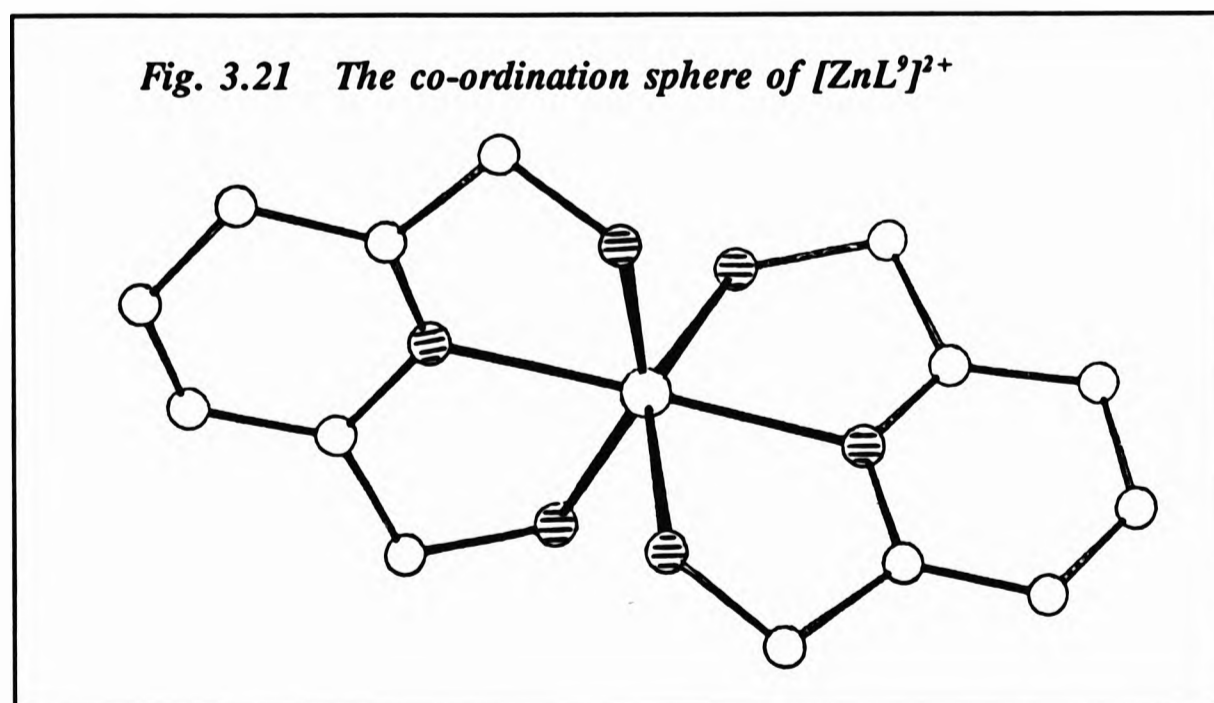


Fig. 3.20 The (a) *facial* and (b) *meridional* isomers adopted by $[18]aneN_6$, and (c) the *meridional* arrangement of $L^7 - L^{10}$, {11}, {12} and {16}

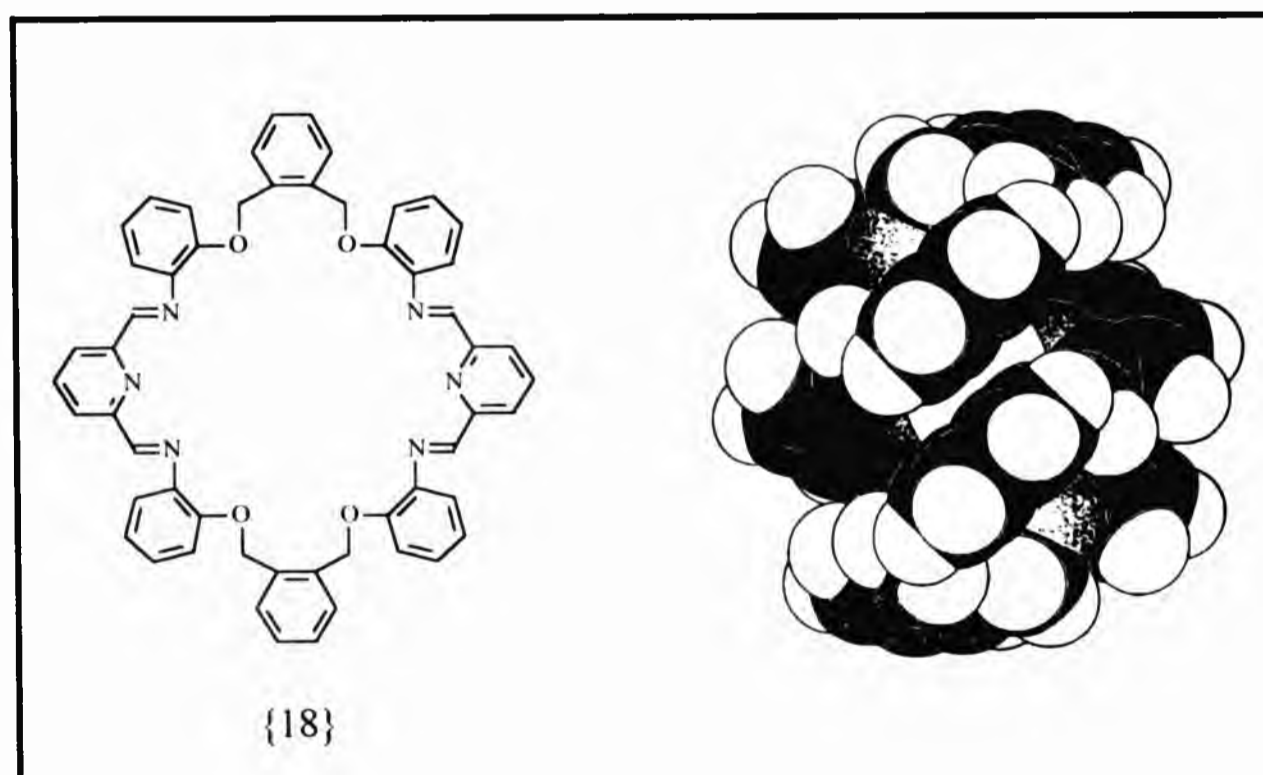
The pyridine groups are *trans* co-ordinated in the complexes of L^9 [N(1f)-Zn-N(1c) = 178.1° , N(1f)-Cd-N(1c) = 174.8° , See Table 3.14] and the coordination of the nitrogen atoms is best described as a pseudo-octahedron, where the pyridyl nitrogen donor atoms occupy the axial sites and the amino nitrogen donor atoms [N(2a), N(2b), N(2d) and N(2e)] define the equatorial plane (Fig. 3.21).



For both $[\text{ZnL}^9]^{2+}$ and $[\text{CdL}^9]^{2+}$, the pyridyl N-M bond is shorter than the amino N-M bond (Table 3.14) and this is a general trend for structures containing the 2,6-pyridinediamine/ diimine substituents.

To this stage, the octahedral wrapping of the ligand around the transition metal was termed "twisting". Ideally the arrangement of the ligand is best described as helical.^[40] Fig. 3.22 shows the distorted octahedral and helical arrangements adopted by the ligands L^9 , {12}, {16} and {17} on co-ordination to transition metals. More evident, is the double helixing described by the 34-membered macrocyclic imine, {18}, with Ni^{2+} , Zn^{2+} , Cd^{2+} and Pb^{2+} (Fig. 3.23), prepared in this Department,^[41] when the three bonds bridging the two pyridyl units are extended to eleven bonds. As was the case for the transition metal complexes of L^7 , L^9 , L^{10} , {12} and {16}, the mononuclear complexes of $[\text{TM}\{18\}]^{2+}$ also exhibit *meridional*, distorted octahedral co-ordination about the metal resulting from the two 2,6-pyridyldiimine head units.

Fig. 3.23 *The double helical structure described by {18} with Zn^{2+} and Ni^{2+} (reproduced with permission from ref. 42)*



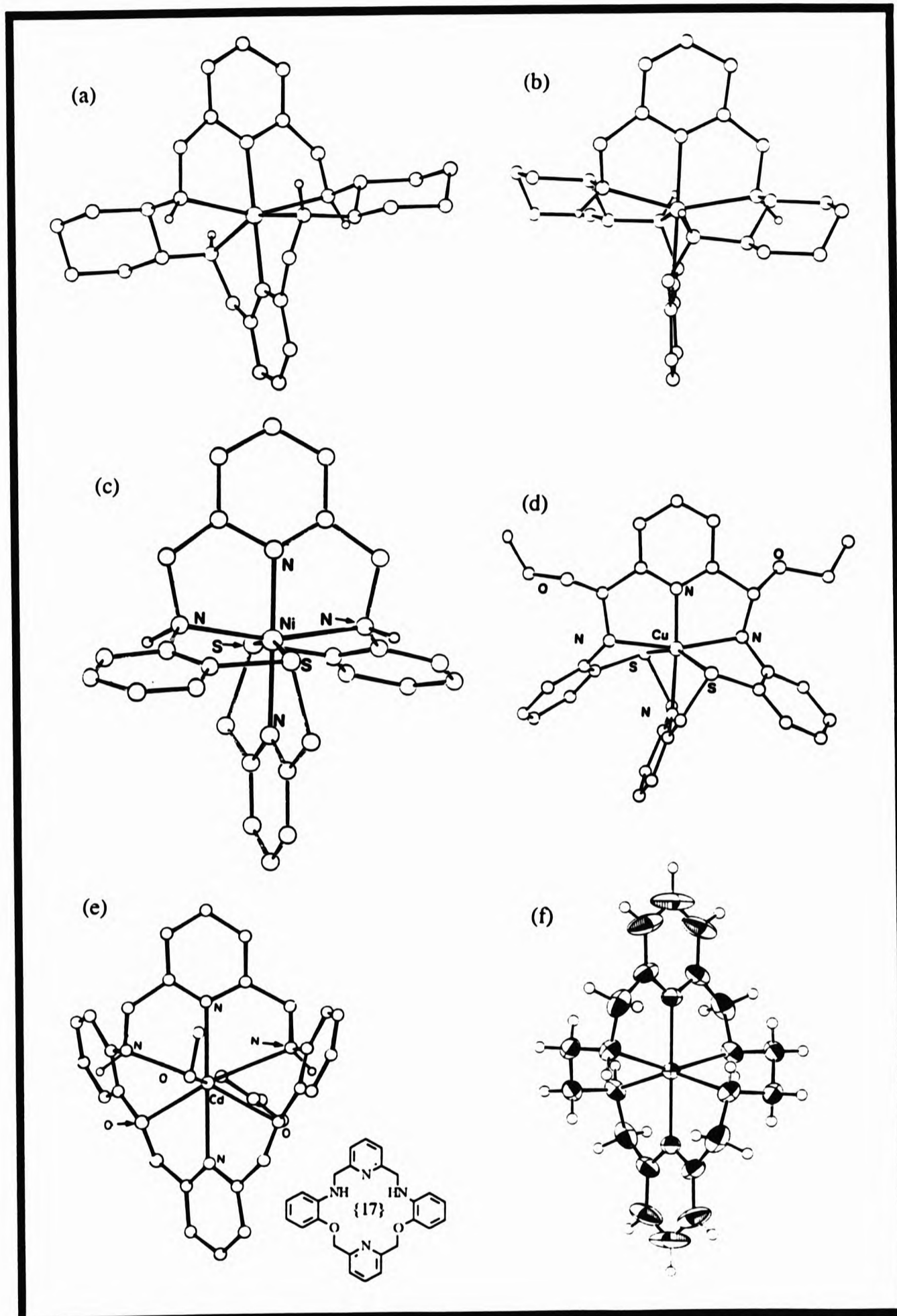


Fig. 3.22 Perspective views of (a) $[ZnL']^{2+}$, (b) $[CdL']^{2+}$, (c) $[Ni\{12\}]^{2+}$, (d) $[Cu\{16\}]^{2+}$, (e) $[Cd\{17\}]^{2+}$ and (f) $[ZnL']^{2+}$ showing the pseudo-octahedral and helical arrangement around the metal [(c), (d), (e) and (f) were reproduced from refs. 20, 20, 39 and 19 respectively]

3.4.2 Yttrium and Lanthanide Metal Complexes of L⁹

Having established the chelating abilities of L⁹ and L¹⁰ with transition metals, further attempts were made to obtain yttrium and lanthanide metal complexes. Two factors were considered, namely the solvent and the counter-ion.

Complexation was carried out by adopting and amending a published procedure^[43] where a solution of the ligand in dichloromethane was dropwise added to a refluxing solution of the metal nitrate in acetonitrile. Colourless crystals of yttrium(III), lanthanum(III), neodymium(III), europium(III), gadolinium(III) and dysprosium(III) complexes of L⁹ were obtained on allowing the resulting mixture to stand at room temperature. These complexes are believed to be the first lanthanide metal complexes of macrocyclic amines.

3.4.2.1 Infrared Spectrophotometry and Magnetic Moments

The IR spectra (Table 3.15) of yttrium and the lanthanide metal complexes of L⁹ resembled those of the transition metal complexes (Table 3.9) with the exception of the nitrate absorption bands as opposed to the perchlorate bands.

Two bands depicting the $\nu(\text{NH})$ stretch were present ranging from 3220 - 3180 cm^{-1} and 3290 - 3260 cm^{-1} and another weak band at 1610 - 1605 cm^{-1} was due to the $\nu(\text{NH})$ bending vibrations. Medium absorptions at 1585 cm^{-1} were due to pyridine ring vibrations. A strong band at 1384 cm^{-1} in all the complexes, except that of lanthanum, suggests the presence of ionic nitrate groups. That at least one of the nitrate groups is bidentate was evident from the nitrate ν_1 and ν_2 vibrations at 1456 - 1466 and 1030 - 1043 cm^{-1} respectively. For the lanthanum complex all three nitrate groups can be bidentate since lanthanum can achieve a maximum co-ordination of 12. For yttrium and the lanthanide metal complexes (excluding that of La^{3+}) the remaining nitrate group can be either monodentate or ionic, thus satisfying the co-ordination of the metal (Chapter 2, Table 2.9), assuming at this stage that the ligand is hexadentate as with the transition metal co-ordination. The magnetic moments of the paramagnetic complexes support the +3 oxidation state of the metals (Table

3.15).

Table 3.15 The major bands^a in the infrared spectra of yttrium and the lanthanide metal complexes of L⁹

COMPLEX	$\nu(\text{NH})_{\text{str}}$	$\nu(\text{NH})_{\text{bend}}$	$\nu(\text{NO}_3^-)$				μ_{eff} (B.M)
			ν_1	ν_2	ν_3	ν_4	
[YL ⁹ (NO ₃) ₂]NO ₃ .MeCN	3280 3199	1607	1451	1036	744	1384	-
[LaL ⁹ (NO ₃) ₃].½H ₂ O	3277 3196	1605	1458	*	*	1314	-
[NdL ⁹ (NO ₃) ₂ MeCN]NO ₃ .MeCN	3284 3188	1605	1446	1033	751	1384	3.8
[EuL ⁹ (NO ₃) ₂ (MeCN)(HNO ₃)]NO ₃	3269	1608	1459	1037	744	1384	3.6
[GdL ⁹ (NO ₃) ₂]NO ₃ .2CH ₂ Cl ₂	3284 3270	1608	1456	1030	740	1384	7.8
[DyL ⁹ (NO ₃) ₂]NO ₃ .2CH ₂ Cl ₂	3274 3215	1609	1466	1043	738	1384	10.4

^ain cm⁻¹, * obscured by ligand vibrations

3.4.2.2 Liquid Secondary Ion Mass Spectrometry

Mass spectrometric analyses indicated that 1:1 metal-to-ligand complexes formed for yttrium and the lanthanide metals complexes of L⁹ (Table 3.16) irrespective of the dimeric species that are possible by the ability of the nitrato group to bridge two metals as for the larger lanthanide metal-imine complexes (Chapter 2).

As was the case repeatedly with all the metal complexes discussed until now, a molecular ion was not detected in the LSIM spectra but the base peak in most of the complexes of yttrium and the lanthanide metals was representative of [LnL⁹(NO₃)₂]⁺ (Ln here also includes Y³⁺). The only exception was the gadolinium complex where the base peak was [GdL⁹(NO₃)]⁺. For the lanthanum and europium complexes the

base peak consisted of $[\text{LnL}^9(\text{NO})_3(\text{MeCN})]^+$ ($\text{Ln} = \text{La}, \text{Eu}$) indicating solvent coordination to the metal.

Table 3.16 The common fragmentations of the LSIM spectra of Y^{3+} and Ln^{3+} complexes of L^9

FRAGMENT	m/z	RELATIVE ABUNDANCE (%)
$[\text{YL}^9(\text{NO}_3)_2]^+$	647	100
$[\text{YL}^9(\text{NO}_3)]^+$	585	55
$[\text{LaL}^9(\text{NO})_3(\text{MeCN}) + \text{H}]^+$	801	31
$[\text{LaL}^9(\text{NO}_3)_2]^+$	697	100
$[\text{NdL}^9(\text{NO}_3)_2]^+$	702	100
$[\text{EuL}^9(\text{NO}_3)_3(\text{MeCN})]^+$	815	100
$[\text{EuL}^9(\text{NO}_3)_2 + \text{H}]^+$	711	60
$[\text{EuL}^9(\text{NO}_3)]^+$	647	40
$[\text{GdL}^9(\text{NO}_3)]^+$	653	100
$[\text{GdL}^9]^+$	591	22
$[\text{DyL}^9(\text{NO}_3)_2]^+$	722	100
$[\text{DyL}^9(\text{NO}_3)]^+$	657	51

3.4.2.3 Nuclear Magnetic Resonance Spectroscopy of $[\text{LaL}^9(\text{NO}_3)_3]$

In contrast to the well defined $[\text{ZnL}^9]^{2+}$ and $[\text{CdL}^9]^{2+}$ ^1H NMR spectra, those of $[\text{LaL}^9(\text{NO}_3)_3]$ consisted of complex multiplet bands when collected both in CDCl_3 and CD_3CN . Other physical and chemical analyses prompted the purity and integrity of this compound and the integration in the ^1H NMR spectrum equalled thirty-eight, the number of protons in $[\text{LaL}^9(\text{NO}_3)_3]$. As with $[\text{L}^8\text{H}_4]\text{Br}_4$, L^9 also has chiral centres which exhibit *R* or *S* configurations. The chiral centres are the non-aromatic nitrogen atoms, N^5 , all of which are identical so the number of possible diastereomers is five, two of them being the *meso* form. The configurations are the same as those given for $[\text{L}^8\text{H}_4]\text{Br}_4$ (Fig. 3.4). This would explain the complexity of the ^1H NMR spectrum (Fig. 3.24).

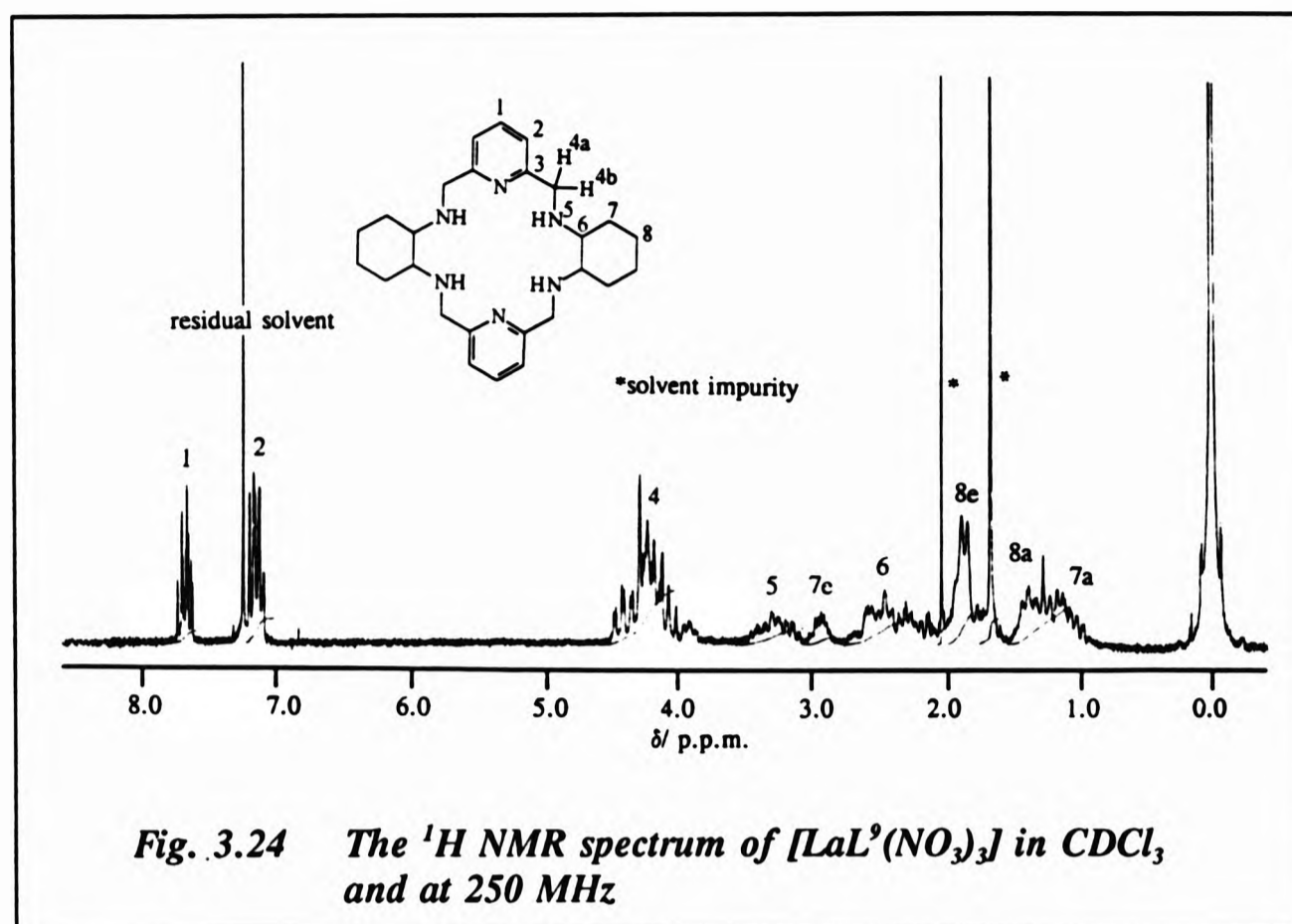


Fig. 3.24 The ¹H NMR spectrum of [LaL⁹(NO₃)₃] in CDCl₃ and at 250 MHz

Table 3.17 shows that the mean chemical shifts are similar to those of [ZnL⁹]²⁺ and [CdL⁹]²⁺. Changes in chemical shifts were not observed on running the spectrum with the addition of D₂O.

The complexity of both ¹H and ¹³C NMR spectra implies that the ligand adopts more than one and possibly all of the five diastereomeric configurations that are possible. The ¹H NMR of [ZnL⁹]²⁺ and [CdL⁹]²⁺ together with their solid state characterisation suggest that the ligand only adopts one of the possible five configurations, *i.e.* the *SSSS* or *RRRR*. This further suggests that for metals with small ionic radii, the ligand pre-organises itself prior to co-ordination, thus preventing steric interaction during the process of twisting and wrapping around the metal. As will be revealed by the X-ray structure of [LaL⁹(NO₃)₃], for larger metals, twisting is not necessary for metal co-ordination, the ligand, therefore, does not have to pre-organise itself to adopt an energy minimum conformation hence it may adopt any of the five diastereomeric forms, one of which was characterised crystallographically.

Table 3.17 The chemical shifts^a of the ¹H and ¹³C NMR spectra of [LaL⁹(NO₃)₃] in CDCl₃

ASSIGNMENT	δ _H	δ _C
1	7.69	139.1
2	7.19	121.0
3	-	159.1
4	4.26	47.6
5	3.32	-
6	2.48	59.0
7e	2.92	31.4
7a	1.19	
8a		24.8
8e	1.84	

^ain p.p.m relative to SiMe₄ as internal standard at 0.0 p.p.m.

3.4.2.4 Solid State Characterisation of [LaL⁹(NO₃)₃]MeCN

The asymmetric unit of the crystal consisted of a neutral complex species (Fig. 3.25) and a molecule of acetonitrile of crystallisation, in contrast to the formulation of [LaL⁹(NO₃)₃].½H₂O derived from microanalytical data.

The lanthanum ion adopts an irregular eleven co-ordinate geometry, six of the co-ordination sites being occupied by the six nitrogen donor atoms of the macrocycle and five sites taken by the oxygen donor atoms of the two bidentate and one monodentate nitrate ligands. The macrocyclic ligand adopts the saddle or butterfly folding observed for [GdL⁵(H₂O)₃]³⁺ (Chapter 2) and the ligand also folds away from the hemisphere containing the two co-ordinating nitrate ligands. As this is the first lanthanide complex of a hexaaza macrocyclic amine, comparisons are not available, although the dihedral angle between the two wings would be expected to be in the same range as that of the imine analogue, [LaL¹(NO₃)₃], of *ca.* 27° (Chapter 2, Table 2.9). Comparisons between [LaL⁹(NO₃)₃] and [LaL¹(NO₃)₃] co-ordination spheres are made in Table 3.18. No significant contrast in the La - N bond lengths is observed between [LaL⁹(NO₃)₃] and [LaL¹(NO₃)₃] implying that the ligand adopts

the same conformation around the metal ion whether it is a tetraamine or a tetraamine, irrespective of the extra flexibility gained by the reduced ligand, L^9 .

Fig. 3.25 *Perspective views of $[LaL^9(NO_3)_3]$ with the acetonitrile molecule omitted*

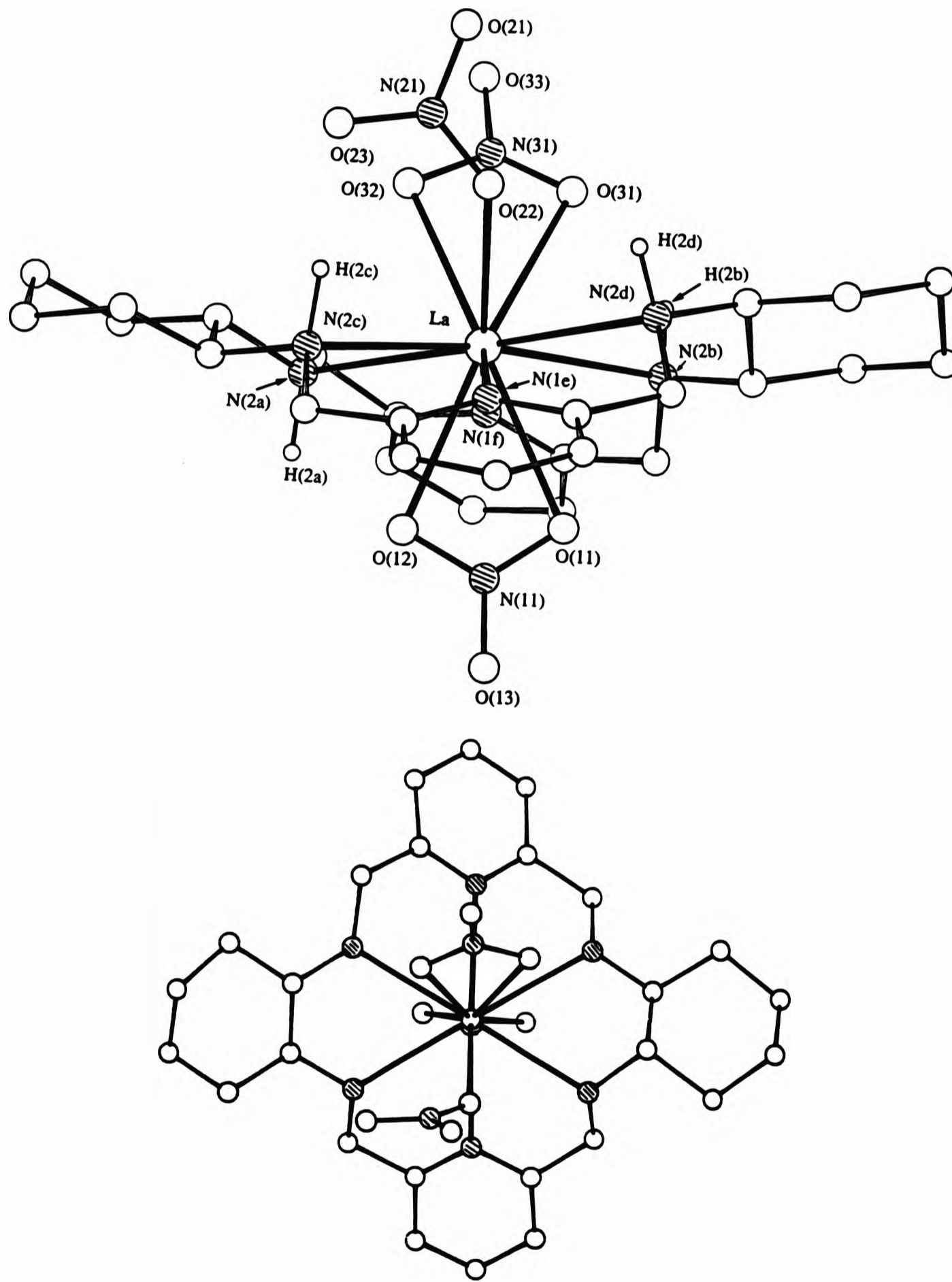
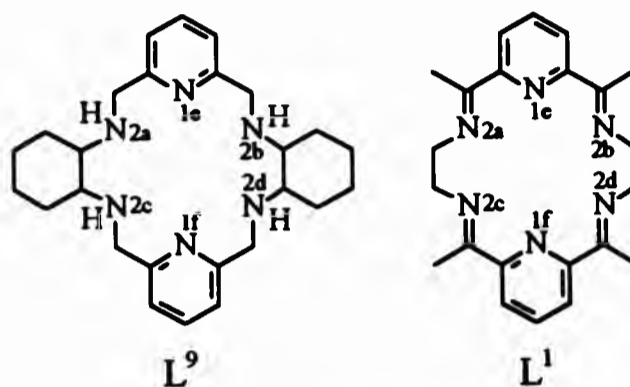


Table 3.18 Dimensions* of the metal ion co-ordination sphere of $[\text{LaL}^{\text{9}}(\text{NO}_3)_3]$ and $[\text{LaL}^{\text{1}}(\text{NO}_3)_3]$ **



Bond Length (Å)	$[\text{LaL}^{\text{9}}(\text{NO}_3)_3]$	$[\text{LaL}^{\text{1}}(\text{NO}_3)_3]$
N(2a) - La	2.770(11)	2.727(7)
N(2b) - La	2.771(11)	2.672(6)
N(2c) - La	2.729(10)	2.704(6)
N(2d) - La	2.719(11)	2.729(6)
N(1e) - La	2.730(11)	2.746(5)
N(1f) - La	2.696(11)	2.746(5)
Bond Angles (°)		
N(1f) - La - N(2a)	117.3(3)	114.2(2)
N(1f) - La - N(2b)	114.9(3)	121.4(2)
N(1f) - La - N(2c)	60.7(3)	58.6(2)
N(1f) - La - N(2d)	61.5(4)	58.7(2)
N(1f) - La - N(1e)	146.3(4)	164.3(1)
N(2c) - La - N(2b)	170.6(5)	179.4(2)
N(2c) - La - N(2a)	61.2(3)	62.9(2)
N(2c) - La - N(2d)	117.3(3)	116.3(2)
N(2c) - La - N(1e)	120.1(3)	120.8(2)
N(1e) - La - N(2a)	60.5(3)	59.2(2)
N(1e) - La - N(2b)	58.2(3)	59.0(2)
N(1e) - La - N(2d)	121.2(3)	116.2(2)
N(2d) - La - N(2b)	63.1(4)	63.6(2)
N(2d) - La - N(2a)	178.3(4)	141.6(2)
N(2a) - La - N(2b)	118.6(3)	116.8(2)

*Estimated standard deviations given in parentheses. **Data taken from ref. 44

The ligand does not conform to the "twist and wrap" about a large metal ion (§ 3.4.1.4) as described for transition metals, but it is also not planar. As described above, and also shown crystallographically (Fig. 3.25), the ligand, L⁹, and hence L⁷, L⁸, and L¹⁰, acquire the same conformation as for their imine analogues on coordination to a lanthanide metal.

The chiral nitrogen centres of L⁹ exhibit wholly *SSSS* or *RRRR* configurations for [ZnL⁹]²⁺ and [CdL⁹]²⁺ respectively. The same ligand when co-ordinated to lanthanum yielded the configuration *SRSS*. As discussed in section 3.4.2.3, for coordination to a large metal, the ligand does not have to pre-organise itself to reach an energy minimum on chelation as the size of the metal is large enough to achieve La - N co-ordination without the necessity to twist and therefore steric strain is not met. The non-pre-organisation leads to the conclusion that the ligand may conform to all five diastereomeric forms on co-ordination to lanthanide metals. The configuration *SRSS* given by the crystallographic structure (Fig. 3.25) was purely coincidental; another crystal would have probably adopted another configuration at the chiral nitrogen sites, *i.e.* another diastereomeric species.

3.5 Conclusion

Reduction and demetallation of 18-membered tetraimine macrocycles has provided a convenient way to isolate such ligands in the metal-free form. The flexibility of these ligands enables their co-ordination to small transition metals, where the ligand twists and octahedrally wraps itself around the metal. Such co-ordination was not possible with imine analogues without the ligand undergoing a rearrangement. Co-ordination of these amines with large metals revealed that the structure adopted by the ligand mimics the butterfly folding of the imine analogues. Whereas for transition metals the ligand adopts only one configuration, the use of lanthanide metals allows the ligand to adopt the five diastereomeric dispositions possible. Extreme stability and inertness was shown by the ligands from the non *NH* exchange in solution.

3.5 References

1. L. F. Lindoy, *The Chemistry of Macrocyclic Ligand Complexes*, Cambridge University Press, Cambridge, 1989, p.48.
2. R. Dewar and E. Fleischer, *Nature*, 1969, **222**, 372.
3. B. Korybut-Daszkiewicz, *J. Chem. Soc., Chem. Commun.*, 1985, 192.
4. S. Mandal and K. Nag, *J. Org. Chem.*, 1986, **51**, 3900.
5. N. W. Alcock, R. G. Kingston, P. Moore and C. Pierpoint, *J. Chem. Soc., Dalton Trans.*, 1984, 1937.
6. D. E. Fenton, B. P. Murphy, A. J. Leong, L. F. Lindoy, A. Bashall and M. McPartlin, *J. Chem. Soc., Dalton Trans.*, 1987, 2543.
7. S. C. Jackels and D. Meyer, *Pat. PCT Int. Appl.*, WO90/ 11282 CL A61 K49/00, 1990.
8. N. A. Bailey, D. E. Fenton, S. J. Kitchen, T. H. Lilley, M. G. Williams, P. A Tasker, A. J. Leong and L. F. Lindoy, *J. Chem. Soc., Dalton Trans.*, 1991, 627.
9. K. E. Krakowiak, J. S. Bradshaw, W. Jiang, N. K. Dalley, G. Wu and R. M. Izatt, *J. Org. Chem.*, 1991, **56**, 2675.
10. K. I. Dhont, W. Lippens, G. Herman and A. M. Goeminne, *Bull. Soc. Chim. Belg.*, 1992, **101**, 1061.
11. R. Menif and A. Martell, *J. Chem. Soc., Chem. Commun.*, 1989, 1521.
12. G. L. Rothermel, Jr., L. Miao, A. L. Hill and S. C. Jackels, *Inorg. Chem.*, 1992, **31**, 4854.
13. D. H. Williams and I. Fleming, *Spectroscopic Methods in Organic Chemistry*, 4th Edn., McGraw-Hill, London, 1987.
14. R. S. Cahn, C. K. Ingold and V. Prelog, *Angew. Chem., Int. Ed. Engl.*, 1966, **5**, 385.
15. A. Streitwieser, Jr., and C. H. Heathcock, *Introduction to Organic Chemistry*, 3rd Edn., Collier MacMillan, New York, 1985.
16. R. J. Fessenden and J. S. Fessenden, *Organic Chemistry*, 4th Edn., Brooks-Cole Publishing Co., California, 1990.

17. N. Harada and K. Nakanishi, *Circular Dichroic Spectroscopy Exciton Coupling in Organic Stereochemistry*, Oxford University Press, Oxford, 1983.
18. J. A. Schellman, *Chem. Rev.*, 1975, **75**, 323.
19. L. H. Bryant, Jr., A. Lachgar, K. S. Coates and S. C. Jackels, *Inorg. Chem.*, 1994, **33**, 2219.
20. K. R. Hanson, *J. Am. Chem. Soc.*, 1966, **88**, 2731.
21. W. B. Jennings, *Chem. Rev.*, 1975, **75**, 307.
22. R. M. Silverstein, G. C. Bassler and T. C. Morrill, *Spectroscopic Identification of Organic Compounds*, 4th Edn., Wiley, Singapore, 1981.
23. S. Chaudhury, unpublished results.
24. S. Waiker, PhD Thesis, University of North London, 1992.
25. P. Guerriero, S. Tamburini, P. A. Vigato, R. Seraglia and P. Traldi, *Org. Mass Spectrom.*, 1992, **27**, 231.
26. P. A. Duckworth, L. F. Lindoy, M. McPartlin and P. A. Tasker, *Aust. J. Chem.*, 1993, **46**, 1787.
27. N. N. Greenwood and A. Earnshaw, *Chemistry of the Elements*, Pergamon Press, Oxford, 1986, p1231.
28. K. F. Purcell and J. C. Kotz, *Inorganic Chemistry*, Holt-Saunders, Hong Kong, 1987.
29. J. E. Huheey, *Inorganic Chemistry, Principles of Structure and Reactivity*, 3rd Edn., Harper International, USA, 1983, p575.
30. N. Nakamoto, *Infrared and Raman Spectra of Inorganic and Co-ordination Compounds*, Wiley, New York, 1970.
31. B. J. Hathaway and A. E. Underhill, *J. Chem. Soc.*, 1961, 3091.
32. A. E. Wickenden and R. A. Krause, *Inorg. Chem.*, 1965, **4**, 404.
33. J. K. M. Sanders and B. K. Hunter, *Modern NMR Spectroscopy, a Guide for Chemists*, Oxford University Press, USA, 1992.
34. M. G. B. Drew, J. Nelson and S. M. Nelson, *J. Chem. Soc, Dalton Trans.*, 1981, 1678.

35. R. K. Harris, *Nuclear Magnetic Resonance Spectroscopy*, Longman, Hong Kong, 1987, p51.
36. M. Kodoma, E. Kimura and S. Yamaguchi, *J. Chem. Soc., Dalton Trans.*, 1980, 2536.
37. T. W. Bell and S. K. Sahni in *Inclusion Compounds, Key Organic Host Systems*, J. L. Atwood, J. E. Davies and D. D. MacNicol (Eds.), Oxford Science Publications, Oxford, 1992, 4, p325.
38. G. H. Searle, *Bull. Chem. Soc. Jpn.*, 1989, 62, 4021.
39. K. R. Adam, S. Donnelly, A. J. Leong, L. F. Lindoy, B. J. McCool, A. B. Bashall, M. R. Dent, B. P. Murphy, M. McPartlin, D. E. Fenton and P. A. Tasker, *J. Chem. Soc., Dalton Trans.*, 1990, 1635.
40. E. C. Constable, *Chem. Ind.*, 1994, 2, 56 and refs therein.
41. I. J. Scowen, PhD Thesis, University of North London, 1993.
42. D. E. Fenton, R. W. Matthews, M. McPartlin, B. M. Murphy, I. J. Scowen and P. A. Tasker, *J. Chem. Soc., Chem. Commun.*, 1994, 1391.
43. J. Forsberg and T. Moeller, *Inorg. Chem.*, 1969, 8, 883.
44. A. M. Arif, J. D. Backer-Dirks, C. J. Gray, A. Hart and M. B. Hursthouse, *J. Chem. Soc., Dalton Trans.*, 1987, 1665.

CHAPTER 4

**Chapter 4: HEXAAZA AND OCTAAZA MACROCYCLES WITH
ADDITIONAL PHENOLIC PENDANT ARM
FUNCTIONALITIES**

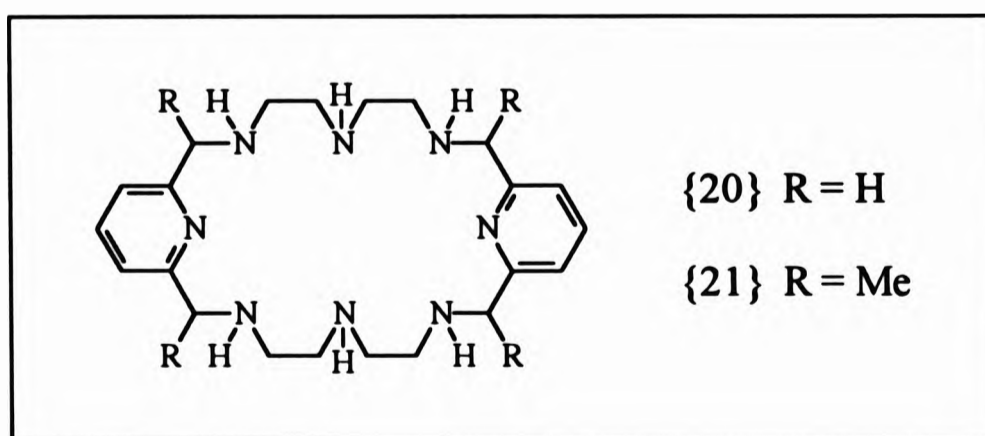
(References to this Chapter are listed on pages 220 - 222)

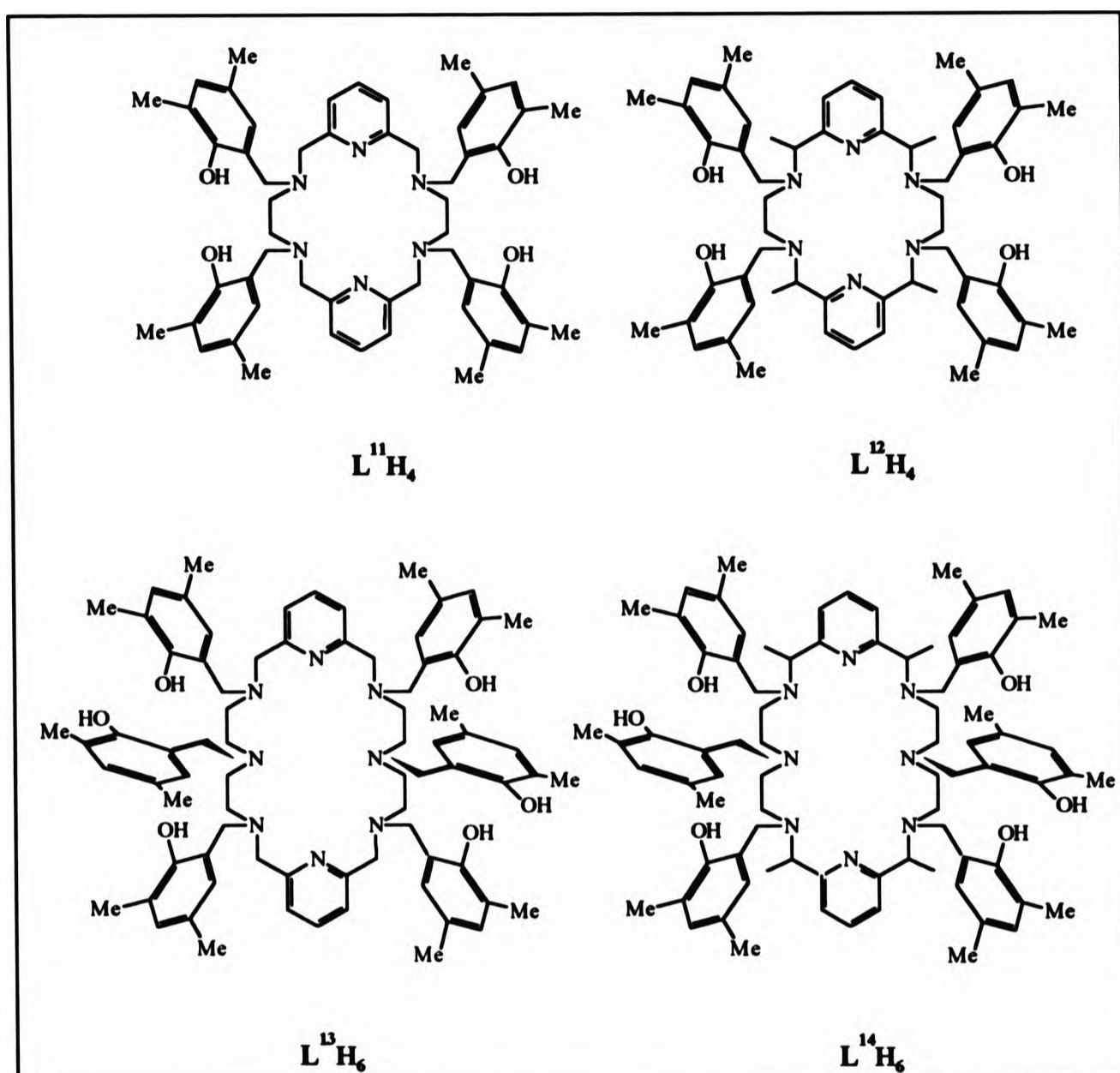
4.1 Introduction

The reduction of the imine bonds to the corresponding amine (chapter 3) exposes the latter functionality to further substitution reactions yielding tertiary nitrogen donors, donors that have received, until recently, limited attention in the field of macrocyclic chemistry.^[1,2] Additionally, the substituting group may be used to alter the chemistry of the macrocyclic ligand regarding its denticity, stability on metal complexation and possibly its solubility.

Functionalities used as pendants include the methylene carboxylate (See Chapter 1), methylene pyridyl,^[3-13] hydroxyethyl^[14,15] and methylene phosphonate^[16-18] but the groups vary depending on the metal to be co-ordinated and the overall use of the ligand and/ or complex.

In this study, the aim was to attach 2,4-dimethylphenol to the secondary amine nitrogen atoms of the ligands L⁷ - L⁹ (discussed in Chapter 3) and also to the octaaza macrocyclic ligands {20} and {21}, linked *via* methylene bridges, followed by transition and lanthanide metal complexation.





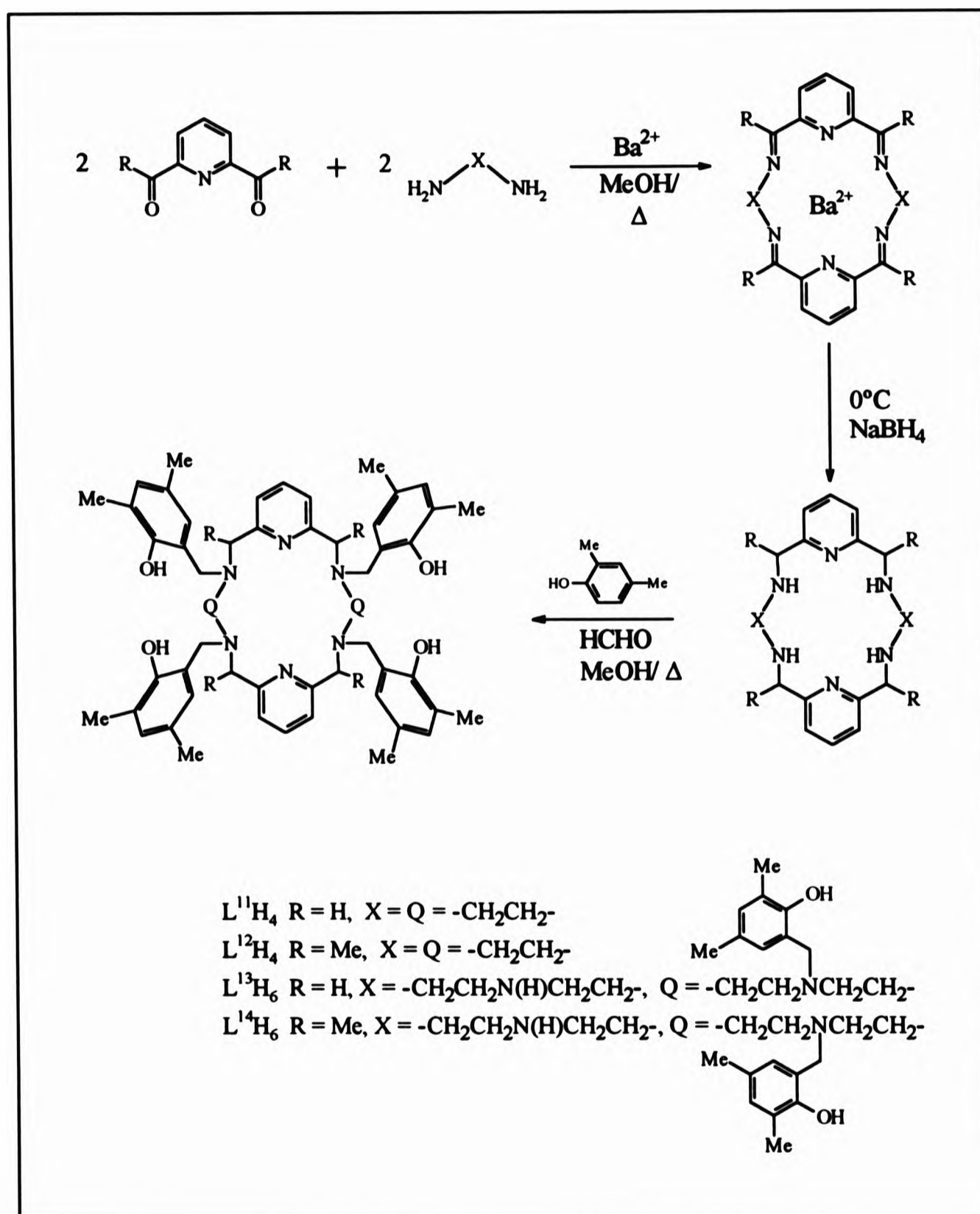
4.2 Synthesis of L^{11} - L^{14} Incorporating the 2-hydroxy-3,5-dimethylbenzyl Pendant arms

The reaction of the non-hydrobrominated amine, L^8 , with 2,4-dimethylphenol and aqueous methanal in a methanolic solution yielded colourless crystals of $L^{12}H_4$. Attempts at carrying out the reaction with the amine as the tetrahydrobromide salt failed resulting in the isolation of the starting amine. In addition, the order in which the reactants were added to the reaction proved to be important. Reactions following the procedure reported by Weighardt *et al.*^[19] and Fanwick *et al.*^[20] did not proceed, *i.e.* refluxing the amine with methanal followed by the addition of 2,4-dimethylphenol. However, when the latter two reagents were reversed in order, the

reaction proceeded successfully. A pure white fluffy solid precipitated instantly, in good yield during reflux, when the reaction was carried out at low methanolic dilution. Well defined colourless crystals were isolated when the reaction was carried out at high dilution and allowed to stand at room temperature for approximately one month. Alternatively, exchanging the solvent from methanol to absolute ethanol on completion of the reaction, caused the precipitation of the solid amorphous product. When the synthesis proved successful the reaction was extended to the formation of $L^{11}H_n - L^{14}H_n$ (for L^{11} and L^{12} , $n = 4$; for L^{13} and L^{14} , $n = 6$) with yields in the range 20 - 50%. The solid state structure of $L^{12}H_4$ was solved *via* a single crystal X-ray crystallography. The new ligands were limited in their solubilities to dichloromethane, acetone, toluene and warm DMSO. Fig. 4.1 shows the three-stage synthesis of $L^{11}H_n - L^{14}H_n$ where, in the first two stages, the products were not pre-isolated.

Attempts to isolate the tetraimine precursors of {20} and {21} according to published non-template procedures^[21-23] under high dilution in acetonitrile were unsuccessful. However, the *in-situ* method using Ba^{2+} as a template in methanol, followed by borohydride reduction and demetallation, which was adopted for the syntheses of the amines L^7 and L^8 (Chapter 3) was convenient and less time consuming, resulting in much higher yields of the required hexaamine. For the purposes of the preparation of $L^{13}H_6$ and $L^{14}H_6$, {20} and {21} were used as oils without further purification, although the hexahydrochloride salts of the hexaamines were isolated as the white solids $[\{20\}H_6]Cl_6 \cdot 2H_2O$ and $[\{21\}H_6]Cl_6 \cdot 4H_2O$. The compounds gave satisfactory IR, EI and NMR analyses (Appendix 1).

Fig. 4.1 The three-stage synthesis of $L^{11}H_4$ - $L^{14}H_6$, incorporating the 2-hydroxy-3,5-dimethylbenzyl pendant arms



4.3 Characterisation of the Ligands

4.3.1 Infrared Spectrophotometry

The IR spectra of the ligands $L^{11}H_4$ - $L^{14}H_6$ were alike. Fig. 4.2 shows a broad band in the range $3500 - 2500 \text{ cm}^{-1}$, superimposed by the strong absorptions of saturated alkyl and aromatic C-H groups, assigned to the O-H group of the phenolic pendant arms. The involvement of intramolecular association tends to diminish the stretching frequency of the O-H stretching vibration, depending on the strength of the hydrogen bond, and suggests that a chelate ring forms (Fig. 4.3) from the intramolecular hydrogen bonding interactions of the hydroxyl proton and the nitrogen atom from which the pendant arm protrudes. Resonance is also occurring. The pattern shown in the spectrum resembles one of a typical carboxylic acid where the exceptional strength of the intermolecular hydrogen bonding, between two carboxylic acid groups on different molecules, is explained on the basis of the large contribution of the ionic resonance structure. Due to strong bonding interactions, a free hydroxyl stretching vibration (*ca.* 3500 cm^{-1}) is not detected. In contrast, the band observed for $L^{11}H_4$ - $L^{14}H_6$ is due to intramolecular hydrogen bonding and not from an intermolecular dimeric structure but probably just as strong.

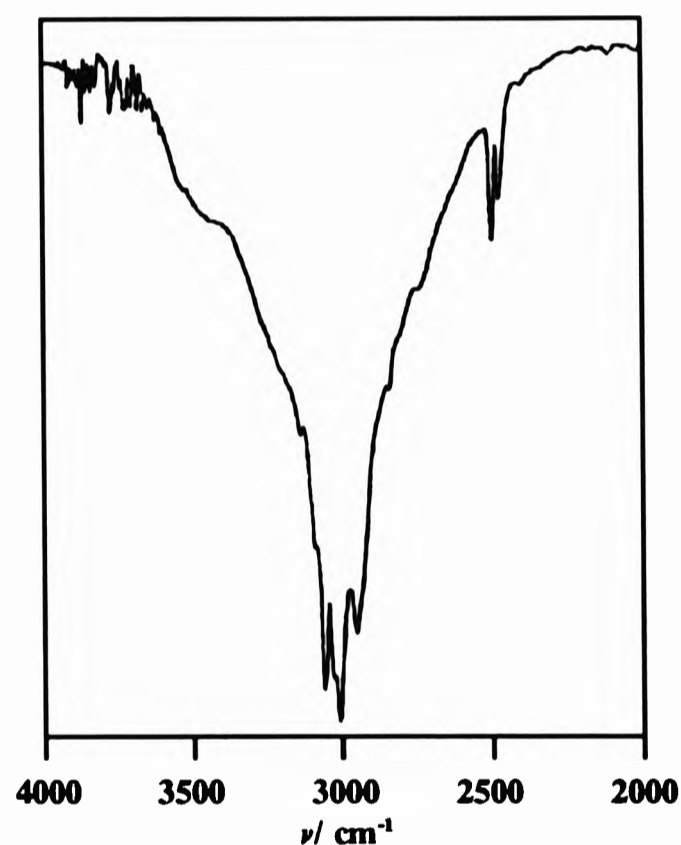


Fig. 4.2 The infrared spectrum of $L^{11}H_4$ - $L^{14}H_6$ in the region $4000 - 2000 \text{ cm}^{-1}$

The substitution of all the amino hydrogen atoms was shown by the absence of the N-H bands at 3285 cm^{-1} . Tertiary amines do not show any characteristic vibrations in the region $3500 - 3200 \text{ cm}^{-1}$ of the IR spectrum.

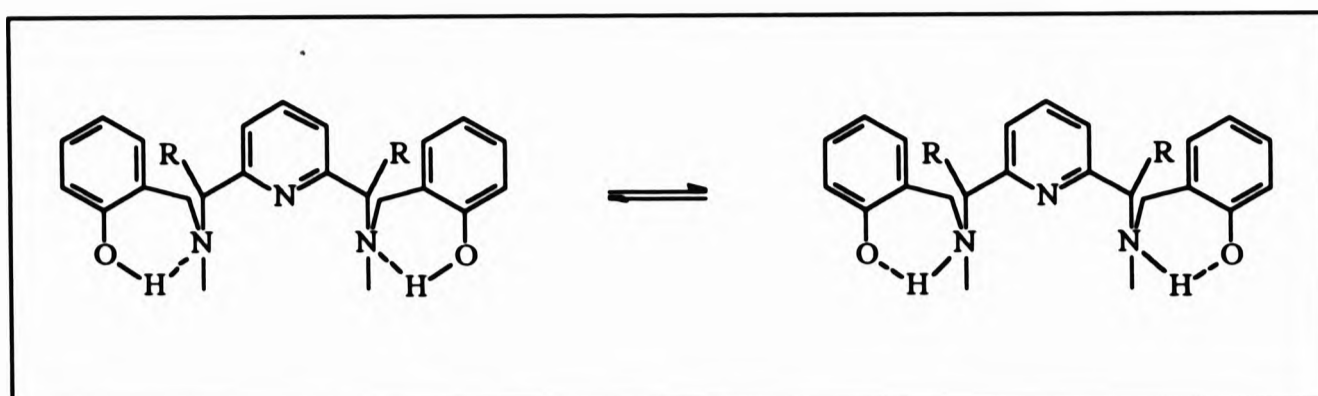


Fig. 4.3 Intramolecular hydrogen bonding leading to chelate ring formation

The weak aromatic C-H stretches absorb at $3006 - 3009 \text{ cm}^{-1}$ and $3054 - 3062 \text{ cm}^{-1}$ adjacent to the more intense alkyl C-H stretches, three bands for $L^{11}\text{H}_4$ and $L^{13}\text{H}_6$ and four for $L^{12}\text{H}_4$ and $L^{14}\text{H}_6$ at $2850 - 2975 \text{ cm}^{-1}$. The extra band at 2938 cm^{-1} for $L^{12}\text{H}_4$ and $L^{14}\text{H}_6$ can be assigned to the C-H stretches of the methyl groups. In the fingerprint region (Table 4.1) all the spectra exhibited characteristic absorptions of skeletal in-plane ring vibrations at $1612 - 1614$, $1587 - 1590$ and $1574 - 1575 \text{ cm}^{-1}$. The O-H stretching vibrations in phenol produced a strong sharp band around 3000 cm^{-1} and O-H bending vibrations around 1377 cm^{-1} . The individual bands are listed in Table 4.1.

Table 4.1 The fingerprint region of the infrared spectra* of $L^{11}\text{H}_4$, $L^{14}\text{H}_6$ and $L^{16}\text{H}_2$

LIGAND	aromatic $\nu(\text{C-H})_{\text{str}}$	alkyl $\nu(\text{C-H})_{\text{str}}$	aromatic $\nu(\text{C-C})_{\text{str}}$	alkyl $\nu(\text{C-H})_{\text{bend}}$	$\nu(\text{O-H})_{\text{bend}}$	$\nu(\text{C-O})_{\text{str}}$	aromatic out-of-plane $\nu(\text{C-H})_{\text{deform}}$
$L^{11}\text{H}_4$	3009 3062	2966 2915 2849	1614w 1590 1574	1485s 1457 1343	1376	1241sh	772
$L^{12}\text{H}_4$	3060 3006	2972 2937 2914 2855	1614w 1588 1574	1485s 1456	1377	1244sh	769
$L^{13}\text{H}_6$	3009 3054	2954 2916 2850	1612w 1590 1573	1485s 1456 1442	1378	1244sh	768
$L^{14}\text{H}_6$	3057	2970 2938 2906 2850	1613w 1587 1575	1485s 1454	1376	1243sh	767
* $L^{16}\text{H}_2$	3011	2937 2861	1612w	1484s 1446	1375	1244sh	769

*in cm^{-1} , *See section 4.6

4.3.2 Liquid Secondary Ion Mass Spectrometry

The LSIM spectra of the ligands had base peaks corresponding to the molecular ion of $[H_nL^x + H]^+$ ($x = 11-14$; $n = 4,6$). One characteristic feature of all the ligands was the cleavage of the whole pendant arm ($-CH_2C_8H_9O$) on decomposition, all the pendant arms being lost consecutively leaving the backbone of the macrocycle. Table 4.2 shows this trend in fragmentation obtained for these ligands.

A trend shown in Table 4.2 is the decrease in the relative abundance as the first two ($L^{11}H_4$ and $L^{12}H_4$) or three ($L^{13}H_6$ and $L^{14}H_6$) pendants are lost. The percentage abundances begin to increase as the remaining pendants are lost. With the exception of $L^{14}H_6$, the second most intense band, after that of the molecular ion, is that representing the backbone of the macrocycle.

A common fragment for all the spectra was representative of $[M/2 + H]^+$. This then leads the way to another fragmentation route by the loss of pendants on this fragment (Table 4.3). The same trend is followed by the relative abundances as in Table 4.2.

Table 4.2 The fragmentation of the ligands $L^{11}H_4$ - $L^{14}H_6$

LIGAND	FRAGMENT	m/z	RELATIVE ABUNDANCE(%)
$L^{11}H_4$	$[L^{11}H_4 + H]^+$	864	100
	$[(L^{11}H_4 + H) - X]^+$	729	11
	$[(L^{11}H_4 + H) - 2X]^+$	594	10
	$[(L^{11}H_4 + H) - 3X]^+$	459	26
	$[(L^{11}H_4 + H) - 4X + 3H]^+$	327	96
$L^{12}H_4$	$[L^{12}H_4 + H]^+$	920	100
	$[(L^{12}H_4 + H) - X + H]^+$	786	8
	$[(L^{12}H_4 + H) - 2X + 2H]^+$	652	5
	$[(L^{12}H_4 + H) - 3X + H]^+$	516	12
	$[(L^{12}H_4 + H) - 4X + 3H]^+$	383	83
$L^{13}H_6$	$[L^{13}H_6 + H]^+$	1218	100
	$[(L^{13}H_6 + H) - X]^+$	1083	10
	$[(L^{13}H_6 + H) - 2X]^+$	948	7
	$[(L^{13}H_6 + H) - 3X + 2H]^+$	815	6
	$[(L^{13}H_6 + H) - 4X + 3H]^+$	681	33
	$[(L^{13}H_6 + H) - 5X + 4H]^+$	547	39
	$[(L^{13}H_6 + H) - 6X + 5H]^+$	413	74
$L^{14}H_6$	$[L^{14}H_6 + H]^+$	1273	100
	$[(L^{14}H_6 + H) - X]^+$	1138	61
	$[(L^{14}H_6 + H) - 2X]^+$	1003	18
	$[(L^{14}H_6 + H) - 3X]^+$	868	20
	$[(L^{14}H_6 + H) - 4X + 2H]^+$	735	16
	$[(L^{14}H_6 + H) - 5X + 3H]^+$	601	89
	$[(L^{14}H_6 + H) - 6X + 5H]^+$	468	43

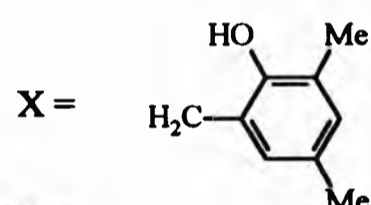


Table 4.3 The second fragmentation route of $L^{11}H_4$ and $L^{12}H_4$

LIGAND	FRAGMENT	m/z	RELATIVE ABUNDANCE (%)
$L^{11}H_4$	$[L^{11}H_4 + H]^+$	864	100
	$[(L^{11}H_4)/2 + H]^+$	433	13
	$[(L^{11}H_4)/2 + H - X]^+$	298	20
	$[(L^{11}H_4)/2 + H - 2X]^+$	163	83
$L^{12}H_4$	$[L^{12}H_4 + H]^+$	920	100
	$[(L^{12}H_4)/2 + H]^+$	460	6
	$[(L^{12}H_4)/2 + H - X]^+$	325	17
	$[(L^{12}H_4)/2 + H - 2X]^+$	190	41

4.3.3 Nuclear Magnetic Resonance Spectroscopy

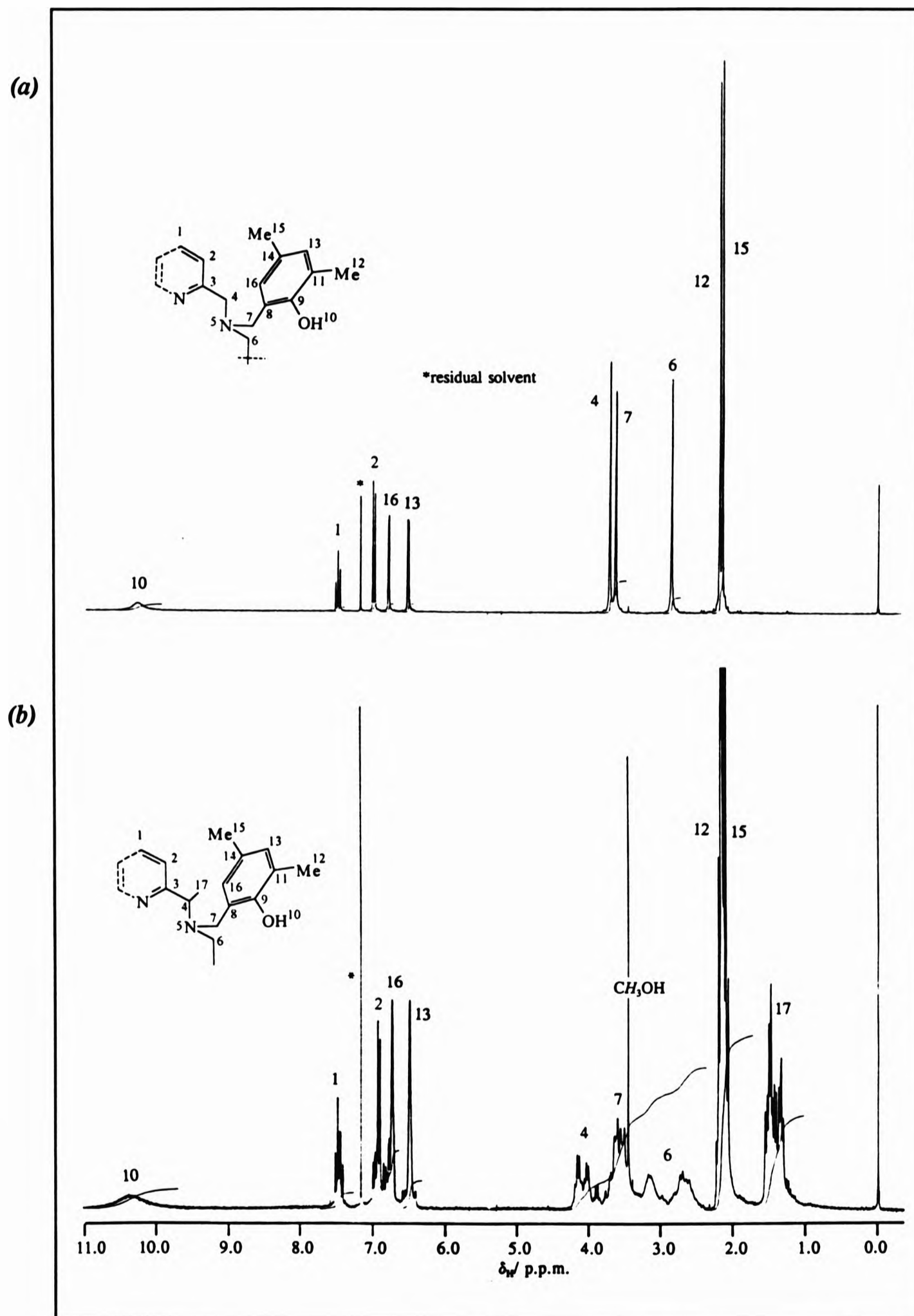
The solution structures of the ligands have been elucidated by ^1H and ^{13}C NMR spectroscopy and where necessary with 2D-COSY spectra also, in CDCl_3 and at 250 MHz. For L^{11}H_4 and L^{12}H_4 , a four-fold symmetry is prominent and this conclusion is prompted by both the ^1H and ^{13}C NMR spectra. For L^{12}H_4 and L^{14}H_6 , the presence of diastereomeric species cause the spectra to be complex yet assignable. The purity and the integral values depicted by the spectra support the tetra- or hexa-substitution of the amine precursors as well as the integrity of the compounds.

4.3.3.1 The NMR Spectra of L^{11}H_4 and L^{12}H_4

The ^1H NMR spectrum of L^{11}H_4 (Fig. 4.4a) depicts a broad peak at δ_{H} 10.38 which collapses on D_2O addition to the NMR solution. This band is assigned to the hydroxyl proton. Generally, the phenolic proton peak is a sharp singlet (due to rapid exchange) and its chemical shift falls in the range δ_{H} 7.5 - 4.0 depending on the concentration, solvent and temperature of the solution. The shift downfield from this range to δ_{H} 10.38 is caused by intramolecular hydrogen bonding^[24] to the tertiary amine nitrogen atom supporting the prediction made in the IR spectrum.

The AB_2 splitting pattern of the pyridine protons was persistent in the spectrum, the typical *triplet*(H^1) and *doublet*(H^2) at δ_{H} 7.55 and 7.06 respectively, the coupling constant between the two protons being $^3J(\text{H}^1, \text{H}^2) = 7.7$ Hz. Further upfield to these bands at δ_{H} 6.84 and 6.57, resonate two doublet bands each integrating for four protons. These are assigned to the aromatic protons of the benzyl ring, the one most downfield being H^{16} , the one at δ_{H} 6.57 being due to H^{13} , the assignments being made due to the proximity of the hydroxyl group and the nitrogen atom, N^5 , causing deshielding. The four-bond coupling, $^4J(\text{H}^{13}, \text{H}^{16})$, is typically 1.63 Hz.^[25] The two singlet bands at δ_{H} 2.19 and 2.16 are ascribed to the protons of the methyl substituents on the phenolic pendant arms. H^{12} being *ortho* and H^{15} *para* to the hydroxyl group suggests that the former protons would resonate downfield to the latter.

Fig. 4.4 The ^1H NMR spectra of (a) $L^{11}\text{H}_4$ and (b) $L^{13}\text{H}_4$ in CDCl_3 and at 250 MHz (relative to SiMe_4 as internal standard at 0.0 p.p.m.)



$L^{11}H_4$ has three methylene groups (H^4 , H^6 and H^7) in different chemical environments and these resonate as three individual *singlets* integrating for eight protons each. The two singlet bands at δ_H 3.74 and 3.66 are assigned to H^4 and H^7 respectively. The distinction between these two bands and that of H^6 was based on the similarity of environments in which the protons H^4 and H^7 are in, *i.e.* both methylene groups are attached to a nitrogen atom and also to an aromatic ring. The extra deshielding caused by the macrocyclic ring allows for H^4 to resonate downfield, at δ_H 3.74, to H^7 . By the process of elimination the band at δ_H 2.87 is labelled H^6 .

The 1H NMR spectrum of $L^{12}H_4$ (Fig. 4.4b) has similar chemical shifts to that of $L^{11}H_4$ with the exception of the presence of the methine and methyl groups and, of course, the general complexity of the bands from the five possible diastereomers (Chapter 3). The chirality about the nitrogen atoms, N^5 , does not affect the NMR spectrum of $L^{11}H_4$ *i.e.* one configuration is adopted. The methyl protons on the backbone of the macrocycle, H^{17} , resonate, on average, at δ_H 1.4, the methine protons, H^4 , at δ_H 4.1. The bands due to the pyridine, benzylic and methylene (H^7 and H^6) protons resonate on average at the same chemical shift as those $L^{11}H_4$. The chemical shifts of both ligands are summarised in Table 4.4. Ideally, as shown for L^8 -*meso* (Chapter 3), the two protons of CH_2^6 are not chemically equivalent but for the purposes of the assignment they are labelled alike.

The off resonance broad band proton decoupled ^{13}C NMR spectrum of $L^{11}H_4$ depicted fourteen bands representing a quarter of the structure (Table 4.5). The spectrum was solved with the aid of DEPT-135 and ^{13}C - 1H COSY spectra, with the knowledge that quaternary carbon atoms are not detected in such spectra. The spectrum of 2,4-dimethylphenol was also helpful as was the spectrum of $[L^7H_4]Br_4$ (Chapter 3, Table 3.4). A similar pattern was given by $L^{12}H_4$ but as multiplets instead of singlet bands (Table 4.5). The quaternary carbon atoms were assigned on the basis of electronegativities and substituent effects.

Table 4.4 The chemical shifts of the ^1H NMR spectra of L^{11}H_4 and L^{12}H_4 in CDCl_3 and at 250 MHz (relative to SiMe_4 at 0.0 p.p.m.)

ASSIGNMENT	δ_{H}	
	$\text{L}^{11}\text{H}_4^*$	$\text{L}^{12}\text{H}_4^{**}$
1	7.55 (t)	7.55
2	7.06 (d)	6.99
3	-	-
4	3.74 (s)	4.11
5	-	-
6	2.87 (s)	2.78 and 3.31
7	3.66 (s)	3.66
8	-	-
9	-	-
10	10.38 (br)	10.53
11	-	-
12	2.19 (s)	2.15
13	6.57 (d)	6.56
14	-	-
15	2.16 (s)	2.15
16	6.84 (d)	6.80
17	-	1.40

* See text for coupling constants ** average value

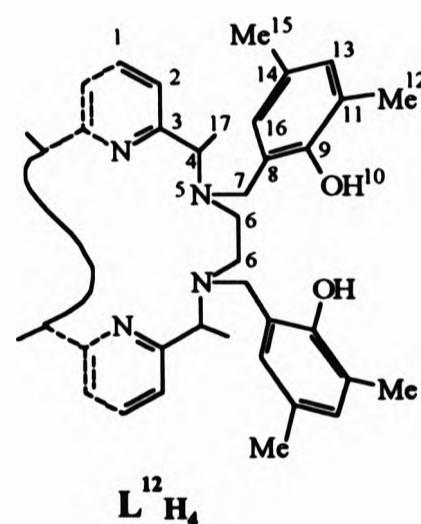
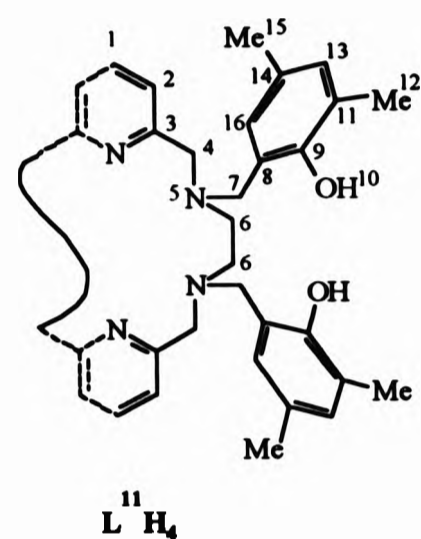
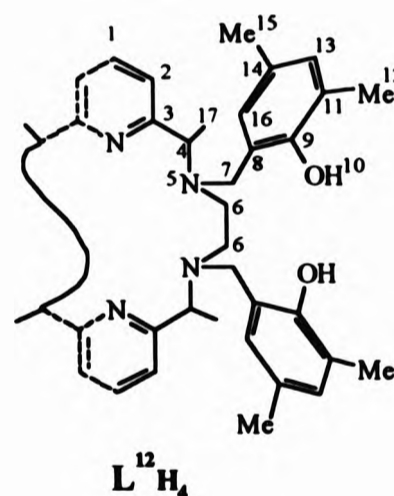
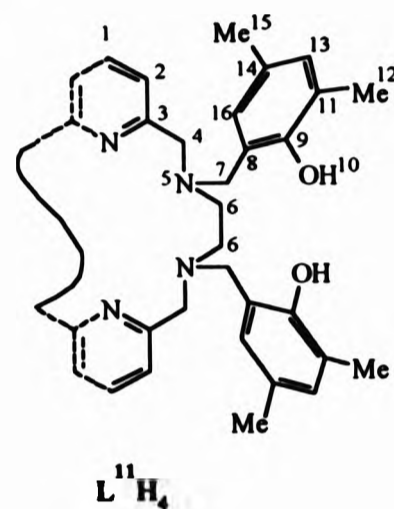


Table 4.5 The chemical shifts of the ^{13}C NMR spectra of L^{H} and L^{H} in CDCl_3 (relative to SiMe_4 as internal standard)

ASSIGNMENT	δ_{C}	
	L^{H}	L^{H} *
1	136.91	136.23
2	122.13	121.4 - 120.2 ^a
3	157.01	160.23
4	58.87	59.67
5	-	-
6	50.85	48.98
7	58.18	54.62
8	127.58	127.64
9	153.28	160.23
10	-	-
11	124.73	124.47
12	20.41	20.42
13	127.14	127.23
14	121.04	121.4 - 120.2 ^a
15	15.74	15.70
16	130.66	130.32
17	-	20.42 and 15.70

* average value, ^a C² and C¹⁴ overlap



4.3.3.2 The NMR Spectra of L¹³H₆ and L¹⁴H₆

The ¹H NMR spectrum of L¹³H₆ (Fig. 4.6, Table 4.6) shows, again, a broad hydroxyl band at δ_H 10.57, this chemical shift being consistent with intramolecular hydrogen bonding. Overall the similarity of this spectrum with that of L¹¹H₄ (Fig. 4.4a) was expected. The *triplet* at δ_H 7.59 from the pyridyl H¹ proton, the *doublet* for the H² proton at δ_H 7.09 and the coupling constant between these protons, ³J(H¹,H²) = 7.7 Hz, are virtually identical

to those of L¹¹H₄. The spectrum suggests that in this structure the protons on the benzylic rings A and B (Fig. 4.5), which resonate at different chemical shifts, are not symmetrically equivalent.

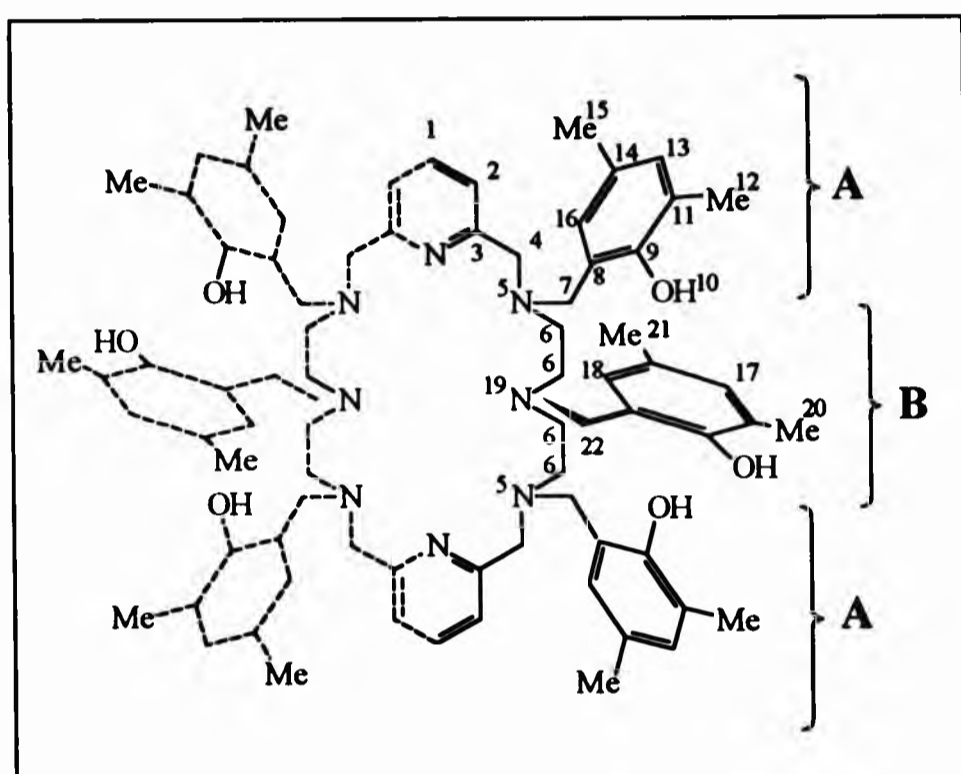
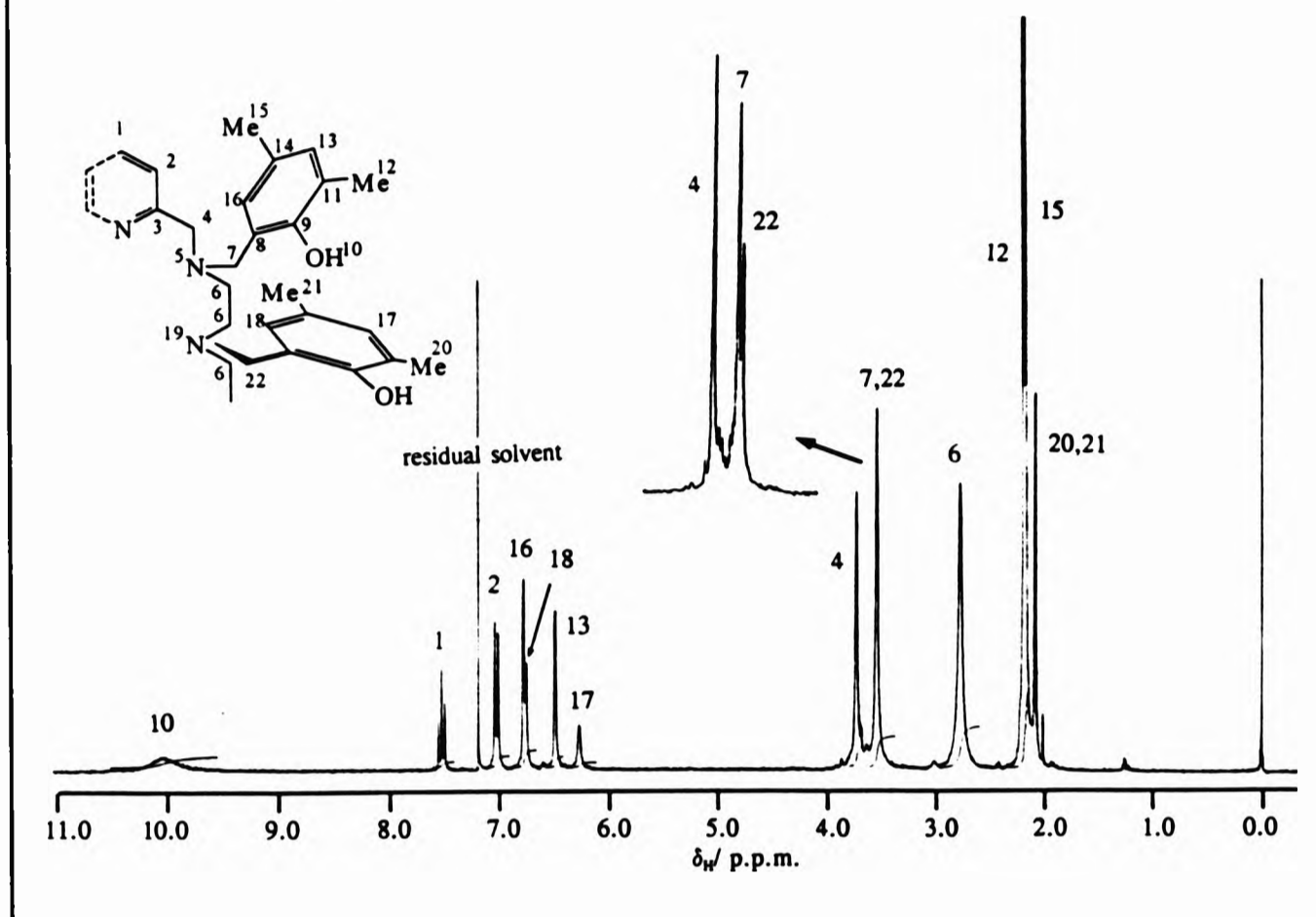


Fig. 4.5 The NMR numbering scheme of L¹³H₆

The protons, H¹⁶ and H¹³ on the benzylic ring A resonate at δ_H 6.83 and 6.54 respectively, each as a doublet band. ¹H-COSY spectra indicated that coupling between these protons does occur. The integration of each of these bands being four suggests that there are four benzylic rings in the same chemical environment. The protons on the ring of pendant B, H¹⁷ and H¹⁸, attached to N¹⁹ resonate at δ_H 6.81 (H¹⁸) and 6.32 (H¹⁷). These are also a pair of doublet bands, shown much clearer in Fig. 4.7, the ¹³C-¹H-COSY spectrum, and are also coupled to each other. The integral values per band is two in this case which is indicative of the two B benzylic rings.

Fig. 4.6 The ^1H NMR spectrum of L^{13}H_6 in CDCl_3 and at 250 MHz with the inset of H^7 run in $(\text{CD}_3)_2\text{CO}$ and at 250 MHz (relative to SiMe_4 as internal standard at 0.0 p.p.m.)

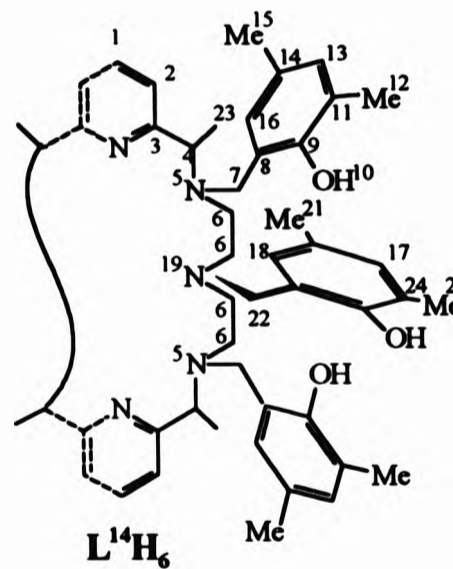
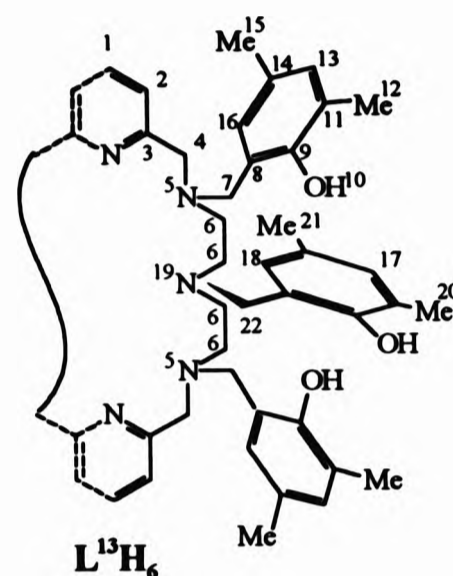


The peak at δ_{H} 3.75, integrating for eight protons is assigned to the methylene protons H^4 and the band at δ_{H} 2.78 is due to the ethylene bridges, H^6 . For the methylene bridges H^7 and H^{22} , the distinction between the pendant arms A and B still applies although not so apparent in the spectrum. Better resolution was obtained when the spectrum was ran in $(\text{CD}_3)_2\text{CO}$ where a band at δ_{H} 3.57 from H^7 with a shoulder at δ_{H} 3.54 due to H^{22} was detected. The pattern is repeated with the methyl protons; two bands at δ_{H} 2.18 and 2.16 are assigned to H^{12} and H^{15} respectively from the pendant arms A and the singlet at δ_{H} 2.07 for proton H^{20} from pendant B.

The ^1H NMR spectrum of L^{14}H_6 in d_6 -DMSO and at 250 MHz is summarised in Table 4.6 and is similar to L^{12}H_4 . Many of the bands which were distinguishable in the spectrum of L^{13}H_6 cannot be made apart in the spectrum of L^{14}H_6 as a result of overlapping and the compound being diastereomeric.

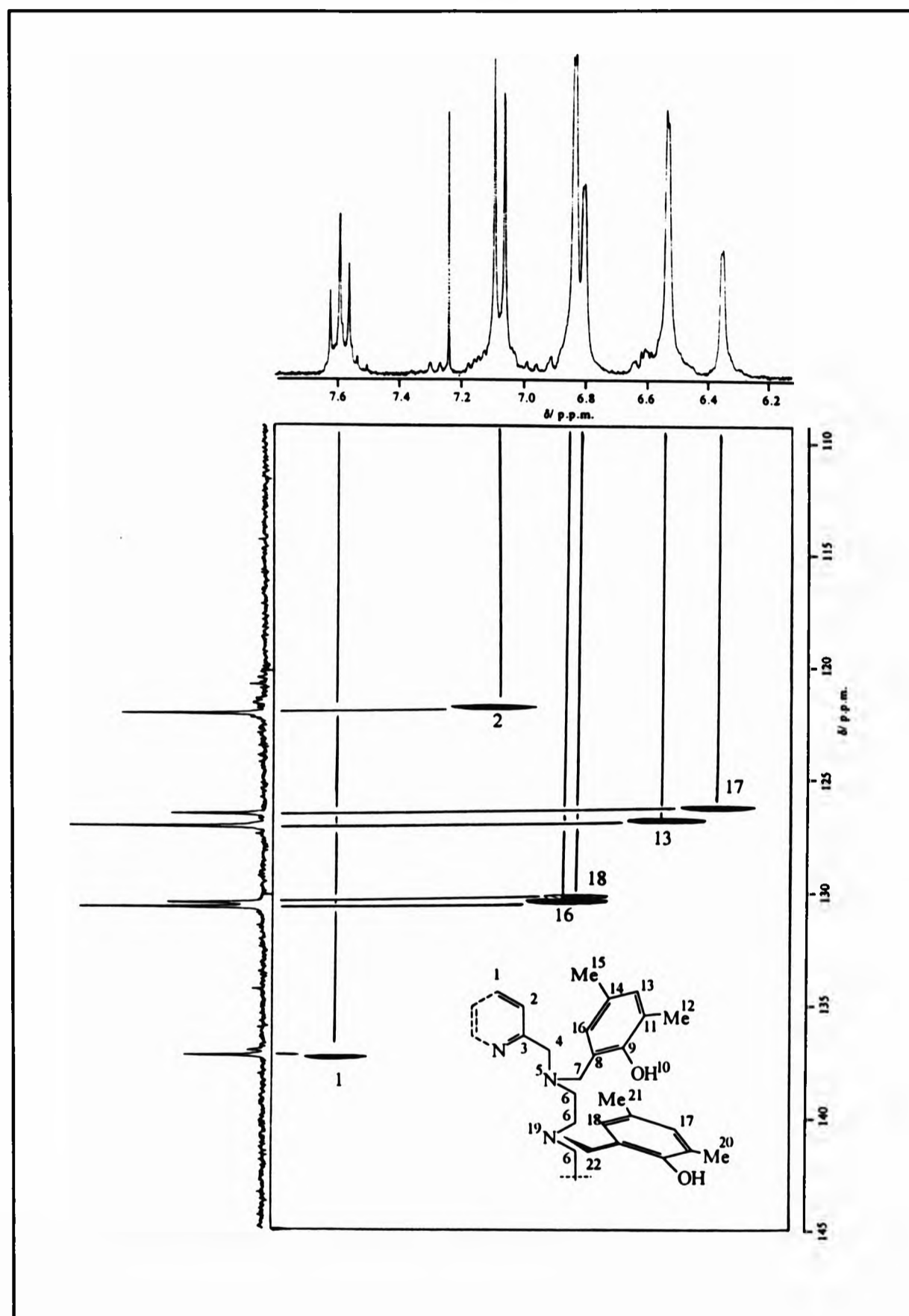
Table 4.6 The chemical shifts of the ^1H NMR spectra of $\text{L}^{13}\text{H}_6^*$ and $\text{L}^{14}\text{H}_6^{**}$ (relative to SiMe_4 as internal standard at 0.0 p.p.m.)

ASSIGNMENT	δ_{H}	
	L^{13}H_6	L^{14}H_6
1	7.59 (t)	7.64
2	7.09 (d)	7.06
3	-	-
4	3.75 (s)	4.61
5	-	-
6	2.78 (s)	2.66
7	3.57 (s)	3.2 - 3.9
8	-	-
9	-	-
10	10.15 (br)	10.15 (br)
11	-	-
12	2.18 (s)	2.3 - 2.6
13	6.54 (d)	6.5 - 6.8
14	-	-
15	2.16 (s)	2.3 - 2.6
16	6.83 (d)	6.5 - 6.8
17	6.32 (d)	6.5 - 6.8
18	6.81 (d)	6.5 - 6.8
19	-	-
20, 21	2.07 (s)	2.3 - 2.6
22	3.54 (s)	3.2 - 3.9
23	-	1.32



* in CDCl_3 , **in d_6 -DMSO

Fig. 4.7 The aromatic region of the ^{13}C - ^1H -COSY spectrum of $L^{13}\text{H}_6$ in CDCl_3



4.3.4 X-Ray Structural Studies of $L^{12}H_4$

The solid state crystal structure of $L^{12}H_4$ has been determined. Fig. 4.8 confirms the tetra-substitution of L^8 by the 2-hydroxy-3,5-dimethylbenzyl pendant arms.

The arrangement adopted by the backbone of the macrocycle is similar to the stepped conformation given by L^8 -*meso* (Chapter 3, § 3.2.4) although for $L^{12}H_4$ the pyridine rings are rearranged such that the pyridyl nitrogen atoms face outward away from the macrocyclic cavity (Fig. 4.9)

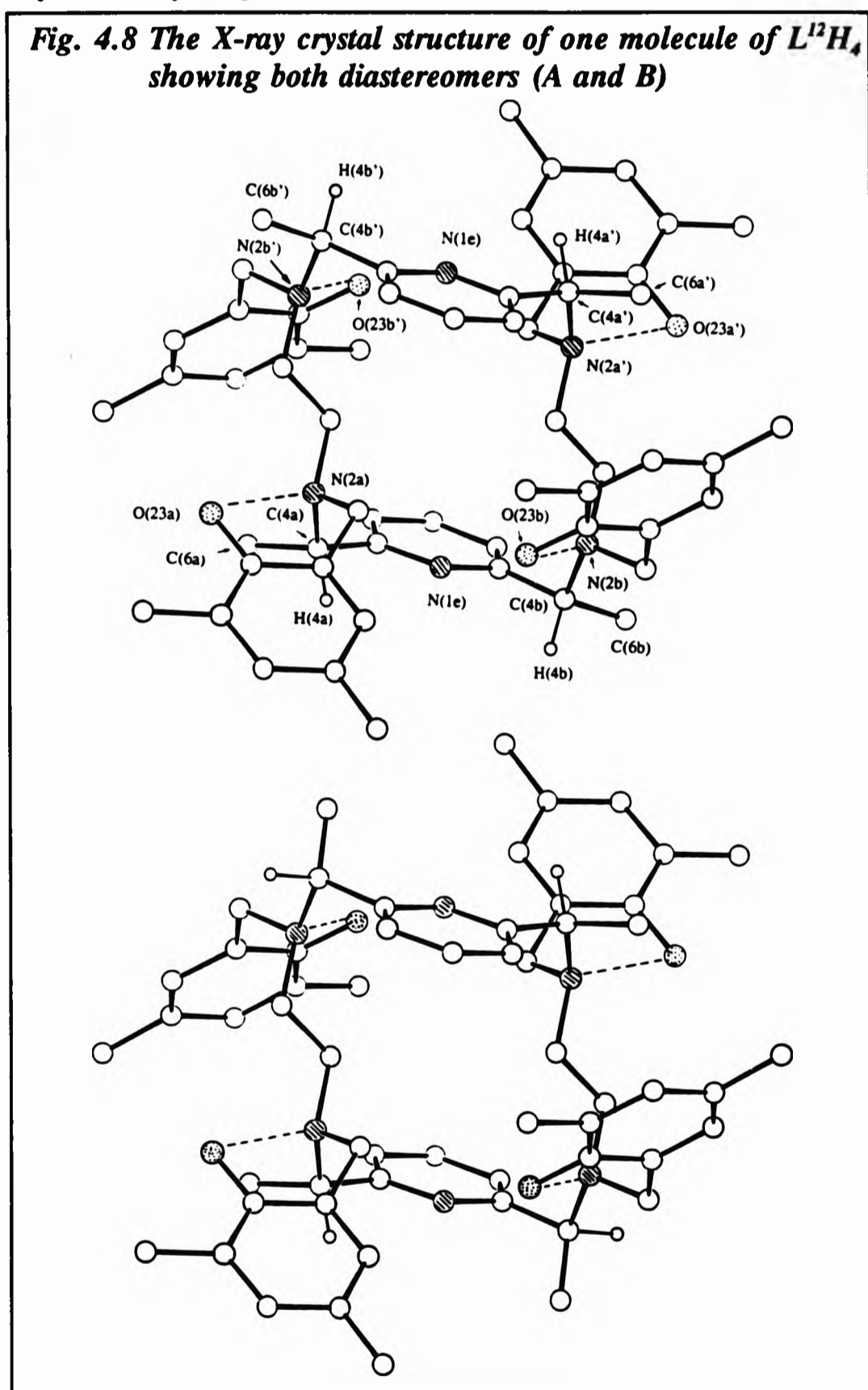
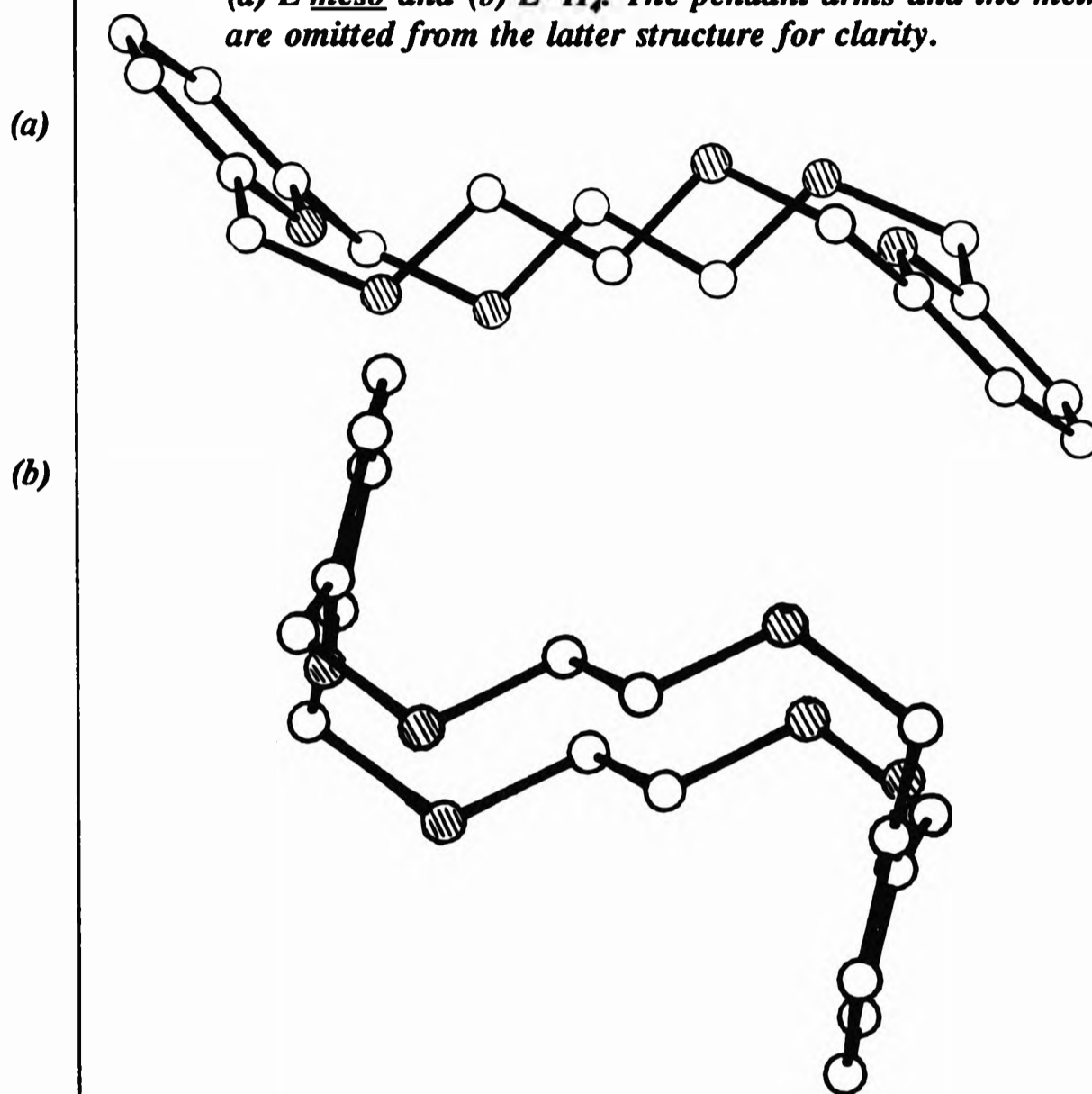


Fig. 4.9 The arrangement of the pyridyl nitrogen atoms in the structures of (a) L^{meso} and (b) $L^{12}H_4$. The pendant arms and the methyl groups are omitted from the latter structure for clarity.



The crystal structure shows the presence of two independent, exactly centrosymmetric, ligand molecules in the crystal and confirms the presence of two different diastereoisomers. These may be deduced from the *ca.* 60:40 disorder of the terminal methyl group C(6a), and the hydrogen atom, H(4a), attached to the chiral carbon atom C(4a) which are explained by the presence at one site of the crystal of isomers with configurations *RSRS* and *SSRR* at the four chiral carbon atoms C(4b'), C(4a'), C(4a) and C(4b) as shown in Fig. 4.8a and Fig 4.8b respectively for the first independent molecule. The second independent molecule is virtually identical to the first apart from the disorder being closer to 50:50 between the two superimposed diastereoisomers.

The two isomers obtained are both *meso*, *RSRS* (Fig. 4.8a) and *SSRR* (Fig. 4.8b) with regards to the asymmetric carbon atoms and also the tertiary nitrogen atoms where both isomers have the same configuration, *RRSS* at the nitrogen centres N(2b'), N(2a'), N(2a) and N(2b) respectively. An important feature in the structure of L¹²H₄ is the intramolecular hydrogen bonding taking place between the hydroxyl hydrogen atom and the lone pair of electrons on the tertiary nitrogen atom, shown in Fig. 4.8 by dashed lines. The position of the hydrogen atoms was not located but the distances O - N(a or b) (2.63 - 2.69 Å) are evident to support this claim. Table 4.7 shows the N...(H)O distances.

Table 4.7 The N...OH distances indicating intramolecular hydrogen bonding in L¹²H₄

Molecule A			Molecule B		
O	N	(Å)	O	N	(Å)
23a	2a	2.65	23c	2c	2.67
23b	2b	2.68	23d	2d	2.63

4.4 Yttrium, Lanthanide and Transition Metal Complexes of L¹¹H₄

Metal complexes of L¹¹H₄ were isolated as pure, well defined crystals when a methanolic solution of the metal salt was added to a refluxing suspension of the ligand in methanol. An excess of the metal salt was necessary for the metal-ligand interaction to occur where yttrium and the lanthanide metals were concerned and stoichiometrically 1:1½ (ligand : metal) was used. Excess metal salt was not essential for the transition metal complexation as an immediate interaction took place and a colour change was observed.

A 1:1, metal-to-ligand, chelation took place as opposed to the polymeric arrangement that can be adopted if the ligand was to chelate to the metal *via* the phenolic groups alone, *i.e.* no involvement of the hexaaza co-ordination from the macrocycle. The polymeric arrangement would not be expected for yttrium and the lanthanide metals

as this would not satisfy the co-ordination of the metal.

In addition to the hexadenticity of the macrocycle, $L^{11}H_4$ also has four deprotonation sites (hence decadentate), therefore maximum co-ordination of yttrium and the lanthanide metals can be achieved through the co-ordination of $L^{11}H_4$ alone. This would be advantageous in that counter-ions or small ligating molecules would not be necessary to counter-balance the charge on the metal and the complex would be neutral and highly stabilised. The high stability in itself would be advantageous for the compounds to be considered as contrast agents for MRI and also as therapeutic agents for *in vivo* location, identification and treatment of tumour cells where the metal chelate must remain intact. Complexes were isolated of yttrium(III), lanthanum(III), neodymium(III), europium(III), gadolinium(III) and dysprosium(III) as well as iron(II) and cadmium(II).

The yttrium and the lanthanide metal complexes possessed the characteristic colour for each metal (Table 4.8). The colourless crystals of the gadolinium(III) complex lost solvent on isolation resulting in a pale yellow-orange colour. The most unusual colour was that of the iron(II) complex which adopted a grey-blue colouration.

A distinguishing feature between the complexes of yttrium, the lanthanide and the transition metals was their solubilities. Whereas the transition metal complexes were readily soluble in methanol, dichloromethane and acetonitrile, the yttrium and the lanthanide metal complexes were sparingly soluble in these solvents and completely soluble when warmed. Solution studies for the latter metal complexes were carried out in DMSO.

4.4.1 Infrared Spectrophotometry and Magnetic Moments

As described above, the charge on the metal was expected to be counter-balanced by the charge on the ligand, $L^{11}H_4$. The IR spectra of yttrium and the lanthanide metal complexes exhibited a strong band at 1384 cm^{-1} characteristic of the un-co-ordinated nitrate ion. Presence of mono- or bi-dentate nitrate ion co-ordination was masked by

ligand vibrations. As a result of metal complexation the intramolecular hydrogen bonding which was observed in the IR spectrum of the ligand was no longer depicted in the spectra of the complexes. A prominent broad band in all the spectra at around 3400 cm^{-1} is assigned to lattice water and/ or methanol. Elemental analyses indicated for the presence of 1 - 2 nitrate ions, 0 - 3 methanol and 0 - 4 water molecules. This aroused suspicions as to whether the hydroxyl groups of $L^{II}H_4$ were at all co-ordinating to the metal and if they were co-ordinating, were they deprotonated or merely bonding through the lone pair of electrons of the oxygen atoms?

For the transition metal complexes, where hydrated metal perchlorate salts were employed, a sharp split perchlorate band at 1089 and 1116 cm^{-1} accompanied by two smaller bands at 949 and 866 cm^{-1} represented the ionic perchlorate ion.

The visible spectrum of the grey-blue iron(II) complex, which was deep blue in methanol, showed one band at 590 nm indicative of octahedral splitting. This suggested that the metal is hexa-co-ordinated from the six nitrogen atoms of the macrocycle. Elemental analyses prompted the presence of two perchlorate counterions both of which are not co-ordinated to the metal as predicted by the IR spectrum. UV-VIS spectra of the lanthanide complexes will be discussed further in section 4.4.5.

Table 4.8 *Magnetic moments of the transition, yttrium and lanthanide complexes of $L^{II}H_4$*

COMPLEX	μ_B (BM)*	COLOUR
$[\text{Fe}(L^{II}H_4)](\text{ClO}_4)_2(\text{MeOH})$	4.9	grey-blue
$[\text{Cd}(L^{II}H_4)](\text{ClO}_4)_2 \cdot 4\text{H}_2\text{O}$	-	white
$[\text{Y}(L^{II}H_2)\text{NO}_3]\text{H}_2\text{O}$	-	white
$[\text{La}(L^{II}H_3)\text{NO}_3] \cdot \text{NO}_3 \cdot 3\frac{1}{2}\text{H}_2\text{O}$	-	white
$[\text{Nd}(L^{II}H_3)\text{NO}_3] \cdot \text{NO}_3 \cdot 4\frac{1}{2}\text{H}_2\text{O} \cdot 2\text{MeOH}$	3.9	lilac
$[\text{Eu}(L^{II}H_3)\text{NO}_3] \cdot \text{NO}_3 \cdot 3\text{MeOH}$	3.6	red-brown
$[\text{Gd}(L^{II}H_3)\text{NO}_3] \cdot \text{NO}_3 \cdot 3\text{H}_2\text{O}$	7.5	white
$[\text{Dy}(L^{II}H_2)\text{NO}_3] \cdot 2\text{H}_2\text{O}$	10.2	white

*at 303 K

A magnetic moment of 4.9 BM at 303 K for this compound is a drop from the expected spin-only value of 5.9 BM for iron(III). This infers that reduction has taken place from $\text{Fe}^{3+}(\text{d}^5) \rightarrow \text{Fe}^{2+}(\text{d}^6)$ and still supports a high spin octahedral environment. Further, this suggests that the hydroxyl groups are unlikely to be co-ordinating to the metal as 8 - 10 co-ordinate iron, although has been isolated, is in fact quite rare, and that iron in the oxidation state +2 has a marked preference for N-donor as opposed to O-donor atoms. The reverse is preferred by iron(III). Analogous complexes of nitrogen donor ligands with iron(II) are more stable than those of iron(III).^[26]

Although suitable crystals of this compound could not be isolated so as to solve the structure without any ambiguity, the metal adopts a six co-ordinate geometry, the six co-ordination sites being taken from the six nitrogen donor atoms from the macrocycle. The overall formula is written as $[\text{Fe}(\text{L}^{\text{H}})](\text{ClO}_4)_2 \cdot \text{MeOH}$.

The magnetic moments (Table 4.8) of the yttrium and the lanthanide metal complexes were as expected for the +3 oxidation state of the metals. From the elemental analyses it was predicted that, with the exception of the yttrium(III) and dysprosium(III), all the complexes consisted of two nitrate ligands, one, as shown by the IR spectra, was ionic, the other bidentate. Of the four pendants only one is deprotonated and co-ordinating to the metal. The yttrium(III) and dysprosium(III) complexes contain one nitrate ligand which implies that two of the benzylic pendant arms are deprotonated and co-ordinating. It cannot be predicted at this stage whether the remaining three or two pendant arms respectively are co-ordinating or rotating freely.

4.4.2 Mass Spectrometry

The base peak for the metal complexes in the LSIM spectra was consistently $[ML^{11}H_n]^+$ (where $n = 4,6$). With the exception of the yttrium, lanthanum and dysprosium complexes, a band representing the sum of the base peak plus one counter-ion was common. For yttrium and dysprosium complexes this band was not observed, and was also not expected, as it is characteristic to detect one counter-ion less than is actually present in the molecular formula.

The common fragmentation pattern of the complexes (Table 4.9) implies that metals are co-ordinated by the six nitrogen donor atoms of the macrocycle and that only one (Cd^{2+} , La^{3+} , Nd^{3+} , Eu^{3+} and Gd^{3+}) or two (Y^{3+} and Dy^{3+}) of the phenolic groups are covalently bonding to the metal per complex. On loss of the counter-ions the complex begins to decompose by the cleavage of a complete pendant arm (2-hydroxy-3,5-dimethylbenzyl), the consecutive loss of all four pendants being typical, leaving the metal co-ordinated to the macrocycle (Table 4.9). In all cases the correct isotopic patterns were present.

For the iron(II) complex two such similar patterns could be postulated (Fig. 4.10) and are by no means the only possible routes to the fragmentation of these compounds. Fig. 4.10 shows that one of these patterns is as described for the complexes of yttrium and the lanthanide metals. The other pathway postulates the loss of the metal prior to the loss of the pendant arms. The relative abundances for the bands representing the latter pattern are relatively low (<6%) so the former pattern is more favourable.

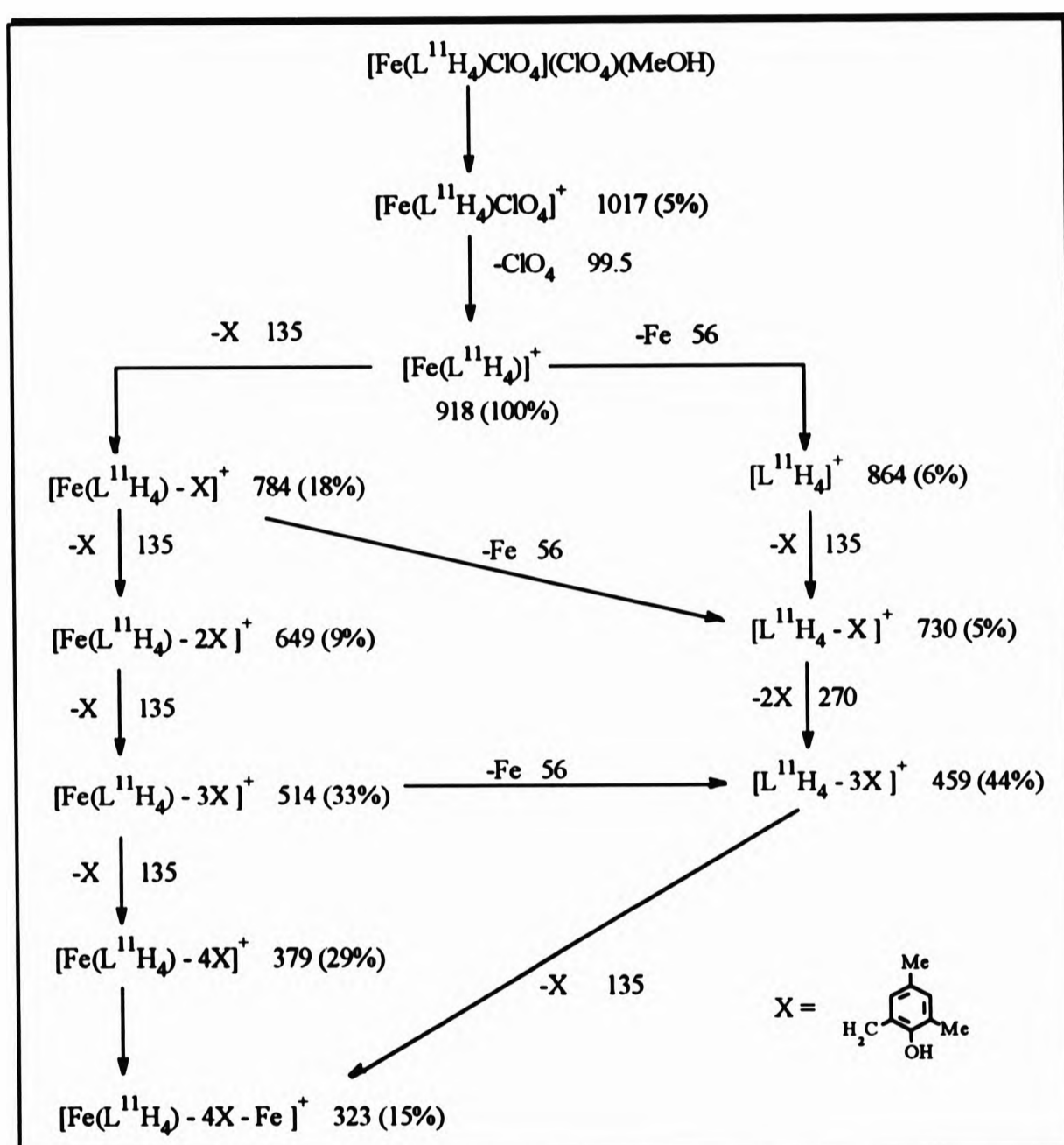


Fig. 4.10 The Two Major Fragmentation Pathways of $[\text{Fe}(\text{L}^{11}\text{H}_4)\text{ClO}_4]^+$

Table 4.9 The common fragmentation pathway of the transition, yttrium and the lanthanide metal complexes of $L^{II}H_4$

The most abundant isotope is quoted

COMPLEX	m/z (% relative abundance)						
	[M - Q] ⁺	[M - 2Q] ⁺	[M - 2Q - X] ⁺	[M - 2Q - 2X] ⁺	[M - 2Q - 3X] ⁺	[M - 2Q - 4X] ⁺	
*[Fe(L ^{II} H ₄)] ²⁺	1017 (5)	918 (100)	784 (18)	649 (9)	514 (33)	379 (29)	
[Cd(L ^{II} H ₄)] ²⁺	-	975 (67)	840 (19)	705 (6)	570 (14)	435 (19)	
[Y(L ^{II} H ₂)] ⁺	-	950 (100)	814 (50)	679 (18)	545 (24)	409 (14)	
[La(L ^{II} H ₃)NO ₃] ⁺	-	1000 (12)	865 (8)	729 (4)	595 (13)	460 (9)	
[Nd(L ^{II} H ₃)NO ₃] ⁺	1067 (18)	1005 (61)	869 (49)	735 (13)	600 (27)	465 (23)	
[Eu(L ^{II} H ₃)NO ₃] ⁺	1078 (21)	1014 (100)	878 (55)	744 (13)	608 (24)	474 (47)	
[Gd(L ^{II} H ₃)NO ₃] ⁺	1082 (13)	1019 (100)	885 (67)	749 (20)	614 (30)	478 (34)	
[Dy(L ^{II} H ₃)] ⁺	-	1023 (100)	888 (30)	752 (34)	618 (17)	484 (40)	

*See also Fig. 4.10

Q = ClO₄, NO₃; X = 2-hydroxy-3,5-dimethylbenzyl

4.4.3 NMR Spectroscopy

^1H NMR spectra were recorded of the complexes $[\text{Y}(\text{L}^{11}\text{H}_2)]^+$, $[\text{La}(\text{L}^{11}\text{H}_3)\text{NO}_3]^+$, $[\text{Nd}(\text{L}^{11}\text{H}_3)\text{NO}_3]^+$, and $[\text{Cd}(\text{L}^{11}\text{H}_4)]^{2+}$ in d_6 -DMSO and at 250 MHz (Fig. 4.12). The spectra were indeed informative of the structure of individual complexes. Those of $[\text{La}(\text{L}^{11}\text{H}_3)\text{NO}_3]^+$ and $[\text{Nd}(\text{L}^{11}\text{H}_3)\text{NO}_3]^+$ had similar splitting patterns and chemical shifts as the ligand (§ 4.3.3.1) irrespective of neodymium being a paramagnetic metal and a NMR shift reagent. Table 4.10 summarises and compares these shifts, the chemical shifts for L^{11}H_4 are reproduced in the Table for comparison.

The major difference in the spectra of the ligand and of its lanthanum(III) and neodymium(III) complexes was the change in shape of the OH band from being broad in the ligand to a sharp band in the complexes, with no dramatic changes in the chemical shift. The change in shape was caused by rapid exchange of the hydroxyl protons.

The similarity in the splitting patterns of the NMR spectra of $[\text{La}(\text{L}^{11}\text{H}_3)\text{NO}_3]^+$ and $[\text{Nd}(\text{L}^{11}\text{H}_3)\text{NO}_3]^+$ and that of the free ligand indicates that the complexes are also symmetry bound in solution. With the knowledge that the co-ordinated nitrate group is bidentate, and that one pendant arm is deprotonated, the only way by which that structure of the La^{3+} and Nd^{3+} complexes can attain a four-fold symmetry is by all four pendant arms co-ordinating to the metal, three of these arms not being deprotonated. Assuming that the macrocycle adopts the butterfly arrangement with lanthanide metals, as discussed in Chapters 2 and 3, then, to retain the symmetry, the pendant arms would have to co-ordinate to the metal from the same hemisphere, the one not containing the co-ordinating nitrate group (Fig. 4.11).

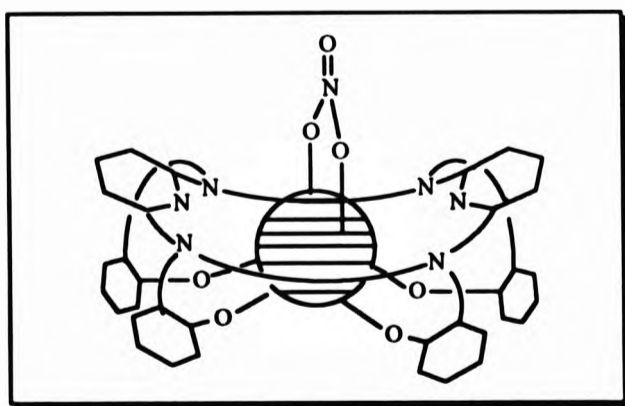


Fig. 4.11 The co-ordination of the phenolic pendant arms and the bidentate nitrate group from opposite hemispheres. (nitrogen co-ordination omitted for clarity)

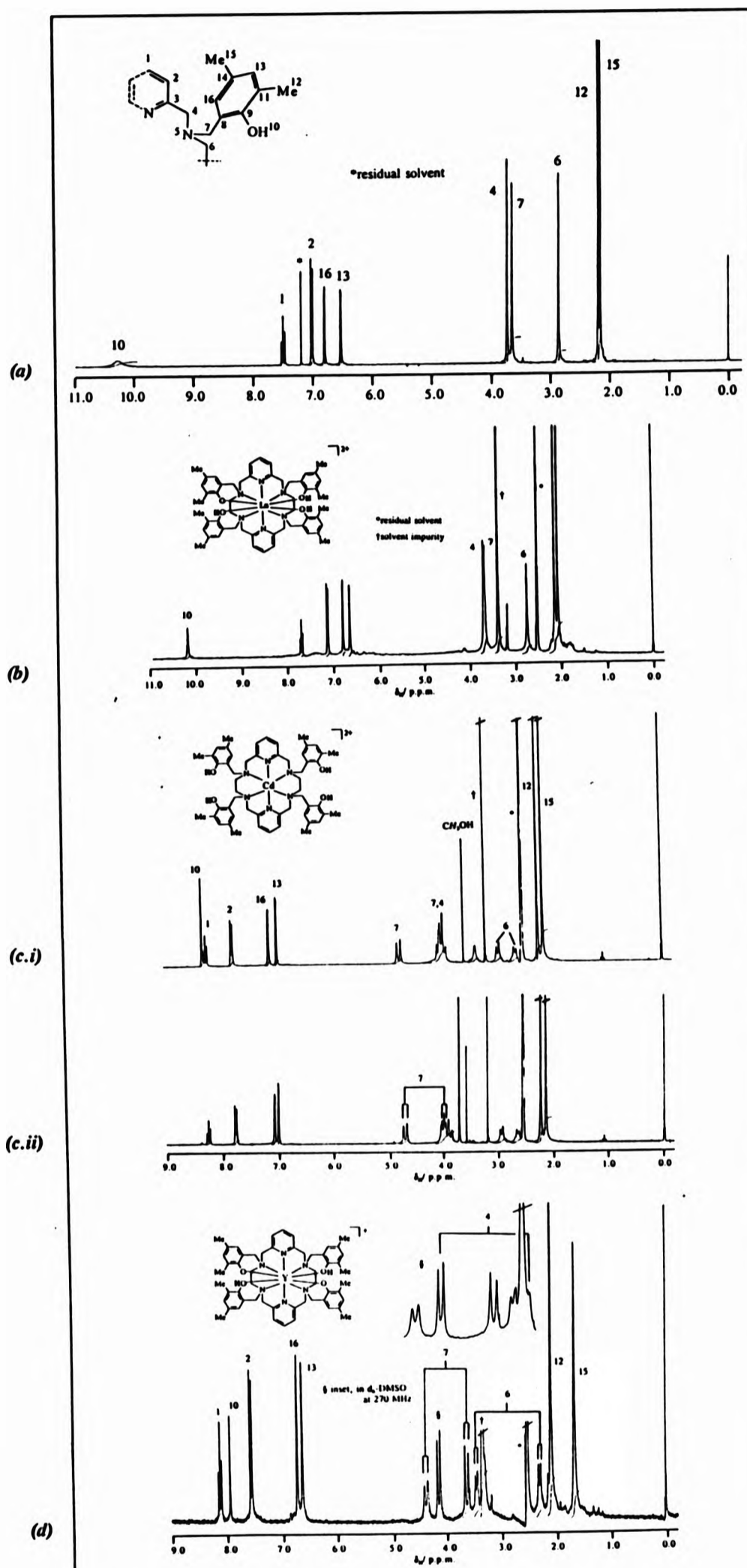
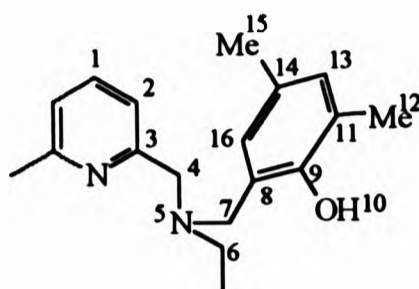


Fig. 4.12 ^1H NMR spectra of (a) $L^1\text{H}$, in CDCl_3 , (b) $[\text{Ln}(\text{L}^1\text{H})\text{NO}_3]^{2+}$ (where $\text{Ln} = \text{La}, \text{Nd}$), in d_5 -DMSO (c.i) $[\text{Cd}(\text{L}^1\text{H})]^{2+}$ in d_5 -DMSO (c.ii) $[\text{Cd}(\text{L}^1\text{H})]^{2+}$ in d_5 -DMSO/ D_2O and (d) $[\text{Y}(\text{L}^1\text{H})\text{NO}_3]^+$ in d_5 -DMSO and at 250 MHz (relative to SiMe_4 as internal standard at 0.0 p.p.m.). Diagrams indicate the co-ordination adopted by the pendant arms. Co-ordinated nitrate groups are omitted for clarity

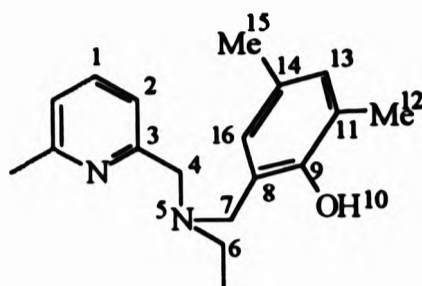
Table 4.10 The ^1H NMR chemical shifts of $\text{L}^{\text{II}}\text{H}_4$ and its La^{3+} , Nd^{3+} , Y^{3+} and Cd^{2+} complexes (relative to SiMe_4 as internal standard at 0.0 p.p.m.)



ASSIGNMENT	δ_{H}				
	$^{\text{a}}\text{L}^{\text{II}}\text{H}_4$	$^{\text{b}}[\text{La}(\text{L}^{\text{II}}\text{H}_3)\text{NO}_3]^+$	$^{\text{b}}[\text{Nd}(\text{L}^{\text{II}}\text{H}_3)\text{NO}_3]^+$	$^{\text{b}}[\text{Y}(\text{L}^{\text{II}}\text{H}_3)\text{NO}_3]^+$	$^{\text{b}}[\text{Cd}(\text{L}^{\text{II}}\text{H}_4)]^{2+}$
1	7.55 (t)	7.71 (t)	7.72 (t)	8.12 (t)	8.28 (t)
2	7.06 (d)	7.13 (d)	7.13 (d)	7.55 (d)	7.69 (t)
3	-	-	-	-	-
4	3.74 (s)	3.68 (s)	3.67 (s)	4.12, 3.3 (d of d)	centred at 3.95 (d of d)
6	2.87 (s)	2.73 (s)	2.72 (s)	3.44, 2.28 (d of d)	2.93, 2.63 (d of d)
7	3.66 (s)	3.65 (s)	3.64 (s)	4.36, 3.61	4.69, 3.96 (d of d)
10	10.38 (br)	10.21 (sh)	10.19 (sh)	8.09 (sh)	8.34 (sh)
11	-	-	-	-	-
12	2.19 (s)	2.12 (s)	2.11 (s)	2.01 (s)	2.22 (s)
13	6.57 (d)	6.64 (d)	6.63 (d)	6.62 (d)	6.97 (d)
15	2.16 (s)	2.05 (s)	2.02 (s)	1.65 (s)	2.12 (s)
16	6.84 (d)	6.79 (d)	6.77 (d)	3.71 (d)	7.11 (d)
$^3J(\text{H}^1, \text{H}^2) / \text{Hz}$	7.7	7.7	7.6	7.7	7.8
$^2J(\text{H}^{16\text{a}}, \text{H}^{16\text{b}}) / \text{Hz}$	-	-	-	c	1.5
$^2J(\text{H}^{4\text{a}}, \text{H}^{4\text{b}}) / \text{Hz}$	-	-	-	13.3	13.9
$^2J(\text{H}^{7\text{a}}, \text{H}^{7\text{b}}) / \text{Hz}$	-	-	-	15.8	16.9
$^2J(\text{H}^{6\text{a}}, \text{H}^{6\text{b}}) / \text{Hz}$	-	-	-	10.2	11.6

^ain CDCl_3 , ^bin d_6 -DMSO, ^c cannot be determined.

Table 4.11 The ^{13}C NMR chemical shifts of $\text{L}^{\text{II}}\text{H}_4$ and its La^{3+} , Y^{3+} and Cd^{2+} complexes^c (relative to SiMe_4 as internal standard at 0.0 p.p.m.)



ASSIGNMENT	δ_{C}			
	^a $\text{L}^{\text{II}}\text{H}_4$	^b $[\text{La}(\text{L}^{\text{II}}\text{H}_3)\text{NO}_3]^+$	^b $[\text{Y}(\text{L}^{\text{II}}\text{H}_2)\text{NO}_3]^+$	^b $[\text{Cd}(\text{L}^{\text{II}}\text{H}_4)]^{2+}$
1	136.91	137.06	139.99	141.68
2	122.13	121.81	121.94	124.12
3	157.01	156.68	156.78	154.11
4	58.18	56.65	56.07	57.19
6	50.85	49.67	49.55	48.63
7	58.67	58.05	56.57	66.23
8	127.58	126.56	155.26	128.15
9	153.28	152.76	150.16	151.90
11	124.73	123.56	124.60	125.18
12	20.41	19.94	19.98	20.07
13	127.04	127.06	129.95	131.00
14	121.04	121.50	120.55	119.43
15	15.74	15.56	15.82	16.66
16	130.66	130.01	130.98	132.01

^ain CDCl_3 , ^bin d_6 -DMSO, ^c ^{13}C NMR spectrum of Nd^{3+} was not recorded

In contrast to the spectra of $[\text{La}(\text{L}^{\text{II}}\text{H}_3)\text{NO}_3]^+$ and $[\text{Nd}(\text{L}^{\text{II}}\text{H}_3)\text{NO}_3]^+$ the ^1H NMR spectrum of $[\text{Y}(\text{L}^{\text{II}}\text{H}_2)\text{NO}_3]^+$ in d_6 -DMSO and at 250 MHz (Fig. 4.12d) was remarkably more complicated. A four-fold symmetry about the structure was depicted by the ^{13}C NMR spectrum in that fourteen bands were observed (Table 4.11) suggesting that all the pendant arms are equivalent. Although the ^{13}C NMR

spectrum was assigned with ease, a ^{13}C - ^1H -COSY spectrum, collected over 60 h, was not adequate to reveal the ^{13}C - ^1H coupling of the region 4.5-2.0 p.p.m. of the ^1H NMR spectrum. Assignment of the ^1H NMR spectrum was based on the collection of a ^1H -COSY spectrum (Fig. 4.13) and by comparison of coupling constants and also the spectra of $[\text{L}^7\text{H}_4]\text{Br}_4$ and L^9 .

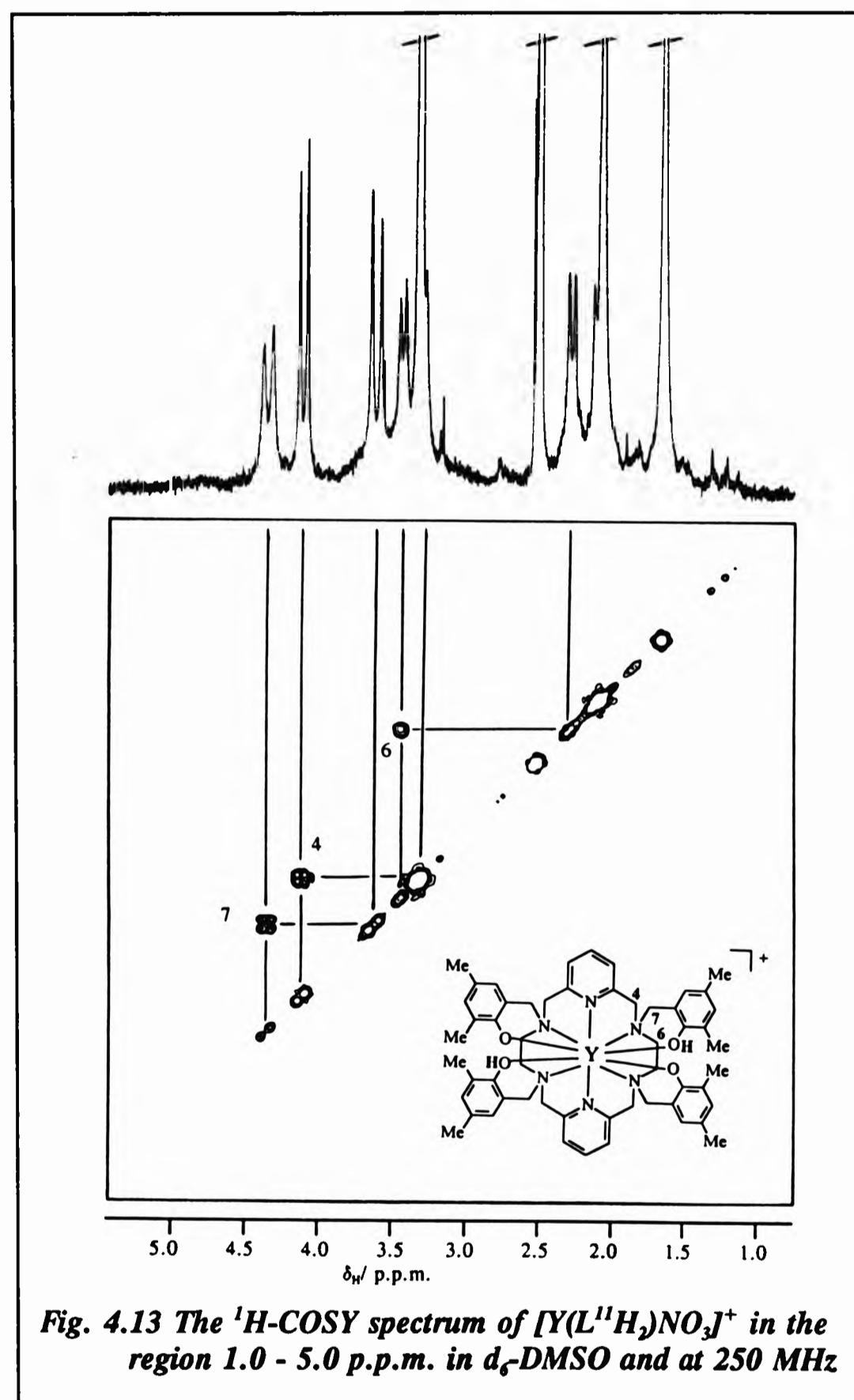


Fig. 4.13 The ^1H -COSY spectrum of $[\text{Y}(\text{L}^{11}\text{H})\text{NO}_3]^+$ in the region 1.0 - 5.0 p.p.m. in d_6 -DMSO and at 250 MHz

The OH band was, again, a sharp singlet but had shifted upfield to δ_{H} 7.93, the intramolecular hydrogen bonding no longer occurring. The triplet (H^1) and the doublet (H^2) bands have shifted downfield to δ_{H} 8.12 and 7.55 from their counterparts in the L^{11}H_4 , $[\text{La}(\text{L}^{11}\text{H}_3)\text{NO}_3]^+$ and $[\text{Nd}(\text{L}^{11}\text{H}_3)\text{NO}_3]^+$ spectra.

Whereas in the free ligand and its lanthanum(III) and neodymium(III) complexes the three different methylene groups, CH_2^4 , CH_2^6 and CH_2^7 resonated as singlet bands at *ca.* δ_{H} 3.6, 2.8 and 3.8 respectively, in the yttrium complex these were each portrayed as two pairs of doublet bands (AB splitting). An A_2B_2 system was not shown for H^6 , *i.e.* the two protons on carbon C^6 are equivalent on the NMR timescale. The *doublet* at δ_{H} 4.36 is coupled to the *doublet* at δ_{H} 3.61 and both are assigned to H^7 [$^2J(\text{H}^{7a},\text{H}^{7b}) = 15.8$ Hz]. The *doublet* at δ_{H} 4.12 is coupled to a *doublet* which is obscured by the impurity band in the solvent at δ_{H} 3.3. The band is revealed when the spectrum was ran at 270 MHz and is shown in Fig. 4.12d. The coupling constant is $^2J(\text{H}^{4a},\text{H}^{4b}) = 13.3$ Hz, this value being similar to that obtained for the proton, H^4 , in the spectrum of L^9 . These bands are therefore assigned to H^4 in this spectrum also. Finally, H^6 is depicted by the two coupled *doublets* at δ_{H} 3.44 and 2.28, the coupling constant between the two protons being, $^2J(\text{H}^{6a},\text{H}^{6b}) = 10.2$ Hz.

The ^1H NMR spectrum of $[\text{CdL}^{11}\text{H}_4]^{2+}$ in d_6 -DMSO (Fig. 4.12c) also shows a symmetrical structure. The arrangement adopted by the macrocyclic backbone is expected to follow the distorted octahedral *twist and wrap* around the metal ion with the pendant arms adopting the same positions as the hydrogen atoms on the secondary amines of $[\text{CdL}^9]^{2+}$ (Chapter 2) without co-ordinating, *i.e.* they are rotating freely. The ligand would possess the configuration *SSSS* or *RRRR* at the nitrogen centres.

The OH band also appears as a sharp singlet but has shifted to δ_{H} 8.32 and collapses on D_2O addition. Consistency is retained by the *triplet-doublet* coupling of H^1 and H^2 [$^3J(\text{H}^1,\text{H}^2) = 7.8$ Hz] at δ_{H} 8.28 and 7.69 respectively with *ca.* 5-6 p.p.m.

downfield shift from the respective bands in the free ligand and La^{3+} , Nd^{3+} and Y^{3+} complexes. The benzylic protons resonate as two *doublets* at δ_{H} 7.11 (H^{16}) and 6.97 (H^{13}) with a coupling constant, ${}^2J(\text{H}^{16}, \text{H}^{13}) = 1.5$ Hz. The methyl proton bands appear as two *singlets* at δ_{H} 2.22 (H^{12}) and 2.12 (H^{15}). The methylene protons, as for the spectrum of $[\text{YL}^{11}\text{H}_2]^+$, follow three AB patterns. The two *doublets* at δ_{H} 2.93 and 2.63 are due to H^6 with a coupling constant, ${}^2J(\text{H}^{6a}, \text{H}^{6b}) = 11.6$ Hz. For H^7 , the *doublet* at δ_{H} 4.69 is coupled to the *doublet* which is situated in the multiplet at $\delta_{\text{H}} \sim 3.9$ (see Fig. 4.12c). This *multiplet* integrates for twelve protons, four of which are from H^7 . The remaining eight protons are from H^4 . Better resolution was obtained on D_2O addition to the NMR sample (inset in Fig. 4.12c). The coupling constant for H^7 is ${}^2J(\text{H}^{7a}, \text{H}^{7b}) = 16.9$ Hz and that of H^4 typically being, 13.9 Hz.

As a summary, the complexes of L^{11}H_4 studied can be divided into two main categories:

- (a) the transition metal complexes where the near octahedral *twist and wrap* is maintained by the hexaaza co-ordination and the pendants are freely rotating in solution,
- (b) the yttrium and lanthanide metal complexes where all the pendant arms co-ordinate to the metal thus the structure being symmetrical but either one or two of the phenolic groups are deprotonated.

4.4.4 The X-Ray Crystal Structure of $[\text{Gd}(\text{L}^{11}\text{H}_3)\text{NO}_3]\text{NO}_3 \cdot 3\text{H}_2\text{O}$

The yellow-orange crystals of $[\text{Gd}(\text{L}^{11}\text{H}_3)\text{NO}_3]\text{NO}_3 \cdot 3\text{H}_2\text{O}$ (Fig. 4.14) showed the cationic complex of $[\text{Gd}(\text{L}^{11}\text{H}_3)\text{NO}_3]^+$ in which the ligand adopts the characteristic boat, butterfly or saddle conformation, as described in Chapters 2 and 3 (§ 2.4.1.3, $[\text{GdL}^5(\text{H}_2\text{O})_3]^{3+}$, and 3.4.2.4, $[\text{LaL}^9(\text{NO}_3)_3]$, respectively) and predicted by NMR solution studies, in contrast to the chair conformation observed in the solid state structure of the ligand, L^{12}H_4 (§ 4.3.4).

The gadolinium ion has an irregular nine-co-ordinate geometry with all the nitrogen donor atoms co-ordinating (Gd - N 2.548 - 2.718 Å), also two oxygen atoms of a bidentate nitrate ligand [Gd - O(1N) 2.501(11) and Gd - O(2N) 2.460(11) Å] and the phenolic oxygen atom O(23a) of one pendant arm, which forms a six membered chelate ring and the shortest metal-ligand bond in the structure [Gd - O(23a) 2.138(10) Å]. The remaining three pendants radiate away from the metal showing no sign of co-ordination (Gd...O 5.390 - 5.626 Å). Also present in the unit cell are three severely disordered water molecules and an ionic nitrate ion. The pendant arms are co-ordinating or protruding below the hemisphere containing the nitrate ligand.

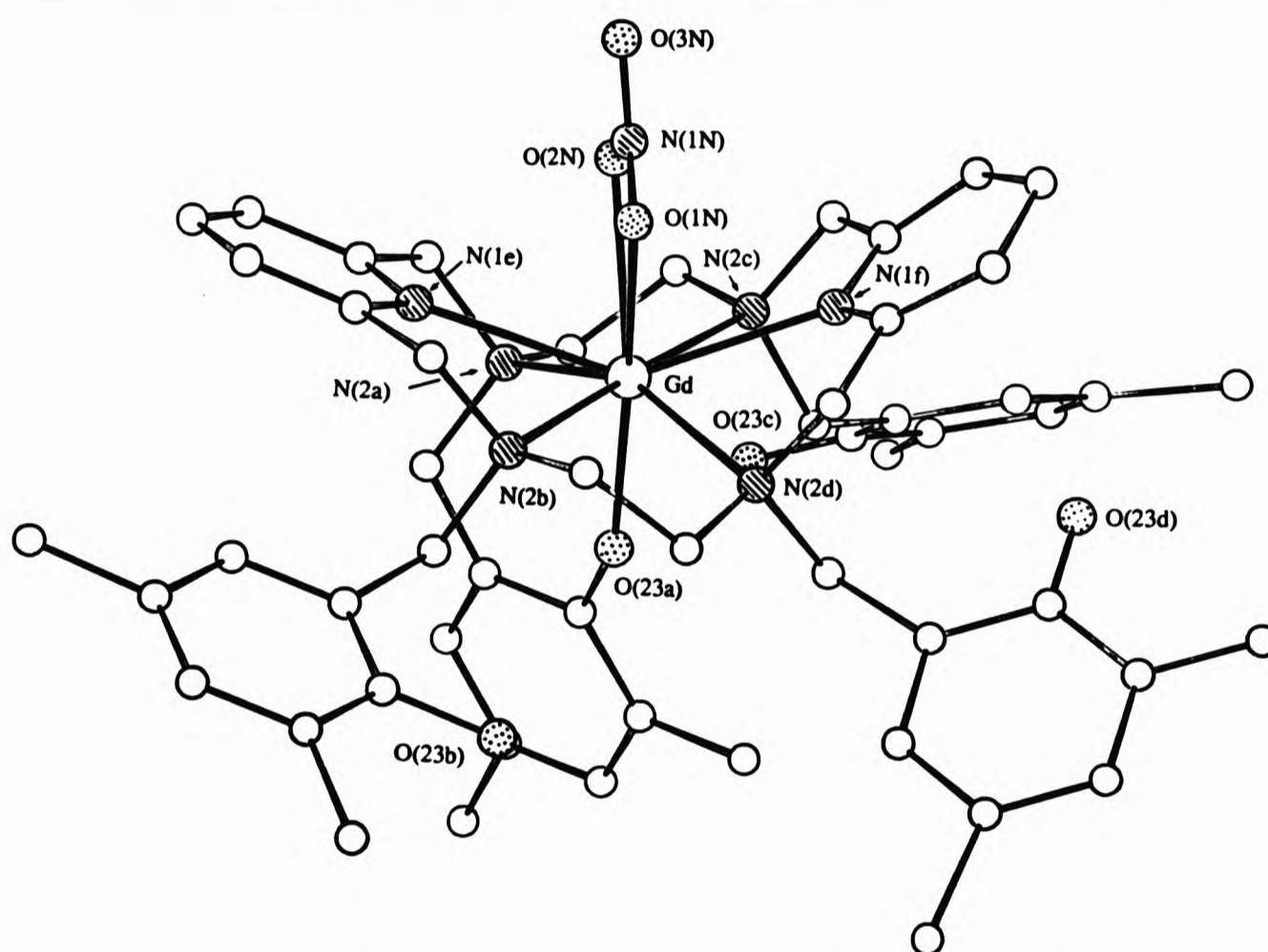


Fig. 4.14 The X-ray crystal structure of $[Gd(L^{11}H_3)NO_3]^+$

The solid state structure does not agree with that predicted using NMR spectroscopy, which suggested that all the pendants should be co-ordinated to the metal ion irrespective of the whether the hydroxyl group is protonated or not. The metal co-ordination adopted, as illustrated by Fig. 4.14, does not prompt steric hinderance,

so there is *room* available for at least two more phenol groups to co-ordinate. Several attempts at diffracting another crystal from the same or another batch proved fruitless.

Macrocycles functionalised with 2-hydroxybenzyl or derivatives of 2-hydroxybenzyl are {22}H₃, {23}H₃ and {24}H₃.

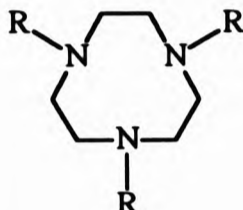
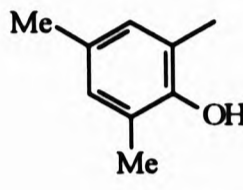
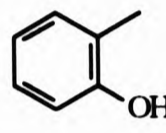
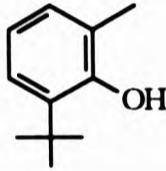
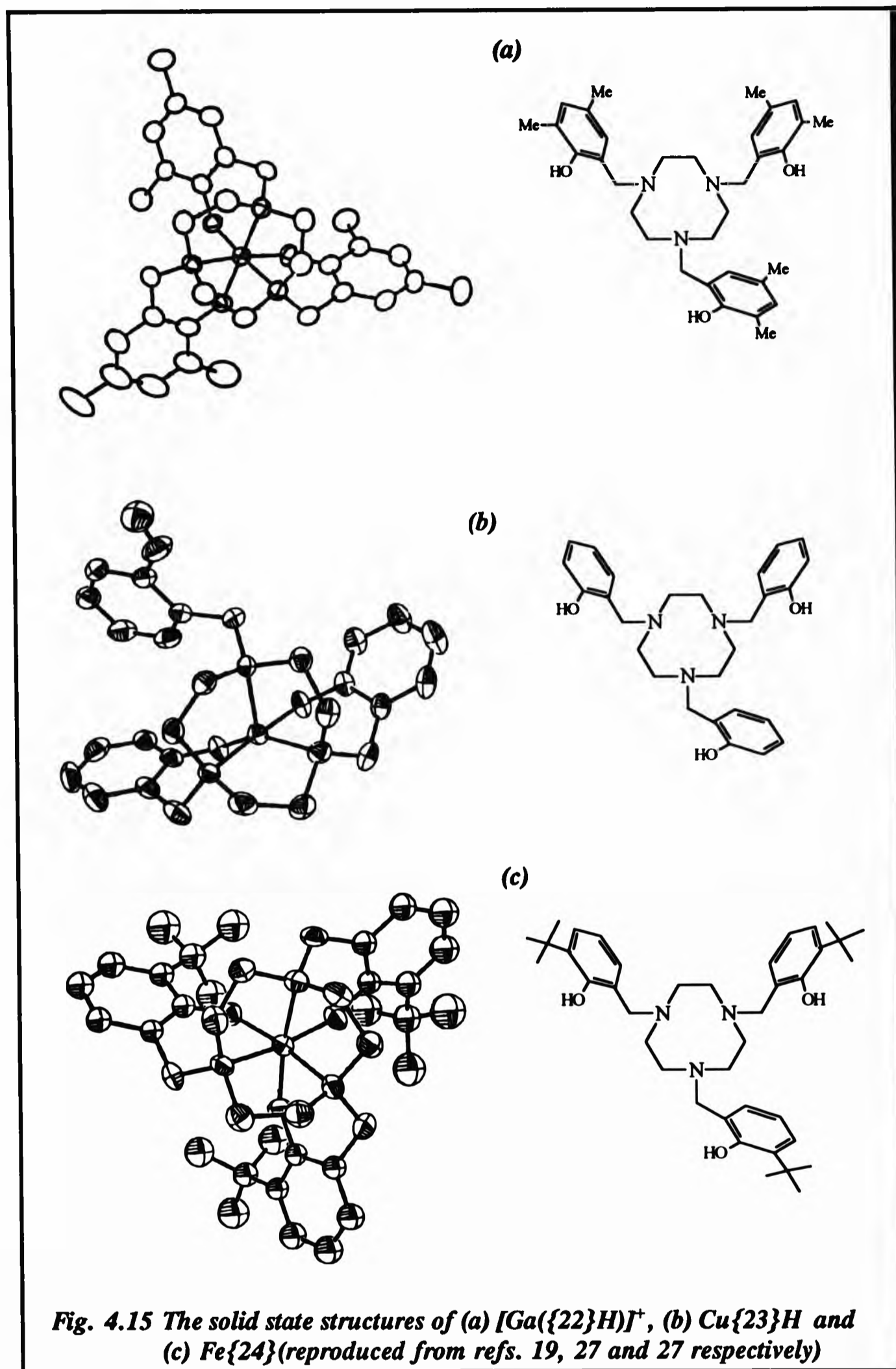
	<u>R</u>		<u>Ref.</u>
		{22}H ₃	19
		{23}H ₃	27
		{24}H ₃	27

Fig. 4.15 shows some crystallographic structures of these ligands with gallium(III), copper(II) and iron(III). Also, as with some of the compounds characterised in this study, [Ga{22}H]ClO₄.MeOH contains one co-ordinated yet protonated phenol group. As with the structure of [Gd(L¹¹H₃)NO₃]⁺, TACN in all the structures shown in Fig. 4.15 adopts a saddle or boat conformation and all the co-ordinating pendants approach the metal from behind the plane of the nitrogen atoms. Cu{23}H forms a neutral complex where one phenolic group is not bound to the metal centre. The cobalt(III) complex of {23}H₃ forms a trinuclear structure, [{23}H₃]₂Co₃²⁺ (Fig. 4.16).

A Co²⁺ ion is in a trigonal prismatic environment of six μ-(alkoxo) bridging oxygen atoms.^[27] The case is similar for [({25}H)₂M₂(μ-OH)]⁺ (where M = Mn, Zn),^[19] shown in Fig. 4.16.



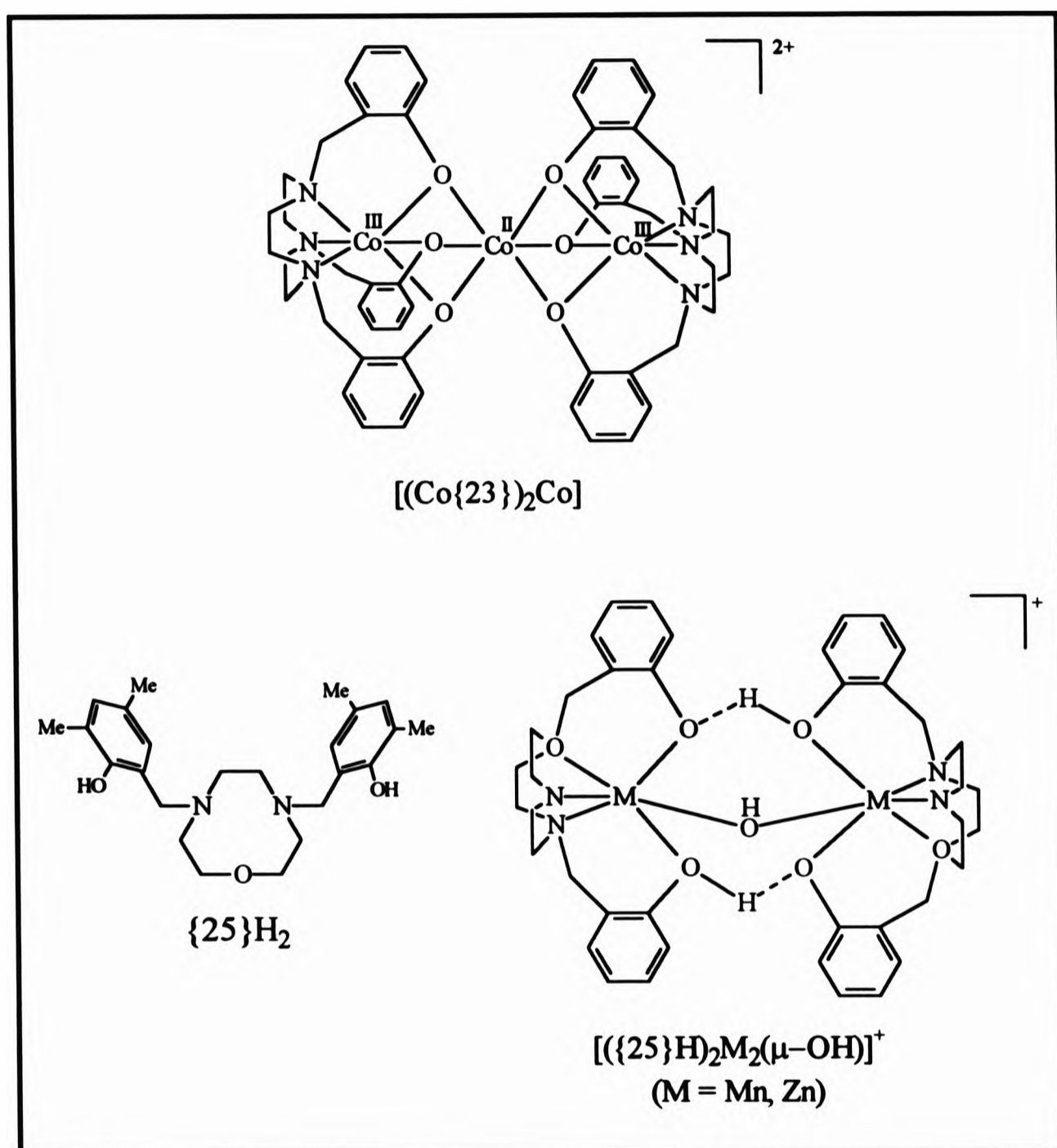


Fig. 4.16 The trinuclear structure of $[(\{23\}_2\text{Co}_3)]^{2+}$ and $[(\{25\}\text{H})_2\text{M}_2(\mu\text{-OH})]^+$ (reproduced from refs. 27 and 19 respectively)

4.4.5. Electronic Spectroscopy

The electronic spectrum of the un-co-ordinated $L^{11}H_4$ in dichloromethane (Fig. 4.17a) exhibits three intense absorption maxima in the region 200 - 300 nm. These bands were in agreement with the UV spectra of phenol and pyridine. The absorption at 234 nm ($\epsilon = 1168 \text{ mol}^{-1} \text{ m}^2$) is due to pyridine whilst the bands at 271 ($\epsilon = 884 \text{ mol}^{-1} \text{ m}^2$) and 289 nm ($\epsilon = 1024 \text{ mol}^{-1} \text{ m}^2$) are from the $\pi \rightarrow \pi^*$ transitions of phenol and phenolate anion respectively. Intramolecular hydrogen bonding in the ligand may cause the splitting observed of the $\pi \rightarrow \pi^*$ transitions. In the spectrum of the hexa-(2-hydroxy-3,5-dimethylbenzyl) ligand, $L^{13}H_6$, the observed bands were broader but the in the same range.

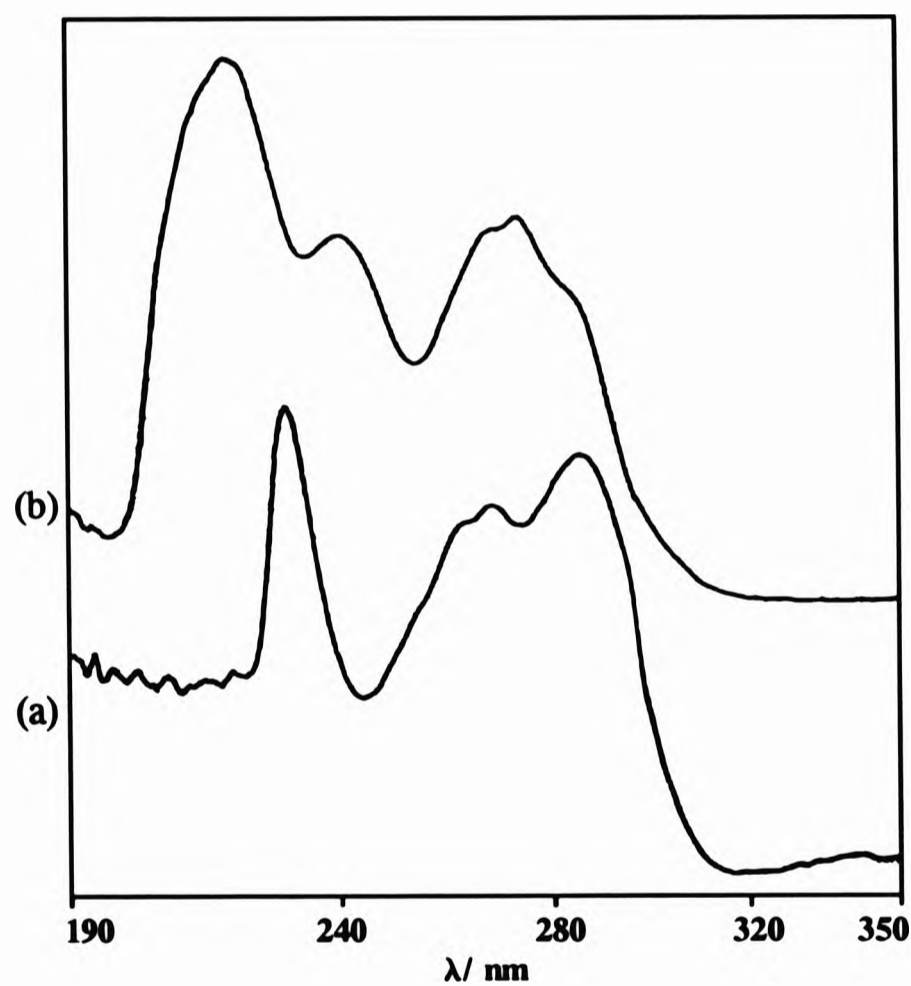


Fig. 4.17 *Electronic spectra of (a) $L^{11}H_4$ in dichloromethane and (b) $[Eu(L^{11}H_4)NO_3]^+$ in methanol at 190 - 350 nm (absorbance is arbitrary)*

The electronic spectrum of $[\text{Fe}(\text{L}^{11}\text{H}_4)]^{2+}$ was discussed previously (§ 4.3.5.1) and it was deduced that the phenol groups do not play any part in metal co-ordination, the band at 590 nm ($\epsilon = 15 \text{ mol}^{-1} \text{ m}^2$) was sufficient evidence for this. Iron-phenolate transitions absorb in the range 450 - 480 nm as given by Fe{23} and Fe{24}.^[27] For $[\text{Eu}(\text{L}^{11}\text{H}_3)\text{NO}_3]^+$ in methanol, bands in the region 200 - 300 nm (Fig. 4.17b) are much broader and have shifted to higher wavelengths (Table 4.12). The absorption bands at 290 ($\epsilon = 1928 \text{ mol}^{-1} \text{ m}^2$), 279 ($\epsilon = 2432 \text{ mol}^{-1} \text{ m}^2$) and 273 nm ($\epsilon = 2340 \text{ mol}^{-1} \text{ m}^2$) are due to $\pi \rightarrow \pi^*$ transitions of the four co-ordinated phenolate pendant arms. A broad band at 443 nm ($\epsilon = 20 \text{ mol}^{-1} \text{ m}^2$) is assigned to the phenolate-to-europium(III) transition. It has been proposed that the absorptivity of this band is roughly additive for successive phenolate binding.^[27]

Table 4.12 *The $\pi \rightarrow \pi^*$ transitions of phenol, phenolate and pyridine for L^{11}H_4 and $[\text{Eu}(\text{L}^{11}\text{H}_3)\text{NO}_3]^+$*

ASSIGNMENT	λ / nm ($\epsilon / \text{mol}^{-1} \text{ m}^2$)	
	^a L^{11}H_4	^b $[\text{Eu}(\text{L}^{11}\text{H}_3)\text{NO}_3]^+$
PHENOL ($\pi \rightarrow \pi^*$)	289 (1024)	290 (1928)
	271 (884)	279 (2432)
	260 (840)	273 (2340)
PYRIDINE ($\pi \rightarrow \pi^*$)	234 (1168)	245 (2360)

^ain dichloromethane, ^bin methanol

The electronic spectrum of $[\text{Nd}(\text{L}^{11}\text{H}_3)\text{NO}_3]^+$, in methanol, is similar to that of $[\text{Eu}(\text{L}^{11}\text{H}_3)\text{NO}_3]^+$ in the region 190 - 350 nm. Any metal ion absorptions in this region were masked by those of the ligand. The UV-VIS region of the metal complexes was recorded in the range 500 - 900 nm and is shown in Fig. 4.18a. The band centres are listed in Table 4.13 together with their extinction coefficients.

Table 4.13 The *f* - *f* transition bands of $[\text{Nd}(\text{L}^{\text{H}})_3\text{NO}_3]^+$
(Assignments are given in Chapter 2)

λ (nm)*	ϵ ($\text{mol}^{-1} \text{m}^2$)
520	2.00
533	1.79
585	3.00
677	1.35
740	2.06
795	2.00
873	1.22

* value indicates band centre

When the spectrum of $[\text{Nd}(\text{L}^{\text{H}})_3\text{NO}_3]^+$ was compared to the spectrum of $[\{\text{NdL}^{\text{S}}(\text{NO}_3)_2\}_2\text{NO}_3(\text{OH})]$ (Chapter 2, Figs. 2.19, 2.20 and Table 2.15) the bands have hardly shifted, the maximum shift being 8 nm, the band being that of the ${}^4\text{I}_{9/2} \rightarrow {}^2\text{G}_{9/2}$ transition at 520 nm. The non-shift is characteristic of lanthanide spectra. The effect of the ligand towards metal *f* - *f* transitions are observed by the changes in the hypersensitive bands. Indeed, when the fine structure of the bands of the spectrum of $[\text{Nd}(\text{L}^{\text{H}})_3\text{NO}_3]^+$ are compared with those of $[\{\text{NdL}^{\text{S}}(\text{NO}_3)_2\}_2\text{NO}_3(\text{OH})]$ they are observed to consist of complicated splitting, in particular the band at 584 nm.

Whereas the similarity of the $[\{\text{NdL}^{\text{S}}(\text{NO}_3)_2\}_2\text{NO}_3(\text{OH})]$ and $\text{Nd}(\text{NO}_3)_3 \cdot 6\text{H}_2\text{O}$ UV-VIS spectra (Chapter 2, Figs. 2.19 and 2.20) suggests that the electrons responsible for the absorptions are not directly involved in the complex formation, the excessive splitting of the major hypersensitive bands at 584 nm (${}^2\text{G}_{9/2}$) and the drop in intensity of the band at 804 nm (${}^4\text{F}_{5/2}$) suggest the contrary. The co-ordination of the four phenolic oxygen (hard base) donor atoms results in greater covalency and it is this ligand effect which is affecting and causing the changes in the hypersensitive bands.

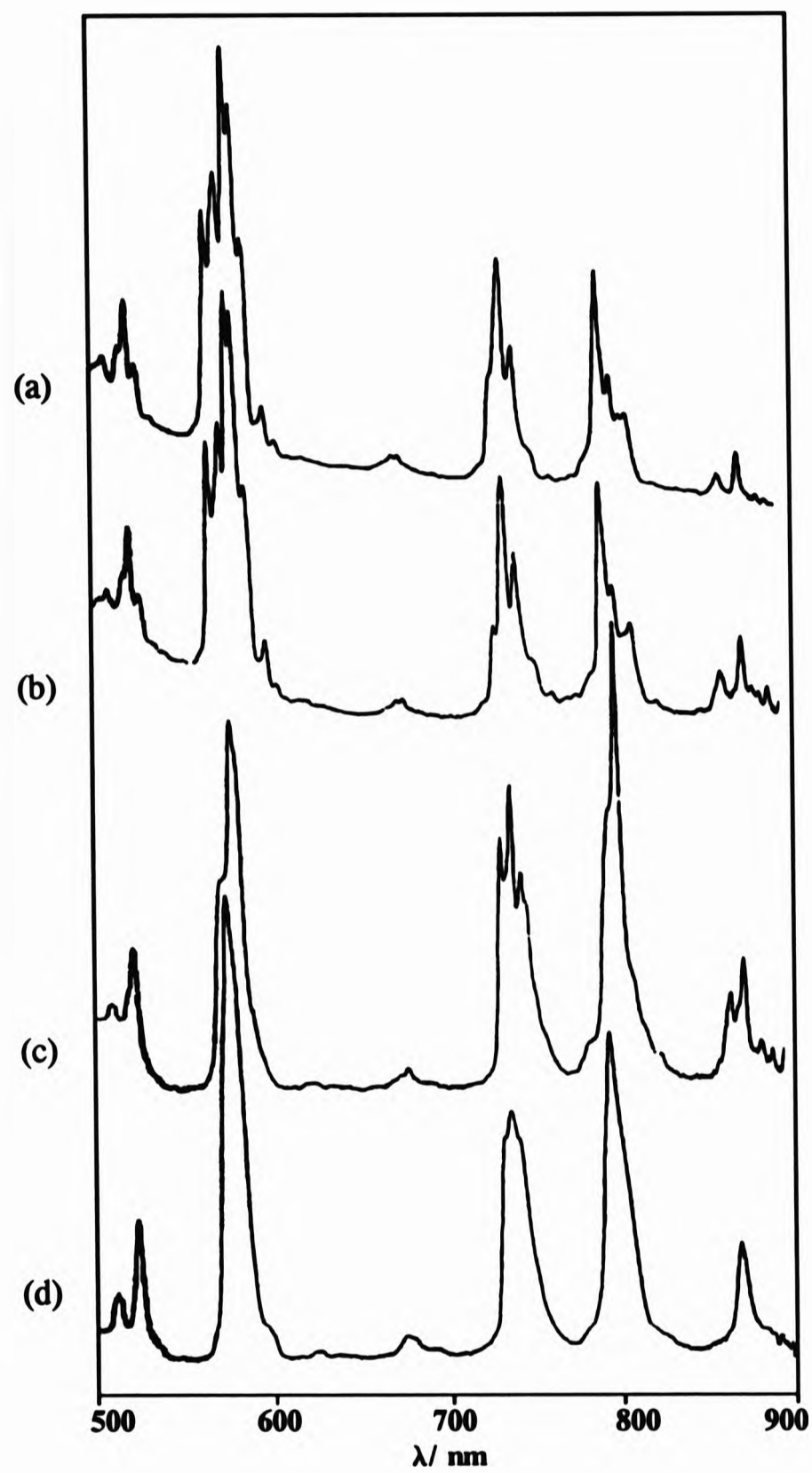


Fig. 4.18 The UV-VIS region of the electronic spectra of (a) $[\text{Nd}(\text{L}^{11}\text{H}_3)\text{NO}_3]^+$, (b) $[\text{Nd}(\text{L}^{11}\text{H}_3)\text{NO}_3]^+/\text{DTPA}$ and (c) $\text{Nd}(\text{NO}_3)_3 \cdot 6\text{H}_2\text{O}/\text{DTPA}$ and (d) $\text{Nd}(\text{NO}_3)_3 \cdot 6\text{H}_2\text{O}$ in methanol at 15 mmol dm^{-3} (absorbance is arbitrary)

The ability of the ligand to hold on to the metal in the presence of DTPAH₅ was investigated using UV-VIS spectroscopy and the overall results are shown in Fig.4.18. The spectra were ran in methanol at pH 7 in the ratios 1:4 ([Nd(L¹¹H₃)NO₃]⁺ : DTPAH₅). The results repeated themselves when spectra were recorded with 1:1 ratios. When this challenge was carried out against the imine, [{NdL⁵(NO₃)₂}]₂NO₃(OH) (Chapter 2) it was noted that the spectrum of [{NdL⁵(NO₃)₂}]₂NO₃(OH)/ DTPA was identical to that of Nd(NO₃)₃.6H₂O /DTPA indicating that [NdDTPAH₂] was being formed in both cases and that the metal was being scavenged from the L⁵ ligand. On challenging [Nd(L¹¹H₃)NO₃]⁺ with DTPAH₅ under the same conditions the spectrum of the mixture containing [Nd(L¹¹H₃)NO₃]⁺/ DTPAH₅ did not undergo any changes from that of the spectrum of neat [Nd(L¹¹H₃)NO₃]⁺ (Fig. 4.18a and Fig. 4.18b). This leads to the conclusion that [Nd(L¹¹H₃)NO₃]⁺ can withstand the challenge from DTPAH₅ which may suggest that neodymium forms a much more stable complex with L¹¹H₄ than with DTPAH₅. The other possibility is that overcrowding of the four co-ordinating pendant arms and the co-ordination of the nitrate ligand from the opposite hemisphere are preventing DTPAH₅ from approaching the metal.

This present work is the first where macrocycles consisting of phenolic pendant arms incorporate lanthanide metals and the relatively high stability of these complexes has been shown, qualitatively, by UV-VIS studies. Some of the most stable complexes of transition metals have been reported with macrocycles functionalised with hydroxybenzyl pendant arms. The stability constant of Fe{22} was determined to be 51.3 compared to 26.3 of Fe(III)EDTAH.^[28] The high stability of the iron(III) complex of {22} is rationalised on the basis of the close fit of the hexa-co-ordinate metal ion in the ligand cavity formed by the pseudo-octahedral arrangement of the ligand nitrogen and phenolic oxygen donor atoms.

4.4.6 Relaxation Rate Measurements of [Gd(L¹¹H₃)NO₃]₂·3H₂O

The relaxation rate of [Gd(L¹¹H₃)NO₃]⁺ was determined at 1 mmol dm⁻³, pH 6, 29°C and at 10 MHz in a mixture of DMSO/ water. A value of $R_1 = 8.2 \text{ dm}^3 \text{ mol}^{-1} \text{ s}^{-1}$ is still higher than that given by [GdDTPA(H₂O)]²⁻ and [GdDOTA(H₂O)]⁻ under the same conditions (Chapter 2, Table 2.14). It is a high value despite the fact that there are no water molecules co-ordinated to the metal ($q = 0$), as shown in the solid state, but there are three lattice water molecules as shown by the X-ray crystal structure (§ 4.4.4). This is an example where outer sphere relaxation may predominate. The gadolinium ion adopts a nine co-ordinate geometry thus there is one vacant co-ordination site for water which may approach from the same hemisphere as the co-ordinating nitrate ligand as the pendants either co-ordinate or rotate freely in solution and overcrowd the opposing hemisphere. But the trend discussed for the imine lanthanide complexes (Chapter 2, § 2.4.1.3) where only one ligand, other than the macrocycle, co-ordinates from the hemisphere containing the nitrate-ion, still applies here. Using a non-co-ordinating counter-ion, such as perchlorate or chloride, would increase the possibility of water co-ordinating to the gadolinium ion.

As expected an increase in T_1 led to a dramatic decrease in the relaxation rate to $R_1 = 2.8 \text{ dm}^3 \text{ mmol}^{-1} \text{ s}^{-1}$ when measured in a mixture of DMSO/ phosphate buffer at pH 6, 37°C and at 10 MHz implying that the phosphate ion has a stronger affinity for the gadolinium ion than the water, nitrate and phenolic ligands.

Taking into account the stability of the complex and the high relaxation rate, [Gd(L¹¹H₃)NO₃]⁺ has potential as a MRI contrast agent, the insolubility being the major drawback.

4.4.7 Fluorescence Experiments of [Eu(L¹¹H₃)NO₃]₂·3MeOH

The fluorescence of chelated lanthanide metals has led to their use as fluorescence probes to gain structural or analytical information.^[29] Some lanthanide ions possess

strongly emissive and long-lived excited states but do not exhibit intense absorption bands. On complexation, light is absorbed by the ligand and electronic energy is transferred to the emitting metal ion. The lanthanide metals that are used for fluorescence experiments are the trivalent ions of samarium, europium, terbium and dysprosium.

The most significant class of ligands is the β -diketones. In aqueous media these have poor fluorescent properties due to the quenching effect of water but are highly applicable as such probes in organic solvents.

The ability of water to quench the fluorescence lifetime of the chelate has been used to determine the number of water molecules co-ordinated to a metal, the results being just as accurate as X-ray crystallography.

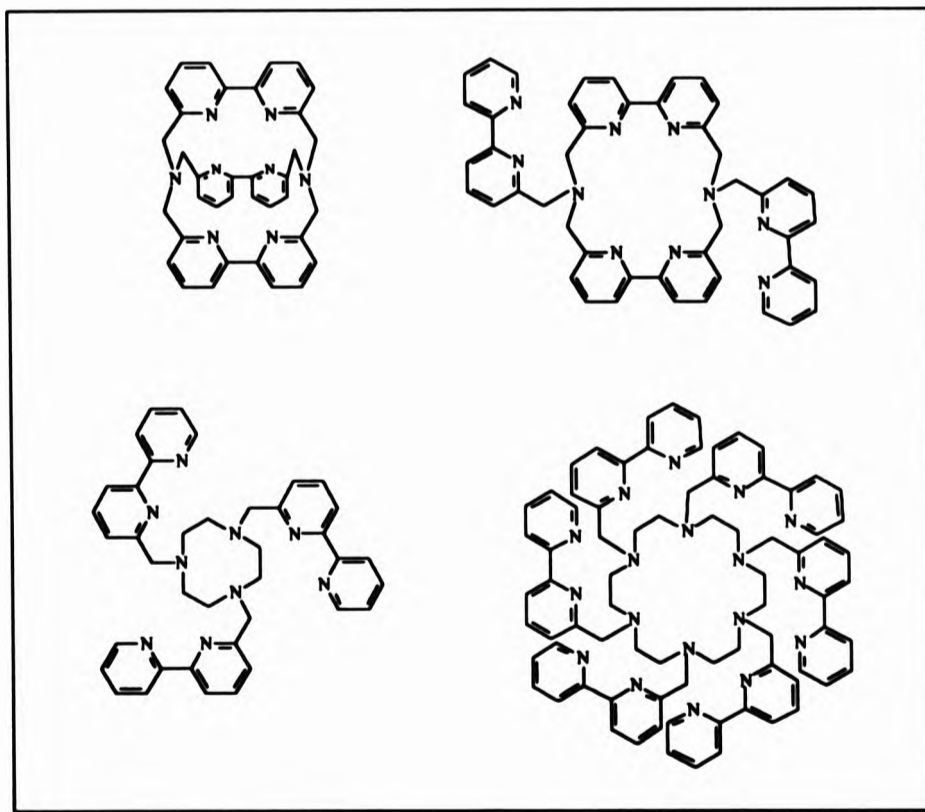
A solution of $[\text{Eu}(\text{L}^{11}\text{H}_3)\text{NO}_3]^+$ in methanol did not show any fluorescent properties when excited at 230 nm. A band at 460 nm was an artefact from the spectrometer (SPEX NOVA 3) which was a band corresponding to twice the excitation wavelength. Emission bands were not observed in the region 500 - 700 nm. Fluorescent enhancers such as acetylacetone and salicylic acid were added to the solution and again fluorescence was not detected. Restrictions in solubility prevented the use of other solvents. Several possibilities can be deduced for the europium(III) complex not possessing fluorescent properties:

1. The ligand $\text{L}^{11}\text{H}_3^-$ may not be able to receive electronic energy or may be unable to transfer it to the resonance level of the europium ion.
2. The solvent, methanol, may play an important part. It is well known that polar solvents do enhance the intensity of fluorescence, the more polar the solvent the greater the fluorescence intensity. The ability of methanol or water to co-ordinate to the metal causes

quenching deactivation of the fluorescent excited state. Thus, the ligand does not shield the metal but exposes it, allowing for metal-to-solvent interaction.

3. The metal-to-ligand covalent character is not restricting the fluorescence of the complex as covalent bonds enhance energy transfer far better than ionic bonds. Strictly speaking, only one phenolic group is covalently bonding to the metal, the remaining three phenol groups form a co-ordinate bond with the metal. That the three co-ordinating phenol groups are protonated is probably having the same effect as the co-ordination of methanol or water molecules in that quenching is taking place.

The deactivation of the excited state occurs as follows: The weak vibronic coupling of Ln(III) ion excited states with OH oscillators of bonded water/ methanol molecules provides an easy path for radiationless de-excitation of Ln(III) ions.^[29] The use of CD₃OD instead of CH₃OH and the conversion of L¹¹H₄ to L¹¹Na₄ will change the stretching frequency and the path for radiationless de-excitation will be limited.



The general conclusion is that the ligands $L^{11}H_4$ - $L^{14}H_6$ are inadequate as fluorescence probes as the metal shielding property is not satisfied. Ligands functionalised with bulky, overcrowding substituents such as dipy have been more successful.^[30-34] Examples are shown above.

4.5 Metal Complexes of $L^{13}H_6$ and $L^{14}H_6$

Isolation of metal complexes of $L^{13}H_6$ and $L^{14}H_6$ was not successful under the same reaction conditions applied for the isolation of metal complexes of $L^{11}H_4$. Addition of the metal salt in methanol to a suspension of the ligand in methanolic solution failed to give a clear solution on reflux even when the quantity of the salt was four-fold. Negative results were also persistent when the following methods were attempted:

- ▶ The metal salt in water was added slowly to a solution of the ligand in acetone at reflux or room temperature.
- ▶ Sodium metal added to a suspension of the ligand in methanol, followed by the addition of the metal salt in methanol at room temperature or reflux.
- ▶ Dropwise addition of a solution of the ligand in dichloromethane to a refluxing solution of the metal salt in acetonitrile or methanol.

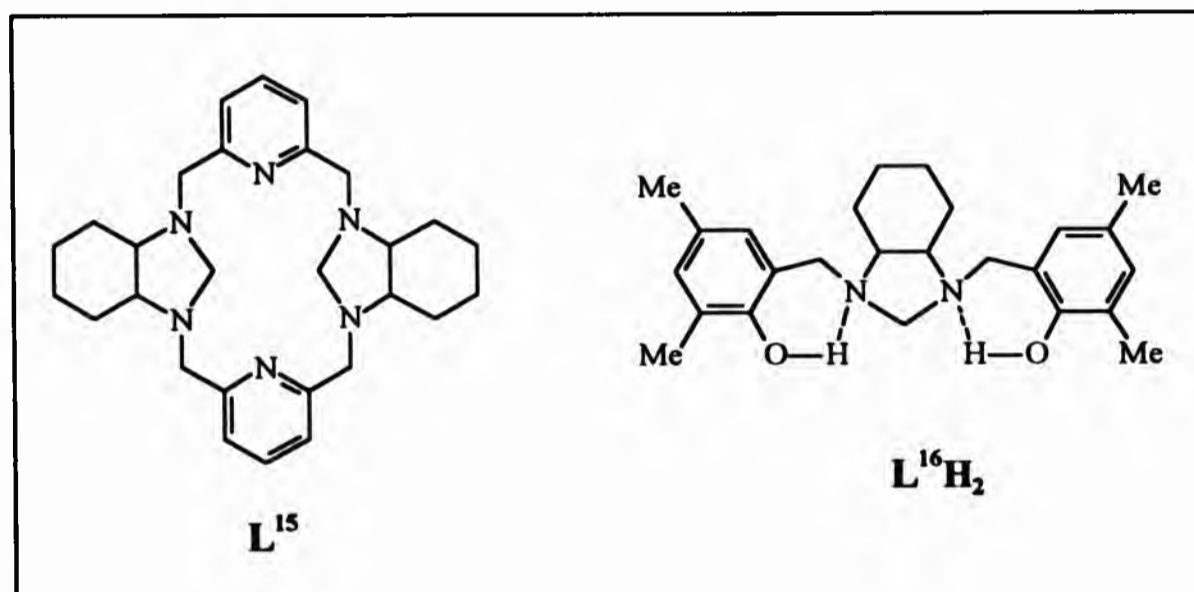
In all cases the unreacted ligand was recovered. The metals used for the complexation were hydrated yttrium, lanthanum, gadolinium, neodymium and europium trinitrate. Where europium was used, a yellow colouration formed but only the ligand was isolated from the reaction mixture.

Solution studies were carried out to investigate whether metal-ligand interaction was taking place. Electronic spectra were run of $Nd^{3+}/L^{13}H_6$ solutions in methanol/

dichloromethane mixtures in the ratios 2:1, 1:1, 3:2, 2:1 and 3:1 respectively and in the range 500 - 900 nm. The spectra were all identical to those of $\text{Nd}(\text{NO}_3)_3 \cdot 6\text{H}_2\text{O}$ and, in particular, changes in the splitting of the hypersensitive band at *ca.* 580 nm had not occurred.

**4.6 The Reaction of L^9 with 2,5-dimethylphenol and aqueous methanal;
Synthesis of L^{15} and L^{16}H_2**

In contrast to the syntheses of L^{11}H_4 , L^{12}H_4 , L^{13}H_6 and L^{14}H_6 the reaction of the amine L^9 with 2,5-dimethylphenol and aqueous methanal yielded large colourless crystals of L^{15} where one molecule of methanal reacted with two amino groups forming a 5-membered ring, reducing the inner great ring from 18- to 16-membered.



The presence of the benzylic ring was not detected in the analyses. The crystals were not soluble in common solvents and the melting point of 336 - 339°C supports the rigidity and stability of the structure. The flexibility of L^9 has been reduced as the tertiary nitrogen atoms have been rigidly locked. The maximum flexibility available to the molecule, as determined by molecular models, is rotation through the methylene groups bridging the pyridine ring and the tertiary nitrogen atoms.

It has to be emphasized that the imine, L^5 and the amine, L^9 , were not isolated prior to the synthesis of L^{15} . Filtering the crystals of L^{15} and allowing the filtrate to stand

afforded feathery white crystals of $L^{16}H_2$, where the Mannich reaction had taken place on the uncyclised (\pm)-*trans*-1,2-diaminocyclohexane. The crystals were readily soluble in methanol, diethyl ether, acetone, toluene, dichloromethane, DMSO and warm acetonitrile. There is the possibility of four hydroxy-3,5-dimethylbenzyl pendant arms attaching to the diaminocyclohexane but steric interactions between adjacent pendant arms on the same or different nitrogen atoms prevent this substitution and instead a methylene group bridges the two nitrogen atoms as for L^{15} . Work carried out in this Department included the attachment of four methylene-phosphonate groups to this diamine.^[34] The tetra-substitution with methylene-phosphonate pendants was achieved when the reaction was carried out in extreme acidic conditions.^[35]

The distinguishing features of the IR spectrum of L^{15} from that of L^9 (Chapter 3, § 3.3.1) was the absence of the sharp band at 3305 cm^{-1} from the N-H stretch and the series of bands ranging from $862 - 714\text{ cm}^{-1}$ which arose from the N-H out-of-plane bend. A new band was observed at 2806 cm^{-1} and was attributed to the C-H stretch of the new methylene groups bridging the two tertiary nitrogen atoms. This wavenumber falls in the range of methylene groups attached to nitrogen atoms.

The C-H stretching region of $L^{16}H_2$ (Table 4.1) shows three bands at 3011 cm^{-1} [$\nu(\text{C-H})$ aromatic] and 2937 and 2861 cm^{-1} [$\nu(\text{C-H})$ alkyl] the latter band primarily being the result of C-H stretching vibrations of cyclohexane.

The absence of the two bands in the region $1590 - 1574\text{ cm}^{-1}$ confirm the absence of the pyridyl group. The C-H and O-H bending vibrations, the C-O stretch and the C-H out-of-plane deformation of $L^{16}H_2$ absorb at similar wavenumbers to the respective vibrations of $L^{11}H_4$, $L^{12}H_4$, $L^{13}H_6$ and $L^{14}H_6$ (Table 4.1).

The EI mass Spectrum of L^{15} was much more informative than the LSIM spectrum although a base peak molecular ion, $[\text{M} + \text{H}]^+$ m/z 459, was detected from both techniques. A band corresponding to half the molecular ion results from two-bond

cleavage, $[M/2]^+$ m/z 229.

The LSIM spectrum of $L^{16}H_7$ yielded a molecular ion $[M + H]^+$ m/z 395 followed by the loss of the two pendant arms consecutively at $[(M + H) - X]^+$ m/z 260 and $[(M + H) - 2X]^+$ m/z 125.

4.6.1 NMR Spectroscopy of L^{15}

Although L^{15} was relatively insoluble, its solubility in $CDCl_3$ was adequate for the collection of NMR spectra. The spectra showed no evidence of protons from the benzylic pendant arm.

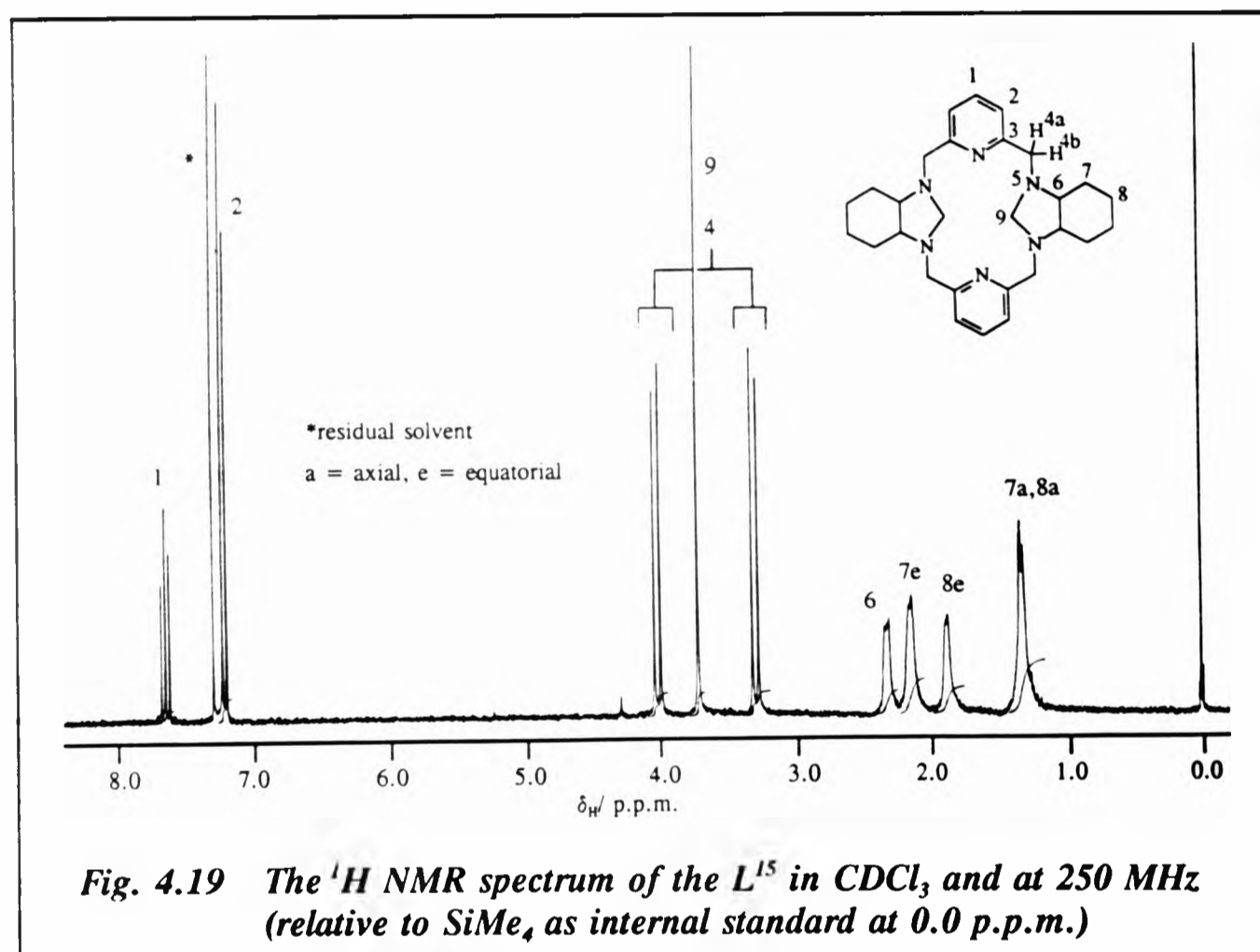


Fig. 4.19 The 1H NMR spectrum of the L^{15} in $CDCl_3$ and at 250 MHz (relative to $SiMe_4$ as internal standard at 0.0 p.p.m.)

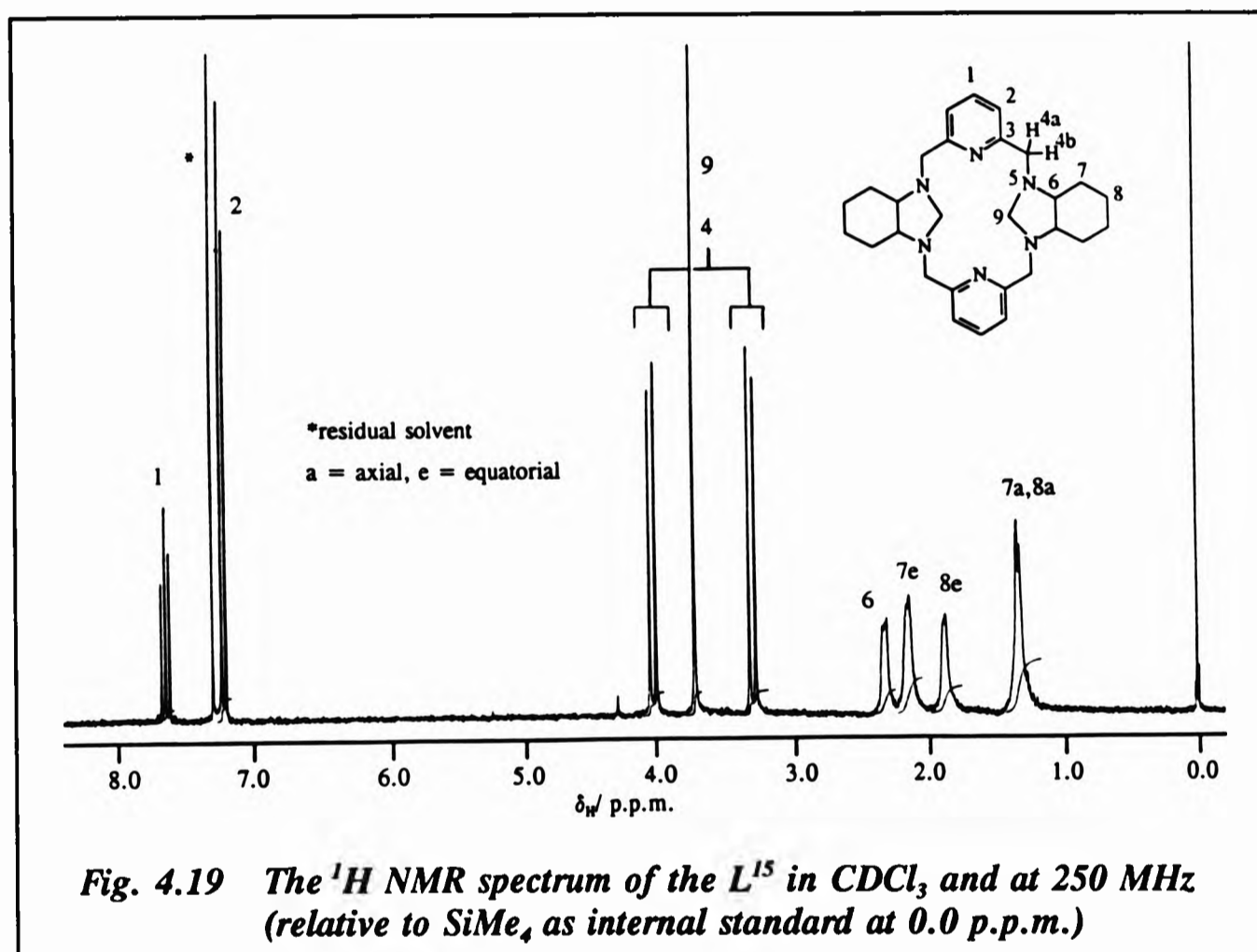
The 1H NMR spectrum of L^{15} (Fig. 4.19) had the same general pattern to that of L^9 with two major differences. The broad NH band at δ_H 2.93 was absent and a singlet peak appeared at δ_H 3.67. This band integrated for four protons and is attributed to the methylene protons, H^9 . The band resonated in between the *doublet of doublets* of the non-equivalent protons, H^{4a} and H^{4b} , which resonate at δ_H 3.99 and 3.23. Whereas for L^9 these formed an AB system, in this case the second order coupling

cleavage, $[M/2]^+$ m/z 229.

The LSIM spectrum of $L^{16}H_2$ yielded a molecular ion $[M + H]^+$ m/z 395 followed by the loss of the two pendant arms consecutively at $[(M + H) - X]^+$ m/z 260 and $[(M + H) - 2X]^+$ m/z 125.

4.6.1 NMR Spectroscopy of L^{15}

Although L^{15} was relatively insoluble, its solubility in $CDCl_3$ was adequate for the collection of NMR spectra. The spectra showed no evidence of protons from the benzylic pendant arm.



The 1H NMR spectrum of L^{15} (Fig. 4.19) had the same general pattern to that of L^9 with two major differences. The broad NH band at δ_H 2.93 was absent and a singlet peak appeared at δ_H 3.67. This band integrated for four protons and is attributed to the methylene protons, H^9 . The band resonated in between the *doublet of doublets* of the non-equivalent protons, H^{4a} and H^{4b} , which resonate at δ_H 3.99 and 3.23. Whereas for L^9 these formed an AB system, in this case the second order coupling

is of the type AM. The coupling constant has also increased from 13.7 Hz for L⁹ to ${}^2J(\text{H}^{\text{a}}\text{H}^{\text{b}}) = 16.1$ Hz for L¹⁵. The chemical shifts of the pyridyl protons were δ_{H} 7.61 for H¹ and δ_{H} 7.18 for H². The coupling constant between the latter two protons was ${}^3J(\text{H}^1, \text{H}^2) = 7.6$ Hz. The chemical shifts of the cyclohexyl protons are assigned on the spectrum (Fig. 4.19).

The off resonance broad band proton decoupled ¹³C NMR spectrum of L¹⁵ consisted of eight bands, again, prompting four fold structural symmetry. These are given in Table 4.14

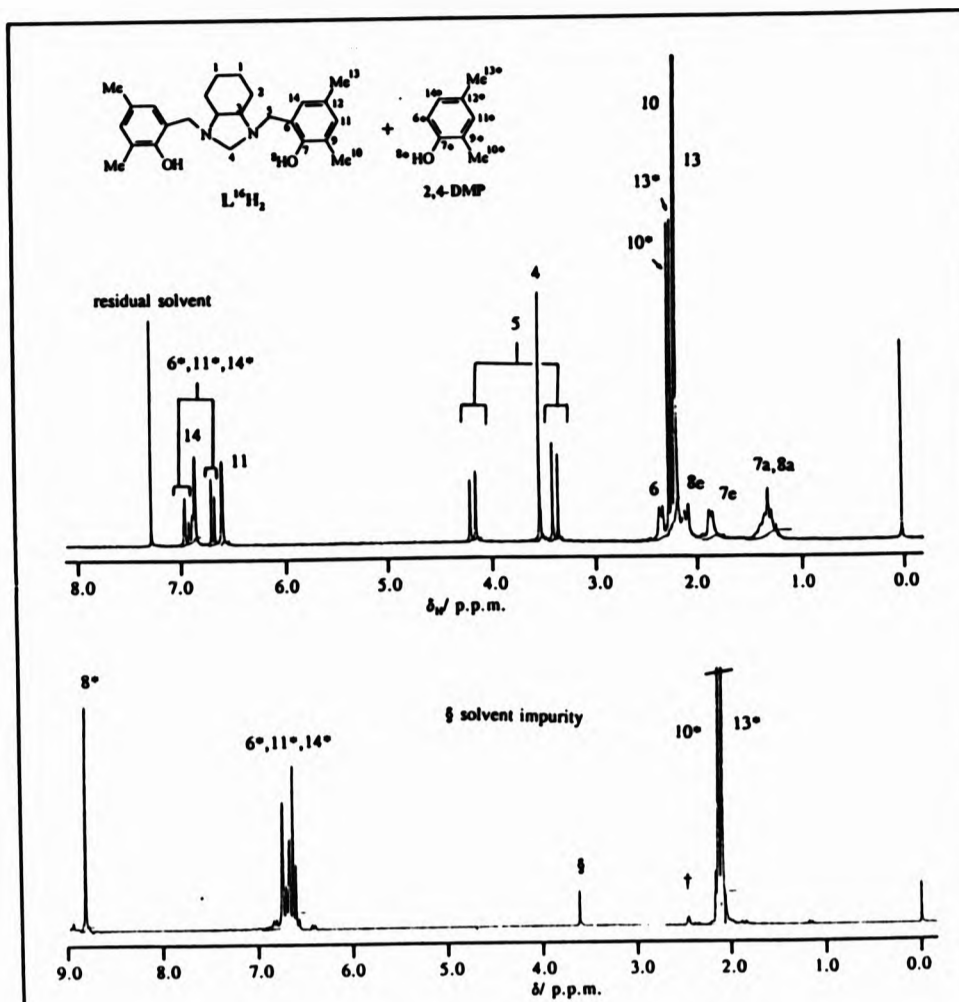
Table 4.14 *The chemical shifts (in p.p.m) of the ¹³C NMR spectrum of L¹⁵ (relative to SiMe₄ as internal standard at 0.0 p.p.m.)*

ASSIGNMENT	δ_{C}
1	137.38
2	122.90
3	157.50
4	58.83
5	-
6	68.21
7	29.12
8	24.36

4.6.2 The NMR Spectroscopy of L¹⁶H₂

Opposing the ¹H NMR spectrum of L¹⁵, the ¹H NMR spectrum of L¹⁶H₂ (Fig. 4.20a) showed the presence of the 2-hydroxy-3,5-dimethylbenzyl pendants but the usual pyridyl triplet-doublet splitting pattern was absent from the region δ_{H} 7.5 - 7.0.

(a)



(b)

refer to Table 4.15 for chemical shifts

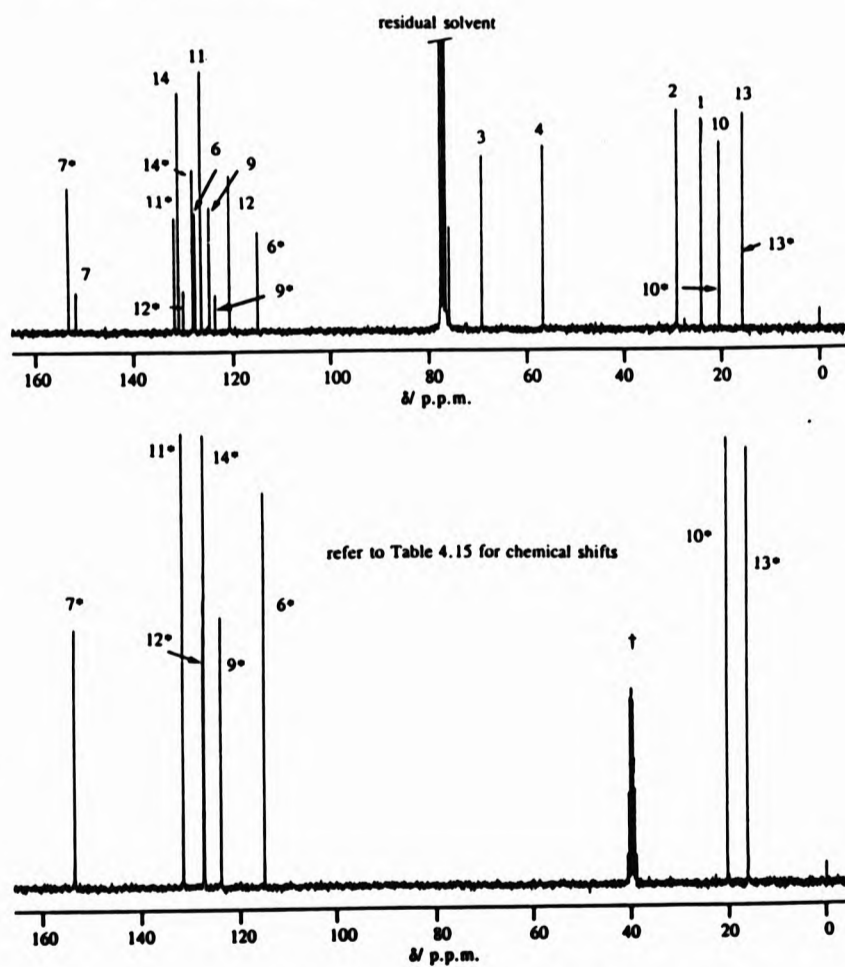


Fig. 4.20 The (a) 1H and (b) ^{13}C NMR spectra of $L^{16}H_2$, with the 2,4-dimethylphenol impurity in $CDCl_3$, and neat 2,4-dimethylphenol in d_6 -DMSO and at 250 MHz (relative to $SiMe_4$, as internal standard at 0.0 p.p.m.)

The two doublet bands from the benzylic ring are depicted at δ_{H} 6.57 and 6.83 and are in similar shifts to those given by L^{11}H_4 and L^{12}H_4 (Table 4.4) and L^{13}H_6 and L^{14}H_6 (Table 4.6). The remaining bands in the region δ_{H} 6.5 - 7.0 were initially confusing but they are in fact aromatic protons from unreacted 2,4-dimethylphenol. This derivation will be discussed further on. The phenolic protons were not observed and this is not a rare occurrence.^[27]

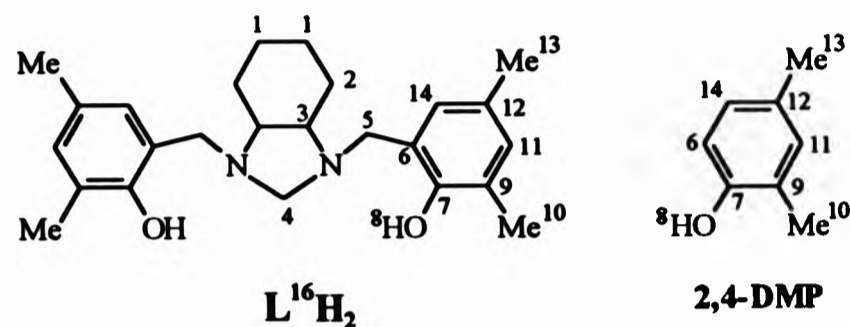
As for L^{15} , the protons from the methylene group bridging the two nitrogen atoms, H^4 , resonate as a *singlet* at δ_{H} 3.51 and integrate for two protons. A *doublet of doublets* at δ_{H} 4.16 and 3.35 are due to the methylene protons, H^5 , indicating that the methylene carbon, C^5 , is prochiral. The coupling constant of these AB protons is ${}^2J(\text{H}^{5a}, \text{H}^{5b}) = 13.7$ Hz. One feature to be noted is that the *doublet* downfield is less intense than the *doublet* upfield yet they each integrate for four protons. Coupling between these two protons, H^{5a} and H^{5b} , was determined by a ${}^1\text{H}$ -COSY spectrum although an explanation for the difference in intensities cannot be derived.

Four bands can be seen in the spectrum arising from the methyl protons although only the two at δ_{H} 2.18 (H^{10}) and 2.17 (H^{13}) are from L^{16}H_2 and these shifts are identical (± 0.01 p.p.m.) to those of L^{11}H_4 (Table 4.4) and L^{13}H_6 (Table 4.6). The bands at δ_{H} 2.25 and 2.22 are from the methyl protons of unreacted 2,4-dimethylphenol.

The cyclohexyl protons were assigned according to the ${}^1\text{H}$ - and ${}^{13}\text{C}$ - ${}^1\text{H}$ -COSY spectra. The multiplet at δ_{H} 1.29 arose from the axial protons of H^7 and H^8 . The equatorial protons, H^{8e} and H^{7e} resonate at δ_{H} 1.8 and 2.08 respectively. The chemical shift of the methine protons, H^6 , is at δ_{H} 2.31.

The off resonance broad band proton decoupled ^{13}C NMR spectrum (Fig. 4.20b and Table 4.15) was extremely complex in the region 110 - 160 p.p.m. Twelve bands were observed in this region which is the number of aromatic carbon atoms in L^{16}H_2 , although the two benzylic rings were expected to be symmetrically equivalent and therefore respective carbon atoms would have that same chemical shifts, *i.e.* only six bands should resonate in this region of the spectrum. When this spectrum was closely compared to the ^{13}C NMR spectra of L^{11}H_4 and L^{13}H_4 , a band at δ_{C} 114 was not present in the latter two spectra and was, therefore, not expected to be in the spectrum of L^{16}H_2 . This band was also present in the spectrum of neat 2,4-dimethylphenol and was assigned to the sp^2 carbon atom adjacent to the hydroxyl group. In L^{11}H_4 and L^{13}H_6 the proton *ortho* to the hydroxyl group is substituted by the methylene group of the pendant arm and hence it is absent from the ^1H NMR spectra of these compounds. The six extra bands detected in this region of the spectrum of L^{16}H_2 and the two extra methyl proton bands support the fact that 2,5-dimethylphenol was present as an impurity irrespective that the compound was crystalline and was washed with cold methanol followed by diethyl ether when it was filtered. This explanation also accounts for the ^1H NMR spectrum. Elimination of the nine protons of 2,4-dimethylphenol from the total integration leaves the correct number of protons for L^{16}H_2 . ^1H - and ^{13}C - ^1H -COSY spectra and also that of 2,4-dimethylphenol aided in separating which signals were from L^{16}H_2 and which from the unreacted 2,4-dimethylphenol bearing in mind that the chemical shifts of the benzylic carbon atoms would alter from the spectrum of neat 2,4-dimethylphenol due to the substitution of the macrocycle which may itself cause deshielding. It should be noted that all the analyses were consistent, in showing the presence of unreacted 2,4-dimethylphenol, on repeating the experiment. Table 4.15 lists the ^{13}C signals of L^{16}H_2 together with those of 2,4-dimethylphenol.

Table 4.15 The ^{13}C NMR chemical shifts of L^{16}H_2 ,* with the 2,4-dimethylphenol impurity and the chemical shifts of neat 2,4-dimethylphenol** (relative to SiMe_4 as internal standard at 0.0 p.p.m.)



ASSIGNMENT	δ_{C}		
	L^{16}H_2	2,4-DMP eliminated from L^{16}	2,4-DMP***
1	24.05		-
2	28.96		-
3	69.99		-
4	56.25		-
5	75.77		-
6	127.87	114.71	114.57 (115.8)
7	151.55	153.03	153.20 (152.9)
8	-	-	-
9	124.56	123.43	123.59 (125.1)
10	20.36	20.42	20.12
11	126.19	131.63**	131.22 (131.1)
12	120.55	129.82	127.13 (130.4)
13	15.57	15.67	15.98
14	130.74	127.38	126.91 (127.4)

* in CDCl_3 , ** in d_6 -DMSO, *** assigned according to empirical parameters for substituted benzene, estimated values are given in parentheses

L^{16}H_2 was isolated in extremely small yields to allow for any syntheses of complexes. Several repeated attempts to isolate lanthanum metal complexes of L^{15} both in dichloromethane and as a suspension in methanol were unsuccessful. Manipulation of molecular models (Fig. 4.21) suggested that the steric hinderance

caused by the inner methylene groups, CH_2^9 , prevent the metal from approaching the macrocyclic hole and the rigidity imposed by the same methylene groups prevent the nitrogen atoms from closing in on the metal.

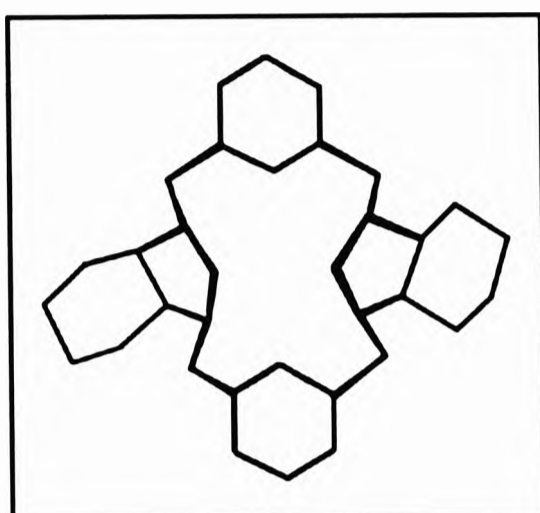


Fig. 4.21 *The minimised structure of L^{15} as predicted by the Alchemy(III) Molecular Modelling package*

Rotation about the methylene groups, CH_2^4 can allow for the ligand to adopt an arrangement such that the inner methylene groups are as far from each other as possible thus exposing the macrocyclic cavity open to the approaching metal. But the nitrogen atoms are rigidly locked, therefore no nitrogen-to-metal bonding takes place even with lanthanum, a metal with a relatively large ionic radius.

4.7 Conclusion

The ligand, $L^{11}\text{H}_4$, on lanthanide metal co-ordination, adopts the butterfly conformation and the characteristic folding of the pyridine rings away from the doubly co-ordinated hemisphere occurs for these complexes also. The energy minimum is achieved when the four pendant arms co-ordinate from the hemisphere below (away) from the pyridine rings (Fig. 4.22).

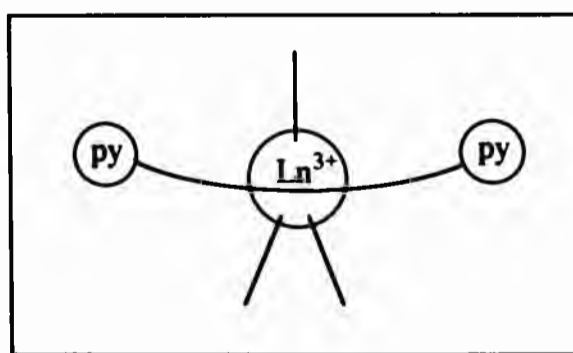


Fig. 4.22 *The characteristic folding of the hexaaza ligands*

As this arrangement is the most stable, diastereoisomerism is not possible, as for the $[LnL^9(NO_3)_3]$ complexes.

Where transition metals are concerned, the pseudo-octahedral, double helixing, about the metal ion is maintained, as for the transition metal complexes of L^9 . The pre-positioning of the pendant arms, forming the configuration *RRRR* or *SSSS* at the tertiary nitrogen centres, also fix the position of co-ordination of the phenol to the metal. Fig. 4.23 (bold

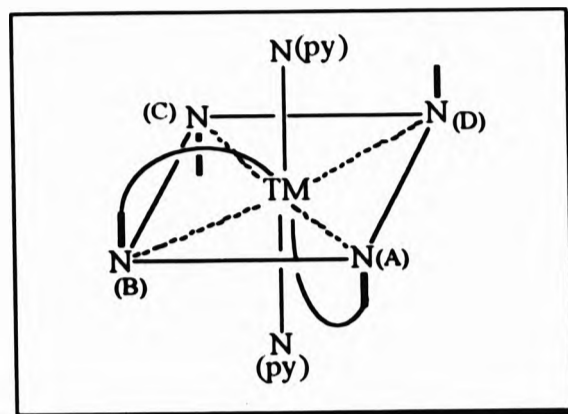


Fig. 4.23 *The proposed co-ordination of the pendant arms on transition metal co-ordination*


lines) shows the arrangement or the protrusion of the pendants from the nitrogen centres. Molecular models have shown that the pendant arm at N(A) can only co-ordinate from below the plane N(A), N(B), N(C) and N(D) as steric interaction from the pendant at N(B) prevents co-ordination from above the plane. The pendant at N(B) is, therefore, restricted to co-ordinating above the plane. But even these proposed arrangements of co-ordination are not possible as the phenolic groups experience steric interaction from the distorted diamino pyridine planes. Thus, the most stable arrangement for transition metal co-ordination of $L^{11}H_4$ is with the pendant arms not co-ordinating to the metal ion.

Repulsion from the cyclohexane rings is also the reason for pendant arms not attaching to the ligand L^9 . The distance between the two tertiary nitrogen atoms on the same cyclohexane ring, is adequate for them to be bridged by a methylene group resulting in the formation of two internal 5-membered rings and the rigid structure of L^{15} .

4.7 References.

1. T. A. Kaden, *Top. Curr. Chem.*, 1984, **121**, 157.
2. P. V. Bernhardt and G. A. Lawrence, *Coord. Chem. Rev.*, 1990, **104**, 297.
3. H. Toftlund and S. Yde-Andersen, *Acta Chem. Scand.*, 1981, **A35**, 575.
4. N. W. Alcock, K. P. Balakrishnan and P. Moore, *J. Chem. Soc., Chem. Commun.*, 1985, 1731.
5. N. W. Alcock, K. P. Balakrishnan and P. Moore, *J. Chem. Soc., Dalton Trans.*, 1986, 1743.
6. E. Kimura, T. Koike, H. Nada and Y. Litaka, *J. Chem. Soc., Chem. Commun.*, 1986, 1322.
7. H. Tsukube, K. Yamashita, T. Iwachido and M. Zenki, *J. Chem. Res. (S)*, 1988, 105.
8. C.-M. Che and W.-T. Tang, *J. Chem. Soc., Dalton Trans.*, 1988, 2879.
9. N. W. Alcock, K. P. Balakrishnan, A. Berry, P. Moore and C. J. Reader, *J. Chem. Soc., Dalton Trans.*, 1988, 1089.
10. G. de M. Norante, M. Di Vaira, F. Mani, S. Mazzi and P. Stoppioni, *J. Chem. Soc., Chem. Commun.*, 1990, 438.
11. E. Asato, S. Hashimoto, N. Matsumoto and S. Kida, *J. Chem. Soc., Dalton Trans.*, 1990, 1741.
12. H. Tsukube, K. Yamashita, T. Iwachido and M. Zenki, *J. Chem. Soc., Perkin Trans. 1*, 1991, 1661.
13. W. S. Szulbinski, P. R. Warburton, D. H. Busch and N. W. Alcock, *Inorg. Chem.*, 1993, **32**, 297.
14. I. A. Fallis, L. J. Farrugia, N. M. Macdonald and R. D. Peacock, *J. Chem. Soc., Dalton Trans.*, 1993, 2759.
15. M. L. Turonek, P. Clarke, G. S. Lawrence, S. F. Lincoln, P.-A. Pittet, S. Politis and K. P. Wainwright, *Inorg. Chem.*, 1993, **32**, 2195.
16. C. F. G. C. Geraldes, A. D. Sherry and W. P. Cacheris, *Inorg. Chem.*, 1989, **28**, 3336.

17. C. J. Broan, K. J. Jankowski, R. Katakay and D. Parker, *J. Chem. Soc., Chem. Commun.*, 1990, 1738.
18. W. Clegg, P. B. Iveson and J. Lockhardt, *J. Chem. Soc., Dalton Trans.*, 1992, 3291.
19. C. Flassbeck, K. Wiegardt, E. Bill, C. Butzlaff, A. X. Trautwein, B. Nuber and J. Weiss, *Inorg. Chem.*, 1992, **31**, 21.
20. D. A. Moore, P. E. Fanwick and M. J. Welch, *Inorg. Chem.*, 1989, **28**, 1504.
21. J. Jazwinski, J.-M. Lehn, R. Meric, J.-P. Vigneron, M. Cesario, J. Guilhem and C. Pascard, *Tetrahedron Lett.*, 1987, **28**, 3489.
22. R. Menif and A. E. Martell, *J. Chem. Soc., Chem. Commun.*, 1989, 3489.
23. K. I. Dhont, W. Lippens, G. Herman and A. M. Goeminne, *Bull Soc. Chim. Belg.*, 1992, **101**, 1061.
24. R. M. Silverstein, G. C. Bassler and T. C. Morrill, *Spectrometric Identification of Organic Compounds*, Wiley, Singapore, 1981.
25. D. H. Williams and I. Flemmings, *Spectroscopic Methods in Organic Chemistry*, M^cGraw-Hill, London, 1987.
26. N. N. Greenwood and A. Earnshaw, *Chemistry of the Elements*, Pergamon, Toronto, 1987, p.1265.
27. U. Auerbach, U. Eckert, K. Weighardt, B. Nuber and J. Weiss, *Inorg. Chem.*, 1990, **29**, 938.
28. E. T. Clarke and A. E. Martell, *Inorg. Chim. Acta*, 1991, **186**, 103.
29. J.-C. Bünzli in *Lanthanide Probes in Life, Chemical, and Earth Sciences*, J.-C. Bünzli and G. R. Choppin (Eds.), Elsevier, Amsterdam, 1989, Chapter 7, p. 219.
30. P. L. Anelli, V. Balzani, L. Prodi and F. Uggeri, *Gazz. Chim. Ital.*, 1991, **121**, 359.
31. L. Prodi, M. Maestri, R. Ziessel and V. Balzani, *Inorg. Chem.*, 1991, **30**, 3798.
32. V. Balzani, J. -M, Lehn, J. van de Loosdrecht, A. Mecati, N. Sabbatini and R. Ziessel, *Angew. Chem. Int. Ed. Engl.*, 1991, **30**, 190.

- 
33. R. Ziessel, M. Maestri, L. Prodi, V. Balzani and A. van Dorsselaer, *Inorg. Chem.*, 1993, **32**, 1237.
 34. M. Constantinou, unpublished results, University of North London.
 35. K. Moedritzer and R. Irani, *J. Org. Chem.*, 1966, **31**, 1603.

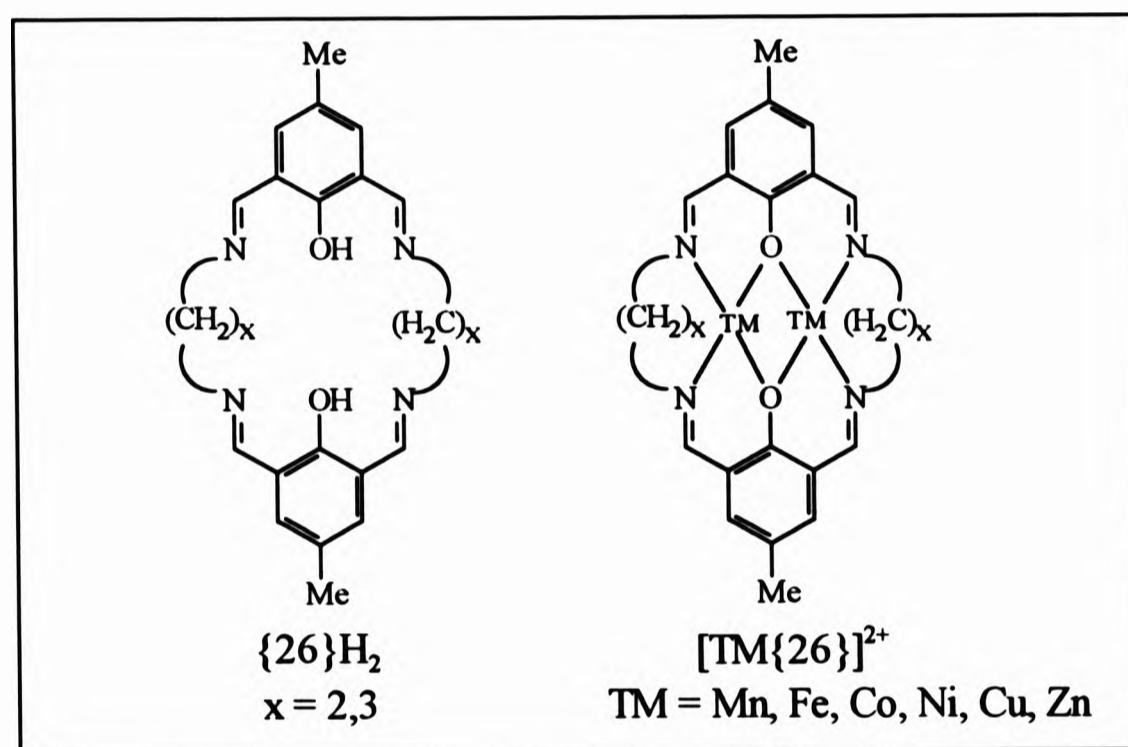
CHAPTER 5

Chapter 5: TETRAAZA MACROCYCLES WITH BRIDGE PHENOLIC GROUPS

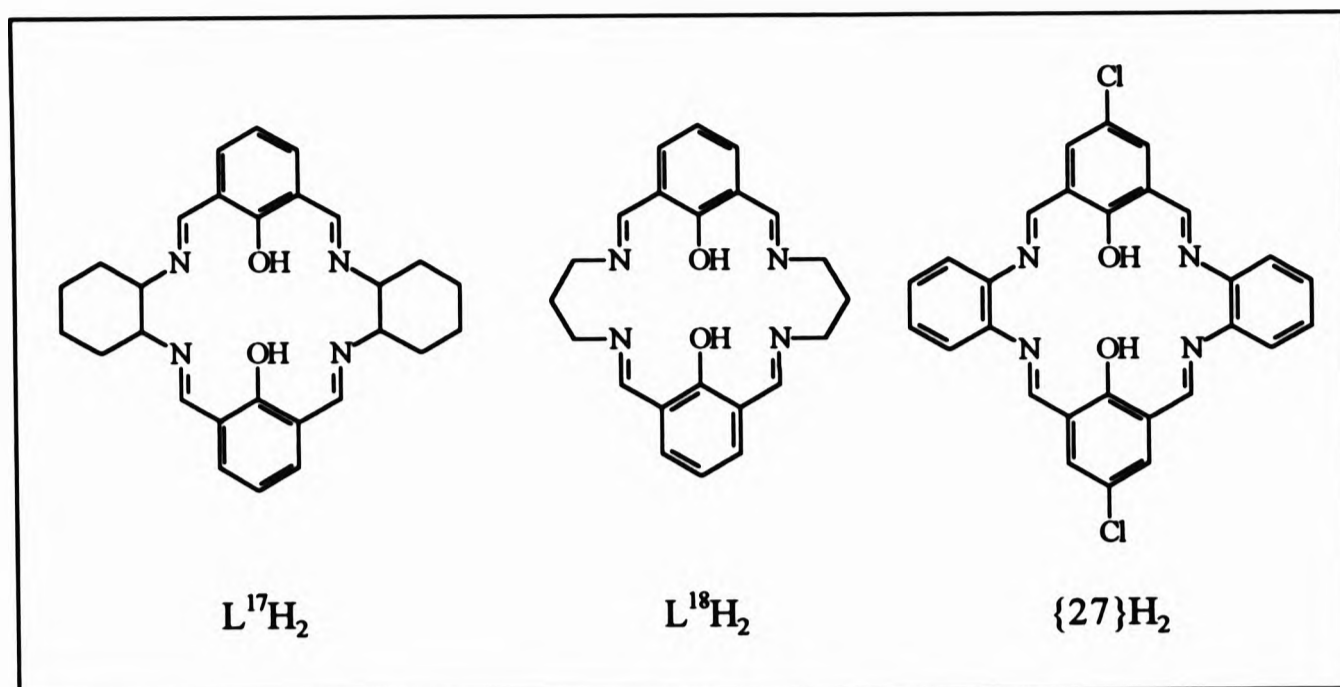
(References to this Chapter are listed on pages 240 and 241)

5.1 Introduction

Robson and Pilkington (1970) first reported the synthesis of {26}H₂ and at the same time observed its binucleating abilities, *i.e.* its capability of securing two metal ions in close proximity.^[1]



On co-ordination with first row transition metals the phenolic protons are lost to give complexes of the type [TM₂{26}]²⁺ in which the phenolic oxygen atoms bridge between metal ions. The decrease in the size of the macrocyclic cavity enables first row transition metals to act as templates, this not being possible for the synthesis of the hexaaza macrocycles, L¹-L⁴. Limited studies have been reported relating such macrocyclic ligands with lanthanide metals. This work consisted of the direct synthesis of L¹⁷H₂ and the template synthesis of the lanthanide metal complexes of L¹⁷H₂ and L¹⁸H₂. The free ligand, L¹⁸H₂ was isolated very recently^[2] as the dimethyl derivative, [{26}H₄](PF₆)₂ (where x = 3).

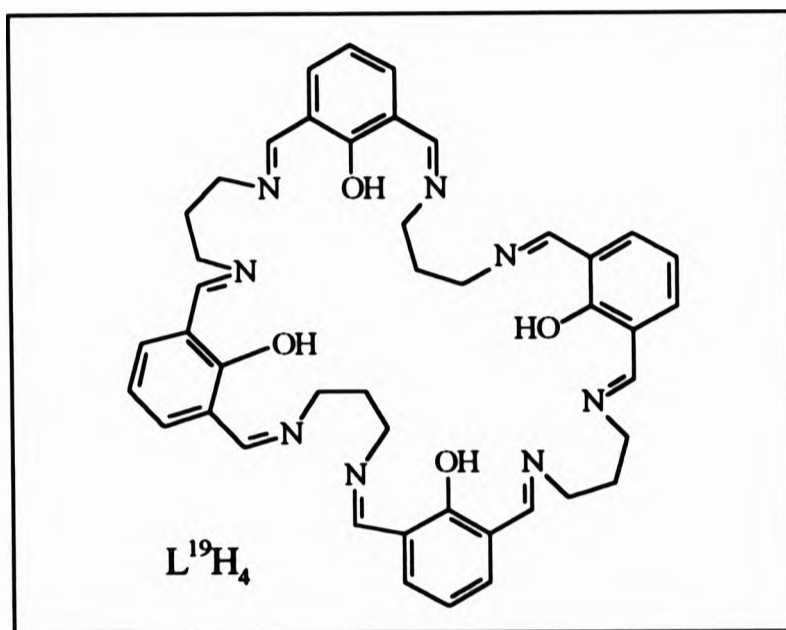


5.2 Synthesis of $L^{17}H_2$ and Lanthanide Metal Complexes of $L^{17}H_2$ and $L^{18}H_2$. Similar to the reaction of 2,6-diformyl-4-chlorophenol with 1,2-diaminobenzene in the absence of a metal template which led to $\{27\}H_2$,¹³¹ the reaction of 2,6-diformylphenol and (\pm)-*trans*-1,2-diaminocyclohexane resulted in a yellow, insoluble [2+2] condensation product, $L^{17}H_2$, with yields of up to 80%.

The insolubility of the ligand prevented its direct complexation with yttrium and the lanthanide metals. However, coloured macrocyclic complexes were isolated when yttrium(III), lanthanum(III), neodymium(III), europium(III), gadolinium(III) and dysprosium(III) were used as templates for both the syntheses of $L^{17}H_2$ and $L^{18}H_2$ in nearly quantitative yields with two types of complex being formed depending on the metal.

With the exception of the dysprosium complex of $L^{18}H_2$, all the yttrium and lanthanide metal complexes formed [2+2] condensation products of the type $[Ln(L^aH)X_q]_p(\text{solvent})$, where $n = 17, 18$; $X = NO_3, OAc, Cl$; $q = 1, 2$; $p = 0-3$. In the cases of yttrium and gadolinium, where metal acetate salts were used the product which precipitated from the reaction mixture consisted of a mixture of the

free ligand, $L^{17}H_2$, and its yttrium or gadolinium metal complex. The metal complex was separated from the ligand by soxhlet extraction in methanol. The reaction of dysprosium trinitrate with 1,3-diaminopropane and 2,6-diformylphenol forms a [4+4] dinuclear product, $L^{19}H_4$.



5.2.1 Infrared Spectrophotometry

A very strong band at 1623 cm^{-1} in the IR spectrum of the ligand, $L^{17}H_2$, confirmed the Schiff condensation, formation of the C=N bonds and that the product was cyclic, by the absence of bands at 3355 and 3274 cm^{-1} from the NH vibrations of the diaminocyclohexane and also the C=O stretch of 2,6-diformylphenol at 1690 and 1660 cm^{-1} . That [2+2] condensation dominated over other possible polymeric species was confirmed by LSIMS with a molecular ion and base peak of $[M + H]^+$ at $m/z\ 457$.

In all the metal template complexes of $L^{17}H_2$ and $L^{18}H_2$, the IR spectra depicted a strong absorption at *ca.* 3400 and 3450 cm^{-1} from lattice water or solvent. Reasons confirming complete cyclisation are the same as those given above for the synthesis of the ligand. Where metal acetate salts were employed, the asymmetric COO^-

stretch appeared as a strong broad absorption centred at 1540 cm^{-1} . The symmetric COO^- stretch appeared as strong broad band at *ca.* 1450 and 1435 cm^{-1} and the O-C-O stretching mode appeared at *ca.* 680 cm^{-1} . These absorption bands conclude that the yttrium and gadolinium acetate complexes contain both ionic and bidentate chelating acetate groups.^[4,5] Where nitrate metal salts were used, ionic nitrate groups were identified by the bands at 1384 , 840 and 720 cm^{-1} and the bidentate groups by the bands at 1310 and 1490 cm^{-1} ($\Delta\nu = 180\text{ cm}^{-1}$). Two counter-ions were present in all the complexes as determined by the elemental analyses which suggests that only one of the two hydroxyl groups in the macrocyclic ligand is deprotonated. It has been suggested that these type of macrocyclic ligands can behave as neutral, mono- or di-anionic according to the synthesis procedure used.^[6,7] Although it was not attempted, the presence of a base, lithium or sodium hydroxide, promotes the formation of complexes containing only one acetate, nitrate or chloride group, whereas, in the absence of a base, complexes containing two or three acetate or nitrate or chloride groups have been obtained, one of these groups almost always being ionic.^[6,7] All the yttrium and lanthanide metal template Schiff bases discussed in this chapter were isolated with the macrocyclic ligand being mono-anionic.

Irrespective of the counter-ion bands all the IR spectra of the complexes showed remarkable similarity. The C=N stretching vibrations absorbed strongly at $1619 - 1638\text{ cm}^{-1}$. In all of the metal complexes the imine band had a shoulder at 1650 cm^{-1} and the explanation for this is that the complexes contain two co-ordinated and two un-co-ordinated imine groups.^[8] This occurrence will be discussed in section 5.2.4. A medium band found at $1530 - 1545\text{ cm}^{-1}$ is characteristic of phenolic C-O acquiring double bond character through conjugation with the imine system in chelating rings,^[9] and a weak band in the region $1030 - 1035\text{ cm}^{-1}$ was assigned to C-O stretching.

5.2.2 Electronic Spectroscopy and Magnetic Moments

The ligand, $L^{17}H_2$, and the yttrium and lanthanide metal complexes of $L^{17}H_2$ and $L^{18}H_2$ were only partially soluble in hot water, dichloromethane and DMSO. Immediate precipitation of both the ligand and the metal complexes from solution prevented the collection of electronic spectra. The observed magnetic moments for the paramagnetic complexes are given in Table 5.1, together with the colouration of all the metal complexes.

Table 5.1 The magnetic moments and colour of the complexes of $L^{17}H_2$, $L^{18}H_2$ and $L^{19}H_4$

COMPOUND	μ_B	COLOUR
$L^{17}H_2$	-	yellow
$[Y(L^{17}H)OAc]OAc.MeOH.2H_2O$	-	yellow
$[La(L^{17}H)(NO_3)]NO_3.1/2H_2O$	-	orange-yellow
$[Nd(L^{17}H)(NO_3)]NO_3.MeOH$	3.1	dark red
$[Eu(L^{17}H)(NO_3)]NO_3.MeOH.3H_2O$	2.9	red-brown
$[Gd(L^{17}H)(OAc)](OAc).3MeOH$	7.5	yellow
$[Dy(L^{17}H)(NO_3)]NO_3.MeOH.31/2H_2O$	9.6	red-brown
$[Y(L^{18}H)](OAc).1/2H_2O$	-	orange-brown
$[La(L^{18}H)(NO_3)]NO_3$	-	orange-brown
$[Nd(L^{18}H)(NO_3)]NO_3.1/2MeOH$	3.3	orange-brown
$[Eu(L^{18}H)(NO_3)]NO_3.H_2O$	3.2	orange-yellow
$[Gd(L^{18}H)(Cl)(H_2O)]Cl.MeOH.2H_2O$	7.6	orange-brown
$[Dy_2(L^{19}H_3)(NO_3)_4(MeOH)H_2O]NO_3.41/2H_2O$	16.1	orange-yellow

The observed magnetic moments agreed with the expected μ_{s+L} values of trivalent lanthanide metals. The dimetallic species, $[Dy_2(L^{19}H_2)(NO_3)_4]^+$ has a value of 16.1 B.M. which is in a reasonably close agreement with the expected value for two metals at 14.7 B.M. This confirms the presence of two metals per unit and also favours the formation of [4+4] condensation, where the two metals are not linked

(the structure of which will be discussed later), to the [2+2] dimeric product. LSIMS also confirmed the dinuclear [4+4] species with a fragment at m/z 1374 (2%) corresponding to $[\text{Dy}_2(\text{L}^{19}\text{H}_3)(\text{NO}_3)_4\text{MeOH}(\text{H}_2\text{O})]^+$. The loss of co-ordinated water formed $[\text{Dy}_2(\text{L}^{19}\text{H}_3)(\text{NO}_3)_4\text{MeOH}]^+$ at m/z 1356 (2%) and the loss the methanol molecule and one nitrate group resulted in $[\text{Dy}_2(\text{L}^{19}\text{H}_3)(\text{NO}_3)_3]^+$ at m/z 1262 (2%).

5.2.3 NMR Spectroscopy

The solution ^1H NMR spectrum of L^{17}H_2 (Fig. 5.2) in CDCl_3 and at 250 MHz is complex indicating that an equilibrium between L^{17}H_2 and the carbinolamine (Fig. 5.1) is taking place.

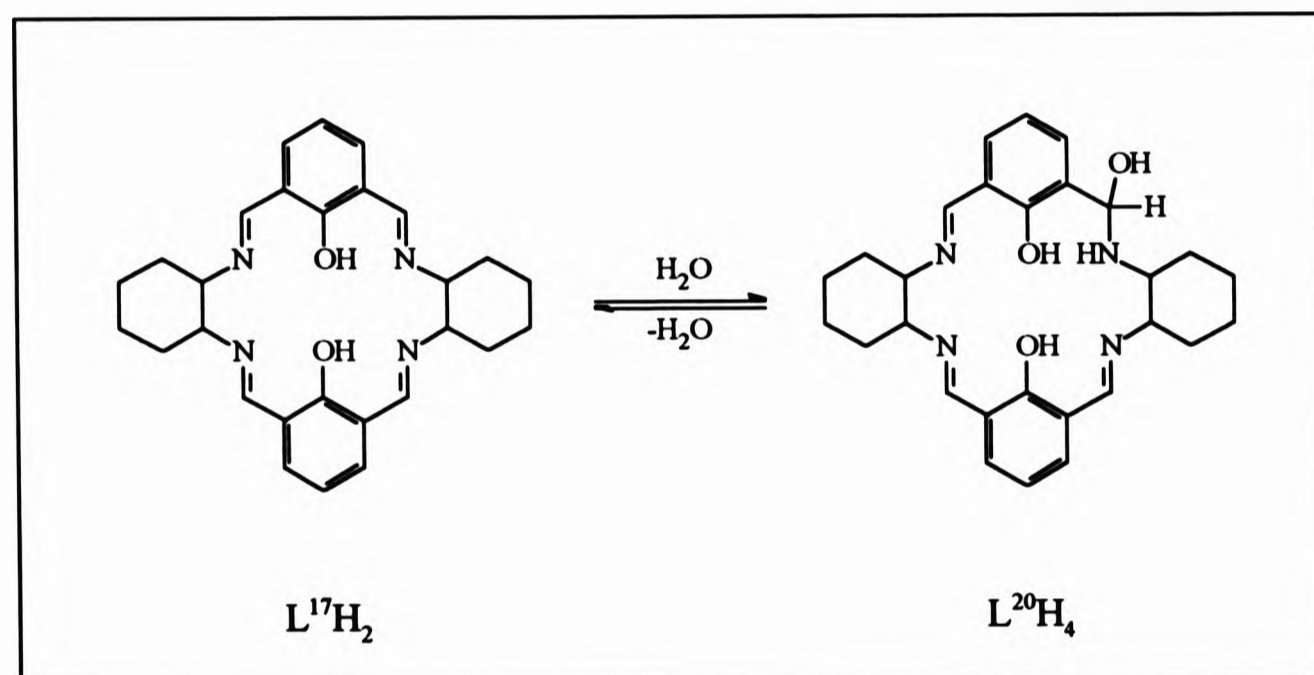


Fig. 5.1 The equilibrium between L^{17}H_2 and L^{20}H_4 in solution

Such complex ^1H NMR spectra were also reported for the template syntheses of {2} (Chapter 2) where an equilibrium was also taking place in solution,^[10] and other examples have been isolated in the solid state^[11] where the imino bond undergoes solvolytic attack.

The ^1H and ^{13}C NMR spectra cannot be solved fully whilst equilibrium is in progress. Four singlet bands at δ_{H} 8.29, 8.05, 7.50 and 7.41 correspond to three imino, $-\text{C}(\text{H})=\text{N}$, protons in L^{20}H_4 and to the single imino proton in L^{17}H_2 . Also, the aromatic region shows, as described for the spectrum in reference 9, seven signals and complex multiplets at δ_{H} 3.1 and 2.2. The cyclohexane protons are grouped as three bands at δ_{H} 1.95, 1.74 and 1.45. Three bands resonate at δ_{H} 14.22, 13.82 and 13.74, the former being broad, the latter two being sharp. These bands are assigned to the OH of both L^{17}H_2 and L^{20}H_4 which collapsed on D_2O addition to the solution. A *doublet* at δ_{H} 6.15 was assigned to the carbinolamine signal, $-\text{C}(\text{H})\text{OH}$, in L^{20}H_4 . The broad *singlet* at δ_{H} 7.49 was ascribed to the NH proton in L^{20}H_4 which couples to the $\text{C}(\text{H})\text{OH}$ of the carbinolamine but does not collapse or shift on addition of D_2O . NMR spectra of the complexes could not be obtained due to the insolubility of the samples; immediate precipitation was observed when the products were warmed in d_6 -DMSO.

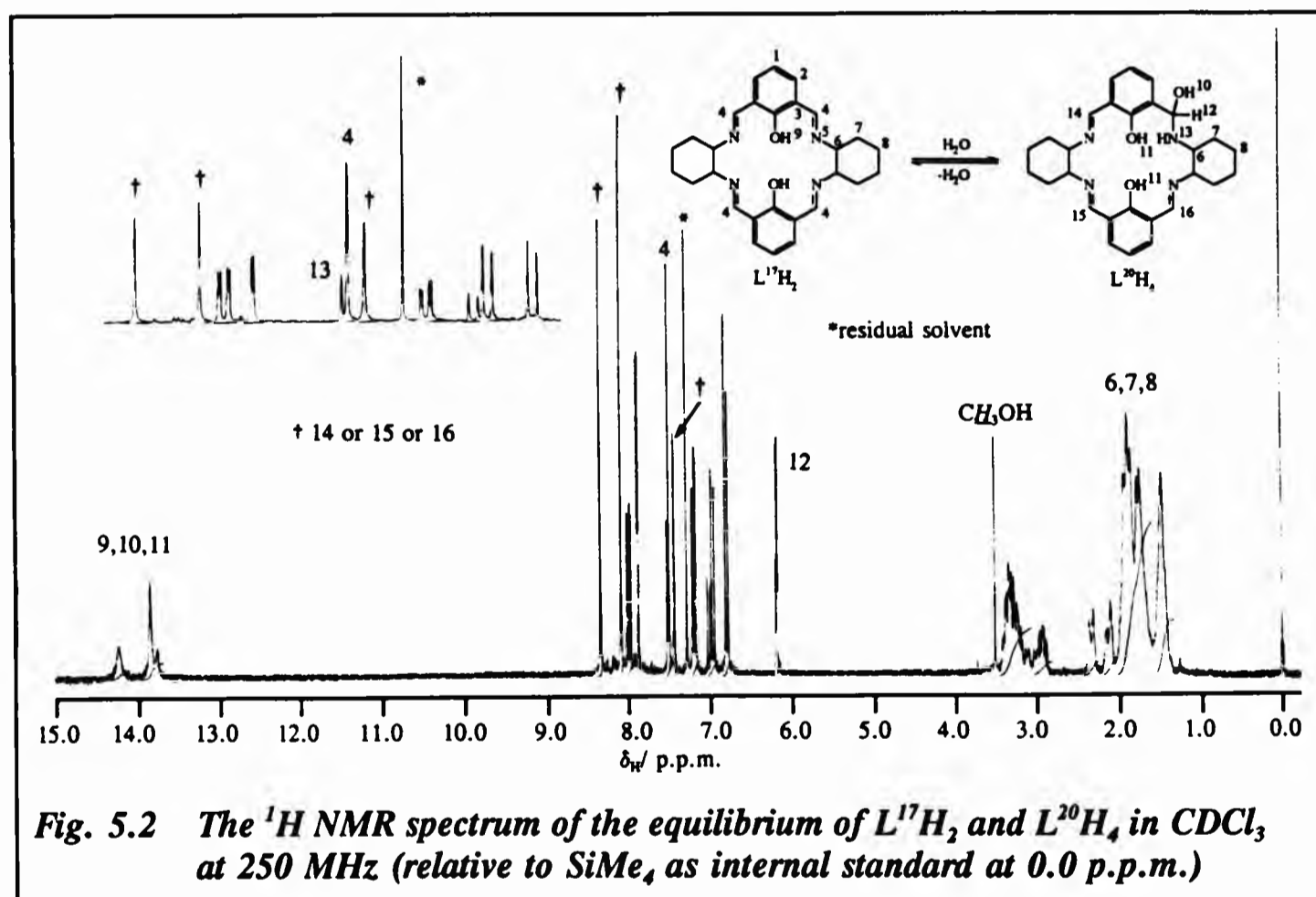


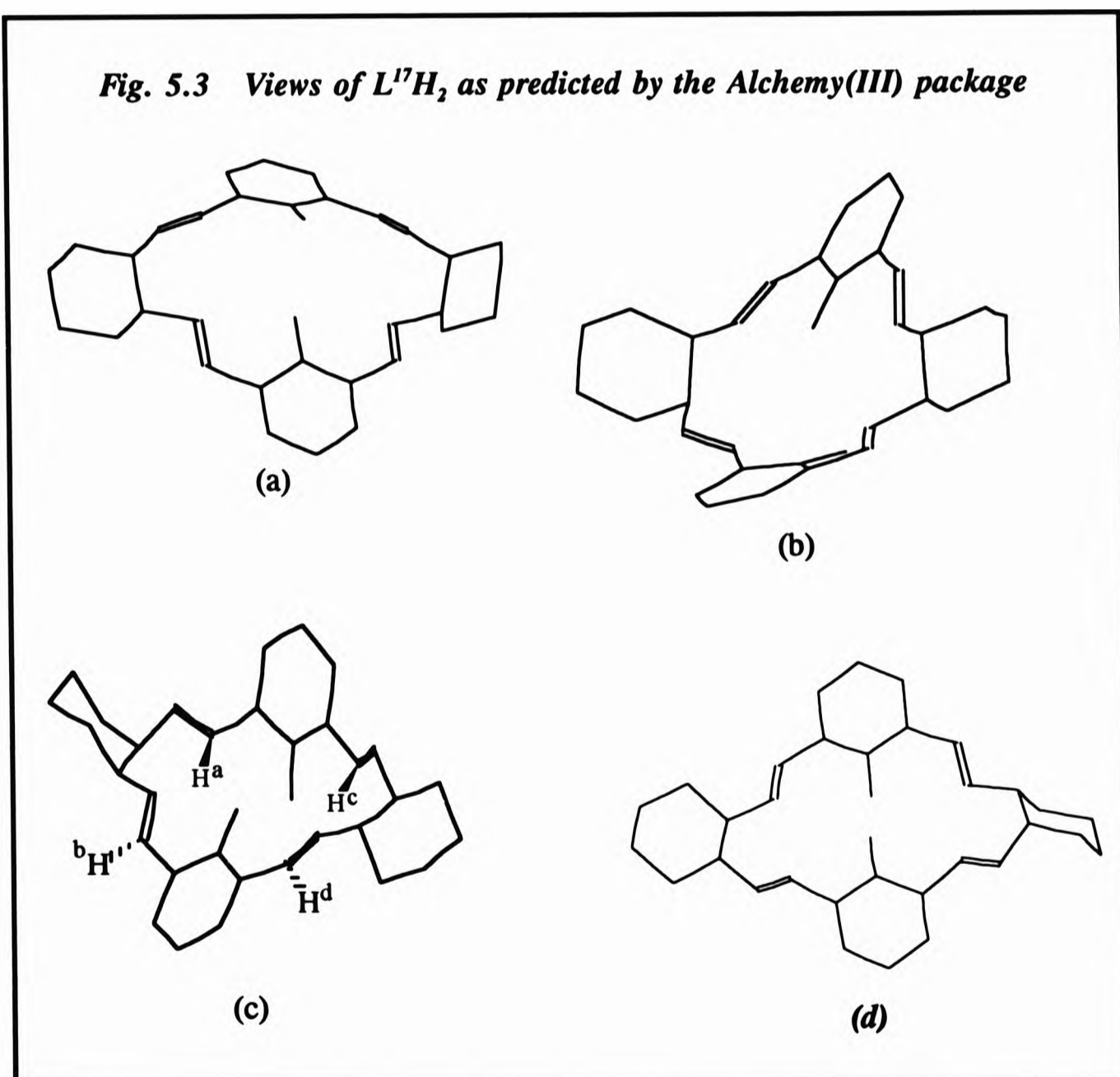
Fig. 5.2 The ^1H NMR spectrum of the equilibrium of L^{17}H_2 and L^{20}H_4 in CDCl_3 at 250 MHz (relative to SiMe_4 as internal standard at 0.0 p.p.m.)

5.2.4 Structure Adaptation of $L^{17}H_2$

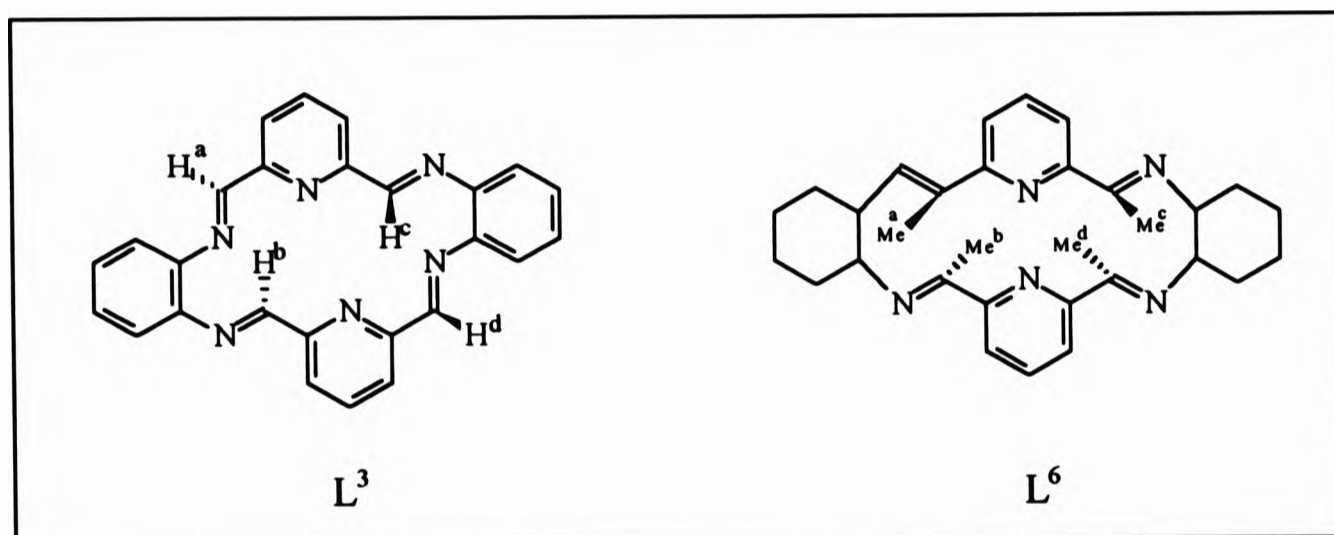
It has been established that the free ligand, $L^{17}H_2$, undergoes solvolytic attack and exists in equilibrium with the carbinolamine, $L^{20}H_4$, in solution. In the solid state the tetraimine formulation, as predicted by IR, LSIMS and microanalysis, is more stable and predominates.

Studies using the Alchemy(III) Molecular Modelling package indicate the same stepped arrangement of $L^{17}H_2$, as described crystallographically for L^6 (Chapter 2).

Fig. 5.3 Views of $L^{17}H_2$, as predicted by the Alchemy(III) package



The comparison between L^3 and L^6 was discussed in Chapter 2. $L^{17}H_2$ adopts a conformation which is different to L^3 ^[12] in that the imino protons, H^{a-d} (Fig. 5.3c) have the same arrangement as for the methyl groups of L^6 . That is, H^a and H^c point behind the plane of the paper and H^b and H^d point out of the plane of the paper. As both L^6 and $L^{17}H_2$ adopt the same conformation, as opposed to that of L^3 , it is reasonable to state that the arrangement (two back, a and c - two forward, b and d) of the former two ligands is dictated by the (\pm)-*trans*- conformation of the diaminocyclohexane. The planar adaptation of 1,2-diaminobenzene causes the alternation of the imine bonds in L^3 (one back - one forward - one back - one forward in the order a, c, b, d).



The structure of $[xH_4](PF_6)_2$, where $x = 3$, (Fig. 5.4) shows a highly unusual folded conformation,^[2] similar to that given by calixarenes,^[13] exposing the nitrogen and oxygen donor atoms.

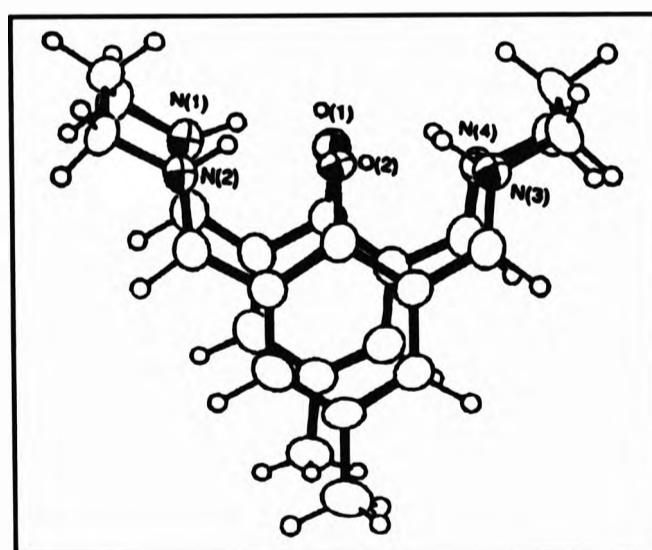
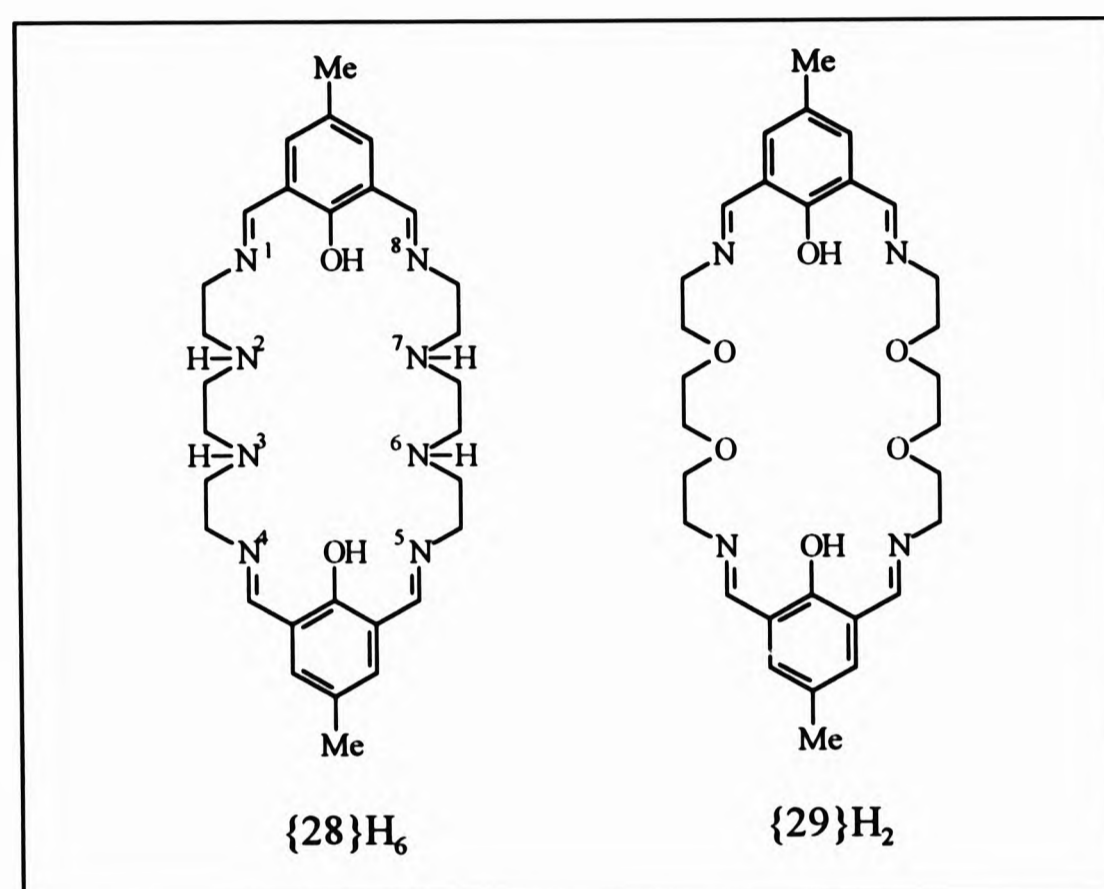


Fig. 5.4 The crystal structure of $[xH_4]^{2+}$ (reproduced from ref. 2)

Although some acyclic compartmental Schiff bases with lanthanide and actinide metals have been reported,^[6,14-16] lanthanide and actinide macrocyclic Schiff bases with bridge phenolic hosts are limited.^[6,16-18] In particular, lanthanide complexes of $\{27\}H_2$ and $L^{18}H_2$ have not been reported.



Kahwa *et al.* have reported dinuclear lanthanide metal complexes of $\{28\}H_6$ ^[17] and $\{29\}H_2$ ^[19] under the same reaction conditions as carried out for this work. Two schemes have been proposed for lanthanide co-ordination to $\{28\}H_6$ depending on the size of the metal.^[17] Firstly, for the larger lanthanide metals, one metal co-ordinates to the phenolic oxygen atom and the nitrogen atoms 1, 2, 7 and 8 whilst the other metal links to the second oxygen atom and the nitrogen atoms 3, 4, 5 and 6. This scheme requires that the metal be large enough to co-ordinate to the three adjacent N-O-N sites. It was also claimed that it became increasingly difficult to prepare complexes of the ligand as the radius of the lanthanide metal decreased. The second scheme involves one metal co-ordinating to both of the oxygen atoms and nitrogen atoms 1, 2, 3 and 4 and the other metal is also co-ordinated to the oxygen atoms but

to the nitrogen atoms 5, 6, 7 and 8. This scheme is favoured by smaller lanthanide metals, Gd - Lu, and is shown by the crystal structure of $[\text{Gd}_2\{29\}(\text{NO}_3)_4]$ ^[18,19] (Fig. 5.5).

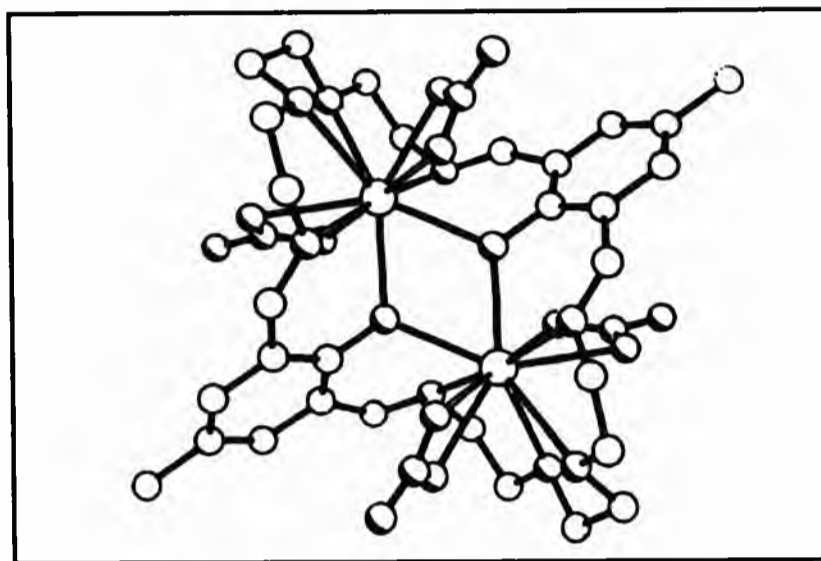


Fig. 5.5 *The crystal structure of $[\text{Gd}_2\{29\}(\text{NO}_3)_4]$ adopting the co-ordination discussed in the second scheme, see text. (reproduced from ref. 19)*

With the support of these schemes it is possible to accept the structure proposed for the dysprosium(III) complex, $[\text{Dy}_2\text{L}^{19}\text{H}_3(\text{NO}_3)_4]^+$ involving [4+4] condensation.

For dysprosium to cause the formation of the L^{19} ligand it would have to undergo the co-ordination described for the second scheme whereas for the formation of L^{18} the dysprosium would have to adopt the co-ordination described by the first scheme. If the co-ordination schemes are to be adhered-to strictly then dysprosium, being one of the smaller lanthanide metals, should favour the synthesis of L^{19} and hence [4+4] condensation. The proposed mechanism would be as follows:

During the template procedure the metal is added to a solution of the 2,6-diformylphenol and co-ordinates to the phenolic oxygen and to one of the aldehydic oxygen atoms as described for the second scheme and shown in Fig. 5.6(a). That the metal only co-ordinates to the phenolic oxygen atom and to only one aldehydic oxygen atom was proved crystallographically by Kahn.^[20]

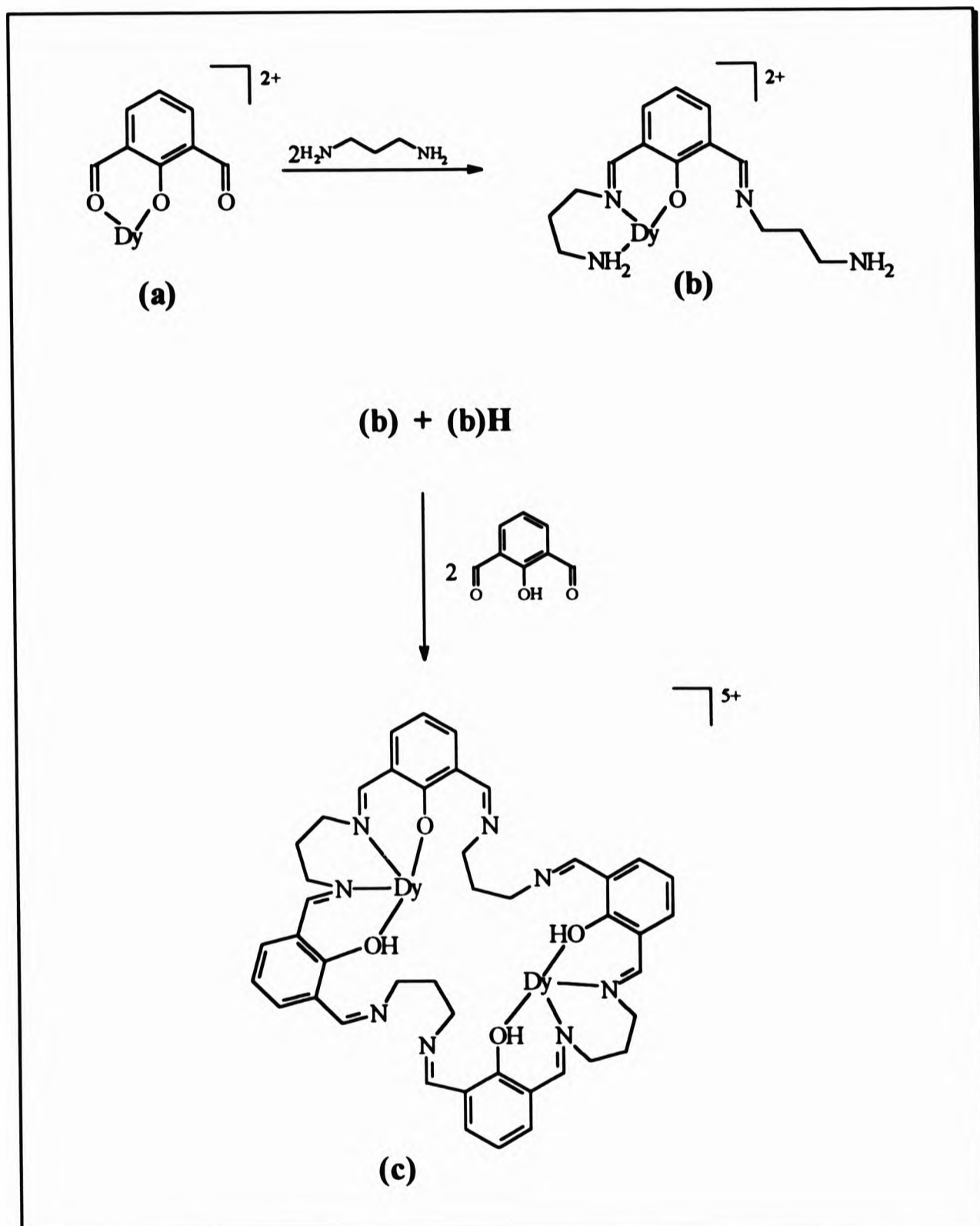


Fig. 5.6 A probable mechanism to the dinuclear [4+4] condensation product $[\text{Dy}_2\text{L}^{\text{19}}\text{H}_3(\text{NO}_3)_4]^{5+}$. Co-ordinated water molecules, nitrate groups and lattice water molecules are omitted for clarity.

On addition of the diamine, the co-ordinated and the free carbonyl oxygen atoms undergo Schiff condensation resulting in the structure given in Fig. 5.6(b). As shown by Kahn^[20] the nitrogen atoms which are not in the same sector as the dysprosium do not co-ordinate to the metal. Two moles of (b) (Fig. 5.6), one in the protonated form, (b)H, then react with two moles of 2,6-diformylphenol to give the cyclised [4+4] condensation product (c). The magnetic moment does not indicate Dy-Dy interaction since the μ_B value obtained was as expected for 2 independent metal ions. The ligand, $L^{19}H_3^-$, therefore, does not behave as a compartmental molecule but as a macrocyclic binucleating ligand in which the two metals ions are co-ordinated at a long distance from each other, with no bridging heteroatoms between them as shown in Fig. 5.6(c).^[21]

The question which arises is: *Why does dysprosium not form [4+4] condensation products with pyridyl as opposed to phenolic bridging and why does neodymium cause the formation of the [2+2] dimeric species, $[NdL^5(NO_2)_2]_2(NO_3)_2(OH)$, where hexaaza compounds (Chapter 2) are concerned?*

The answer to both parts of the question depends on the mechanism of the cyclisation and the metal size. It was mentioned in Chapter 2 that in general all the larger lanthanides (with the exception of lanthanum) would be expected to form dimeric [2+2] condensation products. The thought behind this assumption was that initially lanthanide metal nitrate or acetate salts are dinuclear, *i.e.* $Ln_2(NO_3)_6$, where two nitrate groups bridge two metals. This was proved crystallographically with $Y_2(OAc)_6 \cdot 4H_2O$.^[22] When these salts are used as templates for the hexaaza macrocycle syntheses the larger lanthanide metals are more exposed and protrude from the macrocyclic cavity and this allows for the bridging to be retained. For the smaller lanthanides, the metal is less exposed and *buried* within the macrocyclic cavity compared to the larger metals which brings the two macrocycles very close together thus causing interaction between the two. As a result of this interaction the bridging is caused to break and monomeric species are observed. [2+2] Products are obtained for the hexaaza macrocycles since the lanthanide metal, irrespective of size,

fits snugly into the cavity available from the 2,6-pyridinedialdehyde (Fig. 5.7). The size range of the lanthanide metals allows for a maximum of two dialdehydic units to co-ordinate to the metal. Addition of the diamine results, inevitably, in the [2+2] condensation products. On replacing the pyridine with phenol, the protruding hydroxyl group prevents the co-ordination of one of the carbonyl atoms leading to the mechanism discussed above.

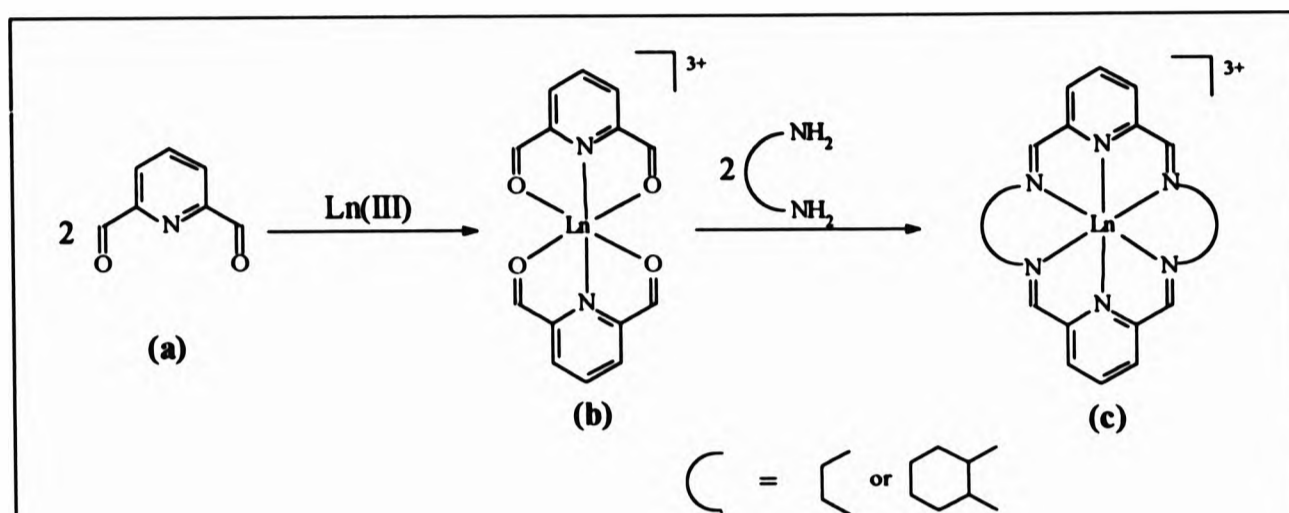


Fig. 5.7 The mode of co-ordination leading to [2 + 2] condensation in hexaaza compounds

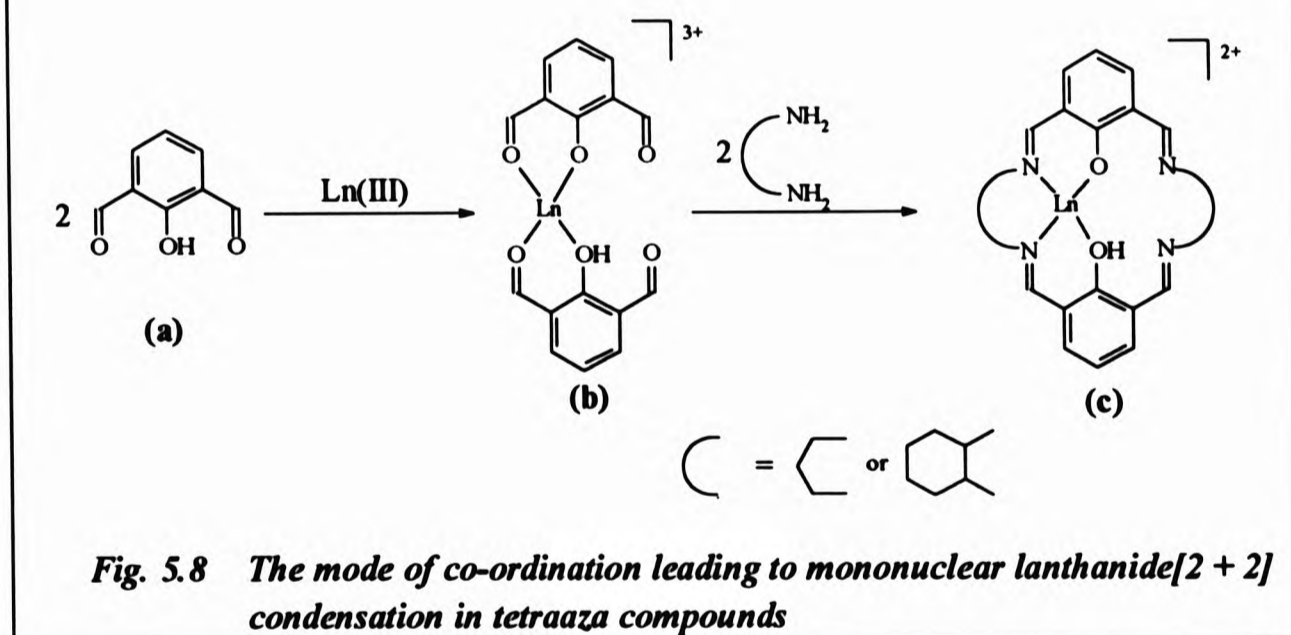
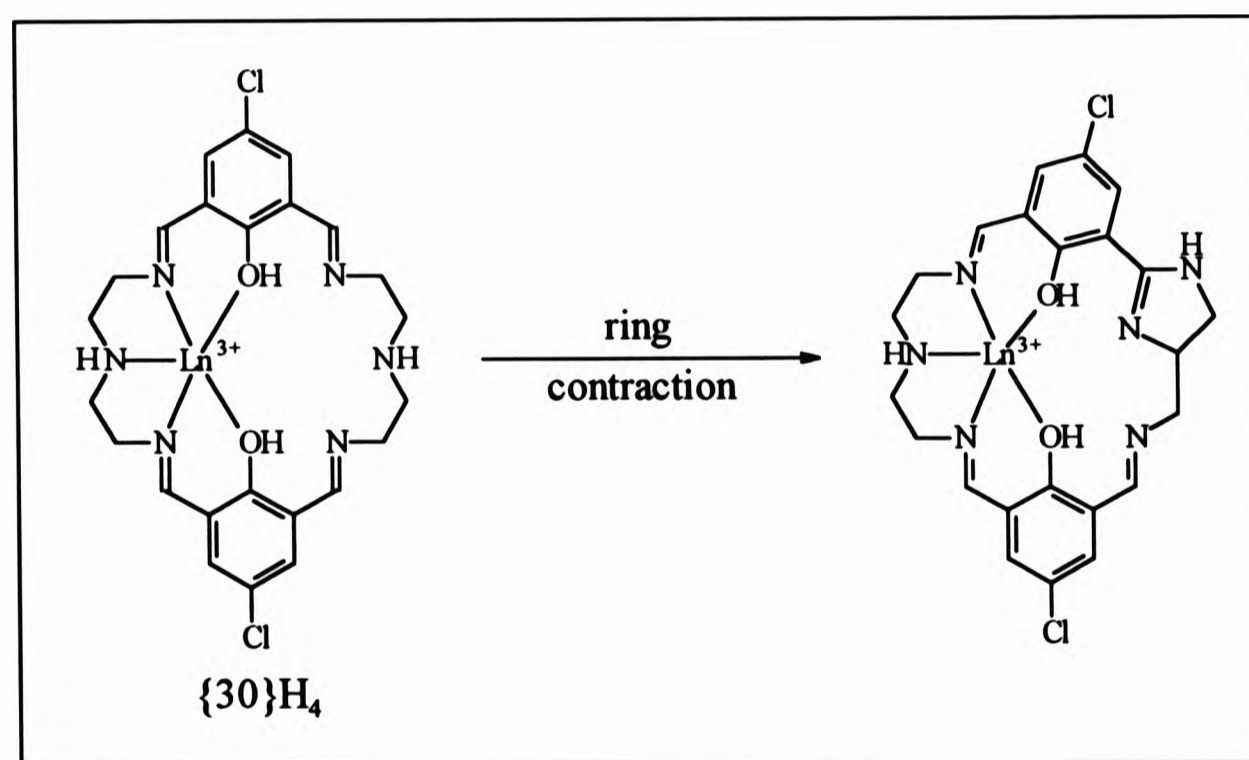


Fig. 5.8 The mode of co-ordination leading to mononuclear lanthanide[2 + 2] condensation in tetraaza compounds

The above mechanisms shed light onto the structure of the [2+2] lanthanide products with 2,6-diformylphenol. The metal is initially co-ordinated by the two molecules of 2,6-diformylphenol, again co-ordination only occurs from one carbonyl oxygen and the phenolic oxygen atoms (Fig. 5.8(b)). Cyclisation then occurs on addition of the

diamine (Fig. 5.8(c)). The co-ordination adopted by the metal as shown by (c), where two imino nitrogen atoms do not co-ordinate, supports the two C=N bands observed in the IR spectra for these complexes at *ca.* 1650 and *ca.* 1630 cm^{-1} .^[23]

For the template synthesis of $\{30\}\text{H}_4$, where the ligand adopts similar co-ordination to that shown in Fig. 5.8(c), ring contraction takes place.^[6] The contraction does not allow for the ligand to increase its denticity towards the metal but makes it "more compact thus allowing a more appropriate spatial arrangement of the donor atoms of the macrocyclic ligand around the lanthanide ion".^[6] Contraction is preferred to solvolysis across the imine bond and Robson and Pilkington^[1] suggested that solvolysis across the imine links for binucleating transition metal ligands or $\{26\}\text{H}_2$ and hence L^{18}H_2 "introduce rather than relieve strain".



5.2.5 Thermogravimetric Analysis

TG analyses were carried out on $[\text{Dy}_2(\text{L}^{19}\text{H}_3)(\text{NO}_3)_4(\text{MeOH})\text{H}_2\text{O}]\text{NO}_3 \cdot 4\frac{1}{2}\text{H}_2\text{O}$ and $[\text{Dy}(\text{L}^{17}\text{H})\text{NO}_3]\text{NO}_3 \cdot \text{MeOH} \cdot 3\frac{1}{2}\text{H}_2\text{O}$.

The thermogram of $[\text{Dy}_2\text{L}^{19}\text{H}_3(\text{NO}_3)_4(\text{MeOH})\text{H}_2\text{O}]\text{NO}_3 \cdot 4\frac{1}{2}\text{H}_2\text{O}$ showed the initial

loss of two water molecules between 60 - 80°C, with a mass decrease of 2.4% (calculated 2.4%). One and a half water molecules followed by one more water molecule were lost in the temperature ranges 80 - 105 and 105 - 130°C respectively. These four and a half water molecules correspond to the water of crystallisation. In the temperature range 130 - 160°C the co-ordinated methanol and water molecules were lost. At temperatures of 200 - 240°C, a mass decrease of 4.2 corresponded to a loss of one nitrate group (calculated 4.1%). At ca. 250°C the sample showed signs of decomposition by changing colour from orange-yellow to brown without melting. These results are summarised in Table 5.2.

Table 5.2 Thermogravimetric analysis of $[Dy_2L^{19}H_5(NO_3)_4(MeOH)H_2O]NO_3 \cdot 4\frac{1}{2}H_2O$

Temperature (°C)	Observed Mass Loss (%)	Calculated Mass Loss (%)	Observed Mass Loss (mol)	Inference
60 - 80	2.4	2.4	36	2H ₂ O
80 - 105	1.8	1.8	27	1½H ₂ O
105 - 130	1.1	1.3	20	1H ₂ O
130 - 160	3.3	3.3	50	1H ₂ O + 1MeOH
160 - 240	4.2	4.1	64	1NO ₃ ⁻

The TGA of $[Dy(L^{17}H)NO_3]NO_3 \cdot MeOH \cdot 3\frac{1}{2}H_2O$ showed a very gradual mass loss up to 160°C. At this temperature the TGA was stopped and the sample was reanalysed by physical and chemical techniques. The colour had not changed from red-brown and the broad band at ca. 3450 cm⁻¹ in the IR spectrum was no longer so prominent. Elemental analysis suggested the total loss of water and methanol such that the compound had become dehydrated. On standing at atmospheric pressure the

weight-loss was not recovered. In general, these compounds decompose at around 250°C confirming the high thermal stability of the macrocycle.

5.6 Conclusion

The synthesis of the novel ligand $L^{17}H_2$ was achieved *via* the direct reaction of 2,6-diformylphenol and (\pm)-*trans*-1,2-diaminocyclohexane and the lanthanide metal complexes of $[L^{17}H]^-$ and $[L^{18}H]^-$ were achieved *via* template procedures. Where dysprosium was the template for the formation of $[L^{18}H_2]$, the [4+4] condensation product, $[L^{19}H_3]^-$ was isolated.

Owing to extreme insolubility of these compounds, solution analyses (*i.e.* UV-VIS, NMR and relaxation rate studies) were restricted. The ability to isolate crystals for crystallographic studies was also affected.

Due to limited availability of 2,6-diformylphenol, this study was restricted to the synthesis of the imino compounds, although borohydride reduction of $L^{17}H_2$ can be achieved by the same procedure which was used to reduce L^5 to L^9 , yielding products which would be more soluble in common solvents.

The reaction of the reduced product of $L^{17}H_2$ with 2,4-dimethylphenol and aq. methanal, would again, cause the formation of the two inner 5-membered rings as for the synthesis of L^{15} with no involvement of 2,4-dimethylphenol due to the repulsion imposed by the cyclohexyl rings.

5.5 References

1. R. Robson and N. H. Pilkington, *Aust. J. Chem.*, 1970, **23**, 225.
2. A. J. Atkins, A. J. Blake and M. Schröder, *J. Chem. Soc., Chem. Commun.*, 1993, 353.
3. P. Guerriero, S. Tamburini, P. A. Vigato, R. Seraglia and P. Traldi, *Org. Mass Spectrom.*, 1992, **27**, 231.
4. K. Nakamoto, *Infrared and Raman Spectra of Inorganic and Coordination Compounds*, 3rd edn., Wiley, New York, 1973.
5. S. D. Robinson and M. F. Uttley, *J. Chem. Soc., Dalton Trans.*, 1973, 1912.
6. P. Guerriero, U. Casellato, S. Tamburini, P. A. Vigato and R. Graziani, *Inorg. Chim. Acta*, 1987, **129**, 127.
7. M. Tadokoro, H. Sakiyama, N. Matsumoto, M. Kodera, H. Okawa and S. Kida, *J. Chem. Soc., Dalton Trans.*, 1992, 313.
8. H. Okawa and S. Kida, *Bull. Chem. Soc. Jpn*, 1972, **45**, 1759.
9. S. K. Mandal and K. Nag. *J. Chem. Soc., Dalton Trans.*, 1983, 2429.
10. K. K. Abid and D. E. Fenton, *Inorg. Chim. Acta*, 1984, **95**, 119.
11. S. Waiker, PhD Thesis, University of North London, 1992.
12. T. W. Bell and F. Guzzo, *J. Chem. Soc., Chem. Commun.*, 1986, 769.
13. A. McKervey and V. Böhmer, *Chem. Br.*, 1992, **28**, 724.
14. W. D. Carlisle, D. E. Fenton, D. C. Mulligan, P. B. Roberts, P. A. Vigato and S. Tamburini, *Inorg. Chim. Acta*, 1987, **126**, 233.
15. I. A. Kahwa, F. R. Fronczek and J. Selbin, *Inorg. Chim. Acta*, 1987, **126**, 227.
16. P. Guerriero, S. Tamburini, P. A. Vigato and C. Bellini, *Inorg. Chim. Acta*, 1991, **189**, 19.
17. I. A. Kahwa, J. Selbin, T. C.-Y. Hsieh and R. A. Laine, *Inorg. Chim. Acta*, 1986, **118**, 179.
18. K. D. Matthews, R. A. Fairman, A. Johnson, K. V. N. Spence, I. A.

- Kahwa, G. L. McPerson and H. Robotham, *J. Chem. Soc., Dalton Trans.*, 1993, 1719.
19. I. A. Kahwa, S. Folkes, D. J. Williams, S. V. Ley, C. A. O'Mahoney and G. L. McPherson, *J. Chem. Soc., Chem. Commun.*, 1989, 1531.
 20. E. Bakalbassis, O. Kahn, J. Sinton, J. C. Trombe and J. Galy, *J. Chem. Soc., Chem. Commun.*, 1991, 755.
 21. P. Guerriero, P. A. Vigato, J.-C. Bünzli and E. Moret, *J. Chem. Soc., Dalton Trans.*, 1990, 647.
 22. S. W. A. Bligh, E. G. Evagorou, M. McPartlin and R. Shah, unpublished results.
 23. H. Okowa and S. Kida, *Inorg. Nucl. Chem. Lett.*, 1971, 7, 751.

CHAPTER 6

Chapter 6: EXPERIMENTAL

(References to this Chapter are listed on page 263)

6.1 Reagents and General Analytical Techniques

The reagents and solvents were generally of GPR grade, obtained commercially from Aldrich Chemical Company Ltd and used without further purification, unless otherwise stated. Radioactive yttrium-90 was provided in a solution of 0.04 mol dm^{-3} hydrochloric acid by Amersham International plc.

TLC was carried out using precoated silica, aluminium or cellulose Merck Kieselgel 60 F₂₅₄ plates. The absorbent used for separatory column chromatography was Merck Kieselgel 60 silica (70 - 230 mesh).

FT-IR spectra were recorded as pressed potassium bromide discs (3 mm or 16 mm) for solid samples, with potassium bromide as background, or as neat, oil or paste films on a Bio-rad FTS-40 spectrometer in the range $400 - 4000 \text{ cm}^{-1}$.

Electronic spectra were carried out on a UV-VIS Shimadzu UV-2100 spectrometer, with 1 cm pathlength, in the range 200 - 900 nm.

Fluorescence spectra were obtained on a Spex Nova 3 spectrometer at the Amersham Laboratories.

Circular dichroism spectroscopy was carried out at Birkbeck College, University of London.

Mass spectrometry was carried out on a Kratos Profile spectrometer with a Sun Data Station and recorded as EI or LSIMS spectra with *m*-nitrobenzyl alcohol as matrix.

High resolution FT-NMR spectra were recorded, at ambient temperature, on a Bruker AM 250 at 250 MHz and less frequently on a Jeol 270 or 500 MHz

spectrometers. Tetramethylsilane was used as internal standard. A Bruker minispec (10 MHz) or multispec (20 MHz) RS 32 connected to an IBM PC/20B data station was employed to detect relaxation times at Birkbeck College, University of London.

Elemental analysis (C, H, N) was determined with a Carlo Elba 1160 instrument.

Room temperature magnetic susceptibilities were measured using a Johnson Matthey balance. The instrument was calibrated with a mercury tetrathiocyanatocobaltate(II), the measurements were carried out in duplicate and the magnetic susceptibilities were corrected for diamagnetism of the ligand.^[1]

Instant thin layer chromatograms were obtained on a Thin Layer Radio-Chromatography phase scanner/analyser at the Amersham International laboratories.

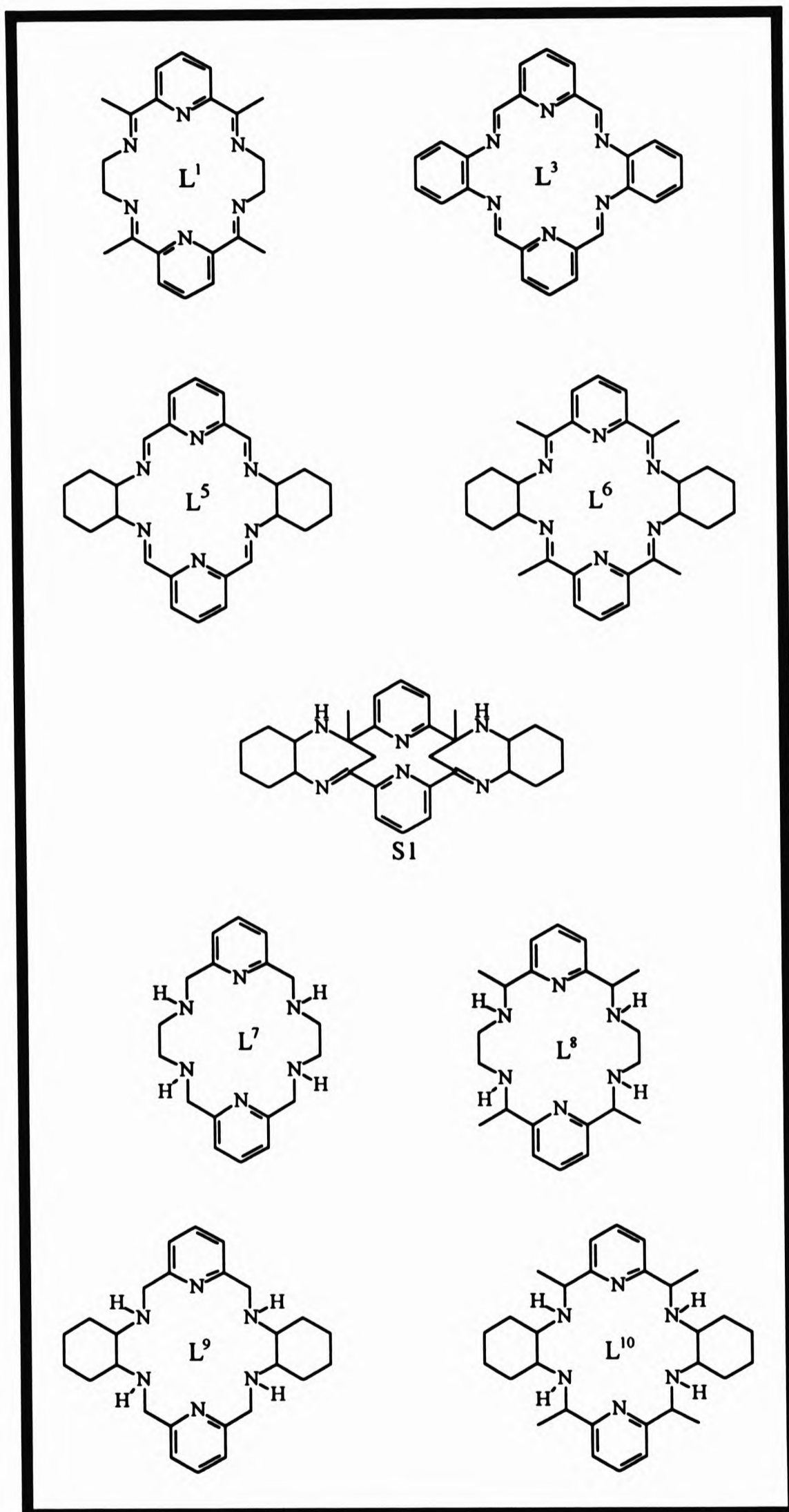
A heating rate of *ca.* 3°C min⁻¹ was used when running thermogravimetric analyses on a Stanton HT-SM Thermobalance.

Melting points were determined on a Gallenkamp melting point apparatus and were uncorrected.

X-ray crystallography data were collected on a Philips PW1100 four-circle diffractometer using Mo-K α radiation from a graphite monochromator.

6.2 Syntheses and Reactions

Precaution: Perchlorate salts are powerful oxidising agents and can be explosive. They should be used in small quantities, behind protective shielding and with extreme caution !



Preparation of 2,6-pyridinedialdehyde.^[2]

Selenium(IV) dioxide (3.99 g, 36 mmol) was added to a well-stirred solution of 2,6-pyridinedimethanol (5.02 g, 36 mmol) in dry, predistilled, 1,4-dioxane (100 cm³) and refluxed for 4 h. The black precipitate was filtered under gravity and discarded. The solvent was removed from the yellow filtrate under reduced pressure and the resulting pink-brown solid was recrystallised from dichloromethane/petroleum ether (40-60°C) (5:1) and dried *in vacuo* to give 2,6-pyridinedialdehyde (4.21 g, 87%). m.p. 113 - 116°C (lit.,^[2] 115 - 117); ¹H NMR (CDCl₃) δ/p.p.m: 8.2 (3H, m, Ar), 10.2 (2H, s); also identified by comparison of its IR spectrum with an authentic sample purchased from Aldrich Chemical Company Ltd.

Preparation of neodymium(III) nitrate hexahydrate.

Neodymium(III) oxide (10.04 g, 29.8 mmol) was dissolved in excess nitric acid (*ca.* 50 cm³) and heated gently on a steam bath until a sticky solid remained. The solid was dissolved in excess methanol which was removed under a stream of nitrogen to give the air stable lavender solid of neodymium(III) nitrate hexahydrate (21.07 g, 81%). The brown ring test was applied to confirm the presence of the nitrate anion; some of the product was dissolved in deionised water and added to a solution of the iron(II) sulphate heptahydrate in water. Slow addition of conc. sulphuric acid resulted in a brown colouration and a brown ring indicative of the nitrate anion. The sample was used without further purification or analysis.

Preparation of phosphate buffer^[3]

Sodium chloride (2.03 g, 34.7 mmol), potassium chloride (0.05 g, 0.7 mmol), sodium phosphate (0.36 g, 3.0 mmol) and potassium phosphate (0.06 g, 3.0 mmol) were dissolved in deionised water (200 cm³) and adjusted to pH 7.4 with dilute hydrochloric acid (6 mol dm⁻³). The solution was made up quantitatively to 250 cm³.

Synthesis of BaL¹(NO₃)₃.

A solution of 1,2-diaminoethane (1.24 g, 20.7 mmol) in methanol (20 cm³) was added dropwise to a refluxing suspension of 2,6-diacetylpyridine (3.26 g, 20.0 mmol) and barium(II) nitrate (2.63 g, 10.0 mmol) in methanol (80 cm³) and

heated for 4 h. The resulting orange-brown mixture was filtered under gravity and the volume of the filtrate was reduced, under reduced pressure, to *ca.* 40 cm³. White crystals of BaL¹(NO₃)₃ (2.74 g, 43%) precipitated on standing at room temperature which were filtered under suction, washed with methanol (2 x 5 cm³) and dried *in vacuo* over calcium chloride. Found: C, 41.8; H, 4.2; N, 17.7. calc. for C₂₂H₂₆N₈O₆Ba: C, 41.6; H, 4.1; N, 17.6%.

Synthesis of [GdL³Cl₂(MeOH)(H₂O)]Cl.1½H₂O.

A solution of 1,2-diaminobenzene (1.62 g, 15.0 mmol) in methanol (20 cm³) was added dropwise, over ½ h, to a refluxing solution of gadolinium chloride hexahydrate (2.79 g, 7.5 mmol) and 2,6-pyridinedialdehyde (2.04 g, 15.1 mmol) in methanol (80 cm³). The mixture was refluxed for 3 h. The solvent was removed under reduced pressure to leave an oil which on work-up with diethyl ether resulted in a bright yellow solid. Recrystallisation from methanol/ diethyl ether gave [GdL³Cl₂(MeOH)(H₂O)]Cl.1½H₂O (3.41 g, 61%) which was filtered under suction, washed with methanol (5 cm³) and diethyl ether (2 x 5 cm³) and dried *in vacuo* over calcium chloride. Found: C, 43.1; H, 3.4; N, 11.1. C₂₇H₂₇N₆O_{3½}Cl₃Gd requires: C, 43.5; H, 3.6; N, 11.3%.

Synthesis of L⁵.

To a refluxing solution of 2,6-pyridinedialdehyde (2.04 g, 15.1 mmol) in methanol (80 cm³) was added dropwise a solution of (±)-*trans*-1,2-diaminocyclohexane (1.7 g, 15.0 mmol) in methanol (10 cm³). The white solid of L⁵ (2.22 g, 68%) precipitated during the 3 h reflux and was filtered hot, washed with methanol (2 x 10 cm³) and diethyl ether (1 x 10 cm³) and dried *in vacuo*. m.p. 349 - 352°C; Found: C, 73.3; H, 7.1; N, 19.9. calc. for C₂₆H₃₀N₆: C, 73.2; H, 7.0; N, 19.7%.

Synthesis of the metal complexes of L⁵.

Two methods were employed depending on the metal salt.

(a) *The use of nitrate or perchlorate salts:* The procedure will be illustrated with gadolinium(III) nitrate and also includes the syntheses of the dimeric products of yttrium(III) and neodymium(III). A solution of (±)-*trans*-1,2-

diaminocyclohexane (1.7 g, 15.0 mmol) in methanol (10 cm³) was added dropwise over ½ h to a solution of gadolinium(III) nitrate hexahydrate (3.38 g, 7.5 mmol) and 2,6-pyridinedialdehyde (2.13 g, 15.0 mmol) in methanol (100 cm³) and heated for 4 h. A white solid precipitated analysing for [GdL⁵(NO₃)₂]NO₃ which was filtered hot under suction, washed with cold methanol (2 x 10 cm³) and diethyl ether (5 cm³) and dried *in vacuo* over calcium chloride. Analytical data are shown in Table 6.1.

- (b) *The use of chloride salts:* The procedure will be illustrated with yttrium(III) chloride. A solution of (±)-*trans*-1,2-diaminocyclohexane (1.3 g, 10.0 mmol) in methanol (5 cm³) was added dropwise over ½ h to a solution of yttrium(III) chloride hexahydrate (1.69 g, 6 mmol) and 2,6-pyridinedialdehyde (1.52 g, 10.0 mmol) in methanol (100 cm³) and heated for 7 h. The volume of the reaction mixture was reduced to *ca.* 40 cm³, under reduced pressure, and allowed to stand at room temperature over several weeks causing the precipitation of the white crystals of [YL⁵Cl₂(H₂O)₂·3½H₂O]. The crystals were filtered under gravity, washed with methanol (2 x 10 cm³) and diethyl ether (5 cm³) and dried *in vacuo* over calcium chloride. Analytical data are shown in Table 6.1.

Synthesis of L⁶.

- (a) *Attempted template synthesis of L⁶ yielding tris-[(±)-trans-1,2-diaminocyclohexane]trinitrato yttrium(III):* To a stirring mixture of 2,6-diacetylpyridine (0.42 g, 2.6 mmol) and yttrium(III) nitrate pentahydrate (0.70 g, 1.9 mmol) in methanol (10 cm³) was added dropwise a solution of (±)-*trans*-1,2-diaminocyclohexane (0.3 g, 2.6 mmol) in methanol (2 cm³). The white crystalline solid of tris-[(±)-*trans*-1,2-diaminocyclohexane]trinitrato yttrium(III) (90 mg, 17%) precipitated instantly from the reaction mixture and was filtered under suction, washed with methanol (2 x 5 cm³) and dried *in vacuo* over calcium chloride. ¹H NMR (D₂O) δ/ p.p.m.: 1.32 (12H, m), 1.76 (6H, m), 1.99 (6H, m), 2.78 (4H, m); ¹³C broad band proton decoupled (D₂O) δ/ p.p.m.: 26.74, 34.69, 57.39.

Table 6.1 Analytical data for the metal complexes of L⁵

Complex	Yield (%)	Found (%)			Required (%)		
		C	H	N	C	H	N
BaL ⁵ (ClO ₄) ₂	44	40.8	4.0	11.1	40.9	3.9	11.0
[LaL ⁵ (NO ₃) ₂]NO ₃	56	41.7	4.3	16.7	41.5	4.0	16.8
[YL ⁵ Cl ₂ (H ₂ O) ₂]Cl.3½H ₂ O	33	43.3	6.0	11.6	43.3	5.7	11.7
{YL ⁵ (NO ₃) ₂ } ₂ .NO ₃ (OH)].MeOH.½H ₂ O	66	45.5	4.8	16.9	45.5	4.7	17.0
{[NdL ⁵ (NO ₃) ₂ } ₂ .NO ₃ (OH)]MeOH.H ₂ O	68	42.1	4.4	15.7	41.9	4.4	15.7
[GdL ⁵ Cl ₂ (H ₂ O)]Cl	64	44.0	5.0	11.1	44.1	4.5	11.9
[GdL ⁵ (NO ₃) ₂]NO ₃	78	39.8	4.4	16.7	40.1	3.9	16.4
[DyL ⁵ (NO ₃) ₂]NO ₃	57	40.4	3.9	16.3	40.3	3.9	16.3

- (b) *Non-template synthesis*: To a refluxing suspension of 2,6-diacetylpyridine (5.04 g, 31.0 mmol) in acetonitrile or methanol (150 cm³) was dropwise added a solution of (\pm)-*trans*-1,2-diaminocyclohexane (3.5 g, 31 mmol) in acetonitrile or methanol (150 cm³) over a period of 2 h. Reflux was continued for 4 h during which the white solid of L⁶ precipitated. The solid was filtered hot, washed with fresh acetonitrile (3 x 15 cm³) and diethyl ether (1 x 10 cm³) and dried *in vacuo* yielding 4.26 g, 57%. m.p. 304 - 315°C (decomp); Found: C, 74.8; H, 7.9; N, 17.4. calc. for C₃₀H₃₈N₆: C, 74.7; H, 7.9; N, 17.4%.
- (c) *In the presence of barium(II)*. Dropwise addition of a solution of (\pm)-*trans*-1,2-diaminocyclohexane (2.1 g, 18.4 mmol) in methanol (20 cm³) to a refluxing solution of 2,6-diacetylpyridine (3.05 g, 18.7 mmol) and barium(II) chloride dihydrate (2.24 g, 9.2 mmol) in methanol (100 cm³) resulted in the precipitation of the white solid of S1 (1.26 g, 28%) which was filtered hot under suction. m.p. 291 - 299°C (decomp); Found: C, 74.9; H, 8.2; N, 17.6. calc. for C₃₀H₃₈N₆: C, 74.7; H, 7.9; N, 17.4%. The filtrate was allowed to stand at room temperature overnight causing the precipitation of the white compound of L⁶ (0.93 g, 21%) which analysed spectroscopically and analytically similar to the compound obtained for reaction (b) above.

Metal complexation of L⁶

(a) *Attempted complexation with lanthanum (III)*:

- (i) *in methanol*. To a refluxing suspension of L⁶ (0.23 g, 0.5 mmol) in methanol (50 cm³) was added dropwise a solution of lanthanum(III) nitrate hexahydrate (0.21 g, 0.5 mmol) in methanol (5 cm³) and reflux continued for 6 h. No change in the reaction mixture took place and L⁶ was recovered uncomplexed (0.22 g, 96% recovery).
- (ii) *in dichloromethane/ acetonitrile*.
Hydroxy-tris[(\pm)-*trans*-1,2diaminocyclohexane] trinitrato lanthanum(III) was obtained when a solution of lanthanum nitrate hexahydrate (0.24 g, 0.5 mmol)

in acetonitrile was added to a refluxing suspension of L^6 in dichloromethane (50 cm^3).

- (b) *Complexation with copper(II)*: A dark green viscous mixture formed when a solution of copper(II) perchlorate hexahydrate (0.59 g, 1.6 mmol) in methanol (10 cm^3) was added to a refluxing suspension of L^6 (0.50 g, 1.0 mmol) in methanol (60 cm^3). A dark brown microcrystalline precipitate was obtained during the 5 h reflux which was filtered hot and recrystallised from acetonitrile yielding $[\text{Cu}L^6(\text{H}_2\text{O})](\text{ClO}_4)_2(\text{MeOH})(\text{H}_2\text{O})$ (0.22 g, 26%); Found: C, 46.0; H, 5.7; N, 10.5. $\text{C}_{31}\text{H}_{46}\text{N}_6\text{O}_{11}\text{Cl}_2\text{Cu}$ requires: C, 45.8; H, 5.7; N, 10.3%.

Synthesis of $[\text{L}^7\text{H}_4]\text{Br}_4$ and $[\text{L}^8\text{H}_4]\text{Br}_4$.

A typical procedure is described for the synthesis of $[\text{L}^8\text{H}_4]\text{Br}_4$: To a refluxing suspension of barium(II) chloride dihydrate (1.12 g, 4.6 mmol) and 2,6-diacetylpyridine (1.54 g, 9.4 mmol) in methanol (150 cm^3) was added dropwise a solution of 1,2-diaminoethane (0.6 g, 9.4 mmol). The mixture was refluxed for 3 h and cooled to 0°C . A first portion of sodium borohydride (2.26 g, 60 mmol) and a second portion (1.14 g, 30 mmol) $\frac{1}{2}$ h later was added to the stirring mixture slowly and in incremental amounts whilst maintaining the temperature at 0°C . The reaction mixture was allowed to reach room temperature whilst stirring overnight and concentrated to dryness under reduced pressure. Extraction of the white solid with dichloromethane ($4 \times 50\text{ cm}^3$) afforded an orange-red oil on removal of the solvent under reduced pressure. Dropwise addition of hydrobromic acid (*ca.* 5 cm^3 of 48% solution in water) to a solution of the oil in methanol (*ca.* 15 cm^3) yielded the white solid of $[\text{L}^8\text{H}_4]\text{Br}_4$ (2.16 g, 68%) which was filtered under suction, washed with methanol ($3 \times 15\text{ cm}^3$) and diethyl ether (15 cm^3) and dried *in vacuo*. Although not necessary, further purification was possible by recrystallisation from deionised water. Found: C, 37.4; H, 5.4; N, 12.1. $\text{C}_{22}\text{H}_{38}\text{N}_6\text{Br}_4$ requires: C, 37.4; H, 5.4; N, 11.9%.

For a typical synthesis of $[\text{L}^7\text{H}_4]\text{Br}_4 \cdot \frac{1}{2}\text{H}_2\text{O}$: yield 51% relative to 5.03 g, 37 mmol of 2,6-pyridinedialdehyde; Found: C, 32.6; H, 4.7; N, 12.7. $\text{C}_{18}\text{H}_{31}\text{N}_6\text{Br}_4\text{O}_{\frac{1}{2}}$ requires: C, 32.8; H, 4.7; N, 12.7%.

Isolation of L⁸-meso:

[L⁸H₄]Br₄ (3.56 g, 5 mmol) was dissolved in a mixture of deionised water/ concentrated hydrochloric acid (10 : 10 cm³) and refluxed for 3 h. The solvent was removed under reduced pressure and the resulting oil was triturated with hot ethanol (ca. 30 cm³) causing the recovery of [L⁸H₄]Br₄ (2.93 g, 83%). Allowing the filtrate to stand overnight at room temperature afforded colourless crystals of L⁸-meso (0.39 g, 11%) which were filtered under gravity, washed with methanol (2 x 10 cm³) and air dried.

Synthesis of L⁹ and L¹⁰.

A typical procedure is described for L⁹: To a refluxing suspension of barium(II) chloride dihydrate (1.83 g, 7.5 mmol) and 2,6-pyridinedialdehyde (2.06 g, 15.3 mmol) in methanol (150 cm³) was added dropwise a solution of (±)-trans-1,2-diaminocyclohexane (1.7 g, 15.0 mmol). The mixture was refluxed for 3 h and cooled to 0°C. A first portion of sodium borohydride (2.28 g, 60 mmol) and a second portion (1.14 g, 30 mmol) ½ h later was added to the stirring mixture slowly and in incremental amounts whilst maintaining the temperature at 0°C. The reaction mixture was allowed to reach room temperature whilst stirring overnight and concentrated to dryness under reduced pressure. Extraction of the white solid with dichloromethane (4 x 100 cm³) afforded an orange oil on removal of the solvent under reduced pressure. TLC indicated the oil to be a two-component mixture with R_f values 0.0 and 0.6. The mixture was chromatographed on a silica (70 - 230 mesh) column and eluted with methanol/ aq. ammonia solution (33%) (5:1). The solid obtained was dissolved in a mixture of toluene/ dichloromethane (80 : 130 cm³) and filtered through glass filter paper. On standing at room temperature the colourless crystals of L⁹.2½H₂O (2.48 g, 68%) were collected. m.p. 121 - 122°C; Found: C, 64.9; H, 8.7; N, 17.6. C₂₆H₄₃N₆O_{2½} requires: C, 65.1; H, 9.0; N, 17.5%.

For a typical synthesis of L¹⁰.3H₂O, yield = 86%; Found: C, 66.4; H, 9.5; N, 15.5. C₃₀H₅₂N₆O₃ requires: C, 66.2; H, 9.6; N, 15.4%.

Transition metal complexes of L⁹ and L¹⁰.

The procedure will be illustrated with the synthesis of $[\text{MnL}^9](\text{ClO}_4)_2$: A solution of manganese(II) perchlorate hexahydrate (0.42 g, 1.12 mmol) in methanol (10 cm³) was added dropwise to a stirring solution of L⁹ (0.51 g, 1.12 mmol) in methanol (40 cm³). Allowing the mixture to stand at room temperature yielded the crystalline $[\text{MnL}^9](\text{ClO}_4)_2$ complex. The product precipitated instantly as an amorphous solid when the reaction mixture was refluxed for *ca.* 1 h. Transition metal complexes of L¹⁰ were prepared in a similar manner. Analytical data are given in Table 6.2.

Lanthanide metal complexes of L⁹.

The procedure will be illustrated with the synthesis of $[\text{LaL}^9(\text{NO}_3)_3] \cdot \frac{1}{2}\text{H}_2\text{O}$: A solution of the ligand, L⁹ (0.53 g, 1.2 mmol) in dichloromethane (20 cm³) was added to a stirring solution of lanthanum(III) nitrate hexahydrate (0.51 g, 1.2 mmol) in acetonitrile (40 cm³) and refluxed for 2 h. The mixture was filtered and diethyl ether was diffused into the filtrate and allowed to stand at room temperature. Colourless crystals of $[\text{LaL}^9(\text{NO}_3)_3] \cdot \frac{1}{2}\text{H}_2\text{O}$ (0.21 g, 23%) formed which were filtered under suction, washed with diethyl ether (5 cm³) and air dried. Analytical data for all the lanthanide metal complexes of L⁹ are listed in Table 6.3.

Synthesis of $[\text{L}^9\text{H}_4](\text{ClO}_4)_4 \cdot 3\text{H}_2\text{O}$.

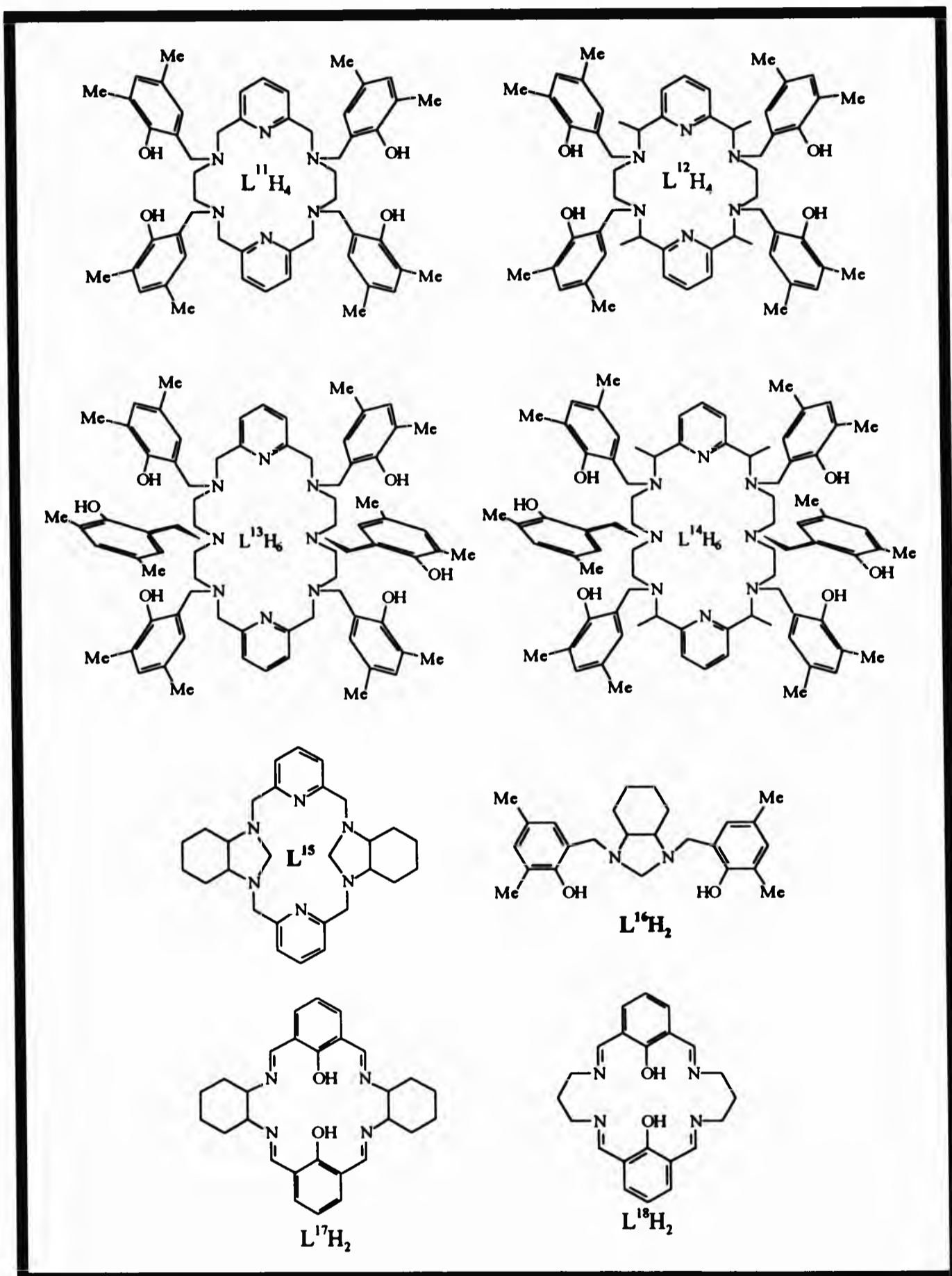
To a solution of L⁹ (0.40 g, 0.92 mmol) in methanol (40 cm³) was added dropwise a solution of gadolinium(III) perchlorate hexahydrate (0.52 g, 0.92 mmol) and a solution of sodium hydroxide (*ca.* 2 cm³, 2 mol dm⁻³) until pH 11 was reached. Allowing the mixture to stand at room temperature for several weeks afforded the white crystalline solid of $[\text{L}^9\text{H}_4](\text{ClO}_4)_4 \cdot 3\text{H}_2\text{O}$ (0.26 g, 34%) which was filtered under suction, washed with methanol (3 x 15 cm³) and diethyl ether (20 cm³) and dried *in vacuo* over calcium chloride. Found: C, 35.0; H, 5.4; N, 9.9. calc. for $\text{C}_{26}\text{H}_{48}\text{N}_6\text{Cl}_4\text{O}_{19}$: C, 35.1; H, 5.4; N, 9.4%.

Table 6.2 Analytical data for the transition metal complexes of L⁹ and L¹⁰

Complex	Yield (%)	Found (%)			Required (%)		
		C	H	N	C	H	N
[MnL ⁹](ClO ₄) ₂	58	45.5	5.5	12.2	45.3	5.5	12.2
[CoL ⁹](ClO ₄) ₃ .2½H ₂ O	59	37.5	4.9	10.0	37.5	5.1	10.0
[CuL ⁹](ClO ₄) ₂ .MeOH	64	44.6	5.7	11.7	44.5	5.8	11.5
[ZnL ⁹](ClO ₄) ₂	68	44.6	5.6	11.9	44.7	5.4	12.0
[CdL ⁹](ClO ₄) ₂	69	42.0	5.1	11.2	42.0	5.1	11.3
[MnL ¹⁰](ClO ₄) ₂ (MeOH)(H ₂ O)	58	41.0	6.6	10.4	40.8	6.6	10.6
[CoL ¹⁰](ClO ₄) ₃ .3½MeOH.3½H ₂ O	54	40.6	7.0	8.6	39.3	6.8	8.5
[CuL ¹⁰](ClO ₄) ₂ .1½H ₂ O	61	45.5	6.2	10.7	46.0	6.3	10.8

Table 6.3 Analytical data for the lanthanide metal complexes of L²

Complex	Yield (%)	Found (%)			Required (%)		
		C	H	N	C	H	N
[YL ² (NO ₃) ₂]NO ₃ .MeCN	24	45.1	5.7	18.9	44.8	5.5	18.7
[LaL ² (NO ₃) ₃] ^{1/2} H ₂ O	23	40.4	4.9	16.5	40.6	5.1	16.4
[NdL ² (NO ₃) ₂ (MeCN)]NO ₃ .MeCN	20	42.9	5.3	17.9	42.6	5.2	18.2
[EuL ² (NO ₃) ₂ (MeCN)(NO ₃ H)]NO ₃	42	38.0	4.9	17.2	38.4	4.8	17.6
[GdL ² (NO ₃) ₂]NO ₃ .2CH ₂ Cl ₂	19	35.7	4.9	13.4	35.5	4.4	13.3
[DyL ² (NO ₃) ₂]NO ₃ .2CH ₂ Cl ₂	20	33.9	4.4	12.2	33.6	4.1	12.2



Synthesis of L¹¹H₄, L¹²H₄, L¹³H₄ and L¹⁴H₄.

The procedure will be described with the synthesis of L¹¹H₄: To a refluxing suspension of barium(II) chloride dihydrate (3.22 g, 13.2 mmol) and 2,6-pyridinedialdehyde (3.56 g, 26.4 mmol) in methanol (150 cm³) was added dropwise a solution of 1,2-diaminoethane (1.6 g, 26.7 mmol) in methanol (10 cm³). The mixture was refluxed for 3 h and cooled to 0°C. A first portion of sodium borohydride (3.95 g, 104 mmol) and a second portion (1.97 g, 52 mmol) ½ h later was added to the stirring mixture slowly and in incremental amounts whilst maintaining the temperature at 0°C. The reaction mixture was allowed to reach room temperature whilst stirring overnight and concentrated to dryness under reduced pressure. Extraction of the white solid with dichloromethane (4 x 150 cm³) afforded an orange-red oil upon removal of the solvent under reduced pressure. The oil was refluxed in methanol (40 cm³) for ½ h before 2,4-dimethylphenol (9.8 g, 80.3 mmol) was added neat and the mixture refluxed for 1 h. Aq. methanal (3.2 g, 106.7 mmol, 37% solution in water) was added dropwise over a period of 1 - 2 h. The white solid of L¹¹H₄ (4.46 g, 39%) precipitated during reflux which was filtered under suction, washed with methanol (3 x 20 cm³) and dried *in vacuo* over calcium chloride. Analytical results are shown in Table 6.4.

Table 6.4 Analytical data for the synthesis of $L^{11}H_6$, $L^{12}H_6$, $L^{13}H_6$ and $L^{14}H_6$											
Ligand	wt di-aldehyde (g)	wt diamine (g)	BaCl ₂ ·2H ₂ O (g) ^d	m.p (°C)	Yield (%)	Found (%)			Required (%)		
						C	H	N	C	H	N
$L^{11}H_4$	3.56 ^a	1.6 ^c	3.22	189 - 191	39	75.1	7.5	9.4	75.1	7.6	9.7
$L^{12}H_4$	2.51 ^b	1.0 ^c	1.87	202 - 205	35	75.7	8.2	9.2	75.7	8.2	9.1
$L^{13}H_6$	3.04 ^a	2.1 ^d	2.44	211 - 212	47	75.1	8.0	9.3	75.0	7.9	9.2
$L^{14}H_6$	1.5 ^b	1.0 ^d	1.12	232 - 236	32	75.7	8.4	9.6	75.5	8.2	8.8

^a2,6-pyridinedialdehyde (M⁺ 135) ^b2,6-diacetylpyridine (M⁺ 163) ^c1,2-diaminoethane (M⁺ 60) ^ddiethylenetriamine (M⁺ 103)

^e(M⁺ 244)

Synthesis of the transition and lanthanide metal complexes of L¹¹H₄.

An example using yttrium(III): To a suspension of L¹¹H₄ (0.25 g, 0.29 mmol) in methanol (40 cm³) was dropwise added a solution of yttrium(III) nitrate pentahydrate (0.16 g, 0.44 mmol) in methanol (5 cm³). Reflux was continued for 2 h during which a colourless solution was obtained. The solution was reduced to ca. 10 cm³, under reduced pressure, and allowed to stand at room temperature. Colourless crystals of [Y(L¹¹H₂)NO₃].H₂O (0.07 g, 22%) were obtained which were filtered under suction, washed with methanol (10 cm³) and dried *in vacuo* over calcium chloride. Analytical data are listed in Table 6.5 for all the metal complexes of L¹¹H₄. In all cases the weight of ligand used was 0.25 g.

Synthesis of L¹⁵ and L¹⁶H₂:

A solution of aq. methanal (2.9 g, 120 mmol) in methanol (30 cm³) was dropwise, added over a period of 1 h, to a refluxing mixture of crude L⁹ (5.09 g, 11.7 mmol) and 2,4-dimethylphenol (11.7 g, 96 mmol). The reaction mixture was refluxed for 6 h and allowed to cool to room temperature. Diffusion of diethyl ether to the mixture caused the precipitation of colourless crystals of L¹⁵ (2.63 g, 49%); Found: C, 73.2; H, 8.3; N, 18.5. calc. for C₂₈H₃₈N₆: C, 73.4; H, 8.3; N, 18.3%. The filtrate was allowed to stand for several weeks from which the feather-like crystals of L¹⁶H₂ formed.

Synthesis of L¹⁷H₂:

To a refluxing solution of 2,6-diformylphenol (0.25 g, 1.7 mmol) in methanol (3cm³) was added a solution of (±)-*trans*-1,2-diaminocyclohexane (0.1 g, 1.7 mmol) in methanol (2 cm³). Reflux was continued for 4 h during which the yellow solid of L¹⁷H₂ (0.30 g, 77%) precipitated and was filtered hot, washed with hot methanol (3 x 3 cm³) and dried *in vacuo* over calcium chloride. Found: C, 73.8; H, 7.0; N, 12.4. calc. for C₂₈H₃₂N₄O₂: C, 73.7; H, 7.0; N, 12.3%.

Table 6.5 Analytical data for the metal complexes of L¹¹H₄

Complex	Yield (%)	Found (%)			Required (%)		
		C	H	N	C	H	N
[Fe(L ¹¹ H ₄)](ClO ₄) ₂ (MeOH)	60	57.2	5.9	7.2	57.4	5.7	7.3
[Cd(L ¹¹ H ₄)](ClO ₄) ₂ .4H ₂ O	88	52.2	5.6	6.7	52.4	5.6	6.8
[Y(L ¹¹ H ₂)NO ₃]	40	62.8	6.2	9.5	63.0	6.3	9.5
[La(L ¹¹ H ₃)NO ₃](NO ₃).3½H ₂ O	17	54.8	5.8	9.4	54.5	5.8	9.4
[Nd(L ¹¹ H ₃)NO ₃](NO ₃).2MeOH.4½H ₂ O	21	52.8	5.9	8.7	52.7	6.4	8.8
[Eu(L ¹¹ H ₃)NO ₃]NO ₃ .3MeOH	36	55.5	5.9	9.1	55.5	6.2	9.1
[Gd(L ¹¹ H ₃)NO ₃]NO ₃ .3H ₂ O	20	54.4	5.8	9.4	54.3	5.8	9.4
[Dy(L ¹¹ H ₂)NO ₃]2H ₂ O	22	57.8	5.8	8.7	57.8	6.1	8.7

Synthesis of the yttrium and lanthanide metal complexes of $L^{17}H_2$.

The synthesis will be illustrated with the preparation of $[Dy(L^{17}H)NO_3]NO_3 \cdot MeOH \cdot 3\frac{1}{2}H_2O$ as an example. 2,5-diformylphenol (1.05 g, 7.0 mmol) in methanol (20 cm³) was added to a solution of dysprosium(III) nitrate pentahydrate (1.53 g, 3.5 mmol) in methanol (60 cm³) and refluxed for ½ h. A solution of (\pm)-*trans*-1,2-diaminocyclohexane (0.8 g, 7.0 mmol) in methanol (10 cm³) was added dropwise to the mixture over 20 min. A red-brown solid precipitated during the 3 h reflux which was filtered hot, washed with methanol (3 x 15 cm³) and diethyl ether (10 cm³) and dried *in vacuo*. Analytical data are given in Table 6.6.

Synthesis of the metal complexes of $L^{18}H_2$ including the synthesis of $[Dy(L^{19}H)(NO_2)_4(H_2O)_2]NO_3 \cdot 5\frac{1}{2}H_2O$:

The method used was similar to that of the syntheses of the metal complexes of $L^{17}H_2$ with the exception that 1,3-diaminopropane was used instead of (\pm)-*trans*-1,2-diaminocyclohexane. The analyses are listed in Table 6.7.

Table 6.6 Analytical data for the metal complexes of L¹⁷H₂

Complex	Yield (%)	Found (%)			Required (%)		
		C	H	N	C	H	N
[Y(L ¹⁷ H)OAc]OAc(MeOH)2H ₂ O	84	54.7	6.1	7.8	54.4	5.9	7.7
[La(L ¹⁷ H)(NO ₃)]NO ₃ .½H ₂ O	94	46.2	4.2	11.5	46.2	4.4	11.6
[Nd(L ¹⁷ H)(NO ₃)](NO ₃)(MeOH)	76	45.9	4.6	11.2	46.1	4.6	11.1
[Eu(L ¹⁷ H)(NO ₃)](NO ₃)(MeOH)3H ₂ O	61	42.5	4.3	10.2	42.6	4.8	10.3
[Gd(L ¹⁷ H)(OAc)](OAc)3MeOH	55	50.5	5.2	6.7	50.8	5.9	6.8
[Dy(L ¹⁷ H)NO ₃]NO ₃ .MeOH.3½H ₂ O	94	41.7	4.7	10.1	41.7	5.0	10.1

Table 6.7 Analytical data for the metal complexes of $L^{18}H_2$

Complex	Yield (%)	Found (%)			Required (%)		
		C	H	N	C	H	N
$[Y(L^{18}H)](OAc) \cdot \frac{1}{2}H_2O$	56	54.0	5.3	10.4	54.2	4.9	10.5
$[La(L^{18}H)(NO_3)]NO_3$	93	41.3	4.0	13.3	41.4	3.6	13.2
$[Nd(L^{18}H)(NO_3)](NO_3)\frac{1}{2}MeOH$	95	40.7	3.7	12.7	41.0	3.5	12.7
$[Eu(L^{18}H)(NO_3)](NO_3)(H_2O)$	92	39.1	3.8	13.1	40.3	3.2	12.8
$[Gd(L^{18}H)(Cl)(H_2O)](Cl)(MeOH) \cdot 2H_2O$	85	40.3	5.5	8.2	40.1	4.8	8.1
$[Dy_2(L^{19}H_3)(NO_3)_4(MeOH)H_2O](NO_3)4H_2O$	71	35.0	3.8	12.0	35.6	4.1	12.0

6.3 References

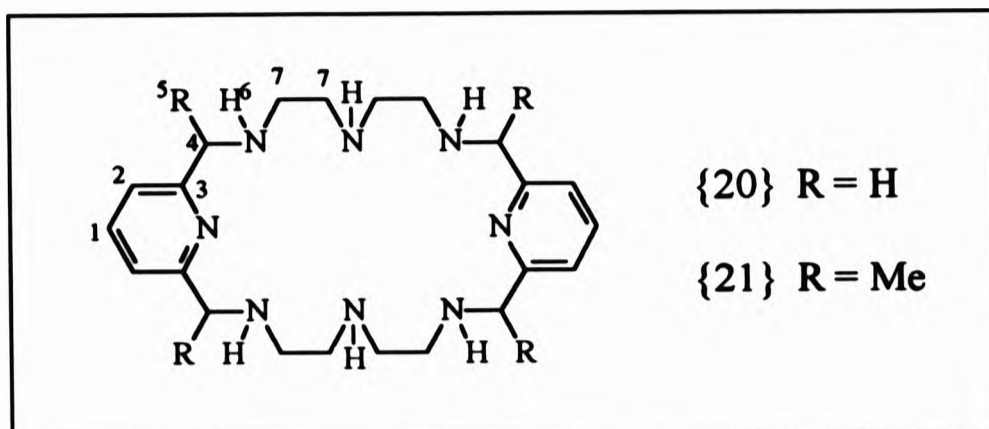
1. A. Earnshaw, *Introduction to Magnetochemistry*, Academic Press, London, 1968.
2. N. W. Alcock, R. G. Kingston, P. Moore and C. Pierpoint, *J. Chem. Soc., Dalton Trans.*, 1984, 1937.
3. J. Sambrook, E. F. Fritsch and T. Maniatis, *Molecular Cloning, A Laboratory Manual*, 2nd edn., Colt Spring Harbour Laboratory Press, U. S. A., 1989.

A P P E N D I X

Appendix	Page
1 Characterisation of $[\{20\}H_6]Cl_6$ and $[\{21\}H_6]Cl_6$	A1
2 Relaxation Rates of $[GdL^5(H_2O)_3].3Cl(3H_2O)$ and $[Gd(L^{11}H_3)NO_3]NO_3.3H_2O$	A2

APPENDIX 1

Characterisation of $\{20\}H_6Cl_6$ and $\{21\}H_6Cl_6$



Yield (%): $\{20\}H_6Cl_6 \cdot 2H_2O$: 64; $\{21\}H_6Cl_6 \cdot 4H_2O$: 59.

IR: (FT-IR, KBr 3 mm disc):

$\{20\}H_6Cl_6 \cdot 2H_2O$: ν_{max}/cm^{-1} 1597m (NH), 1579m (C=N_(py))

$\{21\}H_6Cl_6 \cdot 2H_2O$: ν_{max}/cm^{-1} 1594m (NH), 1577m (C=N_(py))

EI-MS:

$\{20\}H_6Cl_6$: m/z 412 (64%, [M-6HCl]⁺), 206 (37%, [(M-6HCl)/2]⁺)

$\{21\}H_6Cl_6$: m/z 688 (11%, [M]⁺), 468 (56%, [M-6HCl]⁺), 235 (46%, [(M-6HCl)/2]⁺)

¹H NMR

$\{21\}H_6Cl_6$ (diastereomeric): (D₂O): $\delta_H/p.p.m.$ 7.99 (H¹, m); 7.52 (H², m); 4.63 (H⁴, m); 3.38 (H⁷, m); 1.66 (H⁵, m).

Elemental Analysis:

$\{20\}H_6Cl_6 \cdot 2H_2O$: Found: C, 39.8; H, 7.3; N, 16.8%. Calc. for C₂₂H₄₆N₈Cl₆O₂: C, 39.6; H, 6.9; N, 16.8%.

$\{21\}H_6Cl_6 \cdot 4H_2O$: Found: C, 41.0; H, 7.2; N, 14.8%. Calc. for C₂₆H₅₈N₈Cl₆O₄: C, 41.1; H, 7.6; N, 14.8%.

APPENDIX 2

Determination of relaxation times of the gadolinium complexes of L⁵ and L¹¹

The spectrometer was standardised with deionised water and 1 mmol dm⁻³ gadolinium chloride hexahydrate.

Five readings were taken for each concentration and then averaged. The readings were taken in the temperature range 35- 37°C and each solution was at pH 6.

Relaxation times of [GdL⁵(H₂O)₃]Cl₃(3H₂O) at 20 MHz

(a) water system

conc (mmol dm ⁻³)	relaxation delay (s)	T ₁ (s)	R ₁ (dm ⁻³ mmol ⁻¹ s ⁻¹)
0.12	0.24	0.7756	1.2893
0.51	0.57	0.1714	5.8343
0.99	0.66	0.0982	10.1833
1.49	0.94	0.0592	16.8919

$$R_1 = 11.087(\text{conc}) - 0.074$$

$$\text{correlation of data} = 0.999$$

$$\text{at } 1.0 \text{ mmol dm}^{-3}, R_1 = 11.0 \text{ dm}^3 \text{ mmol}^{-1} \text{ s}^{-1}$$

(b) phosphate buffer system

conc (mmol dm ⁻³)	relaxation delay (s)	T ₁ (s)	R ₁ (dm ⁻³ mmol ⁻¹ s ⁻¹)
0.11	3.41	1.4668	0.6818
0.50	2.50	0.4212	2.3742
1.00	1.43	0.2286	4.3745
1.51	1.00	0.1368	7.3099

$$R_1 = 4.680(\text{conc}) + 0.040, \text{ correlation of data} = 0.999$$

$$\text{at } 1.0 \text{ mmol dm}^{-3}, R_1 = 4.6 \text{ dm}^3 \text{ mmol}^{-1} \text{ s}^{-1}$$

Relaxation times of $[\text{Gd}(\text{L}^{11}\text{H}_3)\text{NO}_3]\text{NO}_3(3\text{H}_2\text{O})$ at 10 MHz

(a) DMSO/ water system

conc (mmol dm^{-3})	relaxation delay (s)	T_1 (s)	R_1 ($\text{dm}^{-3} \text{mmol}^{-1} \text{s}^{-1}$)
0.1	0.83	0.8512	1.748
0.5	1.05	0.2350	4.2553
1.0	0.57	0.1263	7.9177
1.5	0.89	0.0818	12.2249
2.0	0.28	0.0604	16.2249

$$R_1 = 7.936(\text{conc}) - 0.2647,$$

correlation of data = 0.9996, $\sigma = 0.1872$

at 1.0 mmol dm^{-3} , $R_1 = 8.20 \text{ dm}^{-3} \text{mmol}^{-1} \text{s}^{-1}$

(b) DMSO/ phosphate buffer system

conc (mmol dm^{-3})	relaxation delay (s)	T_1 (s)	R_1 ($\text{dm}^{-3} \text{mmol}^{-1} \text{s}^{-1}$)
0.1	4.00	0.7944	1.2588
0.5	3.00	0.5682	1.7599
1.0	1.75	0.3574	2.7980
1.5	1.65	0.2950	3.3898
2.0	1.00	0.1974	5.0650

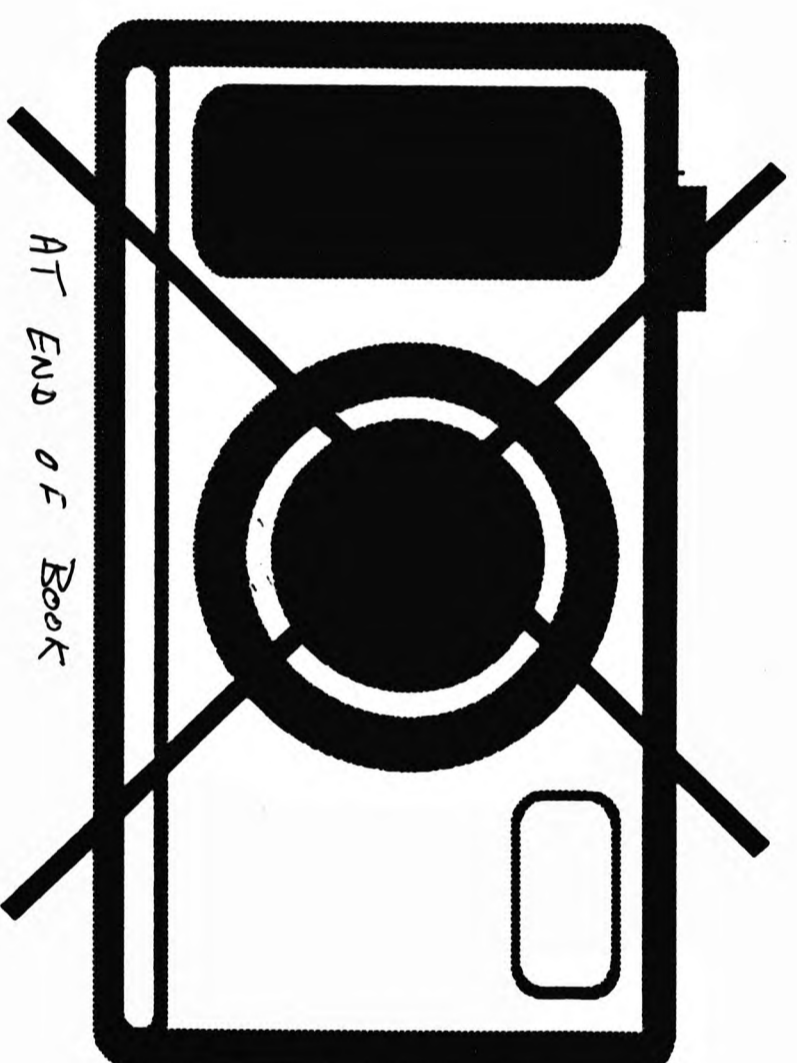
$$R_1 = 1.933(\text{conc}) + 0.8825,$$

correlation of data = 0.9833, $\sigma = 0.3140$

at 1.0 mmol dm^{-3} , $R_1 = 2.82 \text{ dm}^{-3} \text{mmol}^{-1} \text{s}^{-1}$

PUBLICATIONS

**PUBLISHED PAPERS
NOT FILMED FOR
COPYRIGHT REASONS**



THE BRITISH LIBRARY

BRITISH THESIS SERVICE

TITLE LANTHANIDE AND TRANSITION METAL
COMPLEXES OF NITROGEN AND OXYGEN
DONOR MACROCYCLIC LIGANDS.

AUTHOR Evagoras George
EVAGOROU

DEGREE Ph.D

**AWARDING
BODY** University of North London

DATE 1994

**THESIS
NUMBER** DX184647

THIS THESIS HAS BEEN MICROFILMED EXACTLY AS RECEIVED

The quality of this reproduction is dependent upon the quality of the original thesis submitted for microfilming. Every effort has been made to ensure the highest quality of reproduction. Some pages may have indistinct print, especially if the original papers were poorly produced or if awarding body sent an inferior copy. If pages are missing, please contact the awarding body which granted the degree.

Previously copyrighted materials (journals articles, published texts etc.) are not filmed.

This copy of the thesis has been supplied on condition that anyone who consults it is understood to recognise that its copyright rests with its author and that no information derived from it may be published without the author's prior written consent.

Reproduction of this thesis, other than as permitted under the United Kingdom Copyright Designs and Patents Act 1988, or under specific agreement with the copyright holder, is prohibited.

C12

DX

184647